Isotopic, chemical, and crowdsourcing studies of selected water cycle components in arid environments

Dissertation

Doctoral thesis submitted in partial fulfillment of the requirements
for the degree Doctor rerum naturalium (Dr. rer. nat.)

TECHNISCHE
UNIVERSITÄT
DARMSTADT

Department of Materials and Earth Sciences
Technische Universität Darmstadt

Nils Michelsen (Dipl.-Ing. Angewandte Geowissenschaften)

born on 14 August 1980 in Erlenbach am Main, Germany

Supervisor: Prof. Dr. Christoph Schüth
Co-supervisor: Dr. Paul Königer
Examiner: Prof. Dr. Matthias Hinderer
Examiner: Prof. Dr. Susanne Lackner

Darmstadt 2020

Declaration of authorship

I hereby declare that the presented dissertation is based on original research and is the result of my own work. I certify that this dissertation contains no material that has been accepted for the award of any other degree in my name, in any university or other tertiary institution and, to the best of my knowledge and belief, contains no material previously published or written by another person, except where due reference has been made in the text.

Darmstadt, 23 December 2019

Mit Schnellzügen macht man keine Forschungsreisen

August Kekulé (1829-1896)

Abstract

This cumulative thesis comprises five studies (four published, one submitted). The investigations either deal with specific aspects of Saudi Arabia's water cycle or have a methodological character and the developed methods are particularly useful for arid environments.

The first study addresses Riyadh rainfall. Besides major ion analyses, isotope analyses were conducted to calculate a precipitation-weighted Local Meteoric Water Line – a crucial, but hitherto missing reference for past and future groundwater isotope studies.

The second investigation focuses on the next element of the water cycle – the unsaturated zone. Stable isotope fingerprints of sand dune pore waters and meteorological data were used in an isotope model to constrain rain events leading to deep infiltration into dune sands. Interestingly, the derived original (i.e., pre-evaporation) isotopic signatures were not represented in the data set on rainfall (see above) – probably due to the temporally limited nature of the latter.

This observation calls for a long-term monitoring effort targeting the isotopic signature of precipitation in Riyadh and elsewhere in Saudi Arabia. To go beyond the somewhat generic call for more data, concrete advice on which type of cumulative rain sampler to use for such an endeavor is needed. As post-sampling evaporation has to be minimized, several established and new rain collector designs were tested in a laboratory oven. In this experiment, the Tube-dip-in-water collector with pressure equilibration tube proved to be a reliable and contamination-free option.

Building on this knowledge, an automatic counterpart was designed in a fourth study. The microcontroller-based device enables timer-actuated integral rain sampling. The simple low-cost collector is robust and effectively minimizes post-sampling evaporation from the bottles, and the associated isotope fractionation. The excellent performance of the device during an extensive evaporation experiment in a laboratory oven suggests that even multi-week field deployments in warm climates are feasible.

The fifth study deals with shallow groundwater. To reconstruct an unexpected water level rise in a Saudi Arabian cave, a crowdsourcing approach was applied. Chronologically sorted YouTube videos recorded in the cave were screened for suitable reference points (e.g., cave graffiti) that appear in several videos. Then, the distances between these points and the water level were visually estimated and their changes were traced over time. The acquired data helped to identify the likely cause of the piezometric changes – two nearby lakes formed from treated sewage effluent.

Hopefully, the outlined findings can contribute to a better understanding of the hydrogeological system in Saudi Arabia and can help to identify promising paths for future research. The utilized methods might also be of value for other arid areas.

Zusammenfassung

Die vorliegende Dissertation beinhaltet fünf Einzelstudien (vier veröffentlichte, sowie einen eingereichten Artikel). Die Untersuchungen befassen sich mit spezifischen Aspekten des Wasserkreislaufs Saudi-Arabiens oder haben methodischen Charakter, wobei sich die entwickelten Methoden besonders für aride Gebiete eignen.

Das Thema der ersten Studie ist der Niederschlag Riads. Neben Hauptionenanalysen wurden Isotopenanalysen durchgeführt um eine niederschlagsgewichtete „Local Meteoric Water Line“ zu berechnen – eine wichtige aber bislang fehlende Vergleichslinie für ältere sowie zukünftige Isotopenstudien am Grundwasser.

Der Fokus der zweiten Untersuchung ist das folgende Kompartiment des Wasserzyklus – die ungesättigte Zone. Isotopendaten zu Porenwässern in Sanddünen und meteorologische Daten wurden in einem Isotopenmodell kombiniert um Niederschlagsereignisse einzugrenzen, die zu einer tieferen Infiltration in Dünensande führen. Die abgeleiteten Original-Isotopensignaturen (vor der Verdunstung) sind interessanterweise nicht im oben genannten Niederschlagsdatensatz vertreten, vermutlich wegen dessen zeitlicher Limitierung.

Dieses Ergebnis lässt ein Langzeit-Monitoring der Niederschlagsisotopie sinnvoll erscheinen – in Riad, aber auch in anderen Teilen Saudi-Arabiens. In diesem Zusammenhang soll auch ein konkreter Vorschlag zu kumulativen Niederschlagssammlern für ein solches Monitoringprogramm gemacht werden. Da der Verdunstungs-minimierung bei derartigen Sammlern eine besondere Rolle zukommt, wurden mehrere etablierte und neue Sammler in einem Trockenofen getestet. In diesem Experiment wurde der sogenannte „Tube-dip-in-water collector with pressure equilibration tube” als verlässliche und kontaminationsfreie Variante identifiziert.

Darauf aufbauend wurde in einer vierten Studie eine automatische Version dieses Sammlertyps entwickelt, die eine zeitgesteuerte, integrale Niederschlagsbeprobung erlaubt. Dieses einfache, robuste und kostengünstige Modell reduziert die Verdunstung aus den Sammelflaschen und die damit verbundene Isotopenfraktionierung deutlich. Aufgrund der hervorragenden Leistung des Sammlers in einem ausgiebigen Versuch mit einem Trockenofen erscheinen auch mehrwöchige Feldeinsätze des Gerätes in warmen Klimaten möglich.

Die fünfte Studie beschäftigt sich mit flachem Grundwasser. Um den unerwarteten Wasseranstieg in einer saudi-arabischen Höhle zu rekonstruieren, wurde ein Crowdsourcing-Ansatz gewählt. Chronologisch geordnete YouTube-Videos wurden nach Referenzpunkten durchsucht, die in mehreren Videos zu erkennen sind (z.B. Höhlengraffiti). Im Anschluss wurden die Abstände zwischen diesen Punkten und dem Wasserspiegel visuell geschätzt und die zeitliche Entwicklung dieser Abstände verfolgt. Mit den gewonnenen Daten konnte der vermutliche Ursprung des Wasseranstiegs identifiziert werden – zwei nahegelegene Seen die aus behandeltem Abwasser bestehen.

Die hier umrissenen Ergebnisse können hoffentlich zu einem besseren Verständnis der Hydrogeologie Saudi-Arabiens beitragen sowie einen Anstoß zu zukünftigen, weiterführenden Untersuchungen geben. Die hier angewandten Methoden könnten auch für andere aride Gebiete von besonderem Nutzen sein.

Preface

The original idea to write this thesis emerged during my employment as a hydrogeology consultant in Riyadh, Saudi Arabia (2007–2010). At that time, I worked for a company consortium consisting of Gesellschaft für Technische Zusammenarbeit (GTZ) International Services (now Gesellschaft für Internationale Zusammenarbeit, GIZ) and Dornier Consulting. The main task of our multi-disciplinary team was the assessment of several large-scale aquifer systems on the Arabian Peninsula and the most important client was the Saudi Arabian Ministry of Water & Electricity (now Ministry of Environment, Water & Agriculture).

The reports that we submitted during this time comprised multiple volumes addressing a broad range of topics (e.g., geology, hydrology, hydrogeology, water quality, water management, etc.), which allowed me to deepen my knowledge in various fields. Although our studies, and the investigations of previous consultant generations, were comprehensive, I occasionally stumbled upon sub-topics that, in my opinion, deserved more attention. Since many of the concerned aspects were beyond the scope of the projects, a closer look in an academic setting seemed appropriate. The decision to tackle this work was facilitated by two factors – the encouragement by Prof. Dr. Christoph Schüth and Prof. Dr. Randolf Rausch as well as a PhD scholarship awarded to me by the German Federal Ministry of Education and Research (BMBF) as part of their program International Postgraduate Studies in Water Technologies (IPSWaT).

The initial concept had been to incorporate data generated during my consultant time (e.g., hydrochemical and isotope analyses). Given this wealth of unpublished and interesting data, this idea was rather tempting, but I eventually changed my mind. Using only new data meant “loosing” a huge body of information, but also had two crucial advantages. First, the data on which I finally focused were really novel, and second, I did not have to ask anyone for permission to publish it. The latter aspect is important, because the reports of our consortium, and those of previous consultants, have never been published. Many findings in these reports are not surprising or critical, but certain topics are politically sensitive (e.g., natural groundwater radioactivity) and/or of strategic importance.

A second twist of plans was that I eventually deviated from the Saudi-only track. The original strategy had been to write about Saudi Arabia and maybe touch upon a few neighboring countries where necessary from a hydrogeological perspective. At some point, however, I realized that I did not want to become an expert on the kingdom only, but rather use the lessons learnt in a broader context and thus hopefully create knowledge that is also relevant for other (semi-)arid regions.

Following the much debated but at times true academic mantras “publish or perish” and “DOI or it didn’t happen”, the performed work was published in a set of ISI papers and is herein presented in the form of a cumulative dissertation.

ISI publications that are part of this cumulative thesis:

Michelsen, N., Reshid, M., Siebert, C., Schulz, S., Knöller, K., Weise, S.M., Rausch, R., Al-Saud, M., Schüth, C., 2015. Isotopic and chemical composition of precipitation in Riyadh, Saudi Arabia. Chemical Geology 413, 51–62. *(Chapter 2 of this thesis)*

Michelsen, N., van Geldern, R., Roßmann, Y., Bauer, I., Schulz, S., Barth, J.A.C., Schüth, C., 2018. Comparison of cumulative precipitation collectors used in isotope hydrology. Chemical Geology 488, 171–179. *(Chapter 4 of this thesis)*

Michelsen, N., Laube, G., Friesen, J., Weise, S.M., Bait Said, A.B.A., Müller, T., 2019. Technical note: A microcontroller-based automatic rain sampler for stable isotope studies. Hydrology and Earth System Sciences 23(6), 2637–2645. *(Chapter 5 of this thesis)*

Michelsen, N., Dirks, H., Schulz, S., Kempe, S., Al-Saud, M., Schüth, C., 2016. YouTube as a crowd-generated water level archive. Science of the Total Environment 568, 189–195. *(Chapter 6 of this thesis)*

Moreover, the following manuscript has been submitted for publication:

Michelsen, N., Toegl, A., Koeniger, P., Schulz, S., Schüth, C., 2019. Isotopic composition of pore waters in Saudi Arabian dune sands: implications for deep infiltration, evaporation losses, and groundwater recharge estimations. *Submitted for publication. (Chapter 3 of this thesis)*

Additionally, I contributed to a number of ISI publications as co-author. Although most of these articles are also related to my work on the Arabian Peninsula, they are not included in this dissertation.

Additional ISI publications that are not part of this thesis:

Crassard, R., Petraglia, M.D., Drake, N.A., Breeze, P., Gratuze, B., Alsharekh, A., Arbach, M., Groucutt, H.S., Khalidi, L., **Michelsen, N.,** Robin, C.J., Schiettecatte, J., 2013. Middle Palaeolithic and Neolithic Occupations around Mundafan Palaeolake, Saudi Arabia: Implications for Climate Change and Human Dispersals. PLoS ONE 8(7), e69665.

Khan, A., **Michelsen, N.,** Marandi, A., Hossain, R., Hossain, A., Roehl, K.E., Zahid, A., Hassan, Q., Schüth, C., 2019. Processes controlling the extent of groundwater pollution with chromium from tanneries in the Hazaribagh area, Dhaka, Bangladesh. Science of the Total Environment. *In press* (https://doi.org/10.1016/j.scitotenv.2019.136213).

Schulz, S., Horovitz, M., Rausch, R., **Michelsen, N.,** Mallast, U., Köhne, M., Siebert, C., Schüth, C., Al-Saud, M., Merz, R., 2015. Groundwater evaporation from salt pans: Examples from the eastern Arabian Peninsula. Journal of Hydrology 531, 792–801.

Schulz, S., de Rooij, G. H., **Michelsen, N.,** Rausch, R., Siebert, C., Schüth, C., Al-Saud, M., Merz, R., 2016. Estimating groundwater recharge for an arid karst system using a combined approach of time-lapse camera monitoring and water balance modelling. Hydrological Processes 30, 771–782.

Schulz, S., Walther, M., **Michelsen, N.,** Rausch, R., Dirks, H., Al-Saud, M., Merz, R., Kolditz, O., Schüth, C., 2017. Improving large-scale groundwater models by considering fossil gradients. Advances in Water Resources 103, 32–43.

Also among these co-author contributions, some of the work has only been submitted recently:

Darehshouri, S., **Michelsen, N.,** Schüth, C., Schulz, S., 2019. A low-cost environmental chamber to simulate warm climatic conditions. *Submitted for publication.*

The thesis is organized as follows. Chapter 1 is a brief introduction outlining the motivation and some background information on Saudi Arabia. The subsequent Chapters 2 to 6 correspond to the above-mentioned first-author papers. Before each of these chapters, a short preface provides some context and serves as a transition between the sections. Chapter 7 presents some concluding remarks – concerning the situation in Saudi Arabia, but also regarding the broader isotope and crowdsourcing communities. The Acknowledgements section, Chapter 8, is followed by seven appendices. Their numbers correspond to the number of the associated chapter. The Appendices 2 to 6 comprise the Supplementary data published alongside the articles presented in chapters 2 to 6.

Each chapter, preface section, and appendix features its own list of references. The publications represent the final published version (content-wise), but were reformatted for sake of consistency. Figure and table numbers were modified and a consistent reference style was applied.

Table of contents

List of figures

List of tables

List of abbreviations

‰	per mil
δ	delta
θ_g	gravimetric water content
a	slope (of a Local Meteoric Water Line)
AG	Arabian Gulf
AH	auger hole
AS	Arabian Sea
b	intercept (of a Local Meteoric Water Line)
BMBF	Federal Ministry of Education and Research
BWh	hot desert climate (Köppen-Geiger class)
^{14}C	carbon-14
^{36}Cl	chlorine-36
d	deuterium excess
DOI	digital object identifier
EC	electrical conductivity (reference temperature: 25°C)
FAO	Food and Agriculture Organization of the United Nations
GDP	Gross Domestic Product
GIZ	Gesellschaft für Internationale Zusammenarbeit
GMWL	Global Meteoric Water Line
GNIP	Global Network of Isotopes in Precipitation
GTZ	Gesellschaft für Technische Zusammenarbeit
h	hour
^{1}H	hydrogen-1
^{2}H	hydrogen-2 (deuterium)
^{3}H	hydrogen-3 (tritium)
ha	hectare
HDPE	high-density polyethylene
HYSPLIT	HYbrid Single-Particle Lagrangian Integrated Trajectory
IAEA	International Atomic Energy Agency
IPSWaT	International Postgraduate Studies in Water Technologies
ISI	Institute for Scientific Information (see Web of Science, Journal Citation Reports)
lc-excess	Line-conditioned excess
LDPE	low-density polyethylene
LMWL	Local Meteoric Water Line

MA	Major Axis
m asl	meters above sea level
meq	milliequivalent
METAR	Meteorological Aviation Routine Weather Report
MS	Mediterranean Sea
^{16}O	oxygen-16
^{18}O	oxygen-18
OLSR	Ordinary Least Squares Regression
P	precipitation
PE	polyethylene
PP	polypropylene
PTFE	polytetrafluoroethylene (Teflon)
PU	polyurethane
PVC	polyvinyl chloride
PVC-U	unplasticized polyvinyl chloride
PWLSR	precipitation-weighted Least Squares Regression
PWMA	precipitation-weighted Major Axis
PWRMA	precipitation-weighted Reduced Major Axis
RH	relative humidity
RMA	Reduced Major Axis
rmSSE	root mean Sum of Squared Errors
RS	Red Sea
SE	standard error
t	ton
T	temperature
Temp.	temperature
TU	tritium unit
UFZ	Helmholtz Centre for Environmental Research
V-SMOW	Vienna Standard Mean Ocean Water
WMO	World Meteorological Organization
x	fractional evaporative loss

1. Introduction

Although this thesis deals with a range of methods that are applicable to arid environments in general, some of the work was motivated by the situation in one specific country – Saudi Arabia. As many parts of the world exhibit an arid climate and deserve more attention by the water community (see Blume et al., 2017), the question why this specific country was selected is justified, and hence addressed in the following section.

1.1. Why Saudi Arabia?

To a large extent the decision to do research in Saudi Arabia was driven by personal experience in the kingdom (see Preface). Yet, there are additional reasons, including a limited number of water-related publications and a high water stress (Grassert et al., 2013) underscoring the relevance of water research in Saudi Arabia. Moreover, the large size of the country – with about 2,150,000 km² (FAO, 2019a) Saudi Arabia is the world's 12th biggest country – and the associated diversity of environmental settings played a role. Finally, also the country's economic wealth had a certain relevance in the decision. Some of these aspects are elaborated on in the following paragraphs.

Since research can potentially help to address water-related problems, one could (possibly naively) hypothesize that water-scarce countries should be well-represented in the corresponding scientific literature. To test this hypothesis, a simple bibliometric analysis was conducted. The Web of Science database was searched for individual country names in the *Topic* field of English articles that appeared in the last 50 years in a set of water-focused journals: Advances in Water Resources, Groundwater, Hydrogeology Journal, Hydrological Processes, Hydrological Sciences Journal, Hydrology and Earth System Sciences, Hydrology Research, Journal of Hydrology, Water Research, and Water Resources Research (for details on the search, see Appendix 1).

The result of this search is shown in Fig. 1-1, along with some auxiliary data on the countries. For Saudi Arabia, 67 publications were found. Although this number is higher than that of many other countries, we have to keep in mind that the kingdom is one of the biggest (see above) and driest countries of the world (mean annual precipitation of 59 mm; FAO, 2019a). Both aspects should increase the chance of finding water-related publications. Moreover, the country's economic situation, here expressed via the Gross Domestic Product (GDP; 646 billion US$), should allow for extensive water research leading to corresponding publications.

In view of these facts, a total number of 67 seems relatively small. It roughly corresponds to the value of Luxembourg (65) and is much lower than the number found for the Netherlands (363), for example. Even if one restricts the comparison to arid countries, the total of 67 seems rather limited. For the smaller and less wealthy countries Jordan, Egypt, Mongolia, and Iran, for instance, 101, 104, 110, and 241 papers were found, respectively.

Of course, many arid countries are even less represented in the scientific literature (some not shown at all in Fig. 1-1, n=0) and deserve attention, but many are small and hence limited in their geo(morpho)logic diversity (e.g., Bahrain, Qatar, Kuwait), logistically difficult, and/or dangerous to work in (e.g., Iraq, Libya, Mauritania).

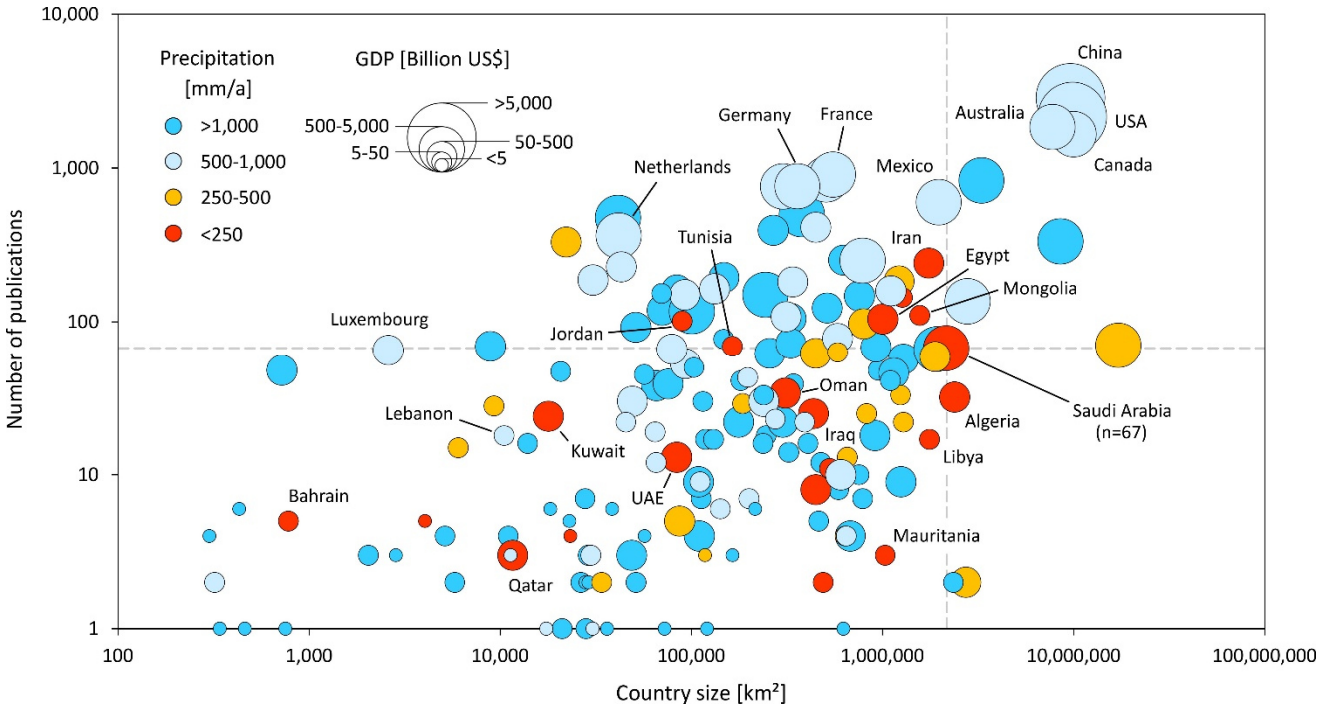

Fig. 1-1. Number of found publications per country, along with country area, precipitation, and GDP data (FAO, 2019a). Note: For several countries, no publications were found (not shown). The grey dashed lines indicate the "coordinates" of Saudi Arabia, i.e., its size (about 2,150,000 km²) and the corresponding number of publications (n=67).

Hence, Saudi Arabia's aridity, minor role in the literature, and size make it a tempting experimental site. Further, its economic wealth led to a decent infrastructure facilitating field logistics and, equally important, allowed the country to afford a history of large-scale aquifer assessments by several generations of consultants. These mostly unpublished reports represent a valuable source of information (in the present case accessible through GIZ and Dornier Consulting, see Preface), upon which further research can be built.

1.2. Background information on Saudi Arabia

The following section is not meant as a comprehensive characterization of the climatology or (hydro)geology of Saudi Arabia. It does not provide a detailed description of the development of the country's water sector either. This would be clearly beyond the scope of this introduction. One could write entire books and PhD theses about each of those topics and others have literally done so (e.g., MAW, 1984, 1988; Powers, 1966; Schulz, 2017; Vincent, 2008).

Instead, the intention behind the following paragraphs is to provide the reader with a *brief* summary of relevant aspects that are necessary to put the subsequent chapters in perspective.

1.2.1. Climate

Saudi Arabia features a hot desert climate (Köppen-Geiger class BWh) with a mean annual precipitation of 59 mm (FAO, 2019a). Higher precipitation depths (e.g., >150 mm) are mostly restricted to mountainous areas (e.g., Asir Mountains in the SW; Fig. 1-2). This also applies to neighboring countries such as Yemen (Asir Mountains) and Oman (e.g., Dhofar Mountains).

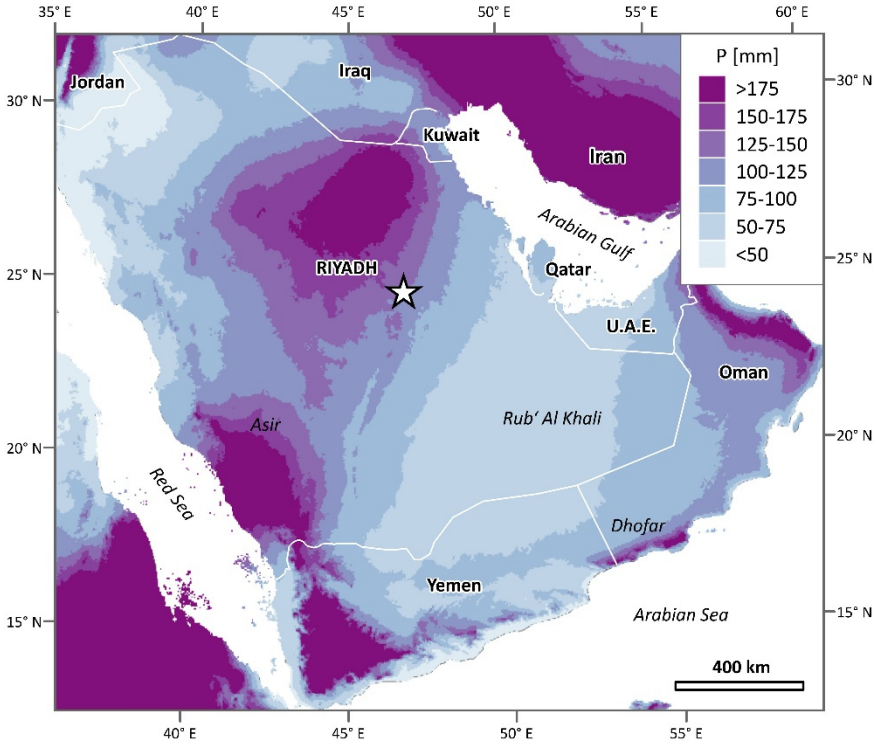

Fig. 1-2. Map showing the mean annual precipitation on the Arabian Peninsula (gridded precipitation data from Fick and Hijmans, 2017).

Given these generally low values, the term "rainy season" does not seem appropriate, but most rain events occur in the cooler months of the year, between November and May.

The small precipitation depths are accompanied by rather high temperatures. In most parts of the country, the mean annual air temperature exceeds 20°C. Lower values are largely restricted to higher elevations (e.g., Asir Mountains). The capital Riyadh, located in Central Saudi Arabia (elevation: approx. 600 m asl) and considered representative for this region, exhibits a mean annual air temperature of 26.8°C (JRCC/PME, 2016). However, higher values are not uncommon, particularly in the Rub' Al Khali Desert (meaning "Empty Quarter") in the SE of the country (Fig. 1-3). It is noteworthy that these are annual averages and individual temperature

measurements can easily yield values above 40°C in summer. For Riyadh, for instance, up to 48°C have been reported (25 July 1987; JRCC/PME, 2016).

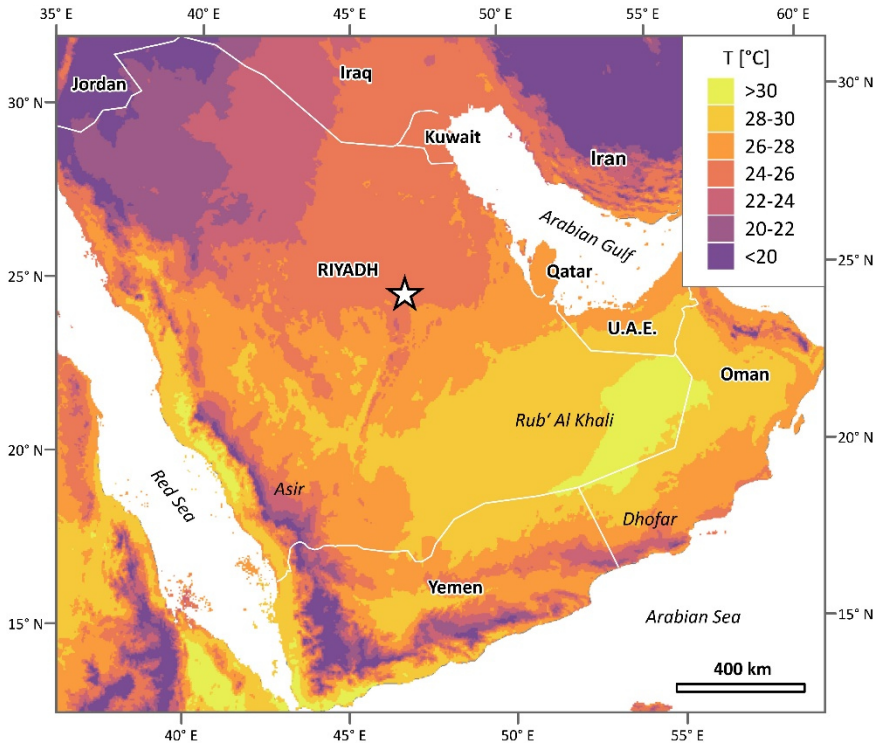

Fig. 1-3. Map showing the mean annual air temperature on the Arabian Peninsula (gridded temperature data from Fick and Hijmans, 2017).

Due to the low precipitation values and high temperatures, relative humidities are low throughout the country. The only exception are relatively narrow coastal bands along the Red Sea and the Arabian Gulf (MAW, 1988). In Riyadh, mean monthly humidity values reach 47 % in winter (December and January), drop down to about 10 % in summer (July), and average at 26 % (JRCC/PME, 2016).

The outlined climate results in pronounced potential evaporation rates. For Riyadh, measurements with evaporation pans have yielded around 100 mm/month in winter and up to about 400 mm/month in summer. The corresponding annual potential evaporation accounts for approx. 2,900 mm (Taher, 2004; see also MAW, 1984, 1988).

As a consequence, natural surface water bodies are a scarce phenomenon in Saudi Arabia. In fact, the kingdom is the world's largest country without a perennial natural river (Al-Shaibani, 2008; cf. Vincent, 2008). The only permanent stream of significant length (roughly 100 km) is the so-called Riyadh River, which largely consists of the capital's treated wastewater (since the 1980s; Mahboob et al, 2014).

To cope with the high water stress (Grassert, 2013), Saudi Arabia has developed a remarkable seawater desalination capacity (Vincent, 2008). However, the backbone of the water supply, particularly for agriculture in the interior part of the country, is still groundwater.

1.2.2. Hydrogeology

Some (renewable) groundwater can be found on the Arabian Shield in Western Saudi Arabia (dominated by Precambrian crystalline basement; Fig. 1-4), either in fractured basement rocks (mostly granitoids) or shallow alluvial aquifers (wadi aquifers; Al-Shaibani, 2008). However, the bulk of the groundwater is hosted by a set of large-scale aquifers on the Arabian Platform adjoining to the east (Fig. 1-4). The latter comprises a thick sedimentary succession with several sandstone and limestone aquifers. These include the Paleozoic Saq, Wajid, and Khuff aquifers, the Triassic Minjur aquifer, the Jurassic Dhruma and Arab aquifers, the Cretaceous Biyadh, Wasia, and Aruma aquifers, the Paleogene Umm Er Radhuma and Dammam aquifers, as well as the Neogene aquifer (for details, see MAW, 1984; Schulz, 2017).

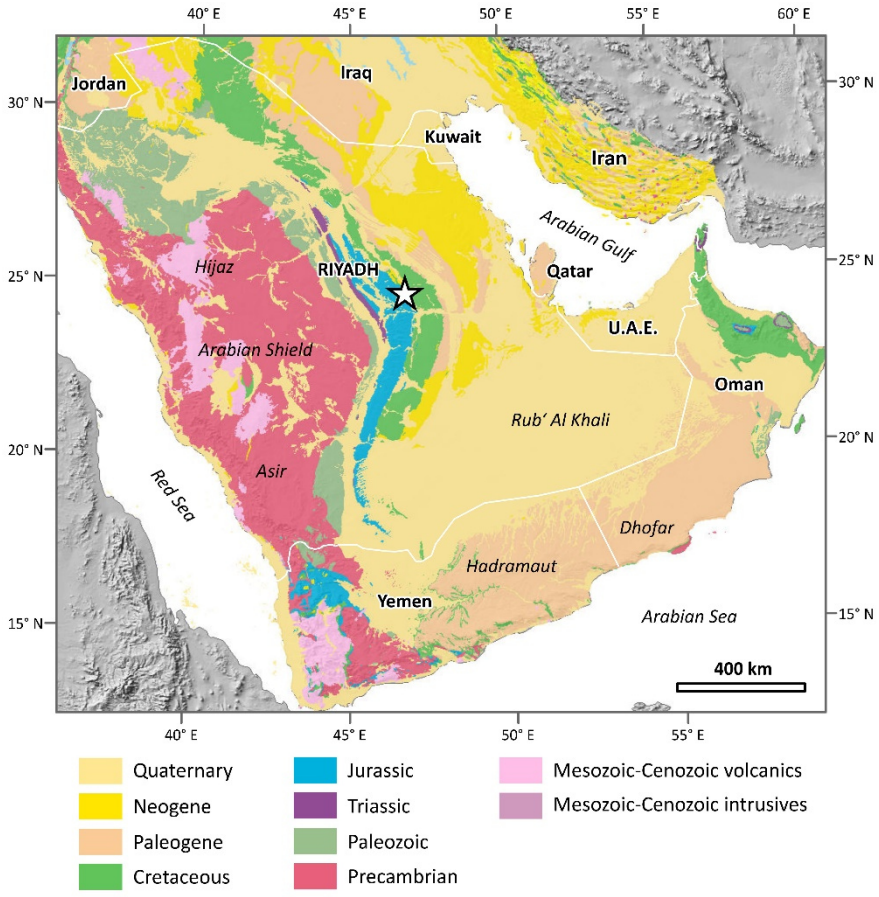

Fig. 1-4. Simplified geological map of the Arabian Peninsula (data source: USGS/ARAMCO, 1963; shaded relief from Natural Earth, 2015).

These aquifers generally have in common that they crop out in a curved band running through the country (roughly N-S) and gently dip towards the east. Hence, the overall groundwater flow direction is from the outcrop (recharge zone) towards the Arabian Gulf. Due to the dipping of the strata, areas with unconfined conditions are rather limited (restricted to the outcrops) and confined and artesian-confined conditions prevail over much of the aquifer system.

Although some groundwater recharge does occur under the currently arid climate, either naturally (e.g., Schulz et al., 2015) or anthropogenically induced (Michelsen et al., 2016, Chapter 6), the bulk of the groundwater is non-renewable or "fossil", i.e., it was recharged during wetter periods in the geological past.

That such wetter conditions did prevail in the past is evident from a number of paleoclimate archives, including petroglyphs (Bednarik, 2017; Guagnin et al., 2015), speleothems (Fleitmann et al., 2004), or lacustrine deposits (McClure, 1976; Rosenberg et al., 2011).

In Saudi Arabia, petroglyphs (also known as rock art) are usually incised into the desert varnish of sandstone outcrops or large boulders and provide a visual impression of the ancient landscape. The depicted animals (e.g., grass-dependent bovine) suggest a savanna type climate (Fig. A1-1). Occasionally, super-imposition and varying degrees of patination (i.e., regrown desert varnish) on the faunal depictions illustrate climatic transitions (Fig. A1-2). However, despite recent efforts (Bednarik, 2002; Macholdt et al., 2018), the direct dating of such depictions remains challenging.

Speleothems and lake deposits, by contrast, represent more quantitative archives. They allow for the estimation of growth/sedimentation rates and the oxygen isotope signature of their calcite ($^{18}O/^{16}O$) can serve as a paleoclimate proxy. Although these archives are datable, different techniques sometimes yielded contrasting results (Rosenberg et al., 2011). Therefore, the exact timing of humid periods in the Late Pleistocene is still under discussion. Concerning the first half of the Holocene, there is general consensus that a wetter climate prevailed, but precipitation amounts and underlying mechanisms are still debated (Enzel et al., 2015).

Although the exact nature and timing of the pluvials are still subject to discussion and groundwater residence time estimations performed by researchers (Sultan et al., 2019; Thatcher et al., 1961) and consultants (e.g., own reports: GIZ/DCo, 2014, 2016, 2017; GTZ/DCo, 2010) are associated with great uncertainties, the mostly fossil character of the groundwater is generally accepted.

1.2.3. Development of the water sector

Historically, i.e., in pre-development times, groundwater use was rather limited. People abstracted water from shallow dug wells, often with the help of animals (Fig. 1-5a), or relied on natural springs (Fig. 1-5b). Where possible, the inhabitants of the region also built qanat systems to tap and distribute groundwater or lake water for irrigation (Al-Bassam and Zaidi, 2016; Kempe and Dirks, 2008; Fig. 1-5c). While shallow groundwater (e.g., in

wadi aquifers) or water exposed in lakes and sinkholes were obvious and easily accessible water sources, it is noteworthy that people were also aware of submarine springs. The latter were tapped in Eastern Saudi Arabia and Bahrain (Rausch et al., 2014; Fig. 1-5d and 1-5e).

Fig. 1-5. Photographs illustrating pre-development water use. a) Dug well with camel lifting water-filled animal skin bags (MAW, 1984), b) Natural spring in the Al Hassa Oasis (300 km ENE of Riyadh, 1937; Facey, 2000), c) Ancient qanat shafts near the Layla Lakes (280 km S of Riyadh), d) and e) Collection of freshwater from a submarine spring near Bahrain with an animal skin bag (1924; ETH, 2019).

Given the small population at that time (at most a few million people instead of the current 33.7 million; FAO, 2019b) and the small demand due to a very limited agricultural sector (Twitchell, 1958), the groundwater use was probably quasi-sustainable (see Al-Bassam and Zaidi, 2016).

To some extent, the rather basic abstraction techniques played a role in this regard as well – although westerners occasionally tried to propagate the use of modern pumps. Harry St. John Bridger Philby, one of the early western travelers on the Arabian Peninsula, visited the Layla Lakes area in 1918 and stated the following in a conversation with a local ruler:

> *"I have seen desert countries brought under cultivation by irrigation and I cannot think that, with the water at your command, we should leave your deserts uncultivated, when with proper machinery and great pumps we could flood them from your great reservoirs."* (Philby, 1922)

The suggested flooding of the desert by means of modern pumps indeed happened, albeit much later (Layla Lakes pump: 1950; Twitchell, 1958), in the course of an agricultural development scheme targeting various parts of the kingdom.

This evolution was largely triggered by the discovery of commercial quantities of oil in 1938. The newly available funds enabled the kingdom to foster its general progress and groundwater abstractions increased dramatically. While also the urban development, the expansion of the road network (Alam, 1989), and the petroleum sector itself required substantial amounts of water (see Schulz et al., 2017), the efforts to boost the agricultural sector had the greatest effects on Saudi Arabia's water resources (Rausch et al., 2014).

Aiming at food security for Saudi citizens, the government set up a program comprising a set of measures to increase agricultural production. This included the i) distribution of land to wheat producers free of charge, ii) provision of grants, subsidies, and free-interest loans, iii) support of modern production techniques, and iv) purchase of crops at prices exceeding world market prices (Al-Hamoudi et al., 1997).

While data on water abstraction rates are scarce and difficult to obtain (Engelhardt et al., 2013), the resulting economic and agricultural development can be conveniently traced utilizing publicly available data (Fig. 1-6).

The general progress is reflected by the nearly constant population growth and the increase in GDP (Fig. 1-6a). The generated petrodollars were used for the above-mentioned subsidies, which in turn triggered a remarkable expansion of agricultural area equipped for irrigation with groundwater (Fig. 1-6b). From the end of the 1970s to 1990, this area roughly increased by a factor of four. This development is mirrored by the wheat production, which skyrocketed from about 0.14 Million tons in 1980 to around 4.12 Million tons in 1992 (Fig. 1-6c). It is also noteworthy that the production of wheat exceeded that of dates. The latter have been the traditional crop of the region, mostly because of the date palm's adaption to the local climate, sandy soils, and water salinities. Wheat self-sufficiency was achieved in 1984 and the surplus was exported, often donated, to less wealthy Arabian and Islamic neighbors (Fig. 1-6d). After the 1991 Gulf War, the Saudis had to review their agriculture policies and subsidies were reduced, leading to a drop in wheat production (Al-Hamoudi et al., 1997; Fig. 1-6c). To reduce the wheat-related water consumption, the country strongly increased its corresponding imports in recent years (Fig. 1-6d).

The agricultural revolution did not remain without consequences. In several areas, groundwater levels dropped significantly and large cones of depression formed. Prominent examples are the Wadi Ad Dawasir area (500 km SW of Riyadh; Al Saud and Rausch, 2012), the area around Kharj (approx. 80 km S of Riyadh; Schulz et al., 2017),

or the Al Hassa Oasis (300 km ENE of Riyadh; Engelhardt et al., 2013). Corresponding drawdowns partly exceeded 100 m (Al Saud and Rausch, 2012).

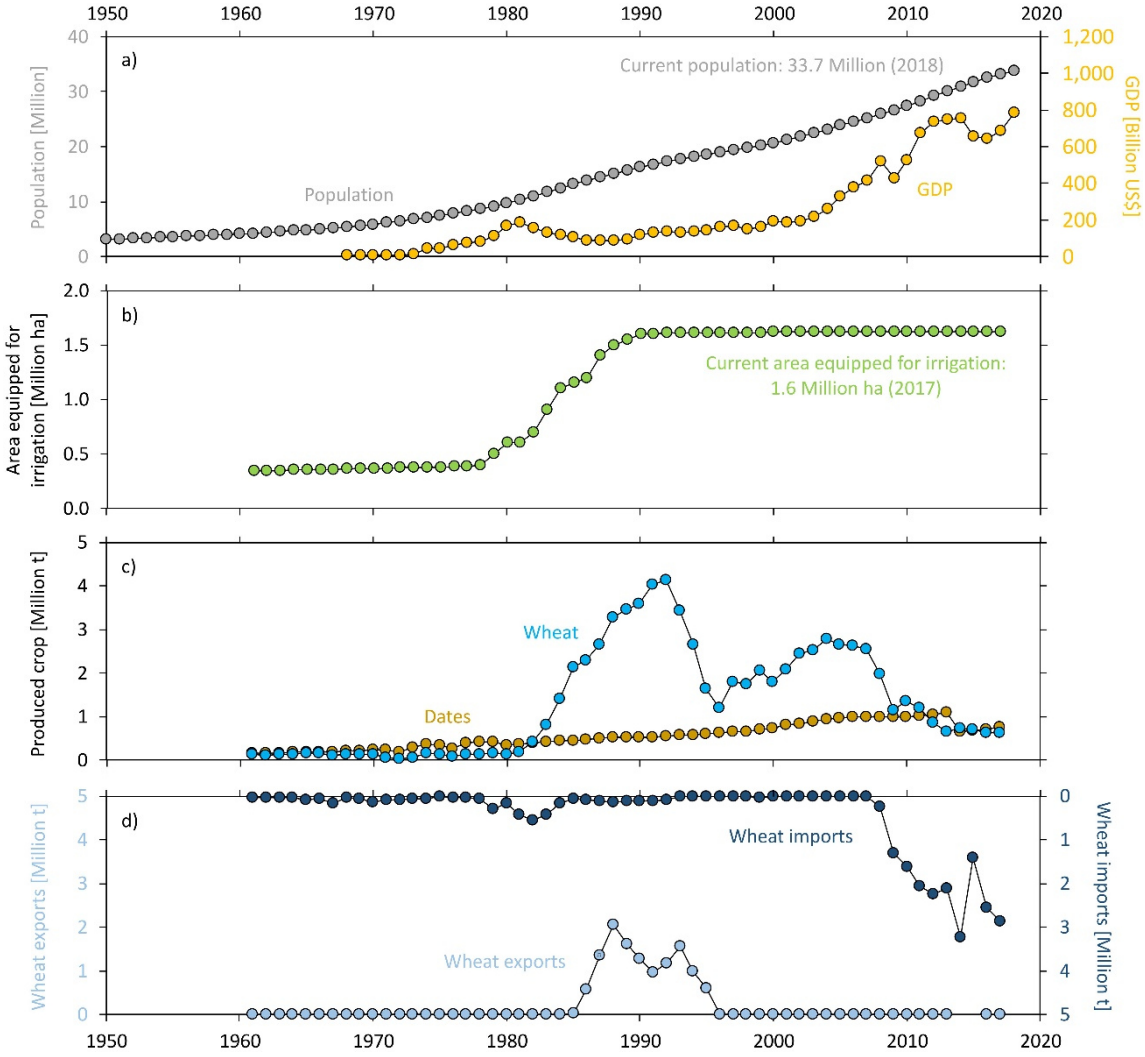

Fig. 1-6. FAO and World Bank data reflecting Saudi Arabia's development. a) Population and economic growth (FAO, 2019b; World Bank, 2019), b) Increase of the agricultural area equipped for irrigation, c) Development of the date and wheat production, d) Development of wheat exports and imports (FAO, 2019b).

Occasionally, the water level drop was also readily apparent at the surface – at locations where water had previously been easily accessible. Onshore and offshore springs in the Eastern Province stopped discharging (Engelhardt et al., 2013; Rausch et al., 2014) and several sinkholes, previously filled with water, fell dry. Prominent examples for the latter phenomenon are the Kharj pools (Fig. 1-7) or the Layla Lakes (Fig. 1-8).

Ancient tumuli suggest a long history of use of the Kharj pools (Fig. 1-7a) and the side walls of the sinkhole still show traces of the pre-development water level. The installation of large pumps led to a remarkable lowering of the water table over the decades (Fig. 1-7b, 1-7c, 1-7d) and nowadays the sinkholes are dry. The Layla Lakes have experienced a similar development. While they had been a popular recreation spot until the 1980s (Fig. 1-

8a, 1-8b), the “proper machinery and great pumps” that Philby had called for in 1918 (see above) had completed their task in the 1990s when the lakes disappeared (Fig. 1-8c, 1-8d).

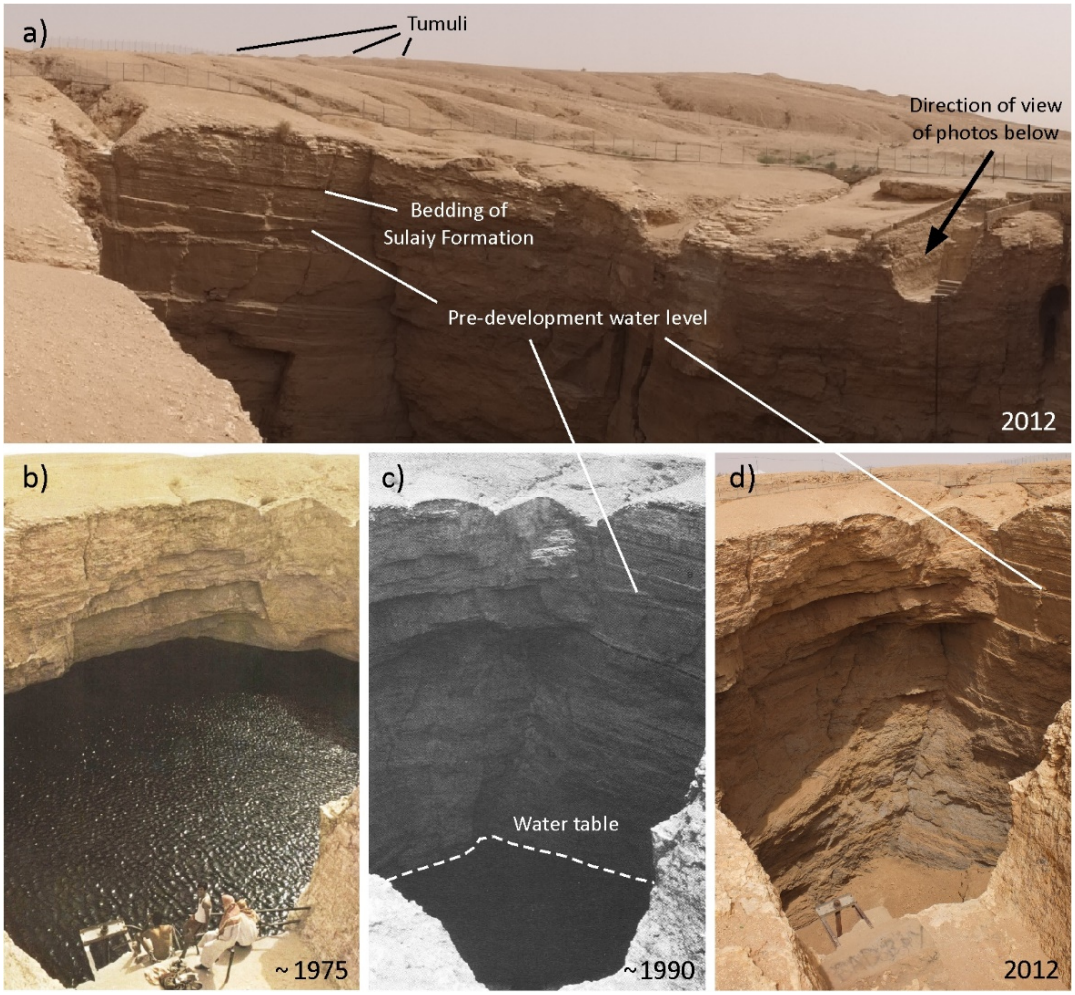

Fig. 1-7. Historic and recent photos of the Ayn Ad Dilh sinkhole, one of the so-called Kharj pools (approx. 80 km SE of Riyadh; 24°6’45’’N 47°15’30’’E). a) Recent overview picture showing traces of the historic water level (not to be confused with the bedding of the Cretaceous Sulaiy formation). Note the water level drop (tens of meters) over the decades: b) mid 1970s (ARAMCO, 1975), c) around 1990 (Vaslet et al., 1991), and d) recent photo from 2012 (own photo of empty sinkhole).

The outlined developments were triggered and/or assessed by multiple generations of consultants from various countries. While initial studies had a rather broad scope and, for instance, included extensive soil surveys to evaluate agricultural potentials, later studies mostly focused on the groundwater itself, particularly deep groundwater, being the kingdom’s main water resource. In any case, the studies were comprehensive and utilized an array of state of the art techniques, including methods from the isotope hydrology toolbox.

Fig. 1-8. Historic and recent photos of the Layla Lakes (280 km S of Riyadh; 22°10'3''N, 46°42'29''E). In the 1970s and 1980s, the lakes were a popular recreation spot among locals and expats, e.g., for a) swimming (photo: Chip Lambert) and b) water skiing (photo: Chris Wheatley). c) In the 1990s, the lakes fell dry and a newly built hotel (background) never went into operation (Kempe and Dirks, 2008). d) A platform and steel pipes belonging to the pumping station are still visible today.

1.2.4. Open questions: isotopes and beyond

Although Kumar and Hadi (2018) recently used the term "futuristic" in the context of isotope applications on the Arabian Peninsula, these methods actually have a long tradition in water studies in this region. In their pioneer work, Thatcher et al. (1961) determined groundwater residence times with the radioactive age tracers ^{3}H (tritium; applicable to young waters, <70 a; see Chapter 2.2.) and ^{14}C (radiocarbon; applicable to older waters, <30,000 a), and reported on the fossil character of Saudi groundwaters (see Chapter 1.2.2.). Such studies were often complemented with stable isotope investigations addressing the isotope ratios $^{18}O/^{16}O$ and $^{2}H/^{1}H$ of the water molecule. These isotope ratios are usually expressed using the delta notation:

$$\delta = (R_{sample}/R_{reference} - 1) \qquad (1\text{-}1)$$

where R is the ratio of the numbers (n) of the heavy and light isotope of an element (e.g., $n(^{18}O)/n(^{16}O)$) in the sample and the reference. The conventionally used standard is Vienna Standard Mean Ocean Water (V-SMOW). The results are then reported in per mil (‰). Negative values mean that the sample is isotopically lighter than the standard ("depleted"). In turn, positive values indicate isotopically heavier water ("enriched").

Due to their stable character and the fact that these isotopes are part of the water molecule itself, they represent conservative and hence nearly ideal tracers with significant fingerprinting potential. The characteristic signature is imprinted during the atmospheric history of the water. Here, it can be subject to a range of isotope effects, including the continental effect, the altitude effect, or the amount effect (Clark and Fritz, 1997; and references therein).

Although stable isotopes are a versatile tool with which one can tackle a range of aspects (e.g., recharge altitudes, cross-formational flow, etc.), the main application in arid areas is to identify paleowaters (e.g., Gat, 1971), i.e., fossil waters that were replenished under wetter and/or cooler climatic conditions in the geological past (see Chapter 1.2.2.). Commonly, such waters are isotopically lighter than current precipitation.

In Saudi Arabia, this method has been extensively used by researchers (Sultan et al., 2008, 2019) and consultants (e.g., own reports: GIZ/DCo, 2014, 2016, 2017; GTZ/DCo, 2010). Yet, the bulk of the performed analyses targeted groundwater only. Over the decades, probably a few thousand Saudi Arabian groundwater samples have been subject to stable isotope analyses. However, data on the isotopic composition of rainfall in the region are surprisingly scarce – although they are urgently needed for comparison purposes. Hence, this topic is addressed in the present thesis (Fig. 1-9; Chapter 2).

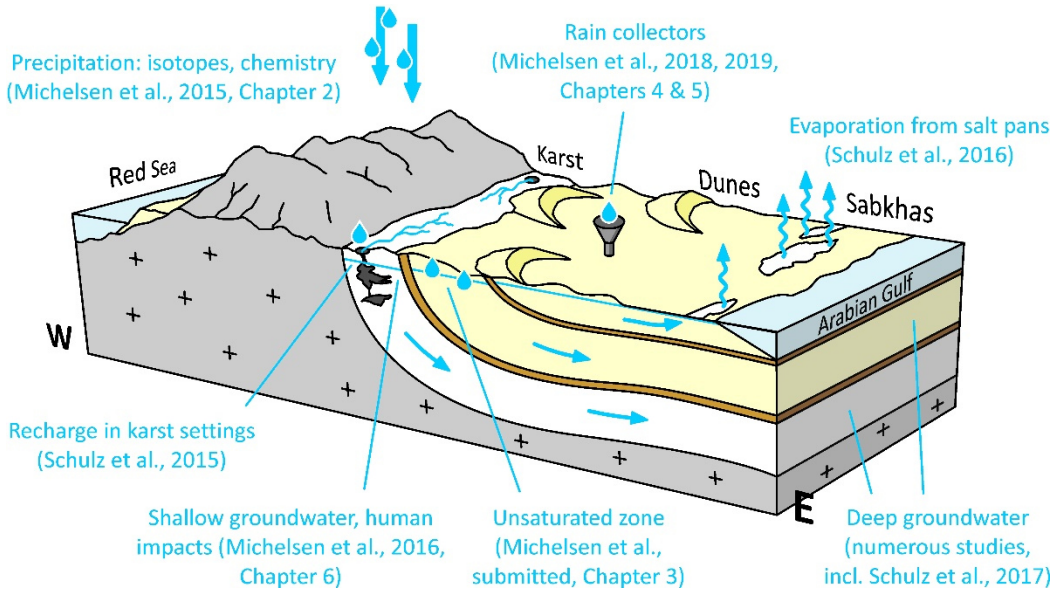

Fig. 1-9. Schematic block diagram summarizing gaps in knowledge and the corresponding first-author ISI publications (Michelsen et al., 2015, 2016, 2018, 2019) and selected co-author ISI publications (Schulz et al., 2015, 2016, 2017).

The subsequent elements of the local water cycle, i.e., the unsaturated zone and shallow groundwater, are underrepresented in the literature as well – most previous studies had focused on deep groundwater (see Chapter 1.2.3.). These issues are tackled in the Chapters 3 and 6. It is noteworthy that the latter chapter also

touches upon the aspect of human interactions with the water cycle and deals with a somewhat untypical case – anthropogenically induced water level *rise*.

These Saudi Arabia-focused investigations are complemented by two studies having a more methodological character. They deal with rain collectors for isotope research and are presented in the Chapters 4 and 5.

Fig. 1-9 gives a graphical overview of all relevant topics addressed in this thesis. It also includes selected co-author studies that were carried out in parallel and have complementary character. Yet, they are not part of this thesis (see Preface).

1.3. References

Alam, M., 1989. Water Resources of the Middle East and North Africa with Particular Reference to Deep Artesian Ground Water Resources of the Area. Water International 14, 122–127.

Al-Bassam, A.M., Zaidi, F.K., 2016. Aqueducts in Saudi Arabia. In: Angelakis, A.N., Chiotis, E., Eslamian, S., Weingartner, H. 8eds.). Underground Aqueducts Handbook. CRC Press, 211–228.

Al-Hamoudi, K.A., Sherif, S.A., Sofian, B.E., 1997. Wheat production in Saudi Arabia between feasibility and efficiency. Agricultural Economics 16, 35–45.

Al Saud, M., Rausch, R., 2012. Integrated Groundwater Management in the Kingdom of Saudi Arabia. In: Rausch, R., Schüth, C., Himmelsbach, T. (eds.). Hydrogeology of Arid Environments. Borntraeger, 1–6.

Al-Shaibani, A.M., 2008. Hydrogeology and hydrochemistry of a shallow alluvial aquifer, western Saudi Arabia. Hydrogeology Journal 16, 155–165.

ARAMCO – Arabian American Oil Company, 1975. The Historic Heartland. ARAMCO World magazine 26(1), 14–25.

Bednarik, R.G., 2002. The Dating of Rock Art: a Critique. Journal of Archaeological Science 29, 1213–1233.

Bednarik, R.G., 2017. Scientific investigations into Saudi Arabian Rock Art: A review. Mediterranean Archaeology and Archaeometry 17(4), 43–59.

Blume, T., van Meerveld, I., Weiler, M., 2017. The role of experimental work in hydrological sciences – insights from a community survey. Hydrological Sciences Journal 62(3), 334–337.

Clark, I.D., Fritz, P., 1997. Environmental Isotopes in Hydrogeology. Lewis Publishers, Boca Raton/New York.

Engelhardt, I., Rausch, R., Keim, B., Al-Saud, M., Schüth, C., 2013. Surface and subsurface conceptual model of an arid environment with respect to mid- and late Holocene climate changes. Environmental Earth Sciences 69, 537–555.

Enzel, Y., Kushnir, Y., Quade, J., 2015. The middle Holocene climatic records from Arabia: Reassessing lacustrine environments, shift of ITCZ in Arabian Sea, and impacts of the southwest Indian and African monsoons. Global and Planetary Change 129, 69–91.

ETH – Eidgenössische Technische Hochschule Zürich, 2019. Bildarchiv der ETH-Bibliothek Zürich. Photo album: Arabien, 1924 (photographer: Arnold Heim). http://doi.org/10.3932/ethz-a-000052764, http://doi.org/10.3932/ethz-a-000052766

Facey, W., 2000. The Story of the Eastern Province of Saudi Arabia. Stacey International, London.

FAO – Food and Agriculture Organization of the United Nations, 2019a. http://www.fao.org/aquastat/en/ (last access: 24 November 2019).

FAO – Food and Agriculture Organization of the United Nations, 2019b. http://www.fao.org/faostat/en/#home (last access: 17 December 2019).

Fick, S.E., Hijmans, R.J., 2017. WorldClim 2: new 1-km spatial resolution climate surfaces for global land areas. International Journal of Climatology 37, 4302–4315.

Fleitmann, D., Matter, A., Pint, J.J., Al-Shanti, M.A., 2004. The speleothem record of climate change in Saudi Arabia. Open-File Report SGS-OF-2004-8, Saudi Geological Survey, Jeddah.

GIZ/DCo – Gesellschaft für Internationale Zusammenarbeit/Dornier Consulting, 2014. Detailed Water Resources Studies of Wasia-Biyadh and Aruma Aquifers, Volume 12 – Environmental Isotopes. Ministry of Water & Electricity, Riyadh.

GIZ/DCo – Gesellschaft für Internationale Zusammenarbeit/Dornier Consulting, 2016. Detailed Water Resources Studies of Khuff, Jilh, Minjur, Dhruma and Overlying Aquifers, Volume 12 – Environmental Isotopes. Ministry of Water & Electricity, Riyadh.

GIZ/DCo – Gesellschaft für Internationale Zusammenarbeit/Dornier Consulting, 2017. Detailed Groundwater Resources Studies in the Rub' Al Khali Desert, Volume 10 – Environmental Isotopes. Ministry of Environment, Water & Agriculture, Riyadh.

GTZ/DCo – Gesellschaft für Technische Zusammenarbeit/Dornier Consulting, 2010. Detailed Water Resources Studies of Wajid and Overlying Aquifers, Volume 12 – Environmental Isotopes. Ministry of Water & Electricity, Riyadh.

Guagnin, M., Jennings, R.P., Clark-Balzan, L., Groucutt, H.S., Parton, P., Petraglia, M.D., 2015. Hunters and herders: Exploring the Neolithic transition in the rock art of Shuwaymis, Saudi Arabia. Archaeological Research in Asia 4, 3–16.

Grassert, F., Reig, P., Luo, T, Maddocks, A., 2013. Aqueduct Country and River Basin Rankings – A Weighted Aggregation of Spatially Distinct Hydrological Indicators. World Resources Institute, Washington, D.C.

JRCC/PME – Jeddah Regional Climate Center South West Asia/Presidency of Meteorology and Environment, 2016. Climate Data for Saudi Arabia. Surface Annual Climatological Report for station Riyadh Old (1985–2010).

Kempe, S., Dirks, H., 2008. Layla Lakes, Saudi Arabia: The world-wide largest lacustrine gypsum tufas. Acta Carsologica 37(1), 7–14.

Kumar, U.S., Hadi, K., 2018. Futuristic isotope hydrology in the Gulf region. Applied Water Science 8, 25.

Macholdt, D.S., Al-Amri, A.M., Tuffaha, H.T., Jochum, K.P., Andreae, M.O., 2018. Growth of desert varnish on petroglyphs from Jubbah and Shuwaymis, Ha'il region, Saudi Arabia. The Holocene 28(9), 1495–1511.

Mahboob, S., Alkkahem Al-Balwai, H.F., Al-Misned, F., Al-Ghanim, K.A., Ahmad, Z., 2014. A study on the accumulation of nine heavy metals in some important fish species from a natural reservoir in Riyadh, Saudi Arabia. Toxicological & Environmental Chemistry 96(5), 783–798.

MAW – Ministry of Agriculture and Water, 1984. Water Atlas of Saudi Arabia. MAW, Riyadh.

MAW – Ministry of Agriculture and Water, 1988. Climate Atlas of Saudi Arabia. MAW, Riyadh.

Michelsen, N., Dirks, H., Schulz, S., Kempe, S., Al-Saud, M., Schüth, C., 2016. YouTube as a crowd-generated water level archive. Science of the Total Environment 568, 189–195.

Michelsen, N., Laube, G., Friesen, J., Weise, S.M., Bait Said, A.B.A., Müller, T., 2019. Technical note: A microcontroller-based automatic rain sampler for stable isotope studies. Hydrology and Earth System Sciences 23(6), 2637–2645.

Michelsen, N., Reshid, M., Siebert, C., Schulz, S., Knöller, K., Weise, S.M., Rausch, R., Al-Saud, M., Schüth, C., 2015. Isotopic and chemical composition of precipitation in Riyadh, Saudi Arabia. Chemical Geology 413, 51–62.

Michelsen, N., van Geldern, R., Roßmann, Y., Bauer, I., Schulz, S., Barth, J.A.C., Schüth, C., 2018. Comparison of cumulative precipitation collectors used in isotope hydrology. Chemical Geology 488, 171–179.

Natural Earth, 2015. http://www.naturalearthdata.com (last access: 23 June 2015).

Philby, H.St.J.B., 1922. The Heart of Arabia. Constable and Company, London.

Powers, R.W., Ramirez, L.F., Redmond, C.D., Elberg, E.L., 1966. Geology of the Arabian Peninsula – Sedimentary Geology of Saudi Arabia. USGS, Washington D.C.

Rausch, R., Dirks, H., Kallioras, A., Schüth, C., 2014. The riddle of the springs of Dilmun – does the Gilgamesh Epic tell the truth? Groundwater 52(4), 640–644.

Schulz, S., 2017. Experimental and numerical studies on the water balance of the Upper Mega Aquifer system, Arabian Peninsula. Dissertation, Technische Universität Darmstadt.

Schulz, S., Horovitz, M., Rausch, R., Michelsen, N., Mallast, U., Köhne, M., Siebert, C., Schüth, C., Al-Saud, M., Merz, R., 2015. Groundwater evaporation from salt pans: Examples from the eastern Arabian Peninsula. Journal of Hydrology 531, 792–801.

Schulz, S., de Rooij, G. H., Michelsen, N., Rausch, R., Siebert, C., Schüth, C., Al-Saud, M., Merz, R., 2016. Estimating groundwater recharge for an arid karst system using a combined approach of time-lapse camera monitoring and water balance modelling. Hydrological Processes 30, 771–782.

Schulz, S., Walther, M., Michelsen, N., Rausch, R., Dirks, H., Al-Saud, M., Merz, R., Kolditz, O., Schüth, C., 2017. Improving large-scale groundwater models by considering fossil gradients. Advances in Water Resources 103, 32–43.

Sultan, M., Sturchio, N.C., Alsefry, S., Emil, M.K., Ahmed, M., Abdelmohsen, K., AbuAbdullah, M.M., Yan, E., Save, H., Alharbi, T., Othman, A., Chouinard, K., 2019. Assessment of age, origin, and sustainability of fossil aquifers: A geochemical and remote sensing-based approach. Journal of Hydrology 576, 325–341.

Sultan, M., Sturchio, N., Al Sefry, S., Milewski, A., Becker, R., Nasr, I., Sagintayev, Z., 2008. Geochemical, isotopic, and remote sensing constraints on the origin and evolution of the Rub Al Khali aquifer system, Arabian Peninsula. Journal of Hydrology 356, 70–83.

Taher, S.A., 2004. Estimation of Potential Evaporation: Artificial Neural Networks Versus Conventional Methods. Journal of King Saud University 17(1), 1–14.

Thatcher, L., Rubin, M., Brown, G.F., 1961. Dating Desert Ground Water. Science 134, 105–106.

Twitchell, K.S., 1958. Saudi Arabia. 3rd edition, Princeton University Press, Princeton.

USGS/ARAMCO – United States Geological Survey/Arabian American Oil Company, 1963. Geologic Map of the Arabian Peninsula. Miscellaneous Geologic Investigations, Map I-270 A, scale 1:2,000,000. USGS, Washington D.C.

Vaslet, D., Al-Muallem, M.S., Maddah, S.S., Brosse, J.M., Fourniguet, J., Breton, J.P., Le Nindre, Y.M., 1991. Explanatory Notes to the Geologic Map of the Ar Riyad Quadrangle, Sheet 24I, Kingdom of Saudi Arabia. Ministry of Petroleum and Mineral Resource, Jiddah.

Vincent, P., 2008. Saudi Arabia: An Environmental Overview. Taylor & Francis, London.

World Bank, 2019. https://data.worldbank.org/ (last access: 17 December 2019).

Preface to Chapter 2

As mentioned above, only a few analyses of the isotopic composition of rainfall are available for Saudi Arabia. The primary repository for such data is the Global Network of Isotopes in Precipitation (GNIP) that is coordinated by the International Atomic Energy Agency and the World Meteorological Organization (GNIP; IAEA/WMO, 2019). When it comes to monthly data, the most common data type in GNIP, the repository lists only a single station for Saudi Arabia (Jeddah, located on the Red Sea coast), with three $\delta^{18}O$ values, one $\delta^{2}H$ value, and two ^{3}H values. These numbers *per se* are low, but, frankly, they become frustrating in an international context (Fig. 1-10).

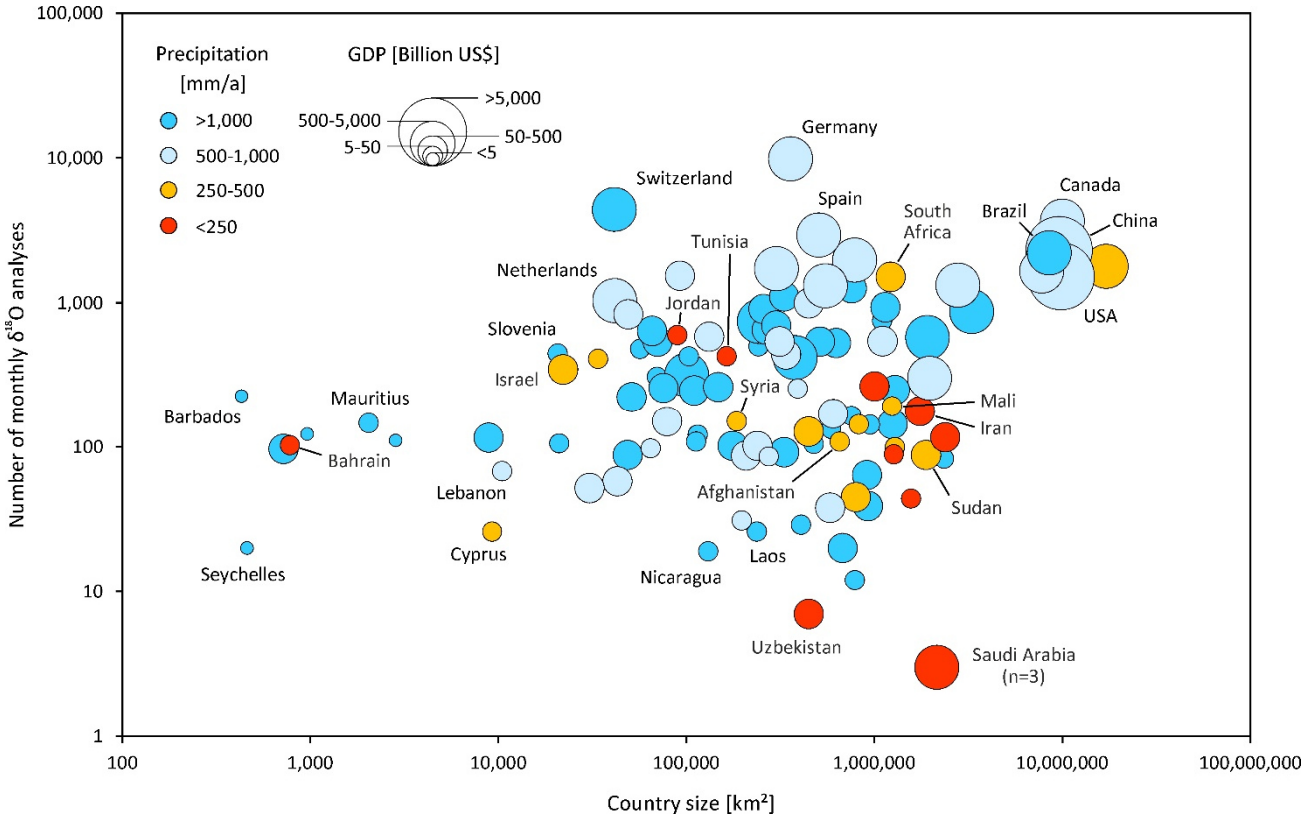

Fig. 1-10. Number of monthly $\delta^{18}O$ analyses per country in the GNIP database (IAEA/WMO, 2019). Note: Numerous countries are not represented in GNIP and are hence not shown. Several countries run national monitoring networks and do not report (all) their data to GNIP. Country area, precipitation, and GDP data were acquired from the Aquastat database (FAO, 2019a).

The plot presents an analysis of the GNIP database on a country basis ($\delta^{18}O$ analyses per country), but also considers some auxiliary data, similar to Fig. 1-1. Due to Saudi Arabia's large size (see Chapter 1) and the small number of $\delta^{18}O$ analyses, the corresponding data point has a unique position within the plot. Further, it stands out due to its large bubble size (relatively high GDP) and its color (low precipitation).

Given this combination of area, wealth, and water scarcity, one would actually expect more data on precipitation, potentially serving as a valuable reference for analyses of groundwaters or pore waters in the

unsaturated zone. In fact, for many smaller and less-wealthy countries more analyses are available in the GNIP database (e.g., Mali, Sudan).

Since the lack of adequate data for Saudi Arabia constitutes a clear gap in knowledge, we tackle this issue in the following chapter. Because data on the chemical composition of rain in the country are limited as well, corresponding analyses were also included in this study.

References

FAO – Food and Agriculture Organization of the United Nations, 2019. http://www.fao.org/aquastat/en/ (last access: 24 November 2019).

IAEA/WMO – International Atomic Energy Agency/World Meteorological Organization, 2019. Global Network of Isotopes in Precipitation. The GNIP Database. http://www.iaea.org/water (last access: 20 November 2019).

2. Isotopic and chemical composition of precipitation in Riyadh, Saudi Arabia

Nils Michelsen [a,*], Mustefa Reshid [a], Christian Siebert [b], Stephan Schulz [b], Kay Knöller [b], Stephan M. Weise [b], Randolf Rausch [c], Mohammed Al-Saud [d], Christoph Schüth [a]

[a] Technische Universität Darmstadt, Institute of Applied Geosciences, Schnittspahnstraße 9, 64287 Darmstadt, Germany

[b] UFZ – Helmholtz Centre for Environmental Research, Theodor-Lieser-Straße 4, 06120 Halle, Germany

[c] Gesellschaft für Internationale Zusammenarbeit International Services, P.O. Box 2730, Riyadh 11461, Saudi Arabia

[d] Ministry of Water & Electricity, Saud Mall Center, King Fahd Road, Riyadh 11233, Saudi Arabia

* Corresponding author (michelsen@geo.tu-darmstadt.de)

Published in Chemical Geology, 2015, Vol. 413, 51–62, DOI: 10.1016/j.chemgeo.2015.08.001

2.1. Abstract

Only limited data on the isotopic and chemical composition of Riyadh rain are currently available. In this study, we complement these data by analyzing integral samples covering 28 precipitation events between 2009 and 2013. Results of stable isotope analyses are used to establish a Local Meteoric Water Line: $\delta^2H = 5.22(\pm0.38) \cdot \delta^{18}O + 14.8(\pm0.9)$ ‰. Moisture source-related isotopic fingerprints are masked by the continental effect, the altitude effect, sub-cloud evaporation, and moisture recycling. The study of one event for intra-storm variability revealed strong isotopic depletion due to rainout and Rayleigh distillation processes, thus highlighting the general need for integral samples. Tritium analyses of grab samples from 12 events yielded concentrations between 2.8 and 6.4 tritium units (TU), which are close to the natural background of a few TU. Major ion concentrations and ratios indicate that solutes are predominantly derived from atmospheric dust originating from limestone outcrops and sabkha deposits. The latter play a role with respect to the elevated Cl^- and Na^+ contents, but are probably also responsible for the SO_4^{2-} and a part of the Ca^{2+} found in Riyadh rain. Observed intra- and inter-storm variabilities of major ion levels necessitate the collection of integral samples and the calculation of precipitation-weighted means, respectively.

The obtained isotopic signatures and the precipitation-weighted mean Cl^- concentration (9.5 mg L^{-1}) may be useful in groundwater assessments, e.g., for the identification of modern recharge and quantification thereof by means of the Chloride Mass Balance method.

2.2. Introduction

For arid countries like Saudi Arabia, a thorough groundwater resources assessment is crucial to enable sound water management. In such studies, the stable water isotopes oxygen-18 (^{18}O) and deuterium (^{2}H) provide a powerful tool to investigate the provenance of groundwaters and the (paleo)climatic conditions during their replenishment. However, to evaluate the isotopic signature of groundwater, that of current precipitation must also be known (Gat, 1971; Wagner and Geyh, 1999).

Usually, such data are retrieved from the closest monitoring station of the Global Network of Isotopes in Precipitation (GNIP, IAEA/WMO, 2015) database. Although the database lists six stations for Saudi Arabia, none of them provides a significant amount of $\delta^{18}O$ and $\delta^{2}H$ analyses (1–13 analyses per station). Even if the entire Arabian Peninsula is considered, the list of stations with a significant data set (i.e., >20 analyses) is rather limited (Fig. 2-1): Bahrain (Bahrain), Salalah (Oman), and Qairoon Hairiti (Oman).

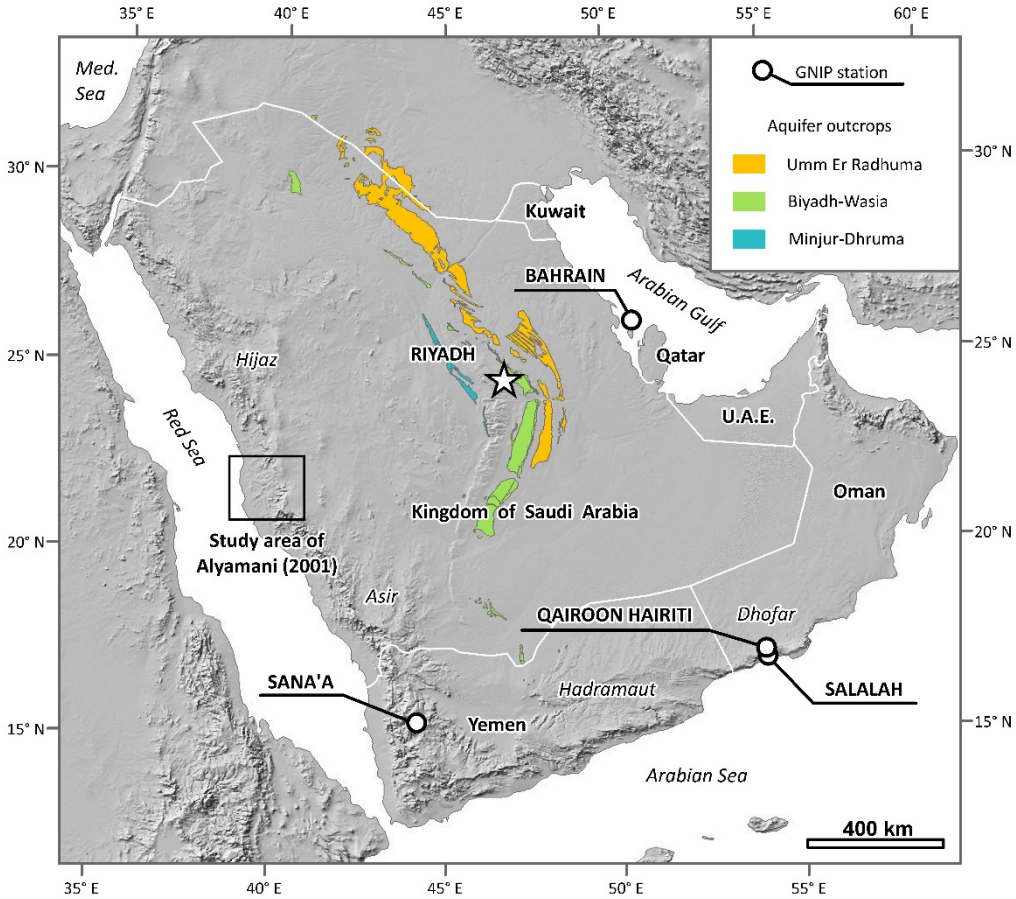

Fig. 2-1. Map showing the countries of the Arabian Peninsula and the available GNIP stations with more than 20 analyses of $\delta^{18}O$ and $\delta^{2}H$ in precipitation (shaded relief from Natural Earth, 2015). Moreover, the map includes the study area of Alyamani (2001, see text) and the outcrops of some major aquifers of Saudi Arabia (MAW, 1984; Powers et al., 1966; USGS/ARAMCO, 1963).

Another source for such isotope data is scientific articles. In this respect, the study by Alyamani (2001) is noteworthy. The author reports isotope analyses for 51 rain samples collected at eight locations in Western Saudi Arabia (4–10 analyses per location; see Fig. 2-1 for study area). Yet, robust isotope data are not available for vast parts of the country. This includes central Saudi Arabia, where some of the major aquifer systems of the Arabian Peninsula have their outcrops, i.e., recharge areas (Fig. 2-1; MAW, 1984; Powers et al., 1966; USGS/ARAMCO, 1963). The isotopic data sets reported for the above-mentioned GNIP stations cannot be expected to be representative for central Saudi Arabia, e.g., because of the continental effect (e.g., −0.3‰/100 km for $\delta^{18}O$ in the Sahara, Sonntag et al., 1976). Also the altitude effect causes significant isotopic shifts (-0.08‰/100 m for $\delta^{18}O$ in W Saudi Arabia, Alyamani, 2001; -0.15‰/100 m for $\delta^{18}O$ in N Oman, Weyhenmeyer et al., 2002).

Due to a lack of isotope data, a Local Meteoric Water Line (LMWL) has never been established for this region (Alsaaran, 2006; Job et al., 1978). Hence, researchers studying groundwater or the unsaturated zone had to seek alternative data sources for precipitation-related data needed for comparison. Some used the Global Meteoric Water Line (GMWL, $\delta^{2}H = 8 \cdot \delta^{18}O + 10‰$; Craig, 1961) as a workaround (Al-Harbi et al., 2008; Bazuhair et al., 1994; Shampine et al., 1979; Subyani, 2004). Others utilized data from the Bahrain GNIP station (BRGM, 1981a; Dincer et al., 1974; Job et al., 1978), despite the distance (Bahrain–Riyadh: 420 km) and difference in elevation (600 m). A few also collected their own, event-based samples – particularly consulting companies working for the Ministry of Agriculture and Water (now Ministry of Water & Electricity): BRGM (1976, n=7), BRGM (1977, n=10), GDC (1980, n=2). While it is common practice to collect samples on a monthly basis (IAEA/WMO, 2015), event samples are occasionally advocated. Crawford et al. (2013) emphasize the opportunity to study the relationships between isotopes in precipitation and synoptic scale weather systems, e.g., by identifying moisture sources of individual events using back-trajectory analysis (compare Leguy et al., 1983). Nevertheless, the quantity of available event-based data is not sufficient to calculate a LMWL, making additional analyses necessary.

Apart from ^{2}H and ^{18}O, hydrogeologists frequently utilize the radionuclide tritium (^{3}H) in groundwater studies, mainly for identifying modern replenishment. The isotope is produced naturally by cosmic radiation, but thermonuclear bomb tests conducted in the 1950s–1980s caused a dramatic rise of ^{3}H concentrations in the atmosphere. Due to washout and decay, atmospheric concentrations have mostly reached natural levels again (Clark and Fritz, 1997). Therefore, groundwater dating relying on bomb-produced tritium in precipitation is close to its expiry date (Fontes, 1985; Kazemi et al., 2006). However, the natural cosmogenic ^{3}H can also be utilized for the estimation of groundwater residence times (Clark and Fritz, 1997; Kazemi et al., 2006). Unfortunately, current ^{3}H levels in Saudi rainwater are unknown.

Besides the isotopic signature of rainfall, its chemical composition is relevant. Knowledge of precipitation chemistry can contribute to an understanding of global element cycling in the atmosphere (Ahmed et al., 1990)

and of air mass circulation (Edmunds, 2010). Rainfall can also be considered the “titrant” in hydrogeochemical processes, being the initial solvent in water–rock interaction (Edmunds, 2010). Additionally, chloride concentrations are a key parameter in the Chloride Mass Balance method for estimating groundwater recharge (Edmunds, 2010) and insufficient data lead to additional uncertainty in the calculation (Bazuhair and Wood, 1996).

Hydrochemical data on rainfall are scarce in arid and semi-arid regions (Ahmed et al., 1990) and particularly in parts of Africa (Edmunds, 2010) and the Arabian Peninsula (Alabdula'aly and Khan, 2000). For central Saudi Arabia, only a few publications are available. Handy and Tucker (1984) report on the chemistry of 12 rain events (April 1983 to March 1984) in Riyadh. Yet, the study suffers from incomplete analyses. Alabdula'aly and Khan (2000) analyzed samples from several rain collectors in Riyadh, but their study covers only four events (March and April 1994).

In light of gaps in the available data, the primary objectives of this study are to provide additional information on the isotopic and chemical composition of rainfall events in Riyadh and to offer insights into the controlling processes. The results will help to improve the understanding of the hydrogeology and hydrochemistry of the aquifer systems of the Arabian Peninsula. For example, they may serve as a basis for estimating groundwater recharge.

2.3. Methods

2.3.1. Study area

The study area is Riyadh, the capital of Saudi Arabia (Fig. 2-1). Average annual precipitation in the city is 112 mm (King Khaled Airport Riyadh; elevation: 614 m above sea level; Al-Saleh, 1997; JRCC/PME, 2015). Most of the rain falls between November and May (MAW, 1984) and receives contributions from various sources. In addition to Mediterranean rainstorms, air masses from the North African continent passing over the Red Sea and storms from the Arabian Sea/Indian Ocean contribute precipitation (Alyamani, 2001; Wagner and Geyh, 1999). Particularly in spring, rain is often associated with dust storms (Wagner, 2011).

Although the climate is generally arid and potential evaporation rates are high, some groundwater recharge occurs, especially from sporadic high-intensity rain events and in settings favorable to recharge like wadis, in which surface runoff is accumulated. Limited recharge may also occur in dune areas (Dincer et al., 1974; Wagner, 2011). Eventually, the infiltrated water reaches the underlying aquifers cropping out in the vicinity of the city (Fig. 2-1). Hence, studying rain samples from Riyadh provides isotopic and chemical fingerprints that are characteristic of current recharge to some of the principal groundwater reservoirs of the Peninsula.

2.3.2. Sampling

To complement the available data, 28 rain events that occurred in Riyadh between 2009 and 2013 were analyzed. Samples were collected at two locations (24.79561°N, 46.75877°E or 24.67946°N, 46.73177°E) using a polypropylene box that was exposed upon the onset of each rain event and emptied immediately after rainfall had ended. In a few cases, a tarp was used instead in order to provide a larger collection area. Both were rinsed with distilled water and dried before usage to avoid contamination. As the isotopic composition can vary during a storm, special care was taken to ensure integral samples representing the entire precipitation event. Aiming at an evaluation of intra-storm variability, a single event was sampled 10 times (intervals of approximately 1 mm).

Representative sub-samples of the total sample were filled in HDPE bottles (15–50 mL). Headspace was minimized and bottles were closed with screw caps and sealed with electrical tape to prevent evaporation. During 12 storms, a larger (0.5 or 1 L), non-integral sample was taken from a roof drain pipe for tritium (^{3}H) analysis.

2.3.3. Isotopic and chemical analysis

The stable isotope signature of water (δ^2H, δ^{18}O) was measured by Laser Cavity Ring-Down Spectroscopy (L-CRD) using Isotopic Liquid Water Analyzers (L1102-i and L2130-i by Picarro, Santa Clara, CA, USA; Helmholtz Centre for Environmental Research, Halle, Germany and Institute of Applied Geosciences, Technische Universität Darmstadt, Germany). The results were expressed in per mil (‰) using the conventional delta-notation relative to Vienna Standard Mean Ocean Water (V-SMOW). As for δ^{18}O, the analytical precision is ±0.1 ‰. In terms of δ^2H, the precision accounts for ±0.8 ‰. Based on the obtained values, the deuterium excess d was calculated as $d = \delta^2H - 8 \cdot \delta^{18}O$ (Dansgaard, 1964). ^{3}H concentrations were measured by Liquid Scintillation Counting (Quantulus 1220 by PerkinElmer, Waltham, MA, USA) after electrolytic enrichment of 400 mL of sample water (enrichment factor of about 20; Helmholtz Centre for Environmental Research, Halle, Germany). Results are reported in tritium units (TU). As the precision is mainly governed by the counting time, no general value is given here. Instead, the individual errors are presented in Table 2-1. Major ion concentrations were determined by Ion Chromatography (882 Compact IC plus by Metrohm, Herisau, Switzerland) at the Institute of Applied Geosciences, Technische Universität Darmstadt, Germany. The precision for the analyzed ions was better than ±3 % (relative standard deviation).

2.3.4. Meteorological data and air mass back-trajectories

To aid interpretation, rain amount and temperature data were necessary. In the case of samples taken in the course of this study, meteorological data were gathered from the closest weather station, King Khaled Airport Riyadh, located approximately 20 km north of the city. Data were accessed online (Weather Underground, Inc., 2015). For samples from previous studies, weather data from BRGM (1981b) and from an online weather archive (Tutiempo Network, S.L., 2015) was considered.

For the rain events sampled in this study, an attempt was made to constrain the associated moisture sources by calculating air mass back-trajectories. These were obtained by means of the HYbrid Single-Particle Lagrangian Integrated Trajectory model (HYSPLIT; Draxler and Rolph, 2015; Rolph, 2015), using the GDAS 1°×1° meteorological data set. Apart from the location, date, and time of the rain event, the suite of required input data comprises the cloud elevation, which was retrieved from hourly weather reports issued by the aforementioned meteorological station (reported as METAR code; Weather Underground, Inc., 2015; for further information see Appendix 2). As most of these data are not available for the rains sampled in previous studies, HYSPLIT modeling was not performed for these events.

2.3.5. Calculation of Local Meteoric Water Lines

Crawford et al. (2014) provide a comprehensive overview on approaches to obtain a LMWL. The corresponding equations, also used in this study, are briefly summarized below (adopted from Crawford et al., 2014; and references therein).

In an Ordinary Least Squares Regression (OLSR), the sum of the squares of the vertical distances between the data points and the line is minimized. The slope of the line is defined as:

$$a_{OLSR} = \frac{\sum_{i=1}^{n} x_i y_i - \frac{\sum_{i=1}^{n} x_i \sum_{i=1}^{n} y_i}{n}}{\sum_{i=1}^{n} x_i^2 - \frac{\left(\sum_{i=1}^{n} x_i\right)^2}{n}} \quad (2\text{-}1)$$

By contrast, the sum of the triangle areas between the points and the best fit line is minimized in the Reduced Major Axis (RMA) approach. Here, the slope of the regression line is calculated as follows:

$$a_{RMA} = \left[\frac{\sum_{i=1}^{n} y_i^2 - \frac{\left(\sum_{i=1}^{n} y_i\right)^2}{n}}{\sum_{i=1}^{n} x_i^2 - \frac{\left(\sum_{i=1}^{n} x_i\right)^2}{n}}\right]^{\frac{1}{2}} \quad (2\text{-}2)$$

The Major Axis (MA) regression aims at minimizing the sum of the squared orthogonal distances between the points and the line. The slope of the latter is given by:

$$a_{MA} = \frac{\left(\sum_{i=1}^{n} V_i^2 - \sum_{i=1}^{n} U_i^2\right) + \sqrt{\left(\sum_{i=1}^{n} V_i^2 - \sum_{i=1}^{n} U_i^2\right)^2 + 4\left(\sum_{i=1}^{n} U_i V_i\right)^2}}{2\sum_{i=1}^{n} U_i V_i} \quad (2\text{-}3)$$

where $U_i = (x_i - \bar{x})$ and $V_i = (y_i - \bar{y})$, and $\bar{x}$ and $\bar{y}$ represent the mean values.

In all three cases, the intercept b is defined as:

$$b = \bar{y} - a\bar{x} \tag{2-4}$$

To calculate the standard errors (SE) for the slope and the intercept, the following equations are applied:

$$SE_a = \frac{\sqrt{\frac{\sum_{i=1}^{n}(y_i - \hat{y}_i)^2}{n-2}}}{\sqrt{\sum_{i=1}^{n}(x_i - \bar{x})^2}} \tag{2-5}$$

$$SE_b = SE_a \sqrt{\frac{\sum_{i=1}^{n} x_i^2}{n}} \tag{2-6}$$

where $\hat{y}_i = ax_i + b$.

The described approaches can be modified by integrating weighting factors that are based on the corresponding precipitation depths p:

$$w_i = \frac{p_i}{\sum_{i=1}^{n} p_i} \tag{2-7}$$

Then the slope of the precipitation-weighted OLSR (PWLSR) becomes:

$$a_{PWLSR} = \frac{\sum_{i=1}^{n} w_i y_i x_i - \sum_{i=1}^{n} w_i x_i \sum_{i=1}^{n} w_i y_i}{\sum_{i=1}^{n} w_i x_i^2 + \sum_{i=1}^{n} w_i x_i} \tag{2-8}$$

For the precipitation-weighted RMA (PWRMA), the slope is:

$$a_{PWRMA} = \frac{\sum_{i=1}^{n} w_i (y_i - \bar{y}_w)^2}{\sum_{i=1}^{n} w_i (x_i - \bar{x}_w)^2} \tag{2-9}$$

where $\bar{y}_w$ and $\bar{x}_w$ are the precipitation-weighted means of y and x.

The slope of the precipitation-weighted MA (PWMA) regression line is defined as:

$$a_{PWMA} = \frac{\left(\sum_{i=1}^{n} w_i V_{wi}^2 - \sum_{i=1}^{n} w_i U_{wi}^2\right) + \sqrt{\left(\sum_{i=1}^{n} w_i V_{wi}^2 - \sum_{i=1}^{n} w_i U_{wi}^2\right)^2 + 4\left(\sum_{i=1}^{n} w_i U_{wi} V_{wi}\right)^2}}{2\sum_{i=1}^{n} w_i U_{wi} V w_i} \tag{2-10}$$

where $U_{wi} = (x_i - \bar{x}_w)$ and $V_{wi} = (y_i - \bar{y}_w)$.

In all three cases, the intercept b is determined as:

$$b_{PW} = \bar{y}_w - a\bar{x}_w \tag{2-11}$$

The standard errors (SE) are then obtained by the following equations:

$$SE_a = \frac{\sqrt{\frac{n\sum_{i=1}^{n} w_i (y_i - \hat{y}_i)^2}{n-2}}}{\sqrt{n\sum_{i=1}^{n} w_i (x_i - \bar{x})^2}} \tag{2-12}$$

$$SE_b = SE_a\sqrt{\sum_{i=1}^{n} w_i {x_i}^2} \quad (2\text{-}13)$$

To evaluate the goodness of fit for the approaches, the average root mean Sum of Squared Errors $rmSSE_{av}$ is considered (for details, see Crawford et al., 2014). The closer to 1.0 the value of this parameter, the better the applied method for the given data set.

All parameters presented above can be calculated conveniently with the LOCAL METEORIC WATER LINE FREEWARE provided by Crawford et al. (2014).

2.4. Results and discussion

2.4.1. Stable isotope signatures

The results of the isotope analyses of this and previous studies are presented in Table 2-1, along with meteorological data. First, we examine the results for the sequentially sampled event (23 April 2012; Sample IDs 21a–21j; Fig. 2-2).

Table 2-1. Results of the isotope analyses (δ values and d given in ‰ V-SMOW) and associated precipitation depths and mean air temperatures of the sampling days.

ID	Sampling Date	Time	Moisture Source[a]	p [mm][b]	Mean T_{air} [°C]	$\delta^{18}O$ [‰]	$\delta^{2}H$ [‰]	d [‰]	^{3}H [TU]	Source
1	3/28/2009	20:00	AG	14.0	19	3.54	30.8	2.5	3.8 ± 0.5	this study
2	4/3/2009	19:00	RS	11.0	16	-2.90	-5.5	17.7		this study
3	12/4/2009	10:15	RS	3.5	16	-2.65	-5.8	15.4	2.8 ± 0.4	this study
4	12/4/2009	19:30	RS	3.5	16	3.04	35.0	10.7		this study
5	12/13/2009	3:45	RS	0.5[c]	17	-0.64	16.8	22.0		this study
6	4/16/2010	20:40	RS	0.5[c]	24	-1.87	3.0	17.9	4.6 ± 0.6	this study
7	5/2/2010	19:40	RS	2.0	26	2.07	20.5	3.9	3.6 ± 0.5	this study
8	5/3/2010	15:45	RS	23.0	26	-0.18	9.8	11.2	4.1 ± 0.5	this study
9	5/5/2010	23:45	RS	3.0	23	2.84	34.3	11.6	6.4 ± 0.8	this study
10	8/3/2010	13:00	AG	1.0	37	9.43	43.1	-32.4		this study
11	1/18/2011	17:00	RS	30.0	8	-0.51	20.3	24.4	2.8 ± 0.5	this study
12	4/12/2011	18:00	RS	1.0	28	3.74	29.6	-0.4	4.0 ± 0.5	this study
13	4/15/2011	5:00	AS	2.5	14	6.74	49.0	-5.0		this study
14	4/15/2011	10:00	AG	2.5	14	-0.91	10.9	18.1		this study
15	4/25/2011	17:00	AS	0.5[c]	30	2.07	22.2	5.7	5.6 ± 0.6	this study
16	4/29/2011	22:15	AS	0.5[c]	30	4.14	20.4	-12.7		this study
17	11/29/2011	8:00	AS	5.0	10	-1.14	17.5	26.7		this study
18	11/29/2011	18:00	AG	5.0	10	-6.53	-29.3	23.0	3.5 ± 0.5	this study
19	4/16/2012	17:05	MS	3.0	26	0.08	11.1	10.4	5.6 ± 0.7	this study
20	4/17/2012	19:15	MS	11.0	25	1.97	24.9	9.1		this study
21	4/23/2012		RS	9.0	26	4.19[d]	42.6[d]	9.1	4.9 ± 0.6	this study
21a	"	17:20				8.10	58.8	-6.0		this study
21b	"	17:35				5.89	51.8	4.6		this study
21c	"	17:50				5.77	54.7	8.6		this study
21d	"	18:05				5.00	53.0	13.1		this study
21e	"	18:20				5.10	50.3	9.5		this study

ID	Sampling Date	Time	Moisture Source[a]	p [mm][b]	Mean T_{air} [°C]	$\delta^{18}O$ [‰]	$\delta^{2}H$ [‰]	d [‰]	^{3}H [TU]	Source
21f	"	18:50				4.42	44.9	9.5		this study
21g	"	20:35				3.65	38.7	9.5		this study
21h	"	20:50				0.71	21.2	15.5		this study
21i	"	21:20				1.77	25.7	11.6		this study
21j	"	23:45				1.53	27.3	15.0		this study
22	10/28/2012	18:45	AS	1.0	28	6.54	27.8	-24.5		this study
23	10/29/2012	0:15	RS	0.5[c]	23	9.45	43.4	-32.2		this study
24	11/19/2012	19:10	AS	2.0	21	3.29	30.6	4.4		this study
25	11/28/2012	23:15	RS	2.0	16	0.46	7.4	3.7		this study
26	11/29/2012	18:00	RS	6.0	13	0.01	23.9	23.8		this study
27	12/18/2012	23:30	RS	3.0	13	0.88	18.1	11.1		this study
28	3/23/2013	23:00	RS	3.0	23	3.70	43.1	13.5		this study
29	3/28/1974	n.a.		5.5	18.5	-0.5	11.7	15.3		Job et al. (1978)
30	1/18/1975	n.a.		1.8	n.a.	4.9	46.9	7.7		BRGM (1976)
31	1/28/1975	n.a.		5.3	n.a.	5.5	44.7	0.7		BRGM (1976)
32	1/29/1975	n.a.		4.3	10.5	0.4	25.0	21.8		BRGM (1976)
33	3/11/1975	n.a.		0.5[c]	23.6	1.5	34.5	22.5		BRGM (1976)
34	3/29/1975	n.a.		31.0	17.2	-0.4	7.6	10.8		BRGM (1976)
35	3/30/1975	n.a.		9.0	15.5	-0.8	11.6	18.0		BRGM (1976)
36	4/21/1975	n.a.		0.8	26	1.9	23.2	8.0		BRGM (1976)
37	3/13/1976	n.a.		10.5	n.a.	-1.2	0.8	10.4		BRGM (1977)
38	3/20/1976	n.a.		13.0	n.a.	-1.2	16.2	25.8		BRGM (1977)
39	3/24/1976	n.a.		0.5[c]	n.a.	-1.1	12.8	21.6		BRGM (1977)
40	3/31/1976	n.a.		0.5[c]	n.a.	-3.6	-12.4	16.4		BRGM (1977)
41	4/20/1976	n.a.		23.2	26.7	-0.6	15.9	20.7		BRGM (1977)
42	4/23/1976	n.a.		7.5	24	-1.7	7.4	21.0		BRGM (1977)
43	4/25/1976	n.a.		2.4	26.2	-2.2	4.1	21.7		BRGM (1977)
44	5/8/1976	n.a.		7.5	29.7	2.2	16.9	-0.7		BRGM (1977)
45	1/5/1977	n.a.		0.5[c]	16.2	-0.3	10.3	12.7		BRGM (1977)
46	5/20/1977	n.a.		0.5[c]	34.3	3.5	17.6	-10.4		BRGM (1977)
47	4/29/1978	n.a.		17.0	24.6	2.1	24.9	8.1		GDC (1980)
48	1/22/1979	n.a.		0.5[c]	20.1	-0.8	-1.8	4.7		GDC (1980)
Precipitation-weighted means (integral samples)						0.37	16.7			

Moisture sources: MS=Mediterranean Sea, RS=Red Sea, AS=Arabian Sea, AG=Arabian Gulf

[a] inferred from air mass back-trajectories (for details on HYSPLIT modeling results see Appendix 2)

[b] if two separate events occurred within one day, the daily rain amount was split in half

[c] the meteorological station reported "0" but a value of 0.5 mm is assumed for display and weighting purposes

[d] arithmetic mean of δ values of samples 21a-21j (mean is used in Fig. 2-3, 2-4, 2-5 and for calculation of LMWL and precipitation-weighted means in the last line of the table)

In the initial phase of the storm, the rain showed enriched isotopic signatures. The sample taken at 17:20, for instance, is characterized by δ values of 8.10 and 58.8 ‰ for ^{18}O and ^{2}H, respectively. In the course of the event, however, the δ values decreased and accounted for 1.53 ‰ ($\delta^{18}O$) and 27.3 ‰ ($\delta^{2}H$) at the end of the event (at 23:45). This isotopic depletion reflects a rainout and Rayleigh distillation process (Clark and Fritz, 1997; Dansgaard, 1964), i.e., isotopic fractionation between vapor and the condensing phase caused a preferential partitioning of the heavy isotopes ^{18}O and ^{2}H into the forming water drops, leaving a depleted vapor reservoir behind. Due to this depletion, subsequent rains become isotopically lighter than the initial ones. The ranges of δ values for ^{18}O and ^{2}H within the event account for approximately 7 and 38 ‰, respectively. Although even

greater ranges are reported in other studies (e.g., Kubota and Tsuboyama, 2003, max. ranges of 12 ‰ for $\delta^{18}O$ and 103 ‰ for $\delta^{2}H$), these values are remarkable since they correspond to approximately half of the total data scatter of the integral samples, with respect to both isotopes. Nevertheless, it is noteworthy that the depletion trajectory, $\delta^{2}H = 5.72(\pm0.52) \cdot \delta^{18}O + 18.6(\pm2.4)$ ‰ (OLSR; not shown in plot), roughly follows the general trend of the integral samples (equation discussed below).

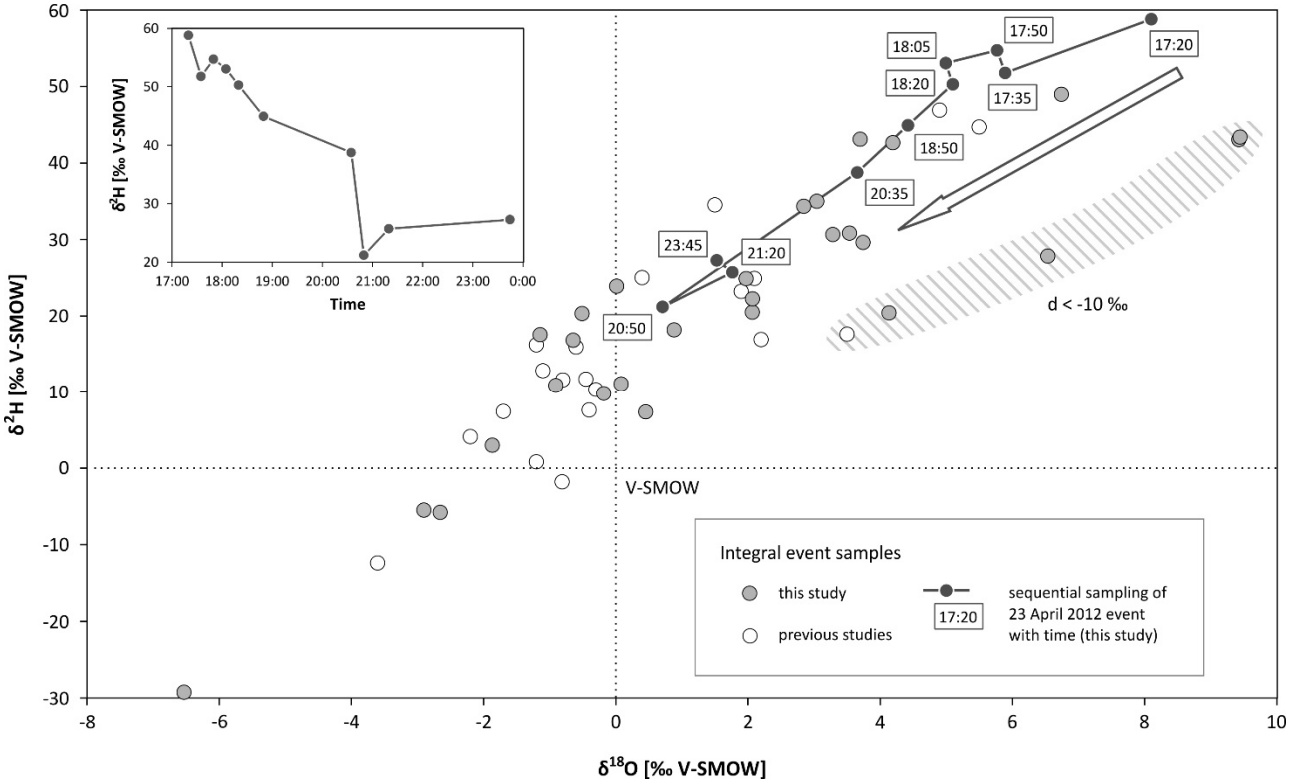

Fig. 2-2. $\delta^{2}H$–$\delta^{18}O$ relationship for the integral samples and the samples collected in the course of the 23 April 2012 event. The inset shows the temporal development of $\delta^{2}H$ during the event.

With respect to the integral event samples, significant scatter is observed in the isotopic composition (Fig. 2-2). The lowest δ values account for -6.53 ‰ (^{18}O) and -29.3 ‰ (^{2}H) and the most enriched rain shows values of 9.45 ‰ (^{18}O) and 43.4 ‰ (^{2}H). The precipitation-weighted means for $\delta^{18}O$ and $\delta^{2}H$ are 0.37 and 16.7 ‰, respectively (last line in Table 2-1). The large spread of the δ values (approximately 16 and 73 ‰ for ^{18}O and ^{2}H) is a common phenomenon (Gat, 1971). In the present case, this data scatter also refers to points that seem to have undergone a positive displacement with a disproportionately high $\delta^{18}O$ component. The resulting small deuterium excess values (d<-10 ‰; hatched area in Fig. 2-2) suggest sub-cloud evaporation from falling drops (Dansgaard, 1964; Ehhalt et al., 1963). During this process, the lighter isotopes are preferentially removed from the water, with $\delta^{18}O$ being relatively more affected.

This interpretation is supported by the analysis shown in Fig. 2-3, which includes precipitation depth and temperature data. It is evident that the concerned rain events (hatched area) were small (<2 mm) and mostly occurred on warm days (23–37°C mean air temperature of sampling day).

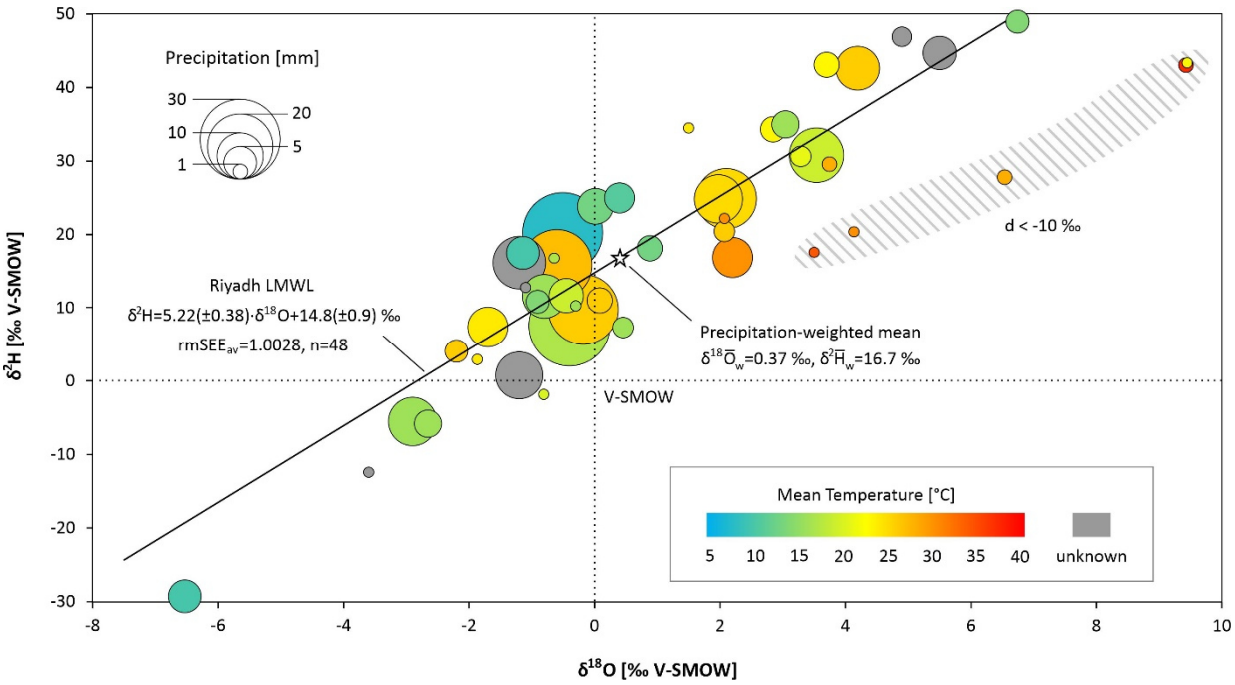

Fig. 2-3. δ^2H–$\delta^{18}O$ relationship for the integral samples in conjunction with precipitation amounts and mean air temperatures of the sampling day.

Within the remaining samples, no distinct correlation between the isotopic signature and the meteoric variables is apparent. Since it would be reasonable to expect a seasonal variation of the δ values (Alyamani, 2001; Weyhenmeyer et al., 2002), we combine the obtained isotopic parameters with the climate chart of Riyadh (Fig. 2-4).

Although the plot does not reveal systematic differences within the rainy season, it shows a clustering of high $\delta^{18}O$ and low d values during the hot summer, when low relative humidity values prevail. This further supports the sub-cloud evaporation hypothesis.

Occasionally, several LMWLs have been established for a given location based on the moisture provenance of rains (Weyhenmeyer et al., 2002). Thus, we grouped events sampled in this study based on their HYSPLIT-derived moisture sources (Fig. 2-5, Table 2-1).

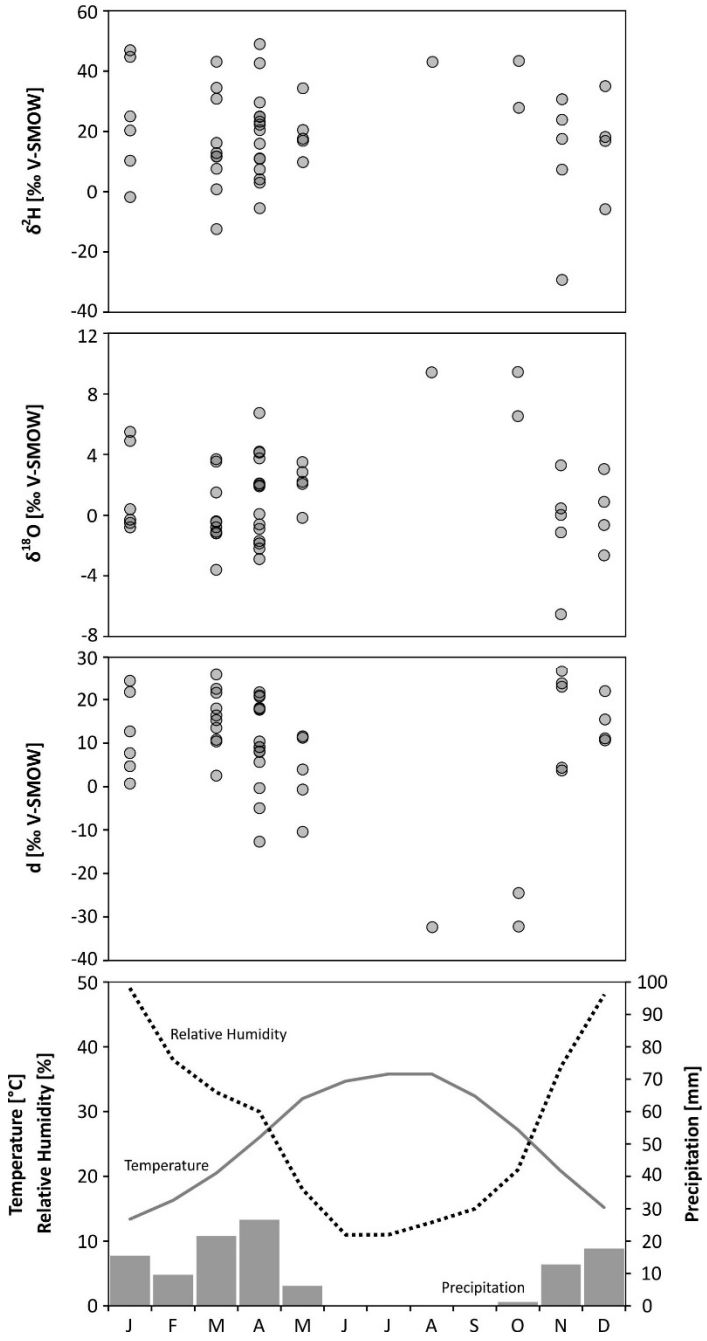

Fig. 2-4. Isotopic signatures of rain events (grouped on a monthly basis), along with long-term climatic means (1985–2010; JRCC/PME, 2015).

Possibly also hampered by the reduced number of data points (events from previous studies were excluded; see Section 2.3.4.), we could not identify systematic patterns. Further, we note that the two rain events with a Mediterranean moisture source do not plot on the Eastern Mediterranean Meteoric Water Line (EMMWL; Gat, 1971, 1984). This might indicate that the original moisture source-related signature is masked, probably by a combination of phenomena (Crawford et al., 2013). In the present case, major factors include: i) altitude effect, ii) continental effect, iii) sub-cloud evaporation, and iv) moisture recycling.

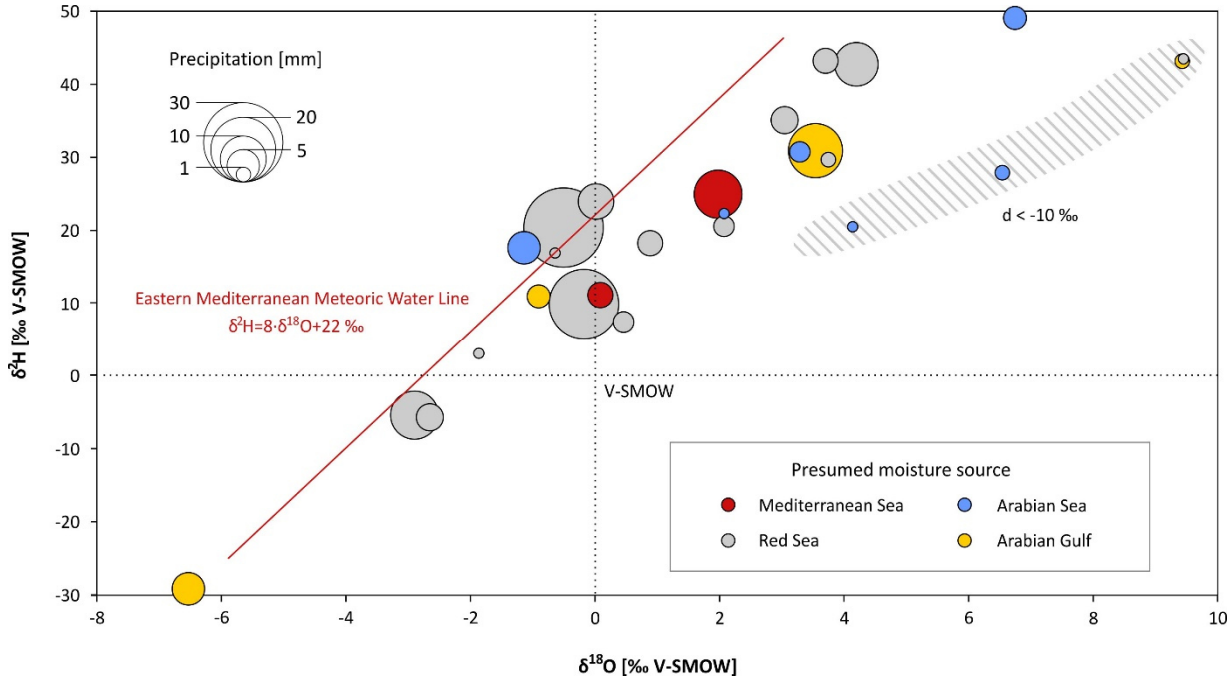

Fig. 2-5. δ^2H–$\delta^{18}O$ relationship for the integral samples collected in this study, classified according to the HYSPLIT-derived moisture sources. For comparison, the Eastern Mediterranean Meteoric Water Line (Gat, 1971, 1984) is included.

The first two effects cause isotopic depletion, possibly along the LMWL. The third process, however, leads to a positive shift with a small slope, thus modifying the LMWL and decreasing the deuterium excess value (see above). The fourth process, in turn, causes the opposite. Re-evaporation of soil moisture and temporary lakes after rainfall generates atmospheric moisture with high deuterium excess values due to kinetic isotope fractionation (Froehlich et al., 2008).

The deuterium excess is often applied to constrain moisture sources (e.g., Fröhlich et al., 2002; Xie et al., 2011) as its numerical value is initially governed by the physical conditions in the vapor source area (relative humidity, air temperature, sea surface temperature; Craig and Gordon, 1965). However, the interplay of the above-mentioned processes is capable of altering the value. Particularly partial evaporation from the falling drop is relevant in arid climate zones (Gat, 1971). Hence, the d value cannot be deemed an unequivocal moisture source indicator in studies conducted in central Saudi Arabia.

Due to the masking effects, it is not reasonable to split the data set to define several LMWLs based on moisture source areas. Instead, we pooled the data points and calculated LMWLs for the entire data set by applying the equations presented in Section 2.3.5. (Table 2-2).

The slopes obtained by OLSR, RMA, and MA are quite small, particularly the ones calculated by OLSR (4.49) and RMA (5.11). These low values are caused by the most divergent δ values in the data set, i.e., outliers linked to sub-cloud evaporation (Hughes and Crawford, 2012). Precipitation from these events would probably evaporate from the soil. From a practical point of view (e.g., recharge estimation), they could thus be neglected (Gat, 1971).

Table 2-2. LMWL parameters obtained by applying the six calculation methods to the Riyadh rainfall isotope data (n= 48).

Method	a	SE_a	b [‰]	SE_b [‰]	$rmSSE_{av}$
OLSR	4.49	0.36	13.6	1.2	1.0536
RMA	5.11	0.35	12.8	1.2	1.0197
MA	5.76	0.41	12.0	1.4	1.0526
PWLSR	5.22	0.38	14.8	0.9	1.0028
PWRMA	5.83	0.39	14.6	0.9	1.0499
PWMA	6.48	0.43	14.4	1.0	1.1373

Leguy et al. (1983), for instance, ignored all events with less than 2 mm of rain. Yet, Hughes and Crawford (2012) point out that choosing such a cut-off value is subjective and might lead to a highly variable outcome. Instead, they favor a precipitation-weighting, which is non-subjective, but still capable of reducing the bias towards small rain events. Also Crawford et al. (2014) recommend precipitation-weighted schemes in such settings. As expected, the slopes obtained by applying the precipitation-weighted regressions PWSLR, PWRMA, and PWMA, are on average greater than those calculated with their non-weighted counterparts. This also applies to the intercepts. With respect to the $rmSSE_{av}$ calculations, it can be summarized that the PWMA yielded the highest value (1.1373), while PWLSR resulted in the lowest value (1.0028). Due to this low $rmSSE_{av}$ and the fact that PWLSR also yielded reasonable standard errors for a and b, we deem this method the most suitable for the present data set and define the following LMWL for Riyadh:

$$\delta^2H = 5.22(\pm0.38) \cdot \delta^{18}O + 14.8(\pm0.9)\ ‰ \text{ (PWLSR; } rmSSE_{av}=1.0028\text{; n=48)} \quad (2\text{-}14)$$

For comparison, we also performed LMWL calculations for selected GNIP stations in the region using the six regression methods. The full set of LMWL parameters is provided in the Supplementary Material (see Appendix 2). A subset, the PWLSR results, is presented in Table 2-3.

Table 2-3. LMWL parameters (all PWLSR) for Riyadh and selected GNIP station in the region (see Fig. 2-1), namely Bahrain (monthly data), Salalah (Oman; event data), Qairoon Hairiti (Oman; event data). For comparison, the parameters for the global data set are included.

Location	Altitude [masl]	Distance to coast [km]	n	$\delta^{18}\overline{O}_w$ [‰]	$\delta^{2}\overline{H}_w$ [‰]	a	SE_a	b [‰]	SE_b [‰]	$rmSSE_{av}$	Data Source
Riyadh	600	360	48	0.37	16.7	5.22	0.38	14.8	0.9	1.0028	this study, refs in Table 2-1
Bahrain	2	1	90	-0.69	7.5	5.48	0.28	11.2	0.7	1.0212	IAEA/WMO (2015)
Salalah	15	4	59	-0.80	5.1	5.18	0.18	9.2	0.3	1.0075	IAEA/WMO (2015)*
Qairoon Hairiti	850	28	43	-0.59	7.3	2.19	0.84	8.6	0.5	1.5253	IAEA/WMO (2015)*
Global	n.a.	n.a.	n.a.	n.a.	n.a.	8.21	0.003	12.6	0.02	1.0040	Crawford et al. (2014)

* data originally published by Wushiki (1991)

The slope for Riyadh (5.22) is lower than the one of the GMWL, but such slopes below 8 are frequently encountered in arid regions. According to Dansgaard (1964) and Clark and Fritz (1997), this is mainly due to non-equilibrium evaporation from falling drops, which predominantly affects light rains. The slope obtained for Riyadh is also comparable to the ones for Bahrain (5.48) and Salalah (5.18). The slope for Qairoon Hairiti (2.19), however, is exceptionally low and has to be treated with care. Coastal sites, often dominated by first stage rainout, frequently exhibit data points scattering in circles or ellipses in the δ^2H vs. $\delta^{18}O$ plot. Consequently, defining a LMWL in such a case is not straightforward (Crawford et al., 2014). This is also reflected by the relatively large standard error of 0.84 and the high $rmSSE_{av}$ of 1.5253. Moreover, the great spread of slopes calculated by the six methods for Qairoon Hairiti is noteworthy — the slopes range from 1.94 (OLSR) to 15.14 (PWMA; see Appendix 2). Further, it is interesting to note that the weighted mean isotopic signature of Qairoon Hairiti (28 km inland at an altitude of 850 m asl) is more enriched that the one of Salalah, which is located directly at the coast. Hence, neither an altitude effect nor a continental effect is apparent. In the present case, this is attributable to the fact that the sampling periods for the two sites do not match. Also when comparing these coastal sites with Riyadh, these otherwise widely observed isotope effects are not apparent — on average, Riyadh rain is isotopically heavier than precipitation at the coastal sites. This again illustrates the overriding effect of sub-cloud evaporation triggered by the hot and arid climate prevailing in central Saudi Arabia. In this context, it is also noteworthy that the LMWL equations for Riyadh and Bahrain are somewhat similar. Yet, their isotopic fingerprints, which are not limited to a simple equation, but also comprise absolute δ values and their weighted means, differ clearly.

2.4.2. Tritium concentrations

The ^3H values of the analyzed grab samples range from 2.8 to 6.4 TU (Table 2-1). These values call for a comparison with other ^3H data from the region. However, the most recent ^3H concentrations reported for the Bahrain GNIP station are from November 2002 (59.2 ± 1.6 TU) and April 2003 (3.0 ± 0.3 TU; IAEA/WMO, 2015). Apart from the fact that these analyses are several years old, the great difference between the two values makes comparison difficult. Moreover, the ^3H concentrations of coastal and inland precipitation waters are not directly comparable due to the reverse continental effect described for tritium (e.g., Fontes, 1985; Kattan, 1997). In ocean waters, modern tritium input is diluted due to mixing with old, depleted bottom waters. Hence, the ^3H levels in precipitation over the oceans and coastal regions are often relatively low. While traveling inland, marine vapor mixes with vapor generated by evaporation of rapidly recycled precipitation with more tritium, thus leading to increasing concentrations with distance from the coast.

Also a comparison with the natural background signal is not straightforward. As no pre-bomb rain analyses were conducted in the region, we have to consider natural ^3H levels reported for other parts of the world. Roether (1967) estimated a pre-bomb rain average of 6 ± 1.5 TU for Central Europe. Taking the geomagnetic latitude

effect on cosmogenic tritium production into account (e.g., Masarik and Beer, 1999), the value for the Middle East should be somewhat lower, possibly on the order of a few TU. Hence, the concentrations in Riyadh rain might suggest that the natural background level is approached. Although more measurements over a longer time period would be needed to determine whether ^{3}H levels are stable or still declining, the obtained concentrations can be used in groundwater studies. At least in recharge-favoring settings like wadi aquifers, the tritium method should still be applicable to detect modern recharge, particularly if low-level ^{3}H methods with detection limits down to 0.01 TU (Sültenfuß et al., 2009) are utilized.

2.4.3. Chemical composition

In viewing the chemistry results (Table 2-4), we again first examine the sequentially sampled event (Sample IDs 21a–21j).

Table 2-4. Results of the hydrochemical analyses (ion concentrations given in mg L^{-1}).

ID	Sampling Date	Time	EC [µS cm^{-1}]	Ca^{2+}	Mg^{2+}	Na^{+}	K^{+}	Cl^{-}	SO_4^{2-}	Source
1	3/28/2009	20:00	94	37.7	1.1	7.7	3.0	9.4	22.6	this study
2	4/3/2009	19:00	n.a.	n.a.	n.a.	n.a.	n.a.	n.a.	n.a.	this study
3	12/4/2009	10:15	78	43.5	0.7	3.5	1.3	3.4	10.0	this study
4	12/4/2009	19:30	164	23.2	1.4	11.2	2.9	17.5	24.8	this study
5	12/13/2009	3:45	79	12.6	0.5	2.6	1.2	2.6	12.8	this study
6	4/16/2010	20:40	44	13.7	0.4	1.7	0.8	0.4	3.7	this study
7	5/2/2010	19:40	164	51.9	1.2	6.2	2.2	7.8	28.3	this study
8	5/3/2010	15:45	57	29.9	0.7	1.6	0.7	0.8	6.0	this study
9	5/5/2010	23:45	74	16.0	0.7	2.6	1.0	3.8	10.3	this study
10	8/3/2010	13:00	52	69.3	2.2	7.2	2.6	8.3	48.3	this study
11	1/18/2011	17:00	112	16.2	1.2	3.3	1.4	4.5	11.6	this study
12	4/12/2011	18:00	298	49.1	1.8	6.8	2.3	10.4	25.1	this study
13	4/15/2011	5:00	765	94.6	11.3	38.6	7.9	83.0	92.2	this study
14	4/15/2011	10:00	141	24.3	1.3	3.0	1.0	4.1	9.3	this study
15	4/25/2011	17:00	247	43.5	1.3	3.9	2.4	3.8	17.9	this study
16	4/29/2011	22:15	476	72.5	4.8	14.1	3.8	27.9	57.1	this study
17	11/29/2011	8:00	355	52.2	1.9	13.0	2.2	27.5	43.9	this study
18	11/29/2011	18:00	92	15.4	0.6	1.8	1.4	1.9	6.2	this study
19	4/16/2012	17:05	308	54.3	1.6	5.9	3.3	8.7	14.6	this study
20[a]	4/17/2012	19:15	(1121)[a]	(145.8)[a]	(3.2)[a]	(66.0)[a]	(13.1)[a]	(123.6)[a]	(224.8)[a]	this study
21	4/23/2012		131	22.7	0.5	1.7	1.2	2.2	12.5	this study
21a	"	17:20	217	34.8	0.2	4.5	3.6	6.3	42.9	this study
21b	"	17:35	168	26.4	0.1	3.0	1.9	4.0	24.1	this study
21c	"	17:50	117	19.1	0.2	2.0	1.3	2.3	14.7	this study
21d	"	18:05	139	23.7	0.8	1.7	1.2	2.2	15.7	this study
21e	"	18:20	208	39.6	0.9	1.2	0.8	1.6	8.4	this study
21f	"	18:50	134	25.8	0.5	0.8	0.6	0.9	5.0	this study
21g	"	20:35	76	14.7	0.4	0.7	0.5	0.8	3.1	this study
21h	"	20:50	76	14.0	0.6	0.9	0.6	0.8	2.2	this study
21i	"	21:20	76	13.3	0.7	1.0	0.5	1.2	3.4	this study
21j	"	23:45	97	15.7	0.2	1.4	1.4	2.3	5.5	this study

ID	Sampling Date	Time	EC [µS cm^{-1}]	Ca^{2+}	Mg^{2+}	Na^{+}	K^{+}	Cl^{-}	SO_4^{2-}	Source
22	10/28/2012	18:45	377	63.3	1.7	7.0	3.0	12.1	33.3	this study
23	10/29/2012	0:15	415	57.8	5.2	14.3	3.6	25.5	50.2	this study
24	11/19/2012	19:10	555	58.4	3.9	43.8	3.0	73.5	50.2	this study
25	11/28/2012	23:15	164	25.1	1.9	4.1	2.6	8.9	14.8	this study
26	11/29/2012	18:00	251	32.0	2.6	11.7	2.3	20.3	13.8	this study
27	12/18/2012	23:30	218	23.0	2.5	4.0	1.5	7.3	10.5	this study
28	3/23/2013	23:00	n.a.	72.3	3.6	9.4	2.2	13.3	38.7	this study
29	3/28/1974	n.a.	n.a.	3.2	0.4	3.4	2.0	2.3	3.8	Job et al. (1978)
Prec.-weighted mean (integral samples)				31.5	1.5	6.1	1.8	9.5	17.3	

[a] elevated concentrations due to contamination of the collection vessel with dust; not considered in plots and calculation of precipitation-weighted mean Cl^- concentration

Fig. 2-6, displaying the temporal development of the SO_4^{2-} and Cl^- contents, reveals an overall decrease in concentrations, especially during the initial phase of the storm. The SO_4^{2-} concentrations, for instance, drop sharply from 42.9 mg L^{-1} at 17:20 to 5.0 mg L^{-1} at 18:50 and then remain more or less stable, fluctuating around a few mg L^{-1}. The Cl^- levels are generally lower than the SO_4^{2-} concentrations, but show a similar development.

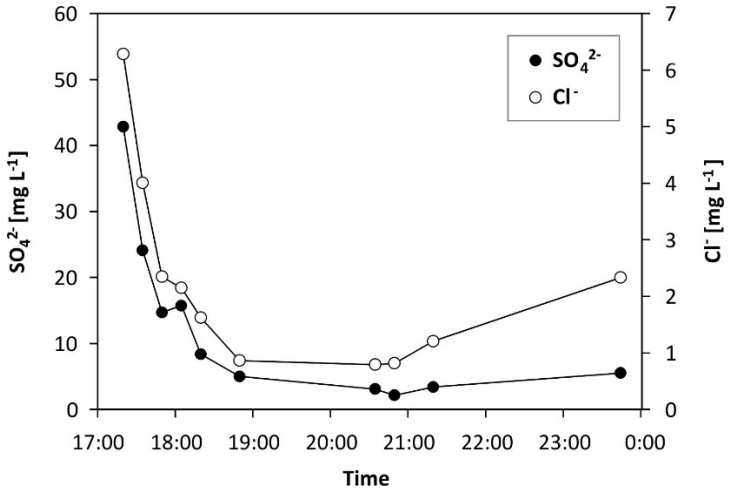

Fig. 2-6. Temporal development of sulfate and chloride concentrations during the 23 April 2012 rain event. Note the secondary concentration axis for chloride.

This pattern, caused by the washout of dust from the atmosphere, is fairly common (e.g., Ahmed et al., 1990; Salameh and Rimawi, 1988). In central Saudi Arabia, the atmosphere is typically dusty (Pósfai et al., 2013) and dust storms and rain events frequently coincide, particularly during spring (Wagner, 2011). The effect may be intensified by partial evaporation from falling drops in the beginning of the event, when the air column is still relatively dry (Gambell and Fisher, 1964). The demonstrated potential for intra-event variability suggests that the collection of integral samples is also crucial in precipitation chemistry studies.

The relationship between ion concentrations in the integral samples and the precipitation amount (Fig. 2-7) is directly related to these washout and evaporation phenomena. The highest concentrations of SO_4^{2-} and Cl^- occur

in rains with precipitation depths below 5 mm. The storms with greater precipitation amounts, on the other hand, show lower concentrations. This indicates that salts washed out from the atmosphere are highly concentrated in the light rains, but are diluted by greater precipitation amounts.

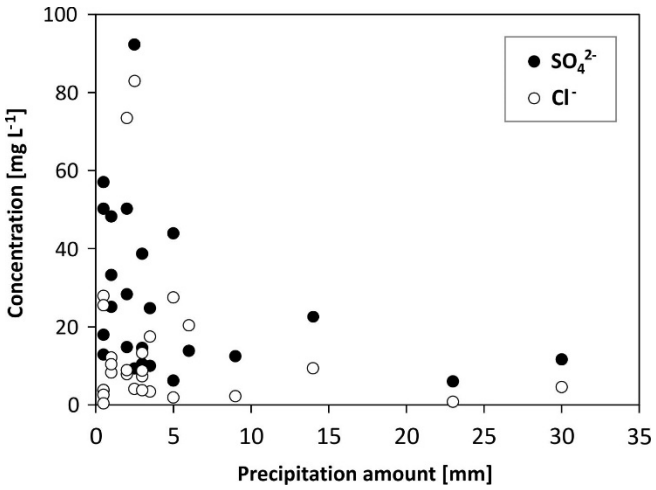

Fig. 2-7. Relationship between concentrations of sulfate and chloride in integral samples and associated rain amounts.

Further, partial evaporation affects light rains to a greater extent (see Section 2.4.1.). Therefore, the calculation of precipitation-weighted means is recommended by many authors (e.g., Ahmed et al., 1990; Wagner, 2011). The corresponding values for the present data set are given in the last row of Table 2-4. Among these means, particularly that for chloride (9.5 mg L^{-1}) may be useful for groundwater recharge estimations utilizing the Chloride Mass Balance method.

In order to study major ion relationships, the obtained concentrations are depicted in scatter plots, along with data from previous studies in Riyadh and Syria (Alabdula'aly and Khan, 2000; Kattan, 1997; Fig. 2-8).

The concentrations and ion ratios obtained in this study compare well with the findings of Alabdula'aly and Khan (2000). Yet, the concentrations in Riyadh rain are mostly quite different from those found for Tartous, a coastal city in Syria (Kattan, 1997). In Fig. 2-8a, the Riyadh samples mostly plot above the samples from Tartous and the line representing seawater dilution (Goldberg, 1963). Thus, the samples from Riyadh contain more Ca^{2+} than one would expect based on the associated Cl^- concentration and an assumed ion ratio similar to that in seawater (Ca^{2+} excess).

Fig. 2-8b exhibits a similar pattern, in this case with an excess of SO_4^{2-}. Thus, dissolution of gypsum or anhydrite dust seems likely (Salameh and Rimawi, 1988). Gypsum dust is known to be present in the atmosphere above Riyadh (Pósfai et al., 2013). Potential sources are anhydrite-dominated formations, which are part of the sedimentary succession (e.g., Jurassic Hith and Tertiary Rus Formation). Yet, corresponding outcrops are rather limited because of dissolution by groundwater and subsequent slumping of overlying strata (Powers et al., 1966).

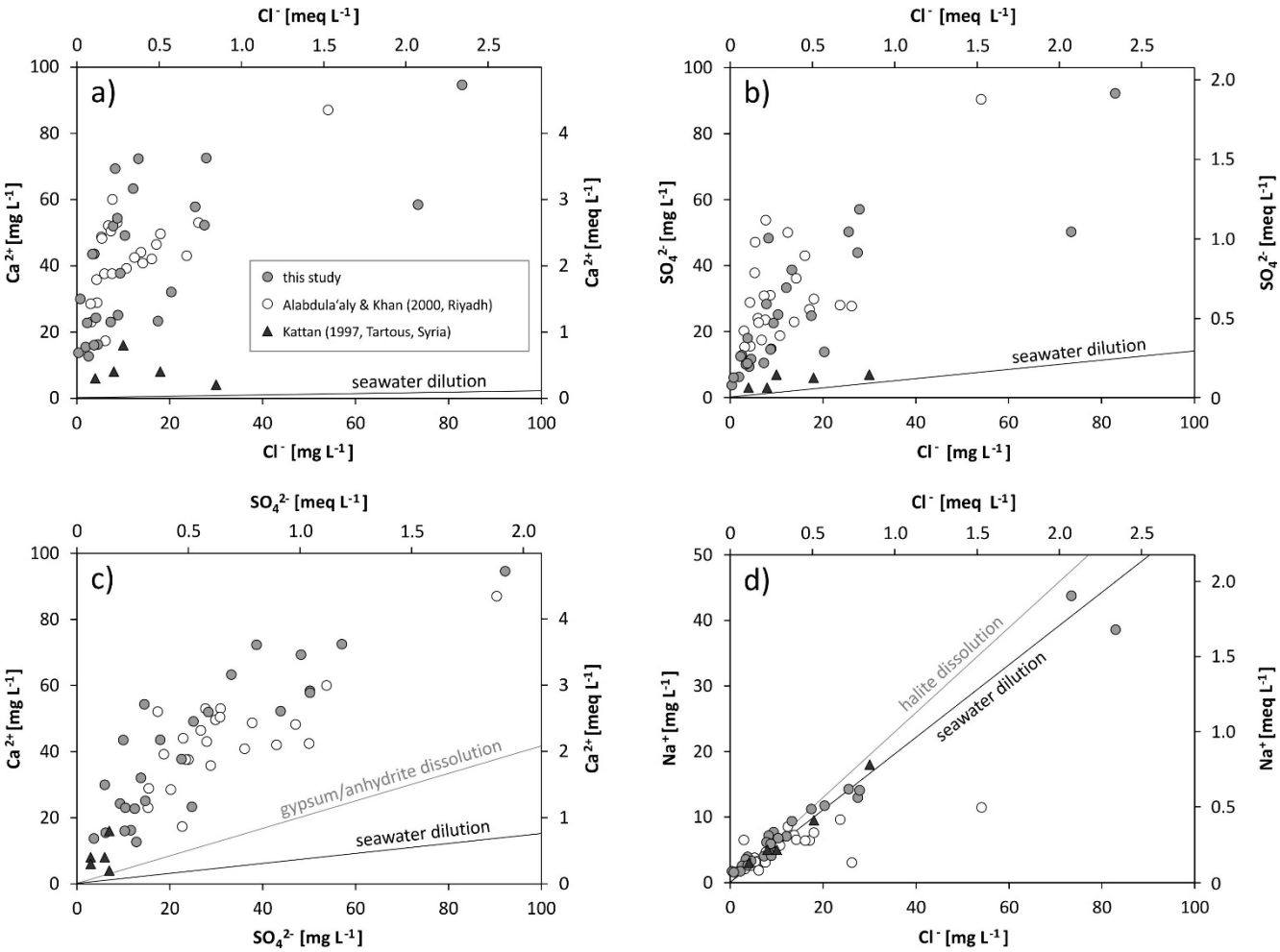

Fig. 2-8. Major ion scatter plots for integral samples. For comparison purposes, published data for Riyadh (Alabdula'aly and Khan, 2000, event samples) and Tartous, a coastal city in Syria (Kattan, 1997, monthly means) are included. The plots also feature lines representing seawater dilution (Goldberg, 1963) and, where applicable, dissolution of selected minerals. Secondary axes present concentrations on a milliequivalent basis (meq L^{-1}).

To verify whether the sampled rains contain dissolved gypsum and/or anhydrite, a Ca^{2+} vs. SO_4^{2-} plot was created (Fig. 2-8c). Here, all Riyadh samples show greater Ca^{2+}/SO_4^{2-} ratios than gypsum and anhydrite (i.e., meq-ratio >1), indicating that the prevailing Ca^{2+} is not fully balanced by SO_4^{2-}. Hence, calcite probably contributes Ca^{2+} as well (Ahmed et al., 1990). Calcite dust has been reported from aerosol investigations (Pósfai et al., 2013) and analyses of deposited dust in Riyadh (Modaihsh, 1997) and Kuwait (Al-Awadhi and AlShuaibi, 2013; Khalaf et al., 1985). The high $CaCO_3$ contents found in the mentioned studies (usually >30 % of the total dust amount) are not surprising, given the fact that limestone outcrops are common in the region, and particularly in the vicinity of Riyadh (e.g., Umm Er Radhuma Formation, Fig. 2-1; Powers et al., 1966; USGS/ARAMCO, 1963). Previous studies in the region have shown that the dissolution of such calcite dust has a buffering effect, shifting rain pH values from the acidic range to circum-neutral conditions (Ahmed et al., 1990; Handy and Tucker, 1984; Salameh and Rimawi, 1988).

Regarding the Na^+ and Cl^- concentrations, it can be stated that most data points lie on or close to the seawater dilution line. This, however, is not much different from the line representing halite dissolution (Fig. 2-8d). The Cl^- and Na^+ concentrations of Riyadh rain are also quite significant and comparable to, or even greater than, the levels found for Tartous. This is somewhat surprising since Tartous is located at the Mediterranean Sea, but the distance between Riyadh and the Arabian Gulf is 360 km. Because sea spray impact typically decreases sharply with distance from the coast (Kattan, 1997), the high Cl^- and Na^+ concentrations encountered in Riyadh must have a different origin. As more than 30,000 km^2 of the Arabian Peninsula are covered by sabkha deposits (salt flats; USGS/ARAMCO, 1963), which are dominated by minerals such as halite, gypsum, anhydrite, calcite, and dolomite (Al-Saafin, 1996), sabkhas could be a source of the solutes in Riyadh rain. Although these salt flats are geomorphologically resistant, wind erosion does occur, as they are relatively exposed due to the flat topography and lack of vegetation (Fryberger et al., 1984; Sanford and Wood, 2001). Al-Saafin (1996) states that halite is often enriched in the top few cm of a sabkha, where it can be dry, powdery, and subject to erosion. The postulated contribution by sabkha dust is further supported by Modaihsh (1997), who found high EC values for dust in Riyadh, which he attributed to eroded sabkha salts. The hypothesis is also consistent with the above-mentioned gypsum/anhydrite input, an observation that would be difficult to explain if the limited outcrops of anhydrite-bearing formations represented the only source.

2.5. Conclusions

Based on the observed intra-storm variability of the isotopic composition of rainwater, we infer that the collection of integral samples covering the entire rain event is crucial. The depletion trajectory, $\delta^2H = 5.72(\pm0.52) \cdot \delta^{18}O + 18.6(\pm2.4)$ ‰ (OLSR), is not much different from the LMWL calculated for the integral samples, $\delta^2H = 5.22(\pm0.38) \cdot \delta^{18}O + 14.8(\pm0.9)$ ‰ (PWLSR). Therefore, non-integral sampling would not dramatically alter the calculated LMWL. Yet, it would not yield the actual isotopic fingerprint (δ value ranges, precipitation-weighted means), which is needed in groundwater studies for comparison. This fingerprint is strongly controlled by mechanisms such as the continental effect, the altitude effect, sub-cloud evaporation from falling drops, and moisture recycling, all masking the composition inherited from the moisture source. Hence, we conclude that the deuterium excess d that is frequently applied to identify moisture sources may not be as helpful in central Saudi Arabia, where partial evaporation can cause a significant decrease in the value. Instead, models like HYSPLIT, so far most commonly applied in dust storm studies in the country (Draxler et al., 2001; Notaro et al., 2013; Pósfai et al., 2013), may be more appropriate to delineate moisture source regions.

The found tritium concentrations of 2.8 to 6.4 TU suggest that natural background levels are approached. However, using ^3H to identify modern groundwater replenishment should still be possible, especially in recharge-favoring environments and if low-level ^3H methods (Sültenfuß et al., 2009) are applied.

The precipitation chemistry indicates that solutes are mainly derived from atmospheric dust, originating from local limestone outcrops and sabkhas. The latter have been demonstrated to play a role with respect to Cl^- and Na^+ as well as SO_4^{2-} and a part of the Ca^{2+}. This hypothesis could be further substantiated by additional isotope studies, e.g., addressing chlorine-36, chlorine-37, and sulfur-34. The key prerequisite would be that the end-members (seawater, sabkha deposits, rocks) are isotopically distinct enough. Moreover, high-volume precipitation samples would be necessary to provide sufficient Cl^- and SO_4^{2-} for the isotope analyses. The idea that a part of the Cl^- might originate from sabkhas should be considered in future aerosol and precipitation chemistry studies in the region. Such investigations frequently include the calculation of enrichment factors for elements relative to sea salt or similar quantifications (sea salt fraction vs. non-sea salt fraction; e.g., Ahmed et al., 1990). For these calculations Cl^- is often regarded as an indicator ion for seawater, i.e., it is assumed that all Cl^- is derived from sea spray. Neglecting a possible non-sea salt contribution of the indicator ion Cl^- leads to erroneous results. Our finding might also have implications for chlorine-36 studies in the region. For calculations of recharge rates or groundwater residence times utilizing this nuclide, the isotopic composition of the chloride input has to be known and ^{36}Cl signatures of sea spray Cl^- and sabkha Cl^- possibly differ significantly (Fontes, 1985).

Based on the encountered chemical evolution of the sequentially sampled rain event, we conclude that collection of integral samples is not only important from an isotope perspective, but also with respect to chemical characterization. Due to inter-storm variability, with precipitation amounts being the major controlling factor of ion concentrations, the calculation of precipitation-weighted means is necessary.

The present study provides robust data on the isotopic and chemical composition of rain in Riyadh. The reported stable isotope signatures and ^3H values could be used for comparison in groundwater studies or unsaturated zone analyses. In the latter, also the precipitation-weighted mean Cl^- concentration (9.5 mg L^{-1}) may be useful for quantitative groundwater recharge estimations utilizing the Chloride Mass Balance method.

2.6. Acknowledgments

Financial support for this study has been provided by the German Federal Ministry of Education and Research (BMBF) through its program International Postgraduate Studies in Water Technologies (IPSWaT; grant no. IPS10/P10). We thank the Ministry of Water & Electricity (Saudi Arabia) for making unpublished consultant reports containing isotope and weather data available. The authors also gratefully acknowledge the NOAA Air Resources Laboratory (ARL) for the provision of the HYSPLIT transport and dispersion model used in this publication. Finally, we thank Matthew Silver for reviewing the draft manuscript for language and two anonymous reviewers for their valuable comments, which helped considerably to improve the manuscript.

2.7. Supplementary data

Supplementary data to this article can be found online at http://dx.doi.org/10.1016/j.chemgeo.2015.08.001 and in Appendix 2.

2.8. References

Ahmed, A.F.M., Singh, R.P., Elmubarak, A.H., 1990. Chemistry of Atmospheric Precipitation at the Western Arabian Gulf Coast. Atmospheric Environment 24A(12), 2927–2934.

Alabdula'aly, A.I., Khan, M.A., 2000. Chemistry of Rain Water in Riyadh, Saudi Arabia. Archives of Environmental Contamination and Toxicology 39, 66–73.

Al-Awadhi, J.M., AlShuaibi, A.A., 2013. Dust fallout in Kuwait city: Deposition and characterization. Science of the Total Environment 461–462, 139–148.

Al-Harbi, O., Hussain, G., Khan, M.M., 2008. Hydrogeochemical Processes and Isotopic Characteristics of Inland Sabkha, Saudi Arabia. Asian Journal of Earth Sciences 1(1), 16–30.

Al-Saafin, A.K., 1996. The Characterization of Sabkhas in the Eastern Parts of Saudi Arabia and its Implications for Engineering. PhD thesis, University of London.

Alsaaran, N.A., 2006. Using Environmental Isotopes for Estimating the Relative Contributions of Groundwater Recharge Mechanisms in an Arid Basin, Central Saudi Arabia. Arabian Journal for Science and Engineering 31(1A), 3–13.

Al-Saleh, M.A., 1997. Variability and Frequency of Daily Rainfall in Riyadh, Saudi Arabia. Geographical Bulletin 39(1), 48–57.

Alyamani, M.S., 2001. Isotopic composition of rainfall and ground-water recharge in the western province of Saudi Arabia. Journal of Arid Environments 49, 751–760.

Bazuhair, A., Al-Sulaiman, K., Abdulaaly, A., Hussein, M.T, Al-Yamani, M.S., 1994. Analysis of the Environmental Isotopes in the Ground Water of the Khulais Basin; West Saudi Arabia. Isotope and Radiation Research 26(1), 27–32.

Bazuhair, A.S., Wood, W.W., 1996. Chloride mass-balance method for estimating ground water recharge in arid areas: examples from western Saudi Arabia. Journal of Hydrology 186, 153–159.

BRGM – Bureau de Recherches Géologiques et Minières, 1976. Hydrogeological Investigations of the Al Wasia Aquifer in the Eastern Province of Saudi Arabia, Appendix 3: Isotopic Analyses. Ministry of Agriculture and Water, Riyadh.

BRGM – Bureau de Recherches Géologiques et Minières, 1977. Al Hassa Development Project, Groundwater Resources Study and Management Programme, Vol. III, Appendix II-7. Results of Isotopic Analyses. Ministry of Agriculture and Water, Riyadh.

BRGM – Bureau de Recherches Géologiques et Minières, 1981a. Ground Water Studies of Al Kharj Area (Saudi Arabia), Appendix 7: Comments on Isotope Analyses. Ministry of Agriculture and Water, Riyadh.

BRGM – Bureau de Recherches Géologiques et Minières, 1981b. Ground Water Studies of Al Kharj Area (Saudi Arabia), Appendix 6: Hydro-Climatology. Ministry of Agriculture and Water, Riyadh.

Clark, I.D., Fritz, P., 1997. Environmental Isotopes in Hydrogeology. Lewis Publishers, Boca Raton/New York.

Craig, H., 1961. Isotopic Variations in Meteoric Waters. Science 133, 1702–1703.

Craig, H., Gordon, L.I., 1965. Deuterium and oxygen 18 variations in the ocean and the marine atmosphere. In: Tongiorgi, E. (ed.), Stable Isotopes in Oceanographic Studies and Paleotemperatures. Spoleto, 9–130.

Crawford, J., Hughes, C.E., Lykoudis, S., 2014. Alternative least squares methods for determining the meteoric water line, demonstrated using GNIP data. Journal of Hydrology 519, 2331–2340.

Crawford, J., Hughes, C.E., Parkes, S.D., 2013. Is the isotopic composition of event based precipitation driven by moisture source or synoptic scale weather in the Sydney Basin, Australia? Journal of Hydrology 507, 213–226.

Dansgaard, W., 1964. Stable isotopes in precipitation. Tellus 16(4), 436–468.

Dincer, T., Al-Mugrin, A., Zimmermann, U., 1974. Study of the Infiltration and Recharge Through the Sand Dunes in Arid Zones with Special Reference to the Stable Isotopes and Thermonuclear Tritium. Journal of Hydrology 23, 79–109.

Draxler, R.R., Gillette, D.A., Kirkpatrick, J.S., Heller, J., 2001. Estimating PM_{10} air concentrations from dust storms in Iraq, Kuwait and Saudi Arabia. Atmospheric Environment 35, 4315–4330.

Draxler, R.R., Rolph, G.D., 2015. HYSPLIT (HYbrid Single-Particle Lagrangian Integrated Trajectory) Model. http://www.arl.noaa.gov/HYSPLIT.php (last access: 17 February 2015), NOAA Air Resources Laboratory, College Park, MD.

Edmunds, W.M., 2010. Conceptual models for recharge sequences in arid and semi-arid regions using isotopic and geochemical methods. In: Wheater, H.S., Mathias, S.A., Li, X. (eds.). Groundwater Modelling in Arid and Semi-Arid Areas. Cambridge University Press, Cambridge, 21–37.

Ehhalt, D., Knott, K., Nagel, J.F., Vodel, J.C., 1963. Deuterium and Oxygen 18 in Rain Water. Journal of Geophysical Research 68(13), 3775–3780.

Fontes, J.C., 1985. Some Considerations on Ground Water Dating Using Environmental Isotopes. Hydrogeology in the Service of Man, Memoires of the 18th Congress of the International Association of Hydrogeologists, Cambridge.

Fröhlich, K., Gibson, J.J., Aggarwal, P.K., 2002. Deuterium Excess in Precipitation and its Climatological Significance. Proceedings of the IAEA conference Study of Environmental Change using Isotope Techniques, 23-27 April 2001, Vienna.

Froehlich, K., Kralik, M., Papesch, W., Rank, D., Scheifinger, H., Stichler, W., 2008. Deuterium excess in precipitation of Alpine regions – moisture recycling. Isotopes in Environmental and Health Studies 44(1), 61–70.

Fryberger, S.G., Al-Sari, A.M., Clisham, T.J., Rizvi, S.A.R., Al-Hinai, K.G., 1984. Wind sedimentation in the Jafurah sand sea, Saudi Arabia. Sedimentology 31, 413–431.

Gambell, A.W., Fisher, D.W., 1964. Occurrence of Sulfate and Nitrate in Rainfall. Journal of Geophysical Research 69(20), 4203–4210.

Gat, J.R., 1971. Comments on the Stable Isotope method in Regional Groundwater Investigations. Water Resources Research 7(4), 980–993.

Gat, J.R., 1984. The stable isotope composition of Dead Sea waters. Earth and Planetary Science Letters 71, 361–376.

GDC – Groundwater Development Consultants, 1980. Umm Er Radhuma Study, Vol. 3, Annex I: Groundwater Chemistry. Ministry of Agriculture and Water, Riyadh.

Goldberg, E.D., 1963. The Oceans as a Chemical System, In: Hill, M.N. (ed.), The Sea – Ideas and Observations on Progress in the Study of the Seas, Vol. 2: The Composition of Sea-Water, Comparative and Descriptive Oceanography. John Wiley & Sons, New York, 3–25.

Handy, A.H., Tucker, R.A., 1984. Rainfall Quality at Selected Sites in Saudi Arabia. Ministry of Agriculture and Water, Water Resources Development Department, open file report 84-604.

Hughes, C.E., Crawford, J., 2012. A new precipitation weighted method for determining the meteoric water line for hydrological applications demonstrated using Australian and global GNIP data. Journal of Hydrology 464–465, 344-351.

IAEA/WMO – International Atomic Energy Agency/World Meteorological Organization, 2015. Global Network of Isotopes in Precipitation. The GNIP Database. http://www.iaea.org/water (last access: 31 July 2015).

Job, C., Moser, H., Rauert, W., Stichler, W., 1978. Chemistry and Isotope Content of Some Wadi Groundwaters in the Central Parts of the Tuwayq Mountains. In: Al- Sayari, S.S., Zötl, J.G. (eds.), Quaternary Period in

Saudi Arabia, Vol. 1: Sedimentological, Hydrogeological, Hydrochemical, Geomorphological, and Climatological Investigations in Central and Eastern Saudi Arabia. Springer, Vienna/New York, 216–226.

JRCC/PME – Jeddah Regional Climate Center South West Asia/Presidency of Meteorology and Environment, 2015. Climate Data for Saudi Arabia. http://jrcc.sa/climate_data_observatory_sa.php (last access: 17 February 2015).

Kattan, Z., 1997. Chemical and environmental isotope study of precipitation in Syria. Journal of Arid Environments 35, 601–615.

Kazemi, G.A., Lehr, J.H., Perrochet, P., 2006. Groundwater Age. Wiley, Hoboken.

Khalaf, F.I., Al-Kadi, A., Al-Saleh, S., 1985. Mineralogical Composition and Potential Sources of Dust Fallout Deposits in Kuwait, Northern Arabian Gulf. Sedimentary Geology 42, 255–278.

Kubota, T., Tsuboyama, Y., 2003. Intra- and inter-storm oxygen-18 and deuterium variations of rain, throughfall, and stemflow, and two-component hydrograph separation in a small forested catchment in Japan. Journal of Forest Research 8, 179–190.

Leguy, C., Rindsberger, M., Zangwil, A., Issar, A., Gat, J.R., 1983. The Relation Between the ^{18}O and Deuterium Contents of Rain Water in the Negev Desert and Air-Mass Trajectories. Isotope Geoscience 1, 205–218.

Masarik, J., Beer, J., 1999. Simulation of particle fluxes and cosmogenic nuclide production in the Earth's atmosphere. Journal of Geophysical Research 104(D10), 12099–12111.

MAW – Ministry of Agriculture and Water, 1984. Water Atlas of Saudi Arabia. MAW, Riyadh.

Modaihsh, A.S., 1997. Characteristics and composition of the falling dust sediments on Riyadh city, Saudi Arabia. Journal of Arid Environments 36, 211–223.

Natural Earth, 2015. http://www.naturalearthdata.com (last access: 23 June 2015).

Notaro, M., Alkolibi, F., Fadda, E., Bakhrjy, F., 2013. Trajectory analysis of Saudi Arabian dust storms. Journal of Geophysical Research – Atmospheres 118, 6028–6043.

Pósfai, M., Axisa, D., Tompa, E., Freney, E., Bruintjes, R., Buseck, P.R., 2013. Interactions of mineral dust with pollution and clouds: An individual-particle TEM study of atmospheric aerosol from Saudi Arabia. Atmospheric Research 122, 347–361.

Powers, R.W., Ramirez, L.F., Redmond, C.D., Elberg, E.L., 1966. Geology of the Arabian Peninsula – Sedimentary Geology of Saudi Arabia. USGS, Washington D.C.

Roether, W., 1967. Estimating the Tritium Input to Groundwater from Wine samples: Groundwater and Direct Run-Off Contribution to Central European Surface Waters. Proceedings of the IAEA conference Isotope in Hydrology, 14-18 November 1966, Vienna.

Rolph, G.D., 2015. Real-time Environmental Applications and Display sYstem (READY). http://www.ready.noaa.gov (last access: 17 February 2015), NOAA Air Resources Laboratory, College Park, MD.

Salameh, E., Rimawi, O., 1988. Hydrochemistry of Precipitation of Northern Jordan. International Journal of Environmental Studies 32, 203–216.

Sanford, W.E., Wood, W.W., 2001. Hydrology of the coastal sabkhas of Abu Dhabi, United Arab Emirates. Hydrogeology Journal 9, 358–366.

Shampine, W.J., Dincer, T., Noory, M., 1979. An Evaluation of Isotope Concentrations in the Groundwater of Saudi Arabia. Proceedings of the IAEA conference Isotope Hydrology 1978, Vol. 2, 19-23 June 1978, Vienna.

Sonntag, C., Neureuther, P., Kalinke, C., Münnich, K.O., 1976. Zur Paläoklimatik der Sahara – Kontinentaleffekt im D- und ^{18}O-Gehalt pluvialer Saharawässer. Naturwissenschaften 63, 479.

Subyani, A.M., 2004. Use of chloride-mass balance and environmental isotopes for evaluation of groundwater recharge in the alluvial aquifer, Wadi Tharad, western Saudi Arabia. Environmental Geology 46, 741–749.

Sültenfuß, J., Roether, W., Rhein, M., 2009. The Bremen mass spectrometric facility for the measurement of helium isotopes, neon, and tritium in water. Isotopes in Environmental and Health Studies 45(2), 83–95.

Tutiempo Network, S.L., 2015. http://www.tutiempo.net/en/Climate/Riyadh/404380.htm (last access: 17 February 2015).

USGS/ARAMCO – United States Geological Survey/Arabian American Oil Company, 1963. Geologic Map of the Arabian Peninsula. Miscellaneous Geologic Investigations, Map I-270 A, scale 1:2,000,000. USGS, Washington D.C.

Wagner, W., 2011. Groundwater in the Arab Middle East. Springer, Berlin/Heidelberg.

Wagner, W., Geyh, M.A., 1999. Application of Environmental Isotope Methods for Groundwater Studies in the ESCWA Region. Geologisches Jahrbuch C(67), Schweizerbart'sche Verlagsbuchhandlung, Stuttgart, Germany.

Weather Underground, Inc., 2015. http://www.wunderground.com/q/locid:SAXX0018 (Almanac function, last access: 17 February 2015).

Weyhenmeyer, C.E., Burns, S.J., Waber, H.N., Macumber, P.G., Matter, A., 2002. Isotope study of moisture sources, recharge areas, and groundwater flow paths within the Eastern Batinah coastal plain, Sultanate of Oman. Water Resources Research 38(10), 1184.

Wushiki, H., 1991. $^{18}O/^{16}O$ and D/H of the Meteoric Waters in South Arabia. Mass Spectroscopy 39(5), 239–250.

Xie, L., Wei, G., Deng, W., Zhao, X., 2011. Daily $\delta^{18}O$ and δD of precipitations from 2007 to 2009 in Guangzhou, South China: Implications for changes of moisture sources. Journal of Hydrology 400, 477–489.

Preface to Chapter 3

Sandy deserts are a dominant feature on the Arabian Peninsula. They cover more than 770,000 km² (Edgell, 2006), which is roughly twice the size of Germany.

These sands have been the subject of numerous studies with a broad range of topics including grain morphologies, heavy mineral spectra, dune ages, vegetation, dune movement and stabilization options (Edgell, 2006; and references therein; El-Nozahy, 1993). Yet, given the enormous size of the sand seas and the crucial role of water in a desert country like Saudi Arabia, the number of studies addressing water in this environment is surprisingly small. One reason might be that water transport and groundwater recharge in dune sands are subtle phenomena – in contrast to karst settings, where the mentioned processes can be rather eye-catching (Michelsen et al., 2016, see Chapter 6; Schulz et al., 2016).

The following chapter presents a study of water in Saudi Arabian dune sands utilizing an isotope-based approach. Although the covered scale is rather small, such studies hold the potential to provide interesting insights and to identify promising paths for future research.

References

Edgell, H.S. (2006). Arabian Deserts – Nature, Origin and Evolution. Springer, Dordrecht.

El-Nozahy, 1993. Grain morphology, grain size and mineralogical composition of linear dune sands, Ad Dahna desert, Saudi Arabia. Neues Jahrbuch für Geologie und Paläontologie – Abhandlungen 188(3), 265–288.

Michelsen, N., Dirks, H., Schulz, S., Kempe, S., Al-Saud, M., Schüth, C., 2016. YouTube as a crowd-generated water level archive. Science of the Total Environment 568, 189–195.

Schulz, S., de Rooij, G. H., Michelsen, N., Rausch, R., Siebert, C., Schüth, C., Al-Saud, M., Merz, R., 2016. Estimating groundwater recharge for an arid karst system using a combined approach of time-lapse camera monitoring and water balance modelling. Hydrological Processes 30, 771–782.

3. Isotopic composition of pore waters in Saudi Arabian dune sands: implications for deep infiltration, evaporation losses, and groundwater recharge estimations

Nils Michelsen [a,*], Anja Toegl [a], Paul Koeniger [b], Stephan Schulz [a], Christoph Schüth [a]

[a] Technische Universität Darmstadt, Institute of Applied Geosciences, Schnittspahnstraße 9, 64287 Darmstadt, Germany

[b] Bundesanstalt für Geowissenschaften und Rohstoffe, Stilleweg 2, 30655 Hannover

* Corresponding author (michelsen@geo.tu-darmstadt.de)

Submitted for publication

3.1. Abstract

The stable isotope ratios $^{18}O/^{16}O$ and $^{2}H/^{1}H$ are a powerful tool in water resources studies. In Saudi Arabia, this tool has been intensively applied to nearly all elements of the water cycle. However, the potential of unsaturated zone isotope studies has not been fully tapped, although this critical zone represents the link between precipitation and the much relied upon groundwater resources. Here, we evaluate water contents and isotope fingerprints of three sand dune profiles from Central Saudi Arabia – two own profiles and one from the literature. The sands are relatively dry (gravimetric soil moisture <4 %) and the pore water isotope signatures fall below the Local Meteoric Water Line, suggesting pronounced evaporation. Applying an isotope model, we calculate evaporation trajectories whose intersections with the Local Meteoric Water Line are deemed to represent the original pre-evaporation isotopic compositions. This exercise helps to constrain rain events responsible for deep percolation – large events (probably tens of millimeters) with a depleted isotopic composition (on average -6.20 and -17.6 ‰ for $\delta^{18}O$ and $\delta^{2}H$, respectively). Interestingly, the identified fingerprint does not match the isotopic signature of precipitation in the area. Given the limited nature of the latter data set (mostly 2009–2013), it seems likely that long-term monitoring efforts are necessary to capture seldom rain events causing efficient infiltration into dune sands, in Saudi Arabia and elsewhere. The resulting improved understanding of the entire isotopic inventory of rain at a given site would reduce the risk of misinterpreting apparent isotopic mismatches between pore (and ground-)waters and precipitation.

3.2. Introduction

The stable isotope ratios of oxygen and hydrogen in the water molecule, $^{18}O/^{16}O$ and $^{2}H/^{1}H$, serve as valuable tracers in water resources assessments, particularly in arid areas (Clark and Fritz, 1997; Gat, 1971, 2010). In Saudi Arabia, one of the world's most water-scarce countries, this tool has been applied to various components

of the water cycle, including precipitation (Alyamani, 2001; Michelsen et al., 2015; Subyani, 2004), surface runoff (Al-Sayari and Zötl, 1978; Subyani, 2004), springs and wells (Al-Sayari and Zötl, 1978; Shampine et al., 1979; Sultan et al., 2008, 2019), seawater (Al-Sayari and Zötl, 1978; Schulz et al., 2015), and even bottled waters (Basheer et al., 2018).

However, the unsaturated zone (particularly dune sands) has received comparatively little attention. This is surprising for a number of reasons. i) This critical zone represents the link between precipitation and the much relied upon groundwater resources. ii) A number of technical developments in the last two decades has facilitated the generation of soil water isotope data (Koeniger et al., 2016; Sprenger et al., 2016), which can also be helpful in the groundwater recharge context (Gaj et al., 2016). iii) In Saudi Arabia, sand dunes are deemed a recharge-favoring environment due to rapid infiltration (Al-Turbak and Al-Hassoun, 1992; Dincer et al., 1974), particularly if the "extinction depth" is reached below which evaporative loss is negligible (Mughal et al., 2015). iv) Eolian sands cover about half of the country's sedimentary area (Powers et al., 1966; USGS/ARAMCO, 1963).

Yet, a few unsaturated zone studies do exist, for example by Dincer et al. (1974) and Al-Sagaby and Moallim (1996, 2001). The former authors investigated pore waters in the Dahna dune belt, about 100 km NE of Riyadh (Fig. 3-1). Although their multi-method approach comprised stable isotope analyses, their evaluation remained somewhat qualitative and the reported direct recharge estimate (approx. 20 mm/a) is solely based on tritium data (^{3}H peak displacement method). The work by the latter authors suffered from analytical constraints. Samples by Al-Sagaby and Moallim (1996) were analyzed in two laboratories, reporting differing results ($\delta^{2}H$ deviations partly >10 ‰). The samples obtained by Al-Sagaby and Moallim (2001) were only analyzed for $\delta^{2}H$ (no $\delta^{18}O$ data available).

It is also noteworthy that, at the time of the mentioned studies, no robust data on the isotopic composition of precipitation were available for Central Saudi Arabia. This knowledge is, however, indispensable to understand pore water stable isotope signals (Sprenger et al., 2016). Without such data it is, for example, not possible to quantify and evaluate evaporation-induced isotopic shifts. As a workaround, Dincer et al. (1974) considered data from Bahrain, the closest monitoring station of the Global Network of Isotopes in Precipitation (GNIP; IAEA/WMO, 2019), despite the distance of about 300 km and an elevation difference of approx. 500 m.

Hence, we here revisit the topic of pore water stable isotope fingerprints in Saudi Arabian dune sands. In doing so, we are particularly interested in a comparison with now available data on the isotopic signature of local rain (Michelsen et al., 2015) and in the question which rain events trigger deep percolation into the prevailing sand dunes.

3.3. Study site

The study site (24°11’47”N, 46°0’20”E) is a shallow, unvegetated interdune valley located about 90 km SW of Riyadh (Fig. 3-1). The area features a set of sub-parallel dune ridges and belongs to the Nafud Qunayfidah, a 2,900 km² large dune field confined in a NW–SE striking valley between two sedimentary escarpments (Edgell, 2006). At the study site, the dunes overlie the Minjur sandstone (Upper Triassic) representing an important aquifer that is used to supply water to the capital (Al-Sagaby and Moallim, 1996).

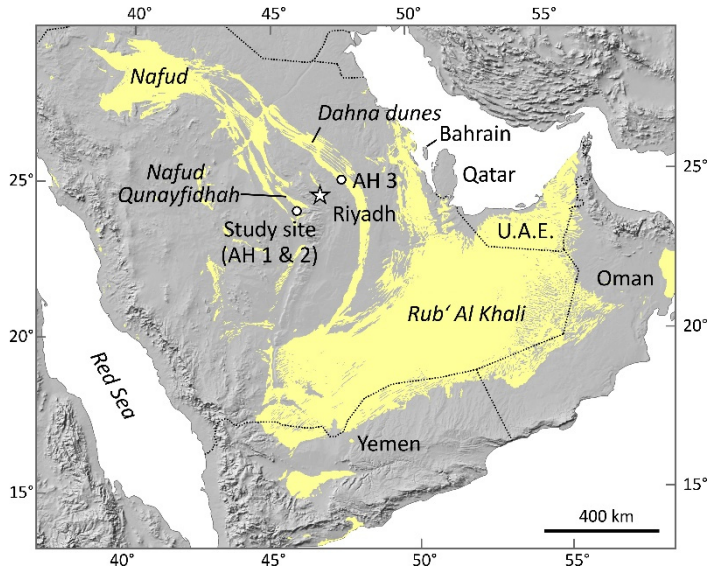

Fig. 3-1. Map of the Arabian Peninsula with eolian sands shown in yellow (USGS/ARAMCO 1963; shaded relief from Natural Earth, 2015). The study site (auger holes AH 1 & 2) is located approx. 90 km SW of Riyadh. AH 3 represents the study site of Dincer et al. (1974).

The area exhibits a hot desert climate (Köppen-Geiger class BWh). The closest weather station (Riyadh) reports a mean annual temperature of 26.8°C and a mean relative humidity of 26 % over a monitoring period from 1985 to 2010. Annual precipitation averages at 93 mm, with most rains occurring between November and May (JRCC/PME, 2016; Fig. A3-1).

The wind regime is bidirectional. Between May and September, N is the prevailing wind direction. From October to April, winds from SSE dominate (Riyadh data; JRCC/PME, 2016). This bidirectional pattern, likely promoted by the geomorphological setting in a valley, causes seasonal switching of windward and leeward sides and apparently results in reversing dunes (McKee, 1979). This means that the dune shape changes seasonally (slip face alternation), which is associated with appreciable sediment movement. The latter was also noted during field visits (seasonal changes of the upper 50 cm in the dune valley). Even short-term changes could occasionally be observed, for instance during a storm in May 2013. However, the general position of the surrounding dunes did apparently not change over several years.

3.4. Methods

For sampling, we used a manual auger set (Eijkelkamp, Giesbeek, Netherlands). The first auger hole (AH 1) was drilled on 9 November 2012. The main purpose was to test the auger and the selected "Riverside" bit under the prevailing conditions. Due to the rather dry nature of the upper meter, this section was stabilized with an improvised assembly consisting of an inverted traffic cone and a short piece of PVC pipe found on-site (Fig. A3-2). Preliminary samples were collected in 1 m intervals (max. depth 6 m) and packed into PE bags (three layers). The second auger hole (AH 2) was created in a distance of 3 m from AH 1 on 22 November 2012, largely using the same technique (stabilization with a 1 m PVC pipe; Fig. A3-3). Sampling intervals varied somewhat and were shorter in the upper section but increased downwards (Table 3-1).

In the laboratory, water was obtained from the samples by cryogenic vacuum extraction in a distillation line similar to that of West et al. (2006). The sand was heated with a heating mantle (200°C) for 3 h and the water was collected in a cold trap immersed in liquid nitrogen. While cryogenic vacuum extraction is commonly considered as a standard technique, it has potential for artefacts, like other methods applied for water extractions (Gaj et al., 2017; Koeniger et al., 2011; Orlowski et al., 2016a, 2016b, 2018; Sprenger et al., 2015). However, we note that dune sands with low silt and clay contents (1 to 6 %) and negligible organic matter concentrations (loss on ignition <0.6 %; see Appendix 3) are probably least prone to such artefacts.

Gravimetric water contents (θ_g) were calculated based on differences in sample mass prior to and after water extraction (Hasselquist et al., 2018; Mahindawansha et al., 2018).

The obtained water was analyzed for its stable isotope signature by Laser Cavity Ring-Down Spectroscopy (L2130-i by Picarro, Santa Clara, CA, USA). Results were expressed in per mil (‰) using the conventional δ-notation relative to Vienna Standard Mean Ocean Water (V-SMOW). The external precisions for $\delta^{18}O$ and $\delta^{2}H$, determined by repeated analyses of a control sample, were ±0.1 ‰ and ±0.8 ‰, respectively.

To indicate deviations from the Local Meteoric Water Line (LMWL), we used the line-conditioned excess (lc-excess; Landwehr and Coplen, 2006), recently experiencing increased popularity (Sprenger et al., 2016):

$$\text{lc-excess} = \delta^{2}H - a \cdot \delta^{18}O - b \qquad (3\text{-}1)$$

where a and b are the slope and the intercept of the LMWL (here $\delta^{2}H = 5.22 \cdot \delta^{18}O + 14.8$ ‰; Michelsen et al., 2015).

In addition, we calculated the deuterium excess d (Dansgaard, 1964) to express deviations from the Global Meteoric Water Line (GMWL; Craig, 1961):

$$d = \delta^{2}H - 8 \cdot \delta^{18}O \qquad (3\text{-}2)$$

3.5. Results and interpretation

The results of the gravimetric water content and isotope analyses for the auger holes AH 1 and 2 are presented in Table 3-1. For comparison, the table also features data from the Dahna dunes by Dincer et al. (1974) from July 1972 (denoted AH 3). All these data are visualized as profiles in Fig. 3-2.

Table 3-1. Gravimetric water contents and pore water stable isotope signatures of the studied dune sands (AH 1 and AH 2). For comparison, data from Dincer et al. (1974) are included (AH 3). The lc-excess and d values are a measure for the deviation from the LMWL (Riyadh; Michelsen et al., 2015) and the GMWL. $\delta^{18}O_{orig}$ and $\delta^{2}H_{orig}$ represent derived original (pre-evaporation) signatures of selected samples (see Section 3.6.1.) and x denotes the calculated fractional evaporative losses (see Section 3.6.2.).

AH	Depth [cm]	θ_g [%]	$\delta^{18}O$ [‰]	$\delta^{2}H$ [‰]	lc-excess [‰]	d [‰]	$\delta^{18}O_{orig}$ [‰]	$\delta^{2}H_{orig}$ [‰]	x [-]
1	100	1.3	16.00	43.7	-55	-84	-	-	-
1	200	1.8	20.95	60.6	-64	-107	-	-	-
1	300	1.8	9.84	27.0	-39	-52	-6.14	-17.3	0.36
1	400	2.0	6.42	21.9	-26	-29	-4.21	-7.2	0.25
1	500	2.2	8.49	25.0	-34	-43	-5.39	-13.3	0.32
1	600	1.9	8.73	29.2	-31	-41	-3.82	-5.1	0.30
2	33	0.4	23.66	61.6	-77	-128	-	-	-
2	43	0.6	25.14	62.7	-83	-138	-	-	-
2	53	0.9	23.03	49.4	-86	-135	-	-	-
2	60	0.8	21.41	58.7	-68	-113	-	-	-
2	67	0.9	22.35	63.6	-68	-115	-	-	-
2	75	1.2	19.94	58.6	-60	-101	-	-	-
2	85	0.9	18.75	49.0	-64	-101	-	-	-
2	95	0.9	16.58	46.0	-55	-87	-	-	-
2	105	0.6	19.06	38.8	-76	-114	-	-	-
2	125	0.9	16.71	41.2	-61	-92	-	-	-
2	145	1.0	13.47	27.8	-57	-80	-10.52	-40.1	0.50
2	165	2.2	11.71	27.6	-48	-66	-8.22	-28.1	0.43
2	185	2.0	11.90	23.3	-54	-72	-10.44	-39.7	0.47
2	205	1.7	8.65	24.7	-35	-45	-5.63	-14.6	0.33
2	255	2.1	10.64	20.5	-50	-65	-10.08	-37.8	0.45
2	333	2.0	6.62	16.1	-33	-37	-6.93	-21.4	0.31
2	355	2.2	6.19	12.6	-34	-37	-7.93	-26.6	0.32
2	400	1.9	7.62	18.7	-36	-42	-7.00	-21.7	0.34
2	450	2.0	6.84	17.5	-33	-37	-6.56	-19.4	0.31
2	500	2.0	3.52	10.8	-22	-17	-5.46	-13.7	0.22
3	45	1.6	-	22	-	-	-	-	-
3	90	2.0	-0.9	2	-8	9	-4.13	-6.8	0.08
3	170	2.4	1.1	9	-12	0	-3.49	-3.4	0.12
3	350	2.9	4.7	13	-26	-25	-5.95	-16.3	0.25
3	430	3.7	5.7	17	-28	-29	-5.42	-13.5	0.27
3	500	3.7	-	14	-	-	-	-	-
3	555	1.9	-	-	-	-	-	-	-
3	600	2.7	5.1	17	-24	-24	-4.73	-9.9	0.24
3	650	3.0	4	12	-24	-20	-5.55	-14.2	0.23
						arithmetic mean	-6.38	-18.5	0.31
						moisture-weighted mean	-6.20	-17.6	0.29

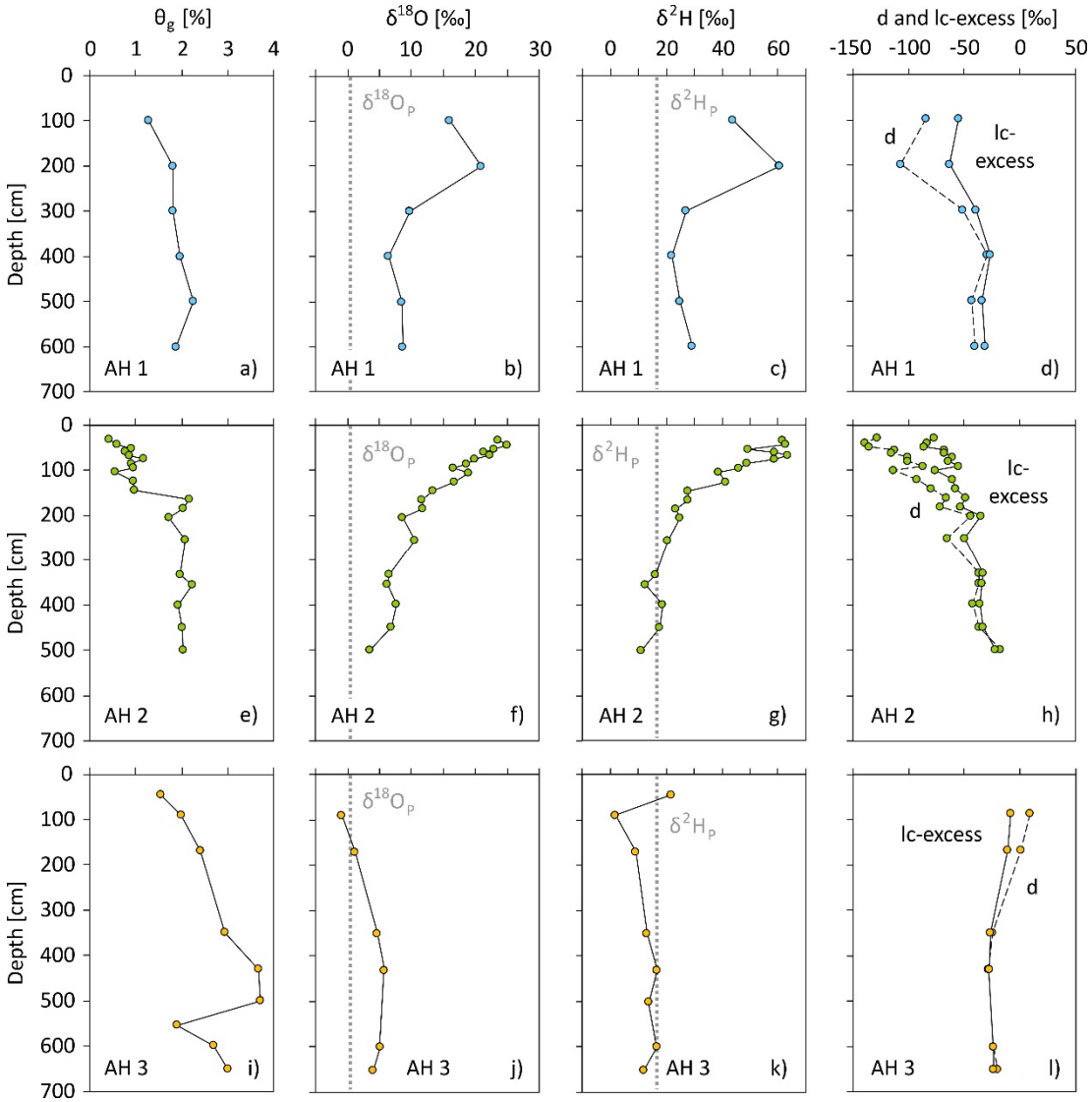

Fig. 3-2. Gravimetric water content, stable isotope, lc-excess, and d profiles for AH 1 (a-d) and AH 2 (e-h) from this study and AH 3 (i-l) from the study by Dincer et al. (1974). Dotted lines in the stable isotope plots indicate the precipitation-weighted mean δ values of Riyadh precipitation ($\delta^{18}O_P$=0.37 ‰, $\delta^{2}H_P$=16.7 ‰; Michelsen et al., 2015).

The gravimetric water contents in AH 1 and 2 are low (<2.5 %), particularly in the upper meter. Below, the values scatter around 2 %. They are hence slightly lower than the water contents of Dincer et al., (1974; 2 to 4 % at depth). Overall, such values and the increasing trend down to a certain depth are typical for Saudi Arabian dune sands. Dincer, for instance, had also collected samples from the Nafud Qunayfidah (in November 1972) and reported water contents below 1 % at the surface and 2 to 3 % at depth (Dincer, 1982).

The stable isotope profiles for AH 1 and 2 show elevated values at the top, reaching more than 20 ‰ ($\delta^{18}O$) and more than 60 ‰ ($\delta^{2}H$). Here, they clearly exceed the precipitation-weighted mean δ values for Riyadh precipitation ($\delta^{18}O_P$=0.37 ‰, $\delta^{2}H_P$=16.7 ‰; Michelsen et al., 2015). At depth, the values stabilize somewhat and fluctuate around 5 to 10 ‰ ($\delta^{18}O$) and around 15 to 25 ‰ ($\delta^{2}H$). The latter range roughly coincides with the

mean δ^2H value for Riyadh precipitation, but the $\delta^{18}O$ values are comparatively high. The AH 3 values are overall lower and hence closer to the precipitation values.

The outlined pattern with high δ values at the top and lower and more stable values at depth is typical for arid settings (Allison and Barnes, 1983; Barnes and Allison, 1983, 1988; Gaj et al., 2016; Tewolde et al., 2019). The enriched section at the top is interpreted as being the result of evaporation (note the lower water contents) and the associated fractionation. Pore waters in greater depths, by contrast, cannot readily evaporate due to the thickness of the stagnant boundary layer.

Despite this match with literature data, the particular shape in the upper part and the depth of greatest enrichment (Allison and Barnes, 1983) should not be over-interpreted (see Koeniger et al., 2016), because of i) our partly large sampling intervals and ii) the sediment dynamics in the top 50 cm (see Section 3.3.).

The isotope profiles are mirrored by the lc-excess and d values (Fig. 3-2). All lc-excess values are negative and in AH 1 and 2 they reach -86 ‰. The corresponding d values are also low and reach -138 ‰. Such low values indicate a remarkable deviation from the LMWL and the GMWL and call for a closer look in the dual isotope space (Fig. 3-3).

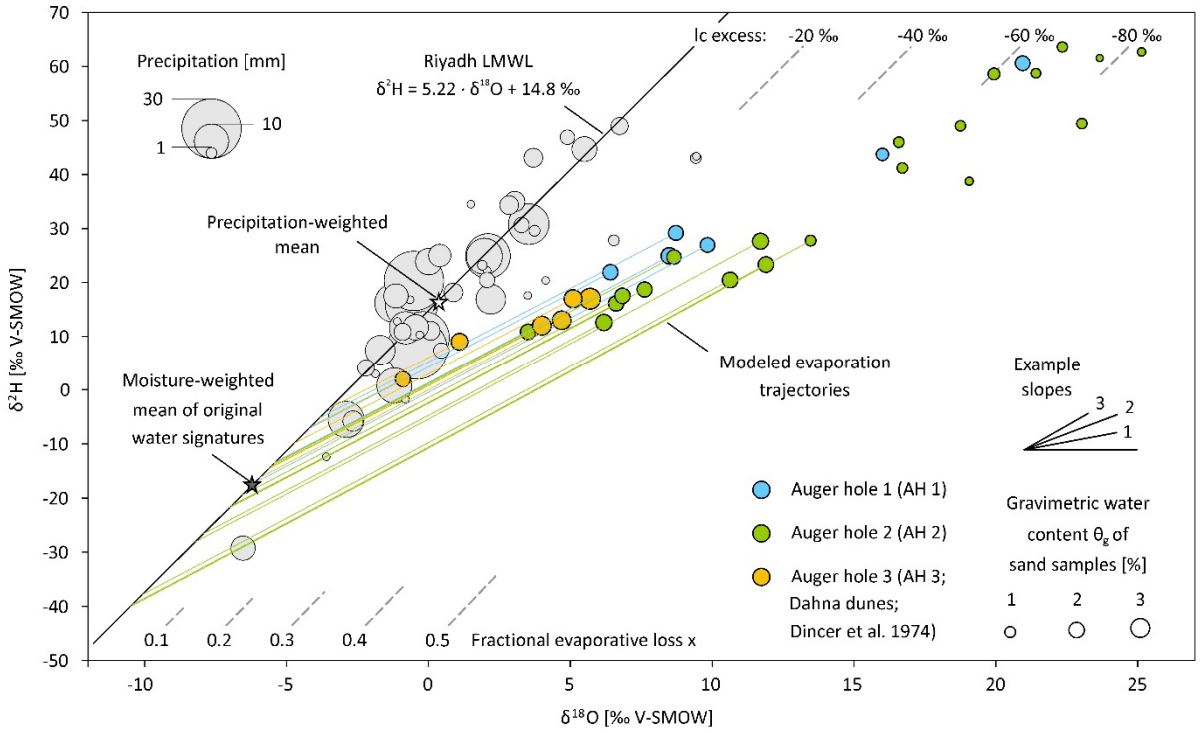

Fig. 3-3. Relation between δ^2H and $\delta^{18}O$ for the studied pore waters (water content θ_g represented by bubble size). For comparison, isotopic data on Riyadh rain events (grey) and the corresponding LMWL are included (rain amount as bubble size; Michelsen et al., 2015). Colored lines are modeled, nearly linear evaporation trajectories (see Section 3.6.1.).

Here, all pore water data points plot below the LMWL and mostly away from the grey circle symbols representing rain events. This particularly applies to waters from the drier parts of the profiles (smaller bubbles). These samples show lc-excess values in the range -55 to -86 ‰ (note the dashed lines at the top of the chart), indicating strong evaporative enrichment. Given their position within the profiles and the low water contents, these waters are unlikely to contribute to groundwater recharge.

Pore waters from the slightly moister samples in the center of the chart ($\delta^{18}O$<15 ‰), corresponding to depths greater than 2 m (AH 1) and 1.4 m (AH 2), are less enriched and plot closer to the Dincer et al. (1974) data points (AH 3). The latter are apparently less evaporation-affected (also note the slightly higher soil moistures, Fig. 3-2). Such pore waters are more likely to eventually become groundwater (Dincer, 1982; Dincer et al., 1974) and we will focus on this group in the following section.

3.6. Discussion

3.6.1. Original water signature

The outlined patterns raise the question which rain events trigger effective infiltration into the dune sands. In this context, the position of the data points in relation to the precipitation-weighted mean composition of Riyadh rain in the dual isotope plot (white star in Fig. 3-3) is noteworthy. While most of the pore waters are relatively enriched in ^{18}O, the $\delta^{2}H$ values often do not differ much from the rain value. Partly, the pore waters are even lighter than the average rain in terms of ^{2}H, implying that it is not necessarily the reported average rain that leads to deep percolation.

Although it is popular to fit a straight “evaporation line” through pore water data points and read the pre-evaporation composition, i.e., the original water signature, from its intersection with the LMWL (Clark and Fritz, 1997; Gat, 2010; Gates et al., 2008; Jin et al., 2018), we refrain from doing so here. Benettin et al. (2018) have alerted the community that such straight regression lines are often a by-product of seasonality effects. Hence, the intersection is entirely driven by geometric considerations and has no significance in its own right. The authors emphasize that isotopic compositions of pore waters are often not related to a single, unique source water, but result from evaporation trajectories that start from seasonally differing original signatures. Hence, they recommend to reconstruct pre-evaporation signatures by modeling an evaporation trajectory for each data point. The intersections with the LMWL then represent the seasonal starting points, which can be averaged.

Following Benettin et al. (2018), we apply the simple and widely used Craig and Gordon (1965) model to construct evaporation trajectories (for details, see Appendix 3). In our case, there is no classical seasonal trend in the isotopic composition of rainfall (Michelsen et al., 2015). Instead, rain mainly occurs erratically between November and May and shows large isotopic inter-event variability, justifying the assumption of an isotopically non-unique soil moisture source. Due to typically large infiltration capacities of Saudi Arabian dune sands (Al-

Turbak and Al-Hassoun, 1992; Dincer et al., 1974) we presume rapid infiltration, followed by slow subsurface evaporation. This means that our model does not require temperature and relative humidity values for each notional event, but warrants the use of annual means (26.8°C and 26 %, respectively; see Section 3.3.).

As data on the isotopic composition of atmospheric vapor δ_A are not available for the area, we assume equilibrium with precipitation (see Gibson et al., 2008). For the latter, we consider the precipitation-weighted mean δ values of Riyadh rainfall (see above).

Finally, we have to set the turbulence parameter n. While for evaporation from open water bodies (e.g., lakes) it is common to use 0.5, the non-turbulent conditions in our case (molecular diffusion through the pore framework) call for a value of 1 (Barnes and Allison, 1983; Benettin et al., 2018; Dubbert et al., 2013; Horita et al., 2008).

With these parameters, we model evaporation trajectories. We initially choose random points on the LMWL and iteratively shift them along the LMWL until the obtained trajectories fit the pore water signatures (colored, nearly straight lines in Fig. 3-3, Fig. A3-4 to A3-6).

The thus obtained individual $\delta^{18}O_{orig}$ and $\delta^{2}H_{orig}$ values range from -10.52 to -3.82 ‰ and from -40.1 to -5.1 ‰, respectively (Table 3-1, Fig. 3-3). While the outlined approach implies “separate water parcels” and piston flow, we are aware that some mixing does occur (through advection, dispersion, and diffusion) and hence average these values. To this end, we consider the associated gravimetric water contents as weighting factors ($\delta_{orig} = (\sum\theta_i \cdot \delta_i)/\sum\theta_i$) and calculate moisture-weighted means of -6.20 and -17.6 ‰, respectively.

Interestingly, this composition deviates from the weighted mean precipitation signature. In fact, it even lies in a part of the plot that is devoid of rain event data points. Yet here, we have to consider the limited temporal extent of the used rain data (mainly 2009–2013). Probably, it is particularly large rain events (likely tens of millimeters) with depleted isotopic signatures (Dincer et al., 1974; see also Jasechko and Taylor, 2015) that cause rapid and deep percolation, but such events were not captured by Michelsen et al. (2015). While Saudi Arabia is largely arid, it occasionally experiences large rain events. In the western part of the country, Walters (1989) studied an event that locally yielded 177 mm within 3 h (23 April 1985). For Riyadh, the largest daily rain on record accounts for about 53 mm (21 March 1995; JRCC/PME, 2016) and return periods of 18 and 50 years have been estimated for daily rains of 40 and 50 mm, respectively (Al-Saleh, 1997).

3.6.2. Evaporative losses

The modeling exercise does not only shed light on the pre-evaporation signature, but also indicates fractional evaporative losses x [-] along each trajectory (dashed lines at the bottom of Fig. 3-3, see also Fig. A3-4 to A3-6). The losses range between 0.08 and 0.50 (Table 3-1) and average at about 0.3.

The modeled losses make it tempting to calculate a first-order soil water balance for the wetter profile sections. To this end, one could simply multiply the mean fractional evaporative loss (0.3) with the long-term annual precipitation amount (93 mm) to obtain the evaporation depth (28 mm). Given that surface runoff is negligible in such dune areas (Dincer et al., 1974) and transpiration is also no relevant process (see Section 3.3.), one could then subtract this value from the precipitation for a rough recharge estimate. This yields an apparent recharge of 65 mm/a. Although tritium has been found in dune sand pore waters of the region (Al-Sagaby and Moallim, 1996; Dincer et al., 1974; see Section 3.2.) and soil moisture in the first few meters increased rapidly after rain events at a nearby dune site (Siebert et al., 2016), the obtained recharge value seems rather high. Other annual recharge estimates for Saudi Arabian dunes account for 0.5 mm (Engelhardt et al., 2013), 1.8 mm (Al-Sagaby and Moallim, 2001), 4 mm (Wagner, 2011), 20 mm (Dincer et al., 1974), and 30 mm (Al-Sagaby and Moallim, 1996). While they show significant scatter, none is close to our first-order estimate.

The shortcoming of this calculation is that the fractional evaporative loss does not represent the entire evaporation. It only reflects the partial loss experienced by waters that found their way into the deeper part of our profile and that are probably associated with larger rain events. Small isolated events, by contrast, only wet the surface or the first few centimeters of the dune sand, where they are prone to complete evaporation (see Gat, 2010). This means that they never leave their isotopic fingerprint in the pore waters at depth (see also Sonntag et al., 1985). Hence, this kind of water balance is misleading, rendering the associated recharge value unreliable.

3.7. Conclusions and outlook

The encountered pore water isotope signatures all fall below the LMWL and show very negative lc-excess values, indicating pronounced evaporative losses. While the latter were quantified with a Craig and Gordon (1965) model for the lower, wetter part of the sand dune profiles, they cannot not be used for a reliable, general soil water balance. Hence, we are unable to provide a groundwater recharge estimate. For this purpose, artificial ^{2}H-labelling and peak displacement tracking in the unsaturated zone might be more promising (see Beyer et al., 2015).

Nevertheless, the modeling exercise indicated that mainly large, isotopically depleted rain events cause deep infiltration. Since the corresponding isotopic fingerprint was absent in the rain data set by Michelsen et al. (2015), it seems that the latter study was too short to capture such rain events. In view of reported return periods of 18 and 50 years for daily rains of 40 and 50 mm (Al-Saleh, 1997), this is however not surprising.

Here, particular care must be taken to not misinterpret the isotope data. Given the presence of tritium in the unsaturated zone (Al-Sagaby and Moallim, 1996; Dincer et al., 1974) and rapid soil moisture response after rain events at a nearby dune site (Siebert et al., 2016), it is likely that the pore waters in the first meters of dune

sands are of modern age (months to decades). However, the mismatch between the derived original signatures and the average rain fingerprint could, in principle, be deemed to indicate a great water age (i.e., paleowater, see Gat, 1971).

To avoid misinterpretations, we need a better overview of possible isotopic rainfall fingerprints at a given site. Interestingly, a few years of precipitation isotope data are often considered sufficient and calls for long-term data sets are mostly focused on the detection of climate change via isotopes (Eastoe and Dettman, 2016). However, in settings like ours, we also need long data series to capture the entire isotopic inventory of local precipitation. Given the availability of suitable cumulative rain collectors minimizing post-sampling evaporation (summarized in Michelsen et al., 2018, 2019) and laser-based isotope analyzers that have lowered analytical efforts and costs (Kerstel et al., 1999; Lis et al., 2008), it is time to initiate such a monitoring program, in Saudi Arabia and other (semi-)arid areas.

3.8. Acknowledgments

We thank Marcel Horovitz for assistance during fieldwork and Mustefa Reshid for guidance in the laboratory. GIZ International Services, Dornier Consulting, and the Ministry of Water & Electricity of Saudi Arabia provided logistical help.

3.9. Supplementary data

Supplementary data for this chapter can be found in Appendix 3.

3.10. References

Al-Basheer, W., Al-Jalal, A., and Gasmi, K., 2018. Isotopic composition of bottled water in Saudi Arabia. Isotopes in Environmental and Health Studies 54(1), 106–112.

Al-Sagaby, I., Moallim, M., 1996. Use of Isotopes to Study Groundwater Recharge Through Sand Dunes in Qasim Area, Saudi Arabia. In: IAEA. Isotope field applications for groundwater studies in the Middle East. TECDOC 890, 11–32.

Al-Sagaby, I., Moallim, M., 2001. Isotope based assessment of groundwater renewal and related anthropogenic effects in water scarce areas: Sand dunes study in Qasim area, Saudi Arabia. In: IAEA. Isotope based assessment of groundwater renewal in water scarce regions. TECDOC 1246, 221–229.

Al-Sayari, S.S., Zötl, J.G., 1978. Quaternary Period in Saudi Arabia, Vol. 1: Sedimentological, Hydrogeological, Hydrochemical, Geomorphological, and Climatological Investigations in Central and Eastern Saudi Arabia. Springer, Vienna/New York.

Al-Saleh, M.A., 1997. Variability and frequency of daily rainfall in Riyadh, Saudi Arabia. Geographical Bulletin 39(1), 48–57.

Al-Turbak, A.S., Al-Hassoun, S.A., 1992. Infiltrometer tests in Ad-Dahna sand dunes. The Arabian Journal for Science and Engineering 17(2A), 119–129.

Allison, G.B., Barnes, C.J., 1983. Estimation of evaporation from non-vegetated surfaces using natural deuterium. Nature 301, 143–145.

Alyamani, M.S., 2001. Isotopic composition of rainfall and ground-water recharge in the western province of Saudi Arabia. Journal of Arid Environments 49, 751–760.

Barnes, C.J., Allison, G.B., 1983. The distribution of deuterium and ^{18}O in dry soils – 1. Theory. Journal of Hydrology 60, 141–156.

Barnes, C.J., Allison, G.B., 1988. Tracing of water movement in the unsaturated zone using stable isotopes of hydrogen and oxygen. Journal of Hydrology 100, 143–176.

Benettin, P., Volkmann, T.H.M., von Freyberg, J., Frentress, J., Penna, D., Dawson, T.E., Kirchner, J.W., 2018. Effects of climatic seasonality on the isotopic composition of evaporating soil waters. Hydrology and Earth System Sciences 22, 2881–2890.

Beyer, M., Gaj, M., Hamutoko, J.T., Koeniger, P., Wanke, H., Himmelsbach, T., 2015. Estimation of groundwater recharge via deuterium labelling in the semi-arid Cuvelai-Etosha Basin, Namibia. Isotopes in Environmental and Health Studies 51(4), 533–552.

Clark, I.D, Fritz, P., 1997. Environmental Isotopes in Hydrogeology. Lewis Publishers, Boca Raton/New York.

Craig, H., 1961. Isotopic variations in meteoric waters. Science 133, 1702–1703.

Craig, H., Gordon, L.I., 1965. Deuterium and oxygen 18 variations in the ocean and the marine atmosphere. In: Tongiorgi, E. (ed.). Stable Isotopes in Oceanographic Studies and Paleotemperatures. Consiglio Nazionale delle Ricerche, Laboratorio di Geologia Nucleare, Pisa, 9–130.

Dincer, T., 1982. Estimating Aquifer Recharge due to Rainfall – A Comment. Journal of Hydrology 58, 179–182.

Dincer, T., Al-Mugrin, A., Zimmermann, U., 1974. Study of the infiltration and recharge through the sand dunes in arid zones with special reference to the stable isotopes and thermonuclear tritium. Journal of Hydrology 23, 79–109.

Dubbert, M., Cuntz, M., Piayda, A., Maguás, C., Werner, C., 2013. Partitioning evapotranspiration – Testing the Craig and Gordon model with field measurements of oxygen isotope ratios of evaporative fluxes. Journal of Hydrology 496, 142–153.

Eastoe, C.J., Dettman, D.L., 2016. Isotope amount effects in hydrologic and climate reconstructions of monsoon climates: Implications of some long-term data sets for precipitation. Chemical Geology 430, 78–89.

Edgell, H.S., 2006. Arabian Deserts – Nature, Origin and Evolution. Springer, Dordrecht.

Engelhardt, I., Rausch, R., Keim, B., Al-Saud, M., Schüth, C., 2013. Surface and subsurface conceptual model of an arid environment with respect to mid- and late Holocene climate changes. Environmental Earth Sciences 69, 537–555.

Gaj, M., Beyer, M., Koeniger, P., Wanke, H., Hamutoko, J., Himmelsbach, T., 2016. In situ unsaturated zone water stable isotope (^{2}H and ^{18}O) measurements in semi-arid environments: a soil water balance. Hydrology and Earth System Sciences 20, 715–731.

Gaj, M., Kaufhold, S., Koeniger, P., Beyer, M., Weiler, M., Himmelsbach, T., 2017. Mineral mediated isotope fractionation of soil water. Rapid Communications in Mass Spectrometry 31, 269–280.

Gat, J.R., 1971. Comments on the Stable Isotope Method in Regional Groundwater Investigations. Water Resources Research 7(4), 980–993.

Gat, J.R., 2010. Isotope Hydrology – A Study of the Water Cycle. Imperial College Press, London.

Gates, J.B., Edmunds, W.M., Darling, W.G., Ma, J., Pang, Z., Young, A.A., 2008. Conceptual model of recharge to southeastern Badain Jaran Desert groundwater and lakes from environmental tracers. Applied Geochemistry 23, 3519–3534.

Gibson, J.J., Birks, S.J., Edwards, T.W.D., 2008. Global prediction of δ_A and $\delta^{2}H$-$\delta^{18}O$ evaporation slopes for lakes and soil water accounting for seasonality. Global Biogeochemical Cycles 22, GB2031.

Hasselquist, N.J., Benegas, L., Roupsard, O., Malmer, A., Ilstedt, U., 2018. Canopy cover effects on local soil water dynamics in a tropical agroforestry system: Evaporation drives soil water isotopic enrichment. Hydrological Processes 32, 994–1004.

Horita, J., Rozanski, K, Cohen, S., 2008. Isotope effects in the evaporation of water: a status report of the Craig–Gordon model. Isotopes in Environmental and Health Studies 44(1), 23–49.

IAEA/WMO – International Atomic Energy Agency/World Meteorological Organization, 2019. Global Network of Isotopes in Precipitation. The GNIP Database. https://nucleus.iaea.org/wiser, (last access: 16 October 2019).

Jasechko, S., Taylor, R.G., 2015. Intensive rainfall recharges tropical groundwaters. Environmental Research Letters 10, 124015.

Jin, K., Rao, W., Guo, Q., Zhang, W., Zheng, F., Wang, S., 2018. Understanding recharge of soil water in a sand dune at the Nuoertu of Badain Jaran Desert using isotopes of H and O. Journal of Radioanalytical and Nuclear Chemistry 318, 1063–1075.

JRCC/PME – Jeddah Regional Climate Center South West Asia/Presidency of Meteorology and Environment, 2016. Climate Data for Saudi Arabia. Surface Annual Climatological Report for station Riyadh Old (1985–2010).

Kerstel, E.R.T., van Trigt, R., Reuss, J., Meijer, H.A.J., 1999. Simultaneous Determination of the $^{2}H/^{1}H$, $^{17}O/^{16}O$, and $^{18}O/^{16}O$ Isotope Abundance Ratios in Water by Means of Laser Spectrometry. Analytical Chemistry 71(23), 5297–5303.

Koeniger, P., Gaj, M., Beyer, M., Himmelsbach, T., 2016. Review on soil water isotope-based groundwater recharge estimations. Hydrological Processes 30, 2817– 2834.

Koeniger, P., Marshall, J.D., Link, T., Mulch, A., 2011. An inexpensive, fast, and reliable method for vacuum extraction of soil and plant water for stable isotope analyses by mass spectrometry. Rapid Communications in Mass Spectrometry 25, 3041-3048.

Landwehr, J.M., Coplen, T.B., 2006. Line-conditioned excess: a new method for characterizing stable hydrogen and oxygen isotope ratios in hydrologic systems. In: IAEA. Isotopes in Environmental Studies, 132–135.

Lis, G., Wassenaar, L.I., Hendry, M.J, 2008. High-Precision Laser Spectroscopy D/H and $^{18}O/^{16}O$ Measurements of Microliter Natural Water Samples. Analytical Chemistry 80(1), 287–293.

Mahindawansha, A., Orlowski, N., Kraft, P., Rothfuss, Y., Racela, H., Breuer, L., 2018. Quantification of plant water uptake by water stable isotopes in rice paddy systems. Plant and Soil 429, 281–302.

McKee, E.D. (1979). A Study of Global Sand Seas. USGS Professional Paper 1052.

Michelsen, N., Laube, G., Friesen, J., Weise, S.M., Bait Said, A.B.A., Müller, T., 2019. Technical note: A microcontroller-based automatic rain sampler for stable isotope studies. Hydrology and Earth System Sciences 23(6), 2637–2645.

Michelsen, N., Reshid, M., Siebert, C., Schulz, S., Knöller, K., Weise, S.M., Rausch, R., Al-Saud, M., Schüth, C., 2015. Isotopic and chemical composition of precipitation in Riyadh, Saudi Arabia. Chemical Geology 413, 51–62.

Michelsen, N., van Geldern, R., Roßmann, Y., Bauer, I., Schulz, S., Barth, J.A.C., Schüth, C., 2018. Comparison of cumulative precipitation collectors used in isotope hydrology. Chemical Geology 488, 171–179.

Mughal, I., Jadoon, K.Z., Mai, M., Al-Mashharawi, Missimer, T.M., 2015. Experimental Measurement of Diffusive Extinction Depth and Soil Moisture Gradients in a Dune Sand Aquifer in Western Saudi Arabia: Assessment of Evaporation Loss for Design of an MAR System. Water 7, 6967–6982.

Natural Earth, 2015. https://www.naturalearthdata.com/ (last access: 23 June 23 2015).

Orlowski, N., Breuer, L., Angeli, N., Boeckx, P., Brumbt, C., Cook, C.S., Dubbert, M., Dyckmans, J., Gallagher, B., Gralher, B., Herbstritt, B., Hervé-Fernández, P., Hissler, C., Koeniger, P., Legout, A., Macdonald, C.J., Oyarzún, C., Redelstein, R., Seidler, C., Siegwolf, R., Stumpp, C., Thomsen, S., Weiler, M., Werner, C., McDonnell, J.J., 2018. Inter-laboratory comparison of cryogenic water extraction systems for stable isotope analysis of soil water. Hydrology and Earth System Sciences 22, 3619–3637.

Orlowski, N., Breuer, L., McDonnell, J.J., 2016a. Critical issues with cryogenic extraction of soil water for stable isotope analysis. Ecohydrology 9, 3–10.

Orlowski, N., Pratt, D.L., McDonnell, J.J., 2016b. Intercomparison of soil pore water extraction methods for stable isotope analysis. Hydrological Processes 30, 3434–3449.

Powers, R.W., Ramirez, L.F., Redmond, C.D., Elberg, E.L., 1966. Geology of the Arabian Peninsula — Sedimentary Geology of Saudi Arabia. USGS, Washington D.C.

Schulz, S., Horovitz, M., Rausch, R., Michelsen, N., Mallast, U., Köhne, M., Siebert, C., Schüth, C., Al-Saud, M., Merz, R., 2015. Groundwater evaporation from salt pans: Examples from the eastern Arabian Peninsula. Journal of Hydrology 531, 792–801.

Shampine, W.J., Dincer, T., Noory, M., 1978. An evaluation of isotope concentrations in the groundwater of Saudi Arabia. In: IAEA. Isotope Hydrology 1987. Vol. II, 443–463.

Siebert, C., Rödiger, T., Schulz, S., Horovitz, M., Merz, R., Friesen, J., Dietrich, P., Michelsen, N., Kallioras, A., Rausch, R., Engelhardt, I., Al-Saud, M., Schüth, C., 2016. New Tools for Coherent Information Base for IWRM in Arid Regions: The Upper Mega Aquifer System on the Arabian Peninsula. In: Borchardt, D., Bogardi, J.J., Ibisch, R.B. (eds.). Integrated Water Resources Management: Concept, Research and Implementation. Springer, 85–106.

Sonntag, Christmann, D., Münnich, K.O., 1985. Laboratory and field experiments on infiltration and evaporation of soil water by means of deuterium and oxygen-18. In: IAEA. Stable and Radioactive in the Study of the Unsaturated Soil Zone, 145–159.

Sprenger, M., Herbstritt, B., Weiler, M., 2015. Established methods and new opportunities for pore water stable isotope analysis. Hydrological Processes 29, 5174–5192.

Sprenger, M., Leistert, H., Gimbel, K., Weiler, M., 2016. Illuminating hydrological processes at the soil-vegetation-atmosphere interface with water stable isotopes. Reviews of Geophysics 54, 674–704.

Subyani, A.M., 2004. Use of chloride-mass balance and environmental isotopes for evaluation of groundwater recharge in the alluvial aquifer, Wadi Tharad, western Saudi Arabia. Environmental Geology 46, 741–749.

Sultan, M., Sturchio, N.C., Alsefry, S., Emil, M.K., Ahmed, M., Abdelmohsen, K., AbuAbdullah, M.M., Yan, E., Save, H., Alharbi, T., Othman, A., Chouinard, K., 2019. Assessment of age, origin, and sustainability of fossil aquifers: A geochemical and remote sensing-based approach. Journal of Hydrology 576, 325–341.

Sultan, M., Sturchio, N., Al Sefry, S., Milewski, A., Becker, R., Nasr, I., Sagintayev, Z., 2008. Geochemical, isotopic, and remote sensing constraints on the origin and evolution of the Rub Al Khali aquifer system, Arabian Peninsula. Journal of Hydrology 356, 70–83.

Tewolde, D.O., Koeniger, P., Beyer, M., Neukum, C., Gröschke, M., Ronelngar, M., Rieckh, H., Vassolo, S., 2019. Soil water balance in the Lake Chad Basin using stable water isotopes and chloride of soil profiles. Isotopes in Environmental and Health Studies 55(5), 459–477.

Wagner, W., 2011. Groundwater in the Arab Middle East. Springer, Berlin/Heidelberg.

Walters, M.O., 1989. A unique flood event in an arid zone. Hydrological Processes 3, 15–24.

West, A.G., Patrickson, S.J., Ehleringer, J.R., 2006. Water extraction times for plant and soil materials used in stable isotope analysis. Rapid Communications in Mass Spectrometry 20, 1317–1321.

USGS/ARAMCO — United States Geological Survey/Arabian American Oil Company, 1963. Geologic Map of the Arabian Peninsula. Miscellaneous Geologic Investigations, Map I-270 A, Scale 1:2,000,000. USGS, Washington D.C.

Preface to Chapter 4

Although the isotopic (and major ion) signatures of Riyadh rainfall presented in Chapter 2 are deemed a first, robust data set, the findings of Chapter 3 suggest that there is more work to be done. Apparently, the rain data set does not reflect the full spectrum of isotopic fingerprints potentially occurring in Central Saudi Arabia. In turn, this indicates a need for a long-term monitoring effort, for example in the form of a cumulative rain collector gathering monthly samples (see GNIP).

Because a simple recommendation to set up such a long-term precipitation monitoring station would be somewhat generic (i.e., appropriate for many parts of the world), it should at least be accompanied by a concrete advice on which sampler type to deploy. This question is rather critical in the present case, given the harsh environmental conditions prevailing in Saudi Arabia. More precisely, the high temperatures and low relative humidities (see Chapter 1.2.1. and Fig. 2-4) represent a challenge when it comes to evaporation suppression – a crucial aspect in precipitation sampling for isotope research. If such samples were collected for major ion analyses, a partial evaporative loss from the collector bottle of a few % would not be too problematic. All ions would simply be subject to evaporative concentration by a few %, which is roughly the long-term precision of a modern ion chromatograph (see Chapter 2.3.3.). In an isotope context, however, this degree of evaporation and the associated fractionation would render the samples unusable. Hence, the IAEA regularly publishes guidelines on how to sample precipitation for isotope analyses and recommends specific sampler types (e.g., Payne, 1983; IAEA, 2014). However, the underlying data that led them to recommend certain techniques and samplers are usually not published, i.e., the reader does not know under which environmental conditions the tests were conducted. Scientific articles on the topic usually report the conditions, but often put emphasis on temperate regions. Prechsl et al. (2014), for instance, tested their samplers in a climate chamber at a temperature of 25°C and a relative humidity of 25 % to „simulate rather extreme field conditions“. In view of their study area in Switzerland, these settings might be considered extreme, but in a Saudi Arabian context, they are everything but extreme. Hence, the following chapter provides a hitherto missing sampler comparison under hot and dry conditions.

References

IAEA, 2014. IAEA/GNIP precipitation sampling guide.

Payne, B.R., 1983. Introduction. In: IAEA. Guidebook on Nuclear Techniques in Hydrology. Technical Report Series No. 91, 1–18.

Prechsl, U.E., Gilgen, A.K. Kahmen, A., Buchmann, N., 2014. Reliability and quality of water isotope data collected with a low-budget rain collector. Rapid Communications in Mass Spectrometry, 28, 879–885.

4. Comparison of precipitation collectors used in isotope hydrology

Nils Michelsen [a,*], Robert van Geldern [b], Yasmin Roßmann [a], Ingo Bauer [a], Stephan Schulz [a], Johannes A.C. Barth [b], Christoph Schüth [a]

[a] Technische Universität Darmstadt, Institute of Applied Geosciences, Schnittspahnstraße 9, 64287 Darmstadt, Germany

[b] Friedrich-Alexander University Erlangen-Nuremberg (FAU), Department of Geography and Geosciences, GeoZentrum Nordbayern, Schlossgarten 5, 91054 Erlangen, Germany

* Corresponding author (michelsen@geo.tu-darmstadt.de)

Published in Chemical Geology, 2018, Vol. 488, 171–179, DOI: 10.1016/j.chemgeo.2018.04.032

4.1. Abstract

Many hydrologic studies require data on the oxygen and hydrogen stable isotope composition ($\delta^{18}O$, $\delta^{2}H$) of precipitation and various collector designs have been suggested for gathering corresponding samples. Yet, it is crucial that these collectors, also known as totalizers, prevent evaporation and associated isotope fractionation. Surprisingly, we were unable to find a comprehensive collector intercomparison in the literature, and much less one that addressed hot and arid conditions.

In this study, we tested six different collector designs over a period of 32 days. They were filled to 20 % of their total volume with water of known isotope composition and placed in a modified laboratory drying oven with a low relative humidity (5 %) and a diurnal temperature change of 26 to 45°C. Evaporative mass losses were determined gravimetrically daily while samples for isotope analyses were collected every four days.

The classic Oil collector, featuring a layer of paraffin oil to prevent evaporation, showed the smallest mass losses and no detectable isotope shift. The Tube-dip-in-water collector with pressure equilibration tube also performed well, although we noted somewhat larger mass losses and isotope shifts. The latter accounted for 0.28 ‰ ($\Delta\delta^{18}O$) and 0.9 ‰ ($\Delta\delta^{2}H$) after 32 days, which is significant, but in view of the extreme conditions, these changes should be still acceptable for most studies. The remaining collectors (Ball-in-funnel, Floating balls, and Float based) all failed.

Under the prevailing conditions, the Tube-dip-in-water collector with pressure equilibration tube seems to represent a good, oil- and thus contamination-free compromise. Nonetheless, also in this system small precipitation amounts are problematic. This may necessitate modifications of the standard design in terms of funnel diameter and bottle geometry. We strongly advise researchers to conduct own tests with their intended collector before field deployment.

4.2. Introduction

The stable isotope ratios of oxygen and hydrogen in the water molecule, $^{18}O/^{16}O$ and $^{2}H/^{1}H$, serve as tracers in a diverse range of scientific disciplines, including hydrology, geology, meteorology, climatology, ecology, food authenticity, and forensics (IAEA, 2014; Terzer et al., 2013). For most isotope-related studies in these fields, the isotope composition of modern precipitation has to be known (IAEA, 2014; Harvey, 2001). The prime source for such data is the Global Network of Isotopes in Precipitation (GNIP; IAEA/WMO, 2018), despite the advent of new databases (e.g., Waterisotopes, 2018) that largely rely on GNIP and other literature data, and the creation of national monitoring networks (e.g., Kralik et al., 2004; Vreča and Malenšek, 2016).

GNIP has provided the spatio-temporal foundation for many isotope studies (Wassenaar et al., 2009) and grows continuously (Terzer, 2015). However, it still has spatial deficiencies (Bowen and Revenaugh, 2003; Rozanski et al., 1993; Terzer et al., 2013; Wassenaar et al., 2009; West et al., 2014) that could not yet be covered by various calls for contributions (IAEA, 2013, 2014; Terzer et al., 2013). Particularly (semi-)arid areas, e.g., in Africa or the Middle East are under-represented in the database (Crawford et al., 2014; Michelsen et al., 2015; Rozanski et al., 1993).

To overcome the lack of data in such regions, researchers used workarounds and considered shallow ground or tap water as proxies for modern precipitation and developed predictive models on a regional (Wassenaar et al., 2009; West et al., 2014) or on the global scale (Bowen and Revenaugh, 2003; Terzer et al., 2013). Nevertheless, we ultimately need more real data, particularly from arid and semi-arid areas. For logistical reasons, their gathering will in most cases involve precipitation collectors yielding an integral monthly sample (cf., Terzer et al., 2016). These collector types are also referred to as “precipitation totalizers” in the literature (IAEA, 2014).

While evaporation from such collectors and the associated isotope fractionation must be prevented in general (IAEA, 2014), this aspect is particularly important in arid areas (Payne, 1983), where high temperatures and low relative humidity values (RH) prevail. Yet, no generally accepted blueprint for a reliable collector in such settings exists. In Table 4-1, we provide an overview of *potential* options and list collectors that have been applied in published isotope studies. This overview reveals a broad spectrum of approaches in terms of complexity and the underlying strategies to avoid secondary evaporation from the collectors. While some types are designed to directly prevent evaporation (e.g., Oil collector), others allow a partial evaporation within the device, but limit atmospheric contact (e.g., Tube-dip-in-water collector).

Due to its effective evaporation reduction, the oil method had already been applied to regular rain gauges more than a century ago (Alter, 1907) and was adopted by the isotope community, in which it has been the gold standard for decades.

Table 4-1. Overview of rain collectors used in stable isotope studies (based on IAEA, 2014; Scholl, 2006; and references cited in the table), including reported or inferred problems.

Type	Comment	Examples	Reported/inferred problems
Oil collector	floating paraffin (or silicon) oil inhibits evaporation	Friedman et al. (1992), Payne (1983), Scholl et al. (1995, 1996), van Geldern et al. (2014)	oil is potential contaminant (Gröning et al., 2012; IAEA, 2014) and can attract insects (Moscati and Scofield, 2011), at times formation of gelatinous phase (Friedman et al., 1992)
Ball-in-funnel collector	table tennis ball in funnel reduces atmospheric contact[a]	Prechsl et al. (2014), Scholl et al. (1995, 1996)	animal vandalism, debris interfering with ball function (Scholl, 2006), significant evaporative loss (Terzer et al., 2016)
Tube-dip-in-water collector (+ pressure equilibration tube)	inlet tube dips in collected water, thus reducing atmospheric contact; long, narrow vent tube for pressure equilibration	Gröning et al. (2012), IAEA (2002, 2014)	significant evaporative loss in case of small rain amounts (Terzer et al., 2016), blocked tube when temperature <0°C (Gröning et al., 2012)
Bag-in-trash-can collector	necked down plastic bag; orifice reduces atmospheric contact	Adams et al. (1995), White et al. (1990)	animal vandalism (Adams et al., 1995)
Inflatable bag collector	initially collapsed bag (or carboy) fills slowly; reduced water surface and headspace	Scholl et al. (1995, 1996), Scholl (2006)	algae growth (Scholl et al., 1995; Scholl, 2006)
U-trap/loop collector	trapped water prevents contact between main sample and atmosphere	Ingraham et al. (1991), McGuire et al. (2005), O'Driscoll et al. (2005)	blocked tube when temperature <0°C
Buried collector	reduced evaporation due to lower subsurface temperature and/or smaller fluctuations	Andreo et al. (2004), Bicalho et al. (2017), Treydte et al. (2014)	evaporation protection not proven (IAEA, 2014)
Electronic autosampler	valve-based, lid-based, etc.; partly incl. cooling unit	Balestrini et al. (2016), Stadler (2003), Stockinger et al. (2016), Welker (2000)	evaporation protection at times questionable (Balestrini et al., 2016; Harvey and Welker, 2000; Tang et al., 1987), costly, power supply needed
Floating balls collector	floating balls reduce water surface	Angermann et al. (2017)[b]	water surface only partially covered
Float collector	floating body reduces water surface	Allen et al. (2014), Muñoz-Villers and McDonnell (2012)	evaporation reduction efficiency unknown

[a] sometimes modified design with ball placed in chamber below funnel (Yasuhara et al., 1993)
[b] styrofoam beads in river-autosampler

For oil separation, researchers used a wide range of tools, including syringes (Stern and Blisniuk, 2002), basters (Beisner et al., 2016), separatory funnels (IAEA, 2014), or spigots (connected to the sampling carboy; Scholl et

al., 2009). Another method was introduced by Green et al. (2015) who simply cut a hole in the bottom of collection bags they had used. Occasionally, water samples were additionally passed through paper filters (Friedman et al., 1992; Scholl et al., 2009). Although Birkel et al. (2016), who simply decanted the oil, assumed no interaction with the water and Ohlanders et al. (2013) found no significant influence of the oil on the water analyses in a dedicated experiment, concerns have been expressed recently. Oil traces could represent a contamination (Prechsl et al., 2014) that may cause complications in the analysis (Gröning et al., 2012). This could become a particular problem in laser spectroscopy (Hartmann et al., 2018; IAEA, 2014). Thus, quantitative oil removal is considered a crucial step that can, however, be challenging (Gröning et al., 2012). For instance, Sánchez-Murillo et al. (2017) reported that they had to discard "samples with suspicious mineral oil presence" after oil removal with a separatory funnel.

Hence, the oil-free Tube-dip-in water collector with pressure equilibration tube has been developed by IAEA (2002). The device was readily adopted in several studies (Brandes et al., 2007; Koeniger et al., 2008; Deshpande et al., 2010; Roa-García and Weiler, 2010), particularly after its formal publication by Gröning et al. (2012) and the production of a commercial version (Palmex Ltd, Zagreb, Croatia)[1]. Since then, it has been used in its original or slightly modified form (Guo et al., 2017) for various collection intervals. These range from single days (Sánchez-Murillo and Birkel, 2016) to periods of three months (Martinez et al., 2015). In addition, several GNIP stations switched from Oil to Tube-dip-in-water collectors (e.g., Müller et al., 2017). Nevertheless, caution is necessary if this collector type is employed in arid areas. In its default configuration (3000 mL sampling bottle; Gröning et al., 2012), it may experience critical in-bottle-evaporative losses, especially when containing only a small amount of water with a correspondingly large headspace (Gröning et al., 2012; Crawford et al., 2017; Terzer et al., 2016).

Given the difficulties in suppressing evaporation from collectors in arid areas and different opinions on the functionality of various samplers (IAEA, 2014; Prechsl et al., 2014; Terzer et al., 2016), we screened the literature for a systematic comparison of available devices. In this exercise, we mainly encountered tests of individual collector designs (Otte et al., 2017; Prechsl et al., 2014; Tappa et al., 2016; Windhorst et al., 2013), partly tested against collectors with no evaporation suppression (Gröning et al., 2012; Weaver and Talma, 2005) or oil-filled devices (Moerman et al., 2013). However, we could not find a comprehensive comparison of all devices, and much less one that addressed hot and arid conditions. In view of the long history of comparative studies that address ordinary rain gauges since about 1955 (summarized in Sevruk et al., 2009), this finding seems surprising. We are quite sure that such tests were performed (cf., IAEA, 2014; Terzer et al., 2016), but apparently the corresponding data have not been published. In order to fill this gap, we tested six collectors – established and unconventional ones – for isotope evaporation effects in a controlled laboratory experiment, mimicking a hot and arid climate. The main objective of this study was to identify the most suitable collector, especially for hot

[1] http://www.rainsampler.com/ (last access: 23 January 2018)

climate conditions that will cause pronounced secondary evaporative isotope shifts, if the design does not effectively prevent evaporation from the collector bottle.

4.3. Methods

4.3.1. Tested collectors

The tests comprised three established models, namely the Oil collector (6 mm layer of paraffin oil), the Tube-dip-in-water collector (type RS 1B, Palmex Ltd, Zagreb, Croatia), and the Ball-in-funnel collector (Prechsl et al., 2014). In addition, we included three more unconventional models – one based on the floating balls principle and two involving a (solid) float (Fig. 4-1).

Floating balls are a standard method to reduce evaporation, for instance in industry or in laboratory experiments (Probert, 1977), however their use in collectors has been rather limited (cf., Angermann et al., 2017), despite their low cost and easy handling. Based on preliminary tests we decided to use two layers of floating balls (each approx. 3 cm thick). The lower layer consisted of LDPE granulate (diameter 3–4 mm) and the upper one was formed from hollow PP balls (diameter 20 mm).

Floats, by contrast, have occasionally been used in collectors (see Table 4-1), but details (material, design) are usually not mentioned. For our experiments, we used a latex-coated Styrodur float (thickness 40 mm; “Float 1”) and a metal float (painted tinplate; “Float 2”; Fig. A4-1 in Appendix 4). Both floats featured a central funnel holding a hollow PP ball (see above) and a lip seal (metallized film).

In addition to these devices, we included a collector without any evaporation reduction mechanism, not as a valid option, but as a reference (“Reference collector”).

To ensure comparability, all collectors had identical volumes (approx. 3000 mL), similar diameters (135-140 mm), and most were made from HDPE as recommended by IAEA (2014, cf., Kralik et al., 2004; Spangenberg, 2012). The float collectors were not bottle-based but custom-made from acrylic glass (Fig. A4-1). All collectors contained 600 mL of water (20 % of bottle volume) with a known isotope composition ($\delta^{18}O$=-8.62 ‰, $\delta^{2}H$=-61.1 ‰ V-SMOW). A rather low filling volume with respect to the total capacity of 3 L was selected to represent typical conditions in arid and semi-arid regions and to avoid a too optimistic scenario in which a large filling volume buffers evaporation effects to a large extent over the time of the experiment. On the other hand, the filling volume was selected to be large enough to allow for several sample collections (each 1.6 mL; see below) during the experiment without significantly reducing the overall volume.

Although combinations of evaporation suppression mechanisms are common (O’Driscoll et al., 2005; Otte et al., 2017; Payne, 1983), they are intentionally not addressed here. Further aspects such as radiation shielding, UV-stability of materials, or thermal insulation are also beyond the scope of this study, although they can be of practical relevance.

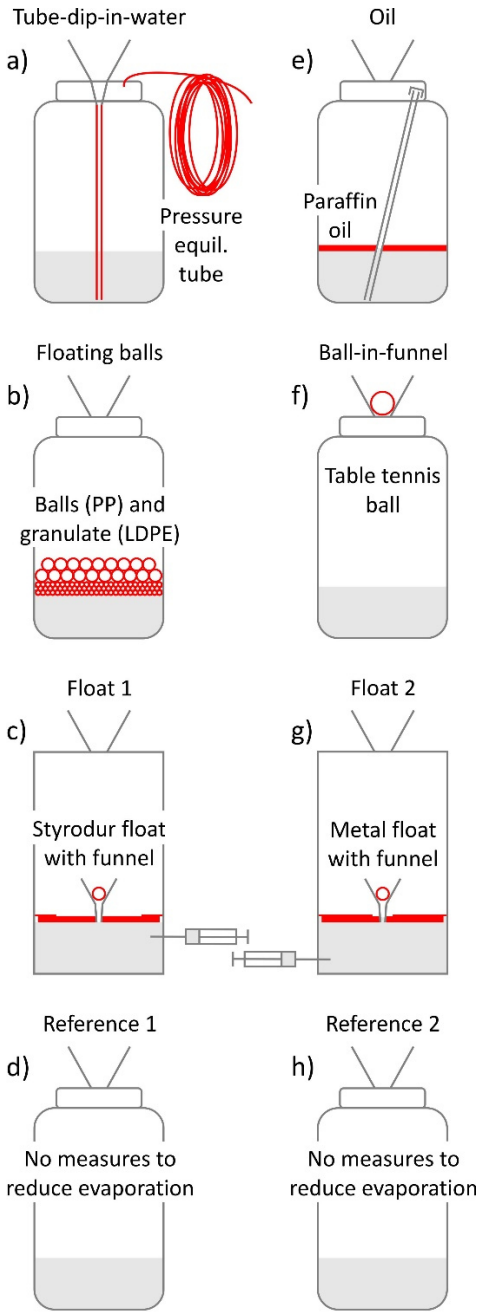

Fig. 4-1. Overview of the tested collectors. Evaporation reduction mechanisms are shown in red. a) to d): 1st run, e) to h): 2nd run. A reference collector without evaporation reduction mechanism was included in each run. For further, general information on the collector types, see Table 4-1.

4.3.2. Experiments

Aiming at controlled conditions, we modified a standard laboratory drying cabinet (T 20, Heraeus, Hanau, Germany). For creating a diurnal temperature regime (Windhorst et al., 2013), we used a socket timer to heat the oven for 12 h per day to temperatures of up to 45°C. After switching off, the oven was allowed to cool down to about 26°C. To accelerate the cooling process, two ice packs were placed in the oven every evening.

Dry conditions were ensured by 1.2 kg of silica gel on a steel mesh tray (changed once every second day) and a continuous flushing of the system with dry air from the pressurized air system of the laboratory (10 L/min, RH<3 %). Aiming at a homogeneous distribution, the dry air entered the oven through a custom-made diffuser and the air flow was further homogenized with a porous filter mat (see Section "Evaporation mapping" and Fig. A4-3 and A4-4 in the Appendix 4).

Because of a limited oven space that did not allow placing all devices inside at the same time, the tests were carried out in two runs, each lasting 32 days. To enable comparisons, we included a reference collector in each run (Fig. 4-1). Evaporative mass losses were determined gravimetrically once a day (Adventurer Pro AV4101, OHAUS, Parsippany, USA). Samples for isotope analyses (1.6 mL in 2 mL vials) were collected every four days, mostly using a pipette. Water from the Oil collector was sampled through an oil-free access pipe (Fig. 4-1e). Samples from the Float collector were taken from a sampling port (Mininert, VICI Precision Sampling, Baton Rouge, USA) with a syringe (Fig. 4-1c, 4-1g, A4-1). Temperature and relative humidity in the oven and in selected collectors were logged every ten minutes (log32 or log32TH, Dostmann electronic, Wertheim, Germany).

4.3.3. Isotope analyses

The water samples were analyzed for $\delta^{18}O$ and $\delta^{2}H$ at the Hydrogeology Stable Isotope Laboratory of the Friedrich-Alexander University Erlangen-Nuremberg. For the analyses, an isotope ratio infrared spectroscopy (IRIS) analyzer, based on wavelength-scanned cavity ring-down spectroscopy, was used (L1102-i WSCRDS, Picarro Inc.). All values are reported in the standard δ-notation in per mil (‰) vs. Vienna Standard Mean Ocean Water (V-SMOW):

$$\delta = (R_{sample}/R_{reference} - 1)$$

where R is the ratio of the numbers (n) of the heavy and light isotope of an element (e.g., $n(^{18}O)/n(^{16}O)$) in the sample and the reference (Coplen, 2011). Four sequential injections of each sample were measured and raw data were corrected for sample-to-sample memory. The reported value is the mean value. The data sets were corrected for instrumental drift during the run and normalized to the V-SMOW/SLAP (Standard Light Antarctic Precipitation) scale by assigning values of 0 ‰ and -55.5 ‰ ($\delta^{18}O$) / 0 ‰ and -427.5 ‰ ($\delta^{2}H$) to V-SMOW2 and SLAP2, respectively (Brand et al., 2014). For normalization, two laboratory reference materials, calibrated directly against V-SMOW2 and SLAP2, were measured in each run. External precision, based on repeated analyses of a control sample, was better than 0.05 ‰ and 0.5 ‰ (±1σ) for $\delta^{18}O$ and $\delta^{2}H$. A detailed description of the analysis procedure is given in van Geldern and Barth (2012).

4.4. Results

4.4.1. Evaporative water losses

The simulated climate conditions (Fig. A4-5) caused considerable evaporative mass losses (Table 4-2; for temporal development, see Table A4-1 and Fig. A4-12).

Table 4-2. Overview of final (fin) evaporative mass losses (Δm), isotope shifts (Δδ), and deuterium excess values (d) after 32 days, and mean RH values. The mass losses Δm_{fin} are expressed as absolute mass losses [g], as percentages of the original water mass of 600 g [%-orig.], and as percentages normalized to the corresponding reference collector [%-ref.] (Δm_{ref}=100 %).

	1st run				2nd run			
	Tube-dip-in-water	Floating balls	Float 1	Ref 1	Oil	Ball-in-funnel	Float 2	Ref 2
Δm_{fin} [g]	8.4	24.7	18.9	21.1	2.8	20.8	25.5	22.1
Δm_{fin} [%-orig.]	1.4	4.1	3.2	3.5	0.5	3.5	4.2	3.7
Δm_{fin} [%-ref.]	40	117	90	100	13	94	115	100
$\Delta\delta^{18}O_{fin}$ [‰]	0.28	1.25	0.75	1.07	0.04	1.05	0.80	0.93
$\Delta\delta^{2}H_{fin}$ [‰]	0.9	3.4	2.2	3.3	0.4	2.2	2.3	2.0
d_{fin} [‰][a]	6.6	1.3	4.1	2.6	8.0	1.7	3.8	2.5
RH_{mean}[b] [%]	93.5[c]	87.7	82.3	n.a.[d]	6.9	n.d.	93.9	n.d.

[a] the deuterium excess ($d = \delta^2H - 8 \cdot \delta^{18}O$; Dansgaard, 1964) of the original filling was 7.9 ‰ (see Table A4-2)
[b] inside the collector
[c] logger failure after approx. 9 days (probably due to condensed water)
[d] logger failure on the first day (probably due to condensed water)

The Oil collector experienced the smallest loss of 2.8 g (after 32 d), which equals 0.5 % of the original mass (%-orig.), followed by the Tube-dip-in-water collector (8.4 g or 1.4 %-orig.). Much larger losses, in the range of 20 to 25 g (3 to 4 %-orig.) were observed for the remaining collectors. The unprotected Reference collectors showed losses of 21.1 and 22.1 g (3.5 and 3.7 %-orig.). This shows that conditions in the two runs were very similar (cf., Fig. A4-5), which implies that the evaporative losses from the two runs can be directly compared. Nevertheless, a normalization was done for each run, i.e., the loss of a given collector was normalized to the loss observed for the corresponding Reference collector (%-ref; Δm_{ref}=100 %). The resulting values reveal that some collectors lost almost the same mass as the Reference collector (Float 1: 90 %-ref., Ball-in-funnel: 94 %-ref.). Particularly noteworthy are the results for the Floating balls (117 %-ref.) and the Float 2 collector (115 %-ref.). These devices showed larger evaporative losses than the Reference collectors that lacked any evaporation reduction mechanism.

4.4.2. Isotope shifts

The deviations from the original isotope composition are shown in dual-isotope plots (δ^2H vs. $\delta^{18}O$) in Fig. 4-2 (for raw data see Tables A4-2 and A4-3). The final shifts after 32 days, $\Delta\delta^{18}O_{fin}$ and $\Delta\delta^2H_{fin}$, are summarized in Table 4-2.

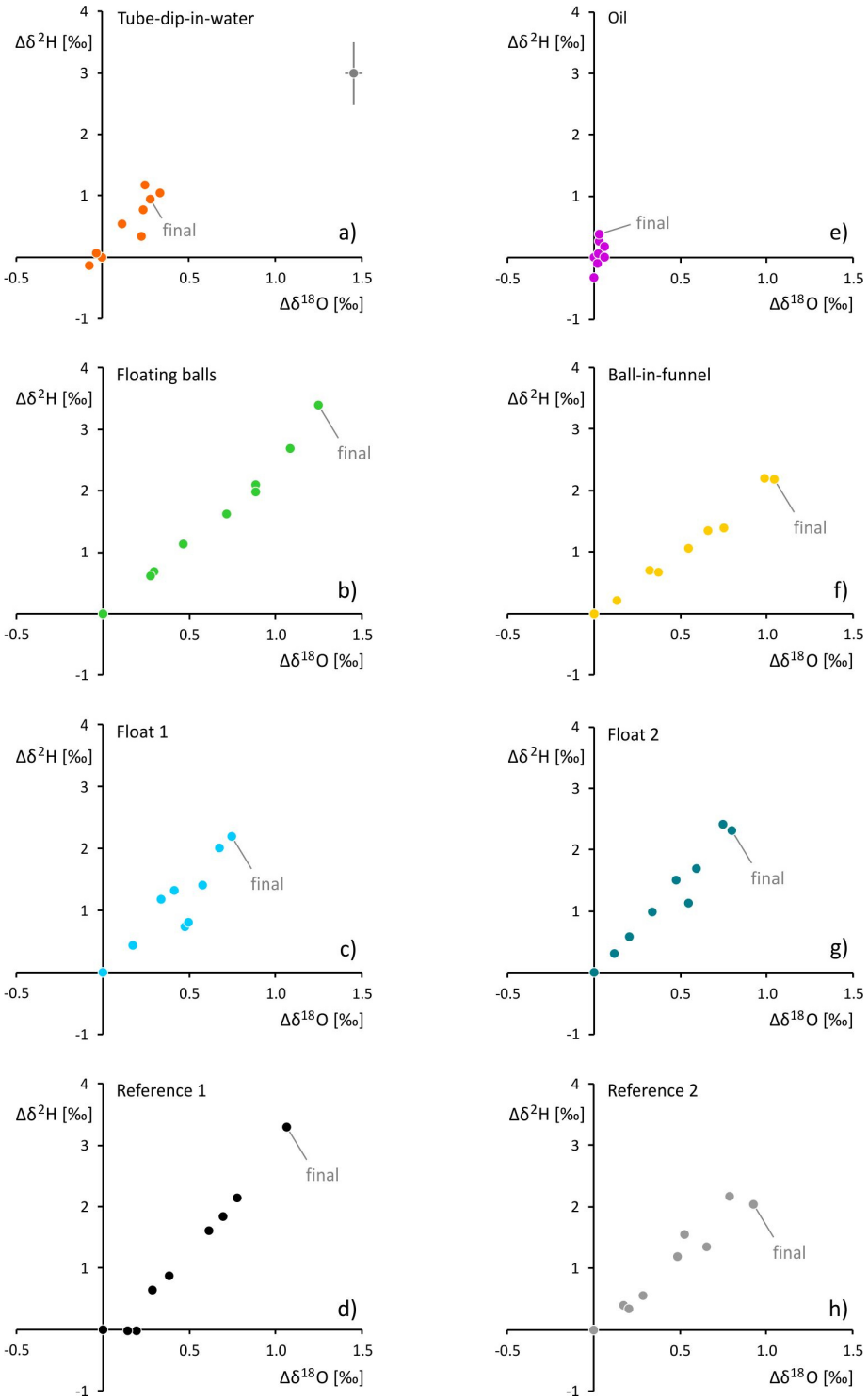

Fig. 4-2. Deviations from the original isotope signature (point of origin) in the dual-isotope space [‰ V-SMOW]. a) to d): 1st run, e) to h): 2nd run. The external precision is exemplarily shown in a).

The Oil collector exhibited the smallest isotope alterations. The corresponding data points scatter around the origin in the dual-isotope space (Fig. 4-2e). Final shifts were 0.04 ‰ and 0.4 ‰ for $\Delta\delta^{18}O_{fin}$ and $\Delta\delta^{2}H_{fin}$, respectively (Table 4-2). Water samples from the Tube-dip-in-water collector showed slight isotopic enrichments with $\Delta\delta^{18}O_{fin}$ and $\Delta\delta^{2}H_{fin}$ accounting for 0.28 and 0.9 ‰ (Fig. 4-2a). For the remaining collectors, we found considerable and systematic enrichments reaching $\Delta\delta^{18}O_{fin}$ values >1 ‰ and $\Delta\delta^{2}H_{fin}$ values exceeding up to 3 ‰.

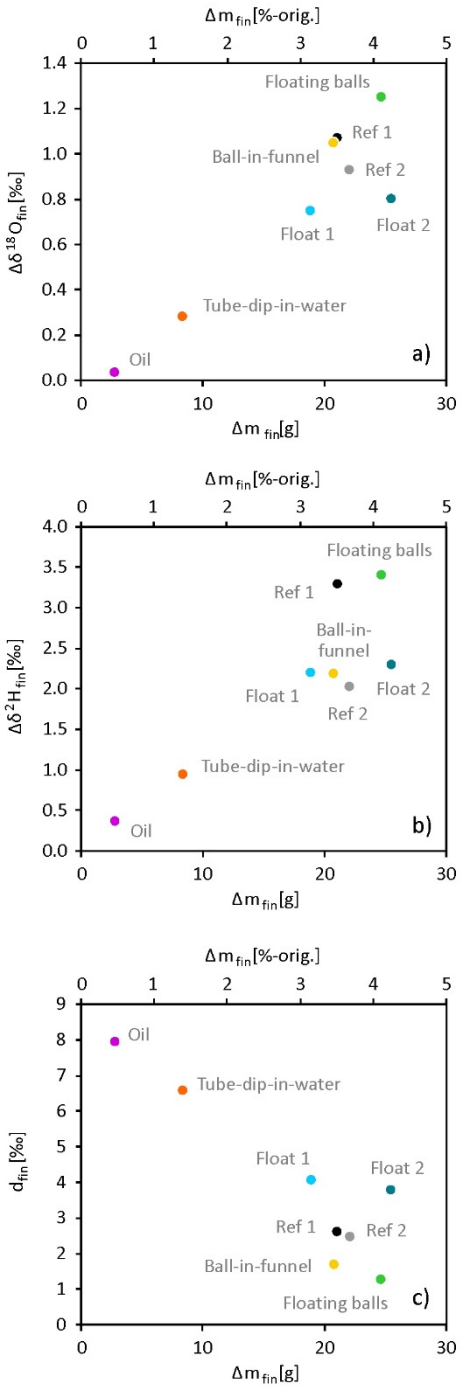

Fig. 4-3. Relation between the final isotope shifts as well as final d values and the corresponding evaporative mass losses. The latter are expressed as absolute masses [g] (lower axes) and as percentages of the original water mass of 600 g [%-orig.] (upper axes).

To incorporate the gravimetric data (Section 4.4.1.), we also plotted the final shifts, $\Delta\delta^{18}O_{fin}$ and $\Delta\delta^{2}H_{fin}$, against the corresponding mass losses (Fig. 4-3a and 4-3b). The smallest changes in isotope composition correspond to relatively small mass losses (<1.5 %-orig.; Oil and Tube-dip-in-water collector). Large isotope shifts are associated with collectors that lost more water (about 3 to 4 %-orig.).

These shifts caused changes in the deuterium excess (d) values (Table 4-2, Fig. 4-3c). While the d values for the Oil and the Tube-dip-in-water collector were still close to the original d value of 7.9 ‰, those for the remaining collectors were significantly lower (1.3 to 4.1 ‰).

4.5. Discussion

For a better understanding of the underlying processes in the various collector designs, we first consider the climate parameters measured inside the collectors, especially the RH values (Table 4-2, Fig. A4-6 to A4-11). A low RH prevailed in the Oil collector (RH_{mean} 6.9 %; Fig. A4-10). This indicates that the 6 mm thick oil layer effectively reduced evaporation and the associated fractionation. The corresponding isotope shifts of 0.04 ‰ ($\Delta\delta^{18}O_{fin}$) and 0.4 ‰ ($\Delta\delta^{2}H_{fin}$) are within the analytical precision. This demonstrates the reliability of oil as an efficient evaporation suppressant and explains its popularity, also for long collection periods such as 6 months (Friedman et al., 1992; Scholl et al., 1995, 1996, 2002) or one year (Gonfiantini et al., 2001; Stern and Blisniuk, 2002).

The Tube-dip-in-water collector, by contrast, does allow for evaporation into the headspace, creating water vapor-saturated conditions (RH_{mean} 93.5 %). These caused continuous re-condensation, which most probably led to the observed logger failure (Table 4-2, Fig. A4-6). To minimize the loss of water vapor, the collector design limits vapor exchange with the oven atmosphere. Nevertheless, the resulting isotope shifts of 0.28 ‰ ($\Delta\delta^{18}O_{fin}$) and 0.9 ‰ ($\Delta\delta^{2}H_{fin}$) are larger than the 2σ external precision for $\delta^{18}O$ (±0.1 ‰) but within the 2σ range for $\delta^{2}H$ (±1 ‰). The shift of the $\delta^{18}O$ value after 32 days considerably exceeds the values observed by Gröning et al. (2012) during their one-year outdoor test in Vienna ($\Delta\delta^{18}O_{fin}$ 0.08 ‰, $\Delta\delta^{2}H_{fin}$ 1.3 ‰). We attribute the shifts in our experiment to two factors: (i) the harsh environmental conditions and (ii) the fact that our collector was only filled to 20 %, causing a high gas/water ratio (cf., Crawford et al., 2017; Gröning et al., 2012; Moerman et al., 2013; Prechsl et al., 2014; Terzer et al., 2016). In view of these rather challenging conditions, we think that the measured isotope shifts observed for the Tube-dip-in-water design can still be deemed acceptable for most studies in isotope hydrology, especially if the collectors are used in regions with temperate to semi-arid climates. It is noteworthy that the problem of high gas/water ratios can be mitigated in real-world applications to some extent by choosing a bigger funnel, a smaller bottle (Gröning et al., 2012) or an “inlet” reducing the effective bottle volume (see Prechsl et al., 2014). Another potential option to decrease the gas volume in months with less precipitation is the prior partial filling of the bottle with displacement objects.

In contrast to the Oil and the Tube-dip-in-water collector, the remaining models showed unacceptably large evaporative losses and isotope shifts. Water evaporated into the headspace in all of the remaining designs, which is indicated by high RH values (RH_{mean}> 80 %). While this evaporation also occurs in the Tube-dip-in-water collector, the critical feature of the other models is the rather short diffusion path out of the collector chamber.

The table tennis ball of the Ball-in-funnel collector was not able to effectively reduce this diffusion, probably because of a small gap between the ball and the not perfectly round funnel. This result is in line with the findings of Terzer et al. (2016), who reported unacceptable isotope effects for this kind of collector and advise against its use. Prechsl et al. (2014) promote the collector, but recommend to empty it within five days after a rain event (if T>25°C and RH<25 %). The gap issue is even more critical in forested areas, where debris or insects fallen into the funnel interfere with the ball function (Scholl, 2006; Scholl et al., 1995).

The Floating balls collector showed the largest mass loss and isotope shift in this study. While the idea behind this collector design is a reduction of the water surface, the results suggest that the opposite has happened. Presumably due to capillary forces, the water between the small granules is pulled upwards, forming concave menisci. This phenomenon probably *increases* the water surface instead of reducing it.

Finally, also the Float collectors' performances were not satisfactory. Our attempt to prevent evaporation by using a lip seal at the outer edge of the float and a small ball in the central funnel was not successful. Interestingly, the Float 2 collector (metal float) showed a significantly higher loss and a slightly larger isotopic enrichment than the Float 1 collector (coated Styrodur float). The intention behind utilizing a metal floating device was to rule out diffusion through the float itself, but it appears its use was counterproductive. We suspect that the metal stored the absorbed heat longer after switching off the oven and thus caused higher water temperatures with more pronounced evaporation during nighttime. The fact that metal collectors can exhibit stronger isotope enrichment than models made from plastic has also been found in experiments reported on by Schürch et al. (2003).

Another aspect that might play a role in case of the low performance collectors is re-condensation upon cooling at the beginning of the night cycle. In this phase, small droplets form on the collector walls and ceilings, which greatly increases the water surface subject to (re-)evaporation (Fig. A4-1). The Reference collectors are subject to this phenomenon too, but the RH values are probably high enough to cause a more intense re-condensation, resulting in the quick formation of larger drops that merge quickly. After reaching a critical mass, these drops flow down the walls, which eventually reduces the total water area available for re-evaporation during the cooler night phase. We observed such larger drops visually, but given the lack of RH data due to logger failure (Reference 1), we do not have direct evidence and the hypothesis that the re-condensation rate plays a role remains somewhat speculative. However, it would explain the finding that the Reference collectors showed smaller mass losses than the Floating balls and the Float 2 collector.

Aiming at further insights into the processes underlying our observations, we also applied the classic Craig and Gordon (1965) model as implemented in the *Hydrocalculator* (Skrzypek et al., 2015; for details, see Section "Craig and Gordon model" in the Appendix 4). To mimic the conditions in our collectors, we did not use the standard settings, but adjusted the kinetic fractionation constant C_k by varying the turbulence parameter n. The latter is often assumed to be 0.5 (Gonfiantini, 1986), but our modeling mostly yielded higher values (indicating more stagnant conditions). In case of the Floating balls collector, for instance, we obtained an n of about 0.8 (Fig. 4-4). This suggests that isotope-fractionating molecular diffusion out of the collectors plays a dominant role in our experiments. Evaporation, by contrast, seems to be less important with regard to fractionation than initially thought. An exception is the Oil collector, in which the oil prevents evaporation in the first place.

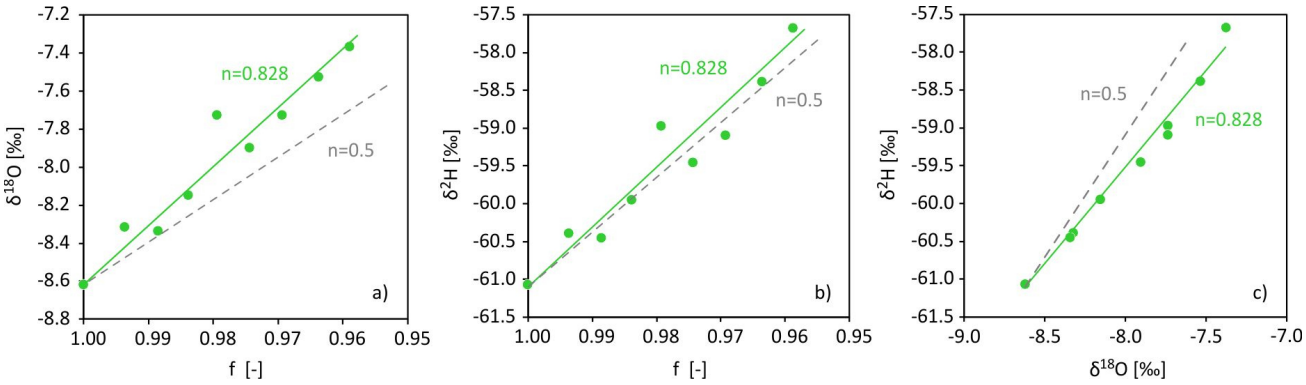

Fig. 4-4. Scatter plots showing the results of the modeling exercise for the Floating balls collector. Note that the lines generated with an n of 0.5 showed unsatisfactory fits, particularly in the $\delta^{18}O$ vs. residual fraction f plot (a) and in the dual-isotope space (c). The corresponding plots for the remaining collectors are presented in Appendix 4 (Figs. A4-13 and A4-14).

If collector designs described in the literature are blindly employed in the field under various climate conditions they were not designed for, impacts on the obtained isotope data seem inevitable. In the rather unlikely case that each integrated sample is affected equally during all seasons and thus shifted by the same value in the dual-isotope plot, the resulting Local Meteoric Water Line (LMWL) will have the correct slope, but an altered intercept. However, it is more likely that samples collected during warmer months are affected to a greater extent. Since these samples are often genuinely enriched in heavier isotopes, their evaporative shift has a leverage effect on the LMWL. This would result in a smaller slope and a modified intercept (e.g., Moerman et al., 2013).

To identify samples affected by evaporation from the collector, the deuterium excess (d) can be considered as a quality assurance/quality control (QA/QC) metric. In our experiment, the low performance devices showed remarkable drops in d, from 7.9 ‰ (original value) down to values between 1.3 and 4.1 ‰ (Fig. 4-3c). Because d can be naturally lowered by sub-cloud evaporation, i.e., partial evaporation from the falling rain drop (Dansgaard, 1964), we do not suggest a general d threshold under which a sample should be regarded as

"suspicious". Yet, we propose that researchers compare calculated d values with empirically determined site-specific threshold values.

4.6. Conclusions and outlook

For our intercomparison of rain collectors, we created extreme conditions with a diurnal temperature regime (26–45°C) and very dry air (5 % RH). This setting allows for an evaluation of the devices in terms of a potential application in warm and arid areas.

The Oil collector exhibited the smallest evaporative losses and lowest isotope shifts. It proved to be the safest option, which shows why it has been the gold standard for decades. While many studies have demonstrated that samples gathered this way could be correctly measured, also with laser-based isotope-analyzers (Ohlanders et al., 2013; van Geldern et al., 2014; Wassenaar et al., 2011), others have expressed concerns. Particularly the potential sample contamination by oil has been highlighted (Gröning et al., 2012; IAEA, 2014; Prechsl et al., 2014). The oil-free Tube-dip-in-water collector with pressure equilibration tube seems to be a viable alternative. Although this method showed measurable isotope shifts under the extreme conditions of this study, we expect a reasonable performance for most isotope hydrology studies, especially compared to the remaining collectors (Ball-in-Funnel, Floating balls, Float 1 and 2). In addition, the device is simple and can be built locally with basic materials or bought from a commercial manufacturer. Sample collection is fast and straightforward, because no oil separation step is involved. Care must be taken when dealing with small amounts of rain. In our study, the collector was filled to 20 % and we already encountered a measurable shift. When lower filling levels are expected, the standard setup should be modified (e.g., larger funnel diameter, smaller bottle volume).

The Tube-dip-in-water collector proved to be a good compromise and we acknowledge a general tendency of researchers to use this published and seemingly established version in isotope hydrology. However, we strongly encourage others to conduct own tests. These should be carried out under environmental conditions expected for the study area, for instance directly in the field. Such real-world tests have the advantage that they reveal shortcomings not considered during the design process. For example, Scholl (2006) reports a case where apparently an animal stole the ball from a Ball-in-funnel collector, presumably because it thought it was an egg. Thirsty animals that opened a device to reach the water and humans that dumped trash in a collector (Adams et al., 1995) are also worth to mention in this context.

The alternative is to conduct such tests in a laboratory setting, allowing a precise control of environmental conditions, which facilitates comparison with other studies. With our simple setup, we have demonstrated that access to a professional climate chamber is no fundamental prerequisite for such tests, but that an ordinary laboratory oven can be modified to improvise a chamber allowing basic control of temperature and humidity as key climate parameters.

In case no prior experiments are conducted to test a collector type, we suggest to use a field control. This means that an additional (rain protected) collector is partly filled with a specific amount of water with known isotope composition and placed next to the rain collector upon installation (Scholl et al., 1995, 1996, 2011). This method at least enables post-sampling evaluation of isotopic integrity.

While this study dealt with rather harsh climatic conditions, it is noteworthy that hot and arid conditions are not the only difficult environment. Also the other extreme, freezing conditions, are challenging and the design of a non-fractionating snow collector remains an issue that must be addressed in the near future.

4.7. Acknowledgments

The first author was financially supported by the German Federal Ministry of Education and Research (BMBF) through its program International Postgraduate Studies in Water Technologies (IPSWaT; grant no. IPS10/P10). We also thank Len Wassenaar and an anonymous reviewer whose valuable comments helped to improve the manuscript.

4.8. Supplementary data

Supplementary data to this article can be found online at https://doi.org/10.1016/j.chemgeo.2018.04.032 and in Appendix 4.

4.9. References

Adams, A.I., Goff, F., Counce, D., 1995. Chemical and Isotopic Variations of Precipitation in the Los Alamos Region, New Mexico. LA-12895-MS, Los Alamos National Laboratory.

Allen, S.T., Brooks, J.R., Keim, R.F., Bond, B.J., McDonnell, J.J., 2014. The role of pre-event canopy storage in throughfall and stemflow by using isotopic tracers. Ecohydrology 7, 858–868.

Alter, J.C., 1907. A Method of Preserving Rainfall. Monthly Weather Review 35(11), 511.

Andreo, B., Liñán, C., Carrasco, F., Jiménez de Cisneros, C., Caballero, F., Mudry, J., 2004. Influence of rainfall quantity on the isotopic composition (^{18}O and ^{2}H) of water in mountainous areas. Application for groundwater research in the Yunquera-Nieves karst aquifers (S Spain). Applied Geochemistry 19, 561–574.

Angermann, L., Jackisch, C., Allroggen, N., Sprenger, M., Zehe, E., Tronicke, J., Weiler, M., Blume, T., 2017. Form and function in hillslope hydrology: characterization of subsurface flow based on response observations. Hydrology and Earth System Sciences 21, 3727–3748.

Balestrini, R., Delconte, C.A., Sacchi, E., Wilson, A.M., Williams, M.W., Cristofanelli, P., Putero, D., 2016. Wet deposition at the base of Mt Everest: Seasonal evolution of the chemistry and isotopic composition. Atmospheric Environment 146, 100–112.

Beisner, K.R., Paretti, N.V., Tucci, R.S., 2016. Analysis of Stable Isotope Ratios ($\delta^{18}O$ and $\delta^{2}H$) in Precipitation of the Verde River Watershed, Arizona, 2003 through 2014. Open-File Report 2016-1053, USGS.

Bicalho, C.C., Batiot-Guilhe, C., Taupin, J.D., Patris, N., Van Exter, S., Jourde, H., 2017. A conceptual model for groundwater circulation using isotopes and geochemical tracers coupled with hydrodynamics: A case study of the Lez karst system, France. Chemcial Geology, https://doi.org/10.1016/j.chemgeo.2017.08.014 (in press).

Birkel, C. Geris, J., Molina, M.J., Mendez, C., Arce, R., Dick, J., Tetzlaff, D., Soulsby, C., 2016. Hydroclimatic controls on non-stationary stream water ages in humid tropical catchments. Journal of Hydrology 542, 231–240.

Bowen, G.J., Revenaugh, J., 2003. Interpolating the isotopic composition of modern meteoric precipitation. Water Resources Research 39(10), 1299.

Brand, W.A., Coplen, T.B., Vogl, J., Rosner, M., Prohaska, T., 2014. Assessment of international reference materials for isotope-ratio analysis (IUPAC Technical Report). Pure and Applied Chemistry 86(3), 425–467.

Brandes, E., Wenninger, J., Koeniger, P., Schindler, D., Rennenberg, H., Leibundgut, C., Mayer, H., Gessler, A., 2007. Assessing environmental and physiological controls over water relations in a Scots pine (*Pinus sylvestris* L.) stand through analyses of stable isotope composition of water and organic matter. Plant, Cell and Environment 30, 113–127.

Coplen, T.B., 2011. Guidelines and recommended terms for expression of stable-isotope-ratio and gas-ratio measurement results. Rapid Communications in Mass Spectrometry 25, 2538–2560.

Craig, H., Gordon, L.I., 1965. Deuterium and oxygen 18 variations in the ocean and the marine atmosphere. In: Tongiorgi, E. (ed.). Stable Isotopes in Oceanographic Studies and Paleotemperatures. Consiglio Nazionale delle Ricerche, Laboratorio di Geologia Nucleare, Pisa, 9–130.

Crawford, J., Hollins, S.E., Meredith, K.T., Hughes, C.E., 2017. Precipitation stable isotope variability and subcloud evaporation processes in a semi-arid region. Hydrological Processes 31, 20–34.

Crawford, J., Hughes, C.E., Lykoudis, S., 2014. Alternative least squares methods for determining the meteoric water line, demonstrated using GNIP data. Journal of Hydrology 519, 2331–2340.

Dansgaard, W., 1964. Stable isotopes in precipitation. Tellus 16(4), 436–468.

Deshpande, R.D., Maurya, A.S., Kumar, B., Sarkar, A., Gupta, S.K., 2010. Rain-vapor interaction and vapor source identification using stable isotopes from semiarid western India. Journal of Geophysical Research 115, D23311.

Friedman, I., Smith, G.I., Gleason, J.D., Warden, A., Harris, J.M., 1992. Stable isotope composition of waters in southeastern California 1. Modern precipitation. Journal of Geophysical Research 97(D5), 5795–5812.

Gonfiantini, R., 1986. Environmental isotopes in lake studies. In: Fritz, P., Fontes, J.C. (eds.). Handbook of Environmental Isotope Geochemistry, Vol. 2: The Terrestrial Environment. Elsevier, Amsterdam, 113–168

Gonfiantini, R., Roche, M.-A., Olivry, J.-C., Fontes, J.-C., Zuppi, G.M., 2001. The altitude effect on the isotopic composition of tropical rains. Chemical Geology 181, 147–167.

Green, M.B., Laursen, B.K., Campbell, J.L., McGuire, K.J., Kelsey, E.P., 2015. Stable water isotopes suggest sub-canopy water recycling in a northern forested catchment. Hydrological Processes 29, 5193–5202.

Gröning, M., Lutz, H.O., Roller-Lutz, Z., Kralik, M., Gourcy, L., Pöltenstein, L., 2012. A simple rain collector preventing water re-evaporation dedicated for $\delta^{18}O$ and $\delta^{2}H$ analysis of cumulative precipitation samples. Journal of Hydrology 448–449, 195–200.

Guo, X., Tian, L., Wang, L., Yu, W., Qu, D., 2017. River recharge sources and the partitioning of catchment evapotranspiration fluxes as revealed by stable isotope signals in a typical high-elevation arid catchment. Journal of Hydrology 549, 616–630.

Hartmann, A., Luetscher, M., Wachter, R., Holz, P., Eiche, E., Neumann, T., 2018. Technical note: GUARD – An automated fluid sampler preventing sample alteration by contamination, evaporation and gas exchange, suitable for remote areas and harsh conditions. Hydrology and Earth System Sciences Discussions, https://doi.org/10.5194/hess-22-4281-2018.

Harvey, F.E., 2001. Use of NADP Archive Samples to Determine the Isotope Composition of Precipitation: Characterizing the Meteoric Input Function for Use in Ground Water Studies. Ground Water 39(3), 380–390.

Harvey, F.E., Welker, J.M., 2000. Stable isotopic composition of precipitation in the semi-arid north-central portion of the US Great Plains. Journal of Hydrology 238, 90–109.

IAEA, 2002. A New Device for Monthly Rainfall Sampling for GNIP. Water & Environment News 16, 5.

IAEA, 2013. Get Involved with GNIP. Water & Environment News 32, 3.

IAEA, 2014. IAEA/GNIP precipitation sampling guide.

IAEA/WMO – International Atomic Energy Agency/World Meteorological Organization, 2018. Global Network of Isotopes in Precipitation. The GNIP Database. https://nucleus.iaea.org/wiser (last access: 11 January 2018).

Ingraham, N.L., Lyles, B.F., Jacobson, R.L., Hess, J.W., 1991. Stable Isotopic Study of Precipitation and Spring Discharge in Southern Nevada. Journal of Hydrology 125, 243–258.

Koeniger, P., Hubbart, J.A., Link, T., Marshall, J.D., 2008. Isotopic variation of snow cover and streamflow in response to changes in canopy structure in a snow-dominated mountain catchment. Hydrological Processes 22, 557–566.

Kralik, M., Papesch, W., Sticher, W., 2004. Austrian Network of Isotopes in Precipitation (ANIP): Quality assurance and climatological phenomenon in one of the oldest and densest networks in the world. In: IAEA. Isotope Hydrology and Integrated Water Resources Management, 146–149.

Martinez, J.L., Raiber, M., Cox, M.E., 2015. Assessment of groundwater–surface water interaction using long-term hydrochemical data and isotope hydrology: Headwaters of the Condamine River, Southeast Queensland, Australia. Science of the Total Environment 536, 499–516.

McGuire, K.J., McDonnell, J.J., Weiler, M., Kendall, C., McGlynn, B.L., Welker, J.M., Seibert, J., 2005. The role of topography on catchment-scale water residence time. Water Resources Research 41, W05002.

Michelsen, N., Reshid, M., Siebert, C., Schulz, S., Knöller, K., Weise, S.M., Rausch, R., Al-Saud, M., Schüth, C., 2015. Isotopic and chemical composition of precipitation in Riyadh, Saudi Arabia. Chemical Geology 413, 51–62.

Moerman, J.W., Cobb, K.M., Adkins, J.F., Sodemann, H., Clark, B., Tuen, A.A., 2013. Diurnal to interannual rainfall $\delta^{18}O$ variations in northern Borneo driven by regional hydrology. Earth and Planetary Science Letters 369–370, 108–119.

Moscati, R.J., Scofield, K.M., 2011. Meteoric Precipitation at Yucca Mountain, Nevada: Chemical and Stable Isotope Analyses, 2006–09. Scientific Investigations Report 2011-5140, USGS.

Müller, S., Stumpp, C., Sørensen, J.H., Jessen, S., 2017. Spatiotemporal variation of stable isotopic composition in precipitation: Post-condensational effects in a humid area. Hydrological Processes 31, 3146–3159.

Muñoz-Villers, L.E., McDonnell, J.J., 2012. Runoff generation in a steep, tropical montane cloud forest catchment on permeable volcanic substrate. Water Resources Research 48, W09528.

O'Driscoll, M.A., DeWalle, D.R., McGuire, K.J., Gburek, W.J., 2005. Seasonal ^{18}O variations and groundwater recharge for three landscape types in central Pennsylvania, USA. Journal of Hydrology 303, 108–124.

Ohlanders, N., Rodriguez, M., McPhee, J., 2013. Stable water isotope variation in a Central Andean watershed dominated by glacier and snowmelt. Hydrology and Earth System Sciences 17, 1035–1050.

Otte, I., Detsch, F., Gütlein, A., Scholl, M., Kiese, R., Appelhans, T., Nauss, T., 2017. Seasonality of stable isotope composition of atmospheric water input at the southern slopes of Mt. Kilimanjaro, Tanzania. Hydrological Processes 31, 3932–3947.

Payne, B.R., 1983. Introduction. In: IAEA. Guidebook on Nuclear Techniques in Hydrology. Technical Report Series No. 91, 1–18.

Prechsl, U.E., Gilgen, A.K. Kahmen, A., Buchmann, N., 2014. Reliability and quality of water isotope data collected with a low-budget rain collector. Rapid Communications in Mass Spectrometry 28, 879–885.

Probert, D., 1977. Inhibition of Evaporation. Applied Energy 3, 257–266.

Roa-García, M.C., Weiler, M., 2010. Integrated response and transit time distributions of watersheds by combining hydrograph separation and long-term transit time modeling. Hydrology and Earth System Sciences 14, 1537–1549.

Rozanski, K., Araguás-Araguás, L., Gonfiantini, R., 1993. Isotopic Patterns in Modern Global Precipitation. In: Swart, P.K., Lohmann, K.C., McKenzie, J., Savin, S. (eds.). Climate change in continental isotopic records. Geophysical Monograph 78, 1–36.

Sánchez-Murillo, R., Birkel, C., 2016. Groundwater recharge mechanisms inferred from isoscapes in a complex tropical mountainous region. Geophysical Research Letters 43, 5060–5069.

Sánchez-Murillo, R., Esquivel-Hernández, G., Sáenz-Rosales, O., Piedra-Marín, G., Fonseca-Sánchez, A., Madrigal-Solís, H., Ulloa-Chaverri, F., Rojas-Jiménez, L.D., Vargas-Víquez, J.A., 2017. Isotopic composition in precipitation and groundwater in the northern mountainous region of the Central Valley of Costa Rica. Isotopes in Environmental and Health Studies 53(1), 1–17.

Scholl, M., 2006. Precipitation isotope collector designs. http://water.usgs.gov/nrp/proj.bib/hawaii/precip_methods.htm (last access: 23 January 2018).

Scholl, M., Eugster, W., Burkard, R., 2011. Understanding the role of fog in forest hydrology: stable isotopes as tools for determining input and partitioning of cloud water in montane forests. Hydrological Processes 25, 353–366.

Scholl, M.A., Gingerich, S.B., Tribble, G.W., 2002. The influence of microclimates and fog on stable isotope signatures used in interpretation of regional hydrology: East Maui, Hawaii. Journal of Hydrology 264, 170–184.

Scholl, M.A., Ingebritsen, S.E., Janik, C.J., Kauahikaua, J.P., 1995. An Isotope Hydrology Study of the Kilauea Volcano Area, Hawaii. U.S. Geological Survey Water-Resources Investigations Report 95-4213.

Scholl, M.A., Ingebritsen, S.E., Janik, C.J., Kauahikaua, J.P., 1996. Use of precipitation and groundwater isotopes to interpret regional hydrology on a tropical volcanic island: Kilauea volcano area, Hawaii. Water Resources Research 32(12), 3525–3537.

Scholl, M.A., Shanley, J.B., Zegarra, J.P., Coplen, T.B., 2009. The stable isotope amount effect: New insights from NEXRAD echo tops, Luquillo Mountains, Puerto Rico. Water Resources Research 45, W12407.

Schürch, M., Kozel, R., Schotterer, U., 2003. The Swiss National Network for the Observation of Isotopes in the Water Cycle (NISOT) – 10-Year Experience of Operation. In: IAEA. International Symposium on Isotope Hydrology and Integrated Water Resources Management. IAEA-CN-104, 336–337.

Sevruk, B., Ondrás, M., Chvíla, B., 2009. The WMO precipitation measurement intercomparisons. Atmospheric Research 92, 376–380.

Skrzypek, G., Mydłowski, A., Dogramaci, S., Hedley, P., Gibson, J.J., Grierson, P.F., 2015. Estimation of evaporative loss based on the stable isotope composition of water using Hydrocalculator. Journal of Hydrology 523, 781–789.

Spangenberg, J.E., 2012. Caution on the storage of waters and aqueous solutions in plastic containers for hydrogen and oxygen stable isotope analysis. Rapid Communications in Mass Spectrometry 26, 2627–2636.

Stadler, H., 2003. Rain Gauge with Integrated Isotope-Sampling Device. In: IAEA. International Symposium on Isotope Hydrology and Integrated Water Resources Management. IAEA-CN-104, 264–265.

Stern, L.A., Blisniuk, P.M., 2002. Stable isotope composition of precipitation across the southern Patagonian Andes. Journal of Geophysical Research 107(D23), 4667.

Stockinger, M.P., Bogena, H.R., Lücke, A., Diekkrüger, B., Cornelissen, T., Vereecken, H., 2016. Tracer sampling frequency influences estimates of young water fraction and streamwater transit time distribution. Journal of Hydrology 541, 952–964.

Tang, A.J.S., Chan, W.H., Orr, D.B., Bardswick, W.S., Lusis, M.A., 1987. An Evaluation of the Precision, and Various Sources of Error, in Daily and Cumulative Precipitation Chemistry Sampling. Water, Air, and Soil Pollution 36, 91–102.

Tappa, D.J., Kohn, M.J., McNamara, J.P., Benner, S.G., Flores, A.N., 2016. Isotopic composition of precipitation in a topographically steep, seasonally snow-dominated watershed and implications of variations from the global meteoric water line. Hydrological Processes 30, 4582–4592.

Terzer, S., 2015. Global Network of Isotopes in Precipitation (GNIP). In: WMO. GCOS – Global Climate Observation System. Final Report, 7th Session of the GTN-H Panel, 20–22.

Terzer, S., Wassenaar, L.I., Araguás-Araguás, L.J., Aggarwal, P.K., 2013. Global isoscapes for $\delta^{18}O$ and $\delta^{2}H$ in precipitation: improved prediction using regionalized climatic regression models. Hydrology and Earth System Sciences 17, 1–16.

Terzer, S., Wassenaar, L.I., Douence, C., Araguas-Araguas, L., 2016. An assessment of the isotopic ($^{2}H/^{18}O$) integrity of water samples collected and stored by unattended precipitation totalizers. Geophysical Research Abstracts 18, EGU2016-15992.

Treydte, K., Boda, S., Graf Pannatier, E., Fonti, P., Frank, D., Ullrich, B., Saurer, M., Siegwolf, R., Battipaglia, G., Werner, W., Gessler, A., 2014. Seasonal transfer of oxygen isotopes from precipitation and soil to the tree ring: source water versus needle water enrichment. New Phytologist 202(3), 772–783.

van Geldern, R., Baier, A., Subert, H.L., Kowol, S., Balk, L., Barth, J.A.C., 2014. Pleistocene paleo-groundwater as a pristine fresh water resource in southern Germany – evidence from stable and radiogenic isotopes. Science of the Total Environment 496, 107–115.

van Geldern, R., Barth, J.A.C., 2012. Optimization of instrument setup and post-run corrections for oxygen and hydrogen stable isotope measurements of water by isotope ratio infrared spectroscopy (IRIS). Limnology and Oceanography: Methods 10, 1024–1036.

Vreča, P., Malenšek, N., 2016. Slovenian Network of Isotopes in Precipitation (SLONIP) – a review of activities in the period 1981–2015. Geologija 59(1), 67–84.

Wassenaar, L.I., Athanasopoulos, P., Hendry, M.J., 2011. Isotope hydrology of precipitation, surface and ground waters in the Okanagan Valley, British Columbia, Canada. Journal of Hydrology 411, 37–48.

Wassenaar, L.I., Van Wilgenburg, S.L., Larson, K., Hobson, K.A., 2009. A groundwater isoscape (δD, $\delta^{18}O$) for Mexico. Journal of Geochemical Exploration 102, 123–136.

Waterisotopes, 2018. http://wateriso.utah.edu/waterisotopes/pages/spatial_db/SPATIAL_DB.html (last access: 11 January 2018).

Weaver, J.M.C., Talma, A.S., 2005. Cumulative rainfall collectors – A tool for assessing groundwater recharge. Water SA 31(3), 283–290.

Welker, J.M., 2000. Isotopic ($\delta^{18}O$) characteristics of weekly precipitation collected across the USA: an initial analysis with application to water source studies. Hydrological Processes 14, 1449–1464.

West, A.G., February, E.C., Bowen, G.J., 2014. Spatial analysis of hydrogen and oxygen stable isotopes ("isoscapes") in ground water and tap water across South Africa. Journal of Geochemical Exploration 145, 213–222.

White, A.F., Peterson, M.L., Wollenberg, H., Flexser, S., 1990. Sources and fractionation processes influencing the isotopic distribution of H, O and C in the Long Valley hydrothermal system, California, U.S.A.. Applied Geochemistry 5, 571–585.

Windhorst, D., Waltz, T., Timbe, E., Frede, H.-G., Breuer, L., 2013. Impact of elevation and weather patterns on the isotopic composition of precipitation in a tropical montane rainforest. Hydrology and Earth System Sciences 17, 409–419.

Yasuhara, M., Marui, A., Kazahaya, K., Suzuki, Y., 1993. An Isotopic Study of Groundwater Flow in a Volcano Under Humid Climatic Conditions. Tracers in Hydrology, IAHS Publ. no. 215, 179–186.

Preface to Chapter 5

The experiments described in the previous chapter have shown that the oil- and thus contamination-free Tube-dip-in-water collector with pressure equilibration tube (Gröning et al., 2012) is rather effective in reducing evaporation. It could be deployed in Saudi Arabia, but of course also other (arid) areas, to collect cumulative samples on a monthly basis. While the collection of monthly samples is traditionally the most common practice, high(er) resolution sampling currently receives increasing attention in the isotope community, also in the context of intra-event studies (see Chapter 2). However, the manual exchange of sampling bottles is time-consuming and an automatic evaporation-free rain sampler would undoubtedly be a useful addition to the isotope hydrologist's toolbox.

An autonomous sampler would also and particularly be helpful, if samples have to be collected in remote areas, which are often devoid of monitoring stations. Unfortunately, the selection of sampler locations is often not entirely based on scientific reasons. Frequently, organizational and logistical factors play a governing role. On the Arabian Peninsula, Riyadh fulfils both criteria (see Chapter 2). The city is located in Central Saudi Arabia, where several major aquifers have their outcrops and thus recharge areas, but obviously, it also helped that the GIZ/Dornier Consulting project office was located there. The GNIP station Bahrain, by contrast, has a long record (since 1961; and hence apparently reliable personnel), but the station is not too helpful from a hydrogeological perspective. It is located at the Arabian Gulf, the discharge zone of the aquifer system. The typical hydrogeologist, however, would prefer a station in the recharge zone, which is, in most cases, in the interior of the peninsula. Depending on the research question, also certain elevations (altitude effect) or distances from the sea (continental effect) could be targeted. As these locations do not necessarily coincide with Saudi Arabia's urban clusters or road network, remote areas might be particularly relevant.

Considering the gained experience with cumulative collectors (see previous chapter), we hence developed an automatic rain sampler for isotope studies, which is introduced in the following chapter.

References

Gröning, M., Lutz, H.O., Roller-Lutz, Z., Kralik, M., Gourcy, L., Pöltenstein, L., 2012. A simple rain collector preventing water re-evaporation dedicated for $\delta^{18}O$ and $\delta^{2}H$ analysis of cumulative precipitation samples. Journal of Hydrology 448–449, 195–200.

5. Technical note: A microcontroller-based automatic rain sampler for stable isotope studies

Nils Michelsen [a,*], Gerrit Laube [b], Jan Friesen [c], Stephan M. Weise [c], Ali Bakhit Ali Bait Said [d], Thomas Müller [b]

[a] Technische Universität Darmstadt, Institute of Applied Geosciences, 64287 Darmstadt, Germany

[b] UFZ – Helmholtz Centre for Environmental Research, Department of Hydrogeology, 04318 Leipzig, Germany

[c] UFZ – Helmholtz Centre for Environmental Research, Department of Catchment Hydrology, 06120 Halle, Germany

[d] Ministry of Regional Municipalities and Water Resources, Salalah, Sultanate of Oman

* Corresponding author (michelsen@geo.tu-darmstadt.de)

Published in Hydrology and Earth System Sciences, 2019, Vol. 23, 2637–2645, DOI: 10.5194/hess-23-2637-2019 ("Highlight article"; https://www.hydrology-and-earth-system-sciences.net/highlight_articles.html)

5.1. Abstract

Automatic samplers represent a convenient way to gather rain samples for isotope (^{18}O and ^{2}H) and water quality analyses. Yet, most commercial collectors are expensive and do not reduce post-sampling evaporation and the associated isotope fractionation sufficiently. Thus, we have developed a microcontroller-based automatic rain sampler for timer-actuated collection of integral rain samples. Sampling periods are freely selectable (minutes to weeks), and the device is low-cost, simple, robust, and customizable. Moreover, a combination of design features reliably minimizes evaporation from the collection bottles. Evaporative losses were assessed by placing the pre-filled sampler in a laboratory oven with which a diurnal temperature regime (21–31°C) was simulated for 26 weeks. At the end of the test, all bottles had lost less than 1 % of the original water amount, and all isotope shifts were within the analytical precision.

These results show that even multi-week field deployments of the device would result in rather small evaporative mass losses and isotope shifts. Hence, we deem our sampler a useful addition to devices that are currently commercially available and/or described in the scientific literature. To enable reproduction, all relevant details on hard- and software are openly accessible.

5.2. Introduction

The stable isotopes ^{18}O and ^{2}H represent nearly ideal tracers that are frequently applied in hydrology and other disciplines. Yet, most applications require data on the isotope composition of precipitation (Bowen and Revenaugh, 2003; Hughes and Crawford, 2013).

Although isotope analyzers have become field-deployable, enabling high-resolution on-site rain analyses (Berman et al., 2009; Herbstritt et al, 2018a; Munksgaard et al., 2011, 2012; Pangle et al., 2013; von Freyberg et al., 2017; Windhorst et al., 2017), many researchers hesitate to take their analyzer to the field due to the risk of damaging the expensive device and due to logistical constraints such as high power demand (Herbstritt et al., 2018b). Hence, most samples are still obtained in more traditional ways for subsequent analysis in the laboratory. They are collected manually (e.g., in intra-event studies; Conroy et al., 2016; Michelsen et al., 2015), with cumulative rain collectors (summarized in Michelsen et al., 2018), or with automatic samplers.

Such automatic samplers, initially mostly developed for precipitation chemistry studies, cover a broad range of designs (see reviews by Krupa, 2002; Laquer, 1990; Robertson et al., 1980). Simple versions of the "linked collection vessels" type (Robertson et al., 1980), featuring a set of serially connected bottles that are consecutively filled, are inexpensive and easy to construct. They have no moving parts and collect samples on a volume basis (Laquer, 1990). Particularly the designs by Kennedy et al. (1979) and Vermette and Drake (1987) are still used nowadays (Fischer et al., 2016, 2017; Hervé-Fernández et al., 2016; Muñoz-Villers and McDonnell, 2013; Saffarpour et al., 2016), albeit sometimes with modifications (Buda and DeWalle, 2009; Qu et al., 2017). Drawbacks of this sampler type comprise the lack of an efficient evaporation reduction mechanism, possibly causing post-sampling fractionation (Fischer et al., 2017), and a potential for cross-contamination of samples.

More complex "automatically segmenting samplers" (Robertson et al., 1980) are commercially available but usually expensive (several thousand euros; Tauro et al., 2018). Further, they often do not minimize evaporation sufficiently (Hartmann et al., 2018; Tauro et al., 2018; Williams et al., 2018). To overcome the latter problem, researchers have occasionally added paraffin oil to the collection bottles of such commercial samplers (Birkel et al., 2011; van Huijgevoort et al., 2016; Sprenger et al., 2017; Tunaley et al., 2017), as recommended by Fergusson (1921). However, a quantitative oil removal is not easy, and oil traces might cause problems during laboratory analyses (Gröning et al., 2012), particularly in laser spectroscopy (IAEA, 2014). Fischer et al. (2016) thus explicitly avoided the oil method and preferred to empty their automatic samplers directly after rainfall events.

The isotope community also developed various custom-made automatic samplers, mostly for high-resolution sampling of rainwater and/or surface water (e.g., Camacho Suarez et al., 2015; Conroy et al., 2016; Coplen et al., 2008; Muller et al., 2015; Neuhaus, 2016, 2018; Siebert, 2015; Terzer-Wassmuth et al., 2018; Zannoni et al., 2019). While some of these collectors are outlined in the corresponding patent specifications (Coplen, 2010; Neuhaus, 2016; Siebert, 2015), several others are only briefly described or not at all. We can imagine that, at least in some of these cases, the researchers did not provide details because they saw their collectors as means to an end, i.e., as tools helping to generate data on which they eventually concentrated.

Notable exceptions in this context are Hartmann et al. (2018) and Nelke et al. (2018), who do provide sufficient details on their devices to enable reproduction. The former authors use a peristaltic pump to inject water directly into airtight vials. Nelke et al. (2018), by contrast, utilize two peristaltic pumps to direct water into aluminum-

lined bags using solenoid valves. Both collectors apparently focus on continuously flowing media (e.g., dripwater, surface water; instead of discontinuous media such as precipitation) and take discrete "snapshot" samples (instead of integral samples) of small to moderate size (12 and 250 mL, respectively). Moreover, their designs have in common that they are rather sophisticated. Yet, complexity can be a double-edged sword. While their technical solutions are certainly elegant, the advanced designs might be somewhat difficult to reproduce.

Another noteworthy open-source device is the autonomous rainfall sampler by Ankor et al. (2019), which collects daily and monthly samples. Here, the water flows by gravity through the partly 3D printed system and is elegantly guided by a split tipping bucket and a "water switch" into the daily and monthly bottles with volumes of 225 mL and 2 L, respectively. Unfortunately, a 13-week field test (mean temperature: 25.3°C) revealed evaporative losses from the pre-filled bottles, resulting in remarkable $\delta^{18}O$ changes. The latter ranged from about 1.10 ‰ to 2.63 ‰, depending on the bottle cap material. Only when paraffin oil was used in the collection bottles (see above) were the isotopic changes acceptable (approx. 0.14 ‰ for $\delta^{18}O$). To mitigate the evaporation effect, the authors suggest a coupled hydrologic–isotopic model that takes advantage of the combined daily and monthly sample collection and allows a back-calculation of the original sample volumes and isotopic compositions. Although such an approach might be an option, we think it would be more straightforward to minimize evaporation from the collection bottles in the first place.

Here, we describe a complementary automatic rain sampler. Our simple, robust, and low-cost collector allows the timer-actuated collection of integral rain samples, with time intervals ranging from minutes to weeks. A combination of design features effectively reduces post-sampling evaporation. In the spirit of open science (see Ankor et al., 2019; Hartmann et al., 2018; Nelke et al., 2018), we provide a detailed description of our customizable collector and its components. Moreover, we present the results of a 26-week test addressing the evaporation reduction capacity of the device in a warm climate.

5.3. Design

The following section gives an overview of the sampler design. Further details (bill of materials, technical drawings, circuit diagram, code, and manuals) enabling reproduction are provided in the Supplement and on the website at https://www.ufz.de/index.php?en=44048 (last access: 15 June 2019) (section Documentation).

The sampler collects rain by a funnel from which the water flows into a distribution unit, the core of the device (Fig. 5-1). It consists of two custom-made uniaxial discs (separated by a 2 mm neoprene rubber seal) with drill holes that are positioned opposite each other. The upper disc (PTFE) is the rotor (rotates clockwise) and has two drill holes fitted with push-in ports. The outer port is the rain inlet, and the inner port is the air outlet. The lower disc (PVC-U) is the stator (remains static) and features 36 ports that are arranged in two circles. The ports of the outer circle are connected to water tubes, and the ports of the inner circle are connected to air tubes (LDPE; see section "Pre-test of tubing materials" in Appendix 5, incl. Fig. A5-1, Table A5-1).

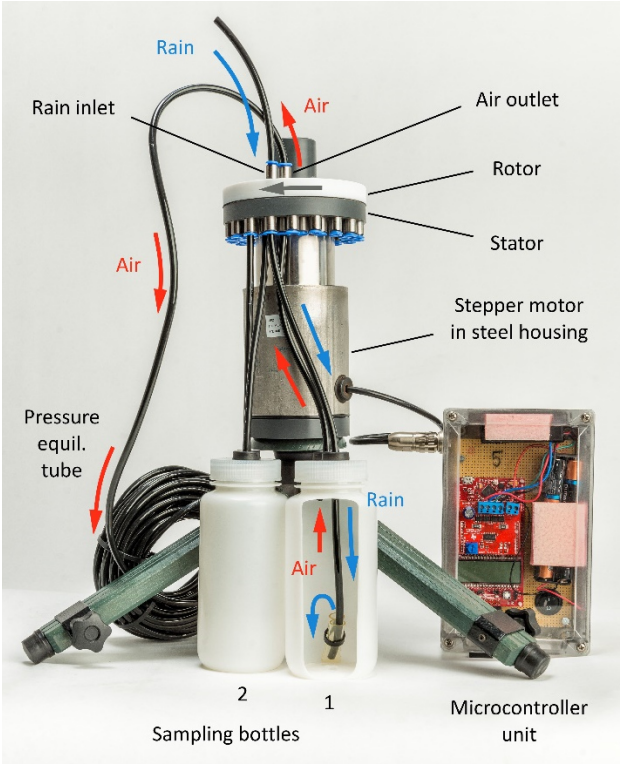

Fig. 5-1. Overview of the automatic sampler principle (photo by André Künzelmann, UFZ). Water (blue arrows) flows from the rain inlet through the distribution unit and into the first bottle (cutaway view). Displaced air (red arrows) leaves the bottle and flows through the distribution unit and the air outlet into a 15 m long pressure equilibration tube. At the end of the sampling interval, the rotor is turned (grey arrow), leading the rain into the second bottle.

Water coming from the funnel flows through the rain inlet into the distribution unit and then through a water tube, into the first 500 mL sampling bottle. All tubes are guided through the bottle caps by means of cable grommets (Fig. A5-2), ensuring a tight connection. With respect to the bottles, we recommend thick-walled HDPE bottles that effectively reduce diffusive water losses (Spangenberg, 2012; Gröning, 2019). For our purposes, we selected 500 mL HDPE wide-mouth bottles by Labsolute (Renningen, Germany; wall thickness approx. 1.7 mm).

To minimize post-sampling evaporation, we adapted the concept of an evaporation-free cumulative collector (Gröning et al., 2012), which has been successfully tested under hot and arid conditions (Michelsen et al., 2018) and is advocated by the IAEA (2014). In this concept, an inlet tube extends to the bottom of the bottle. A few millimeters of rainfall is sufficient to cause a water level rise into the tube, thus decoupling the bottle headspace from the atmosphere. This process can be amplified by inserting the end of the inlet tube into a small container (Gröning et al., 2012; or a short piece of bent tubing; see Fig. 5-1), reducing the amount of rain needed to decouple the air in the bottle from the atmosphere. The air displaced by the inflowing water leaves the bottle through the air tubing that, unlike the inlet tube, extends just below the bottle cap. The air tubing leads from

the bottle cap back to the distribution unit. Here, the air is pushed through the air outlet into a 15 m long pressure equilibration tube (see Gröning et al., 2012; IAEA, 2014).

At the end of the freely selectable sampling interval, a microcontroller (Texas Instruments; for details, see Supplement) triggers a stepper motor to turn the rotor of the distribution unit by 20°. Through this rotation, the first sampling bottle is isolated from the atmosphere – the rotor disc closes the water and air tubes of this bottle. In turn, rain can now flow into the second bottle. The air thus displaced from the second bottle is pushed into the aforementioned pressure equilibration tube; i.e., this tube is shared by all bottles. A tight fit of the rotor is ensured through a spring above the disc, providing sufficient pressure to avoid leakages.

The microcontroller features a display and buttons for convenient programming, avoiding the necessity of a notebook during field setup or maintenance. Moreover, the microcontroller has a set of low power modes that are excessively used. In fact, the microcontroller and the accompanying stepper motor driver are only active during initial setup and between sampling periods, while the distribution unit is driven to the next sampling port. The fact that the distribution unit consumes virtually no power during sampling allows for week-long sampling periods on just two AA batteries for the logic unit and another eight AA batteries for the stepper motor.

The stepper motor and the control unit (microcontroller with accessories and batteries) are each located in a dust- and waterproof enclosure and connected by a waterproof cable (IP68). This robust design loosens the requirements for the overall enclosure. For field deployments (not presented here), a simple plastic storage box was chosen to be sufficient to house the sampling bottles and the automatic collector.

5.4. Evaporation experiment

5.4.1. Methods

After initial tests targeting the functional capabilities of the sampler (timing, rotation angles, etc.), we studied the evaporation reduction efficiency of the device.

To this end, five HDPE bottles (500 mL; Labsolute, Renningen, Germany) were partially filled with water of known isotopic composition ($\delta^{18}O$=-8.53 ‰, $\delta^{2}H$=-60:7 ‰ related to Vienna Standard Mean OceanWater, V-SMOW) and connected with water and gas tubing to the distribution unit (Table 5-1). The latter was not coupled to the microcontroller unit; i.e., the rotor did not move during the test.

Table 5-1. Overview of collected samples and associated water losses and isotopic shifts. Water losses Δm are given as absolute mass losses [g] and as percentages of the original water amount [% orig]. Isotopic signatures ($\delta^{18}O$ and $\delta^{2}H$) and isotopic shifts away from the original composition ($\Delta\delta^{18}O$ and $\Delta\delta^{2}H$) are given in ‰ V-SMOW. Note that the analytical precisions for $\delta^{18}O$ and $\delta^{2}H$ account for ±0.15 ‰ and ±0.6 ‰ (±1σ), respectively.

ID	Description	t [weeks]	Δm [g]	Δm [% orig]	$\delta^{18}O$ [‰]	$\delta^{2}H$ [‰]	$\Delta\delta^{18}O$ [‰]	$\Delta\delta^{2}H$ [‰]
Orig.	Original water	0	n.a.	n.a.	-8.53	-60.7	n.a.	n.a.
Bottle 1	exposed, 100 mL	6	0.17	0.17	-8.32	-60.2	0.21*	0.5*
		16	0.56	0.56	-8.50	-60.6	0.03*	0.1*
		26	0.94	0.94	-8.44	-60.2	0.09*	0.5*
Bottle 2	blocked, 100 mL	6	0.20	0.20	-8.42	-60.4	0.11*	0.3*
		16	0.56	0.56	-8.23	-60.0	0.30*	0.7*
		26	0.93	0.93	-8.46	-60.2	0.07*	0.5*
Bottle 3	blocked, 200 mL	6	0.16	0.08	-8.49	-60.7	0.04*	0.0*
		16	0.46	0.23	-8.49	-60.6	0.04*	0.1*
		26	0.81	0.40	-8.59	-60.9	-0.06*	-0.2*
Bottle 4	blocked, 300 mL	6	0.43	0.14	-8.53	-60.8	0.00*	-0.1*
		16	1.16	0.39	-8.50	-60.5	0.03*	0.2*
		26	2.04	0.68	-8.57	-60.7	-0.04*	0.0*
Bottle 5	blocked, 400 mL	6	0.53	0.13	-8.53	-60.8	0.00*	-0.1*
		16	1.47	0.37	-8.55	-60.7	-0.02*	0.0*
		26	2.41	0.60	-8.60	-60.6	-0.07*	0.1*
Bottle 6	closed, 100 mL	6	0.05	0.05	-8.60	-60.9	-0.07*	-0.2*
		16	0.14	0.14	-8.65	-60.9	-0.12*	-0.2*
		26	0.24	0.24	-8.66	-60.9	-0.13*	-0.2*
Bottle 7	open, 100 mL	6	5.27	5.27	-6.85	-56.1	1.68	4.6
		16	14.18	14.18	-3.70	-46.9	4.83	13.8
		26	24.42	24.42	0.70	-35.2	9.23	25.5

n.a.: not applicable; *: Δδ within analytical precision (|±1σ|= 2σ)

Bottle 1 (filled with 100 mL) was connected to the open ports; i.e., its water and air tubes led to the ports beneath the rain inlet and the air outlet, respectively (Fig. 5-2). A 2 m long rain tube (without funnel) was connected to the rain inlet, and a 15 m long pressure equilibration tube was connected to the air outlet. With this bottle, we wanted to assess how long a sampling bottle can be left "exposed" to the atmosphere (exposed via the rain tube and the pressure equilibration tube).

Bottles 2 to 5 contained different water amounts (100, 200, 300, and 400 mL), and their water and air tubes led to stator ports that were blocked by the rotor disc. Here, the goal was to determine how long a sample can remain in the collector without undergoing critical evaporative mass loss.

This setup was placed for 26 weeks (see Hartmann et al., 2018) in a laboratory drying oven (T 6120 by Heraeus, Hanau, Germany) with which a diurnal temperature regime was simulated (Michelsen et al., 2018). A socket timer triggered a daily 12 h heating period (31°C). After this phase, the oven was allowed to cool down to room temperature (approx. 21°C). To accelerate this cooling process, the oven was opened daily for 3 h. Temperature and relative humidity in the oven were logged in 10 min intervals (DK320 HumiLog ruggedPlus by Driesen + Kern GmbH, Bad Bramstedt, Germany).

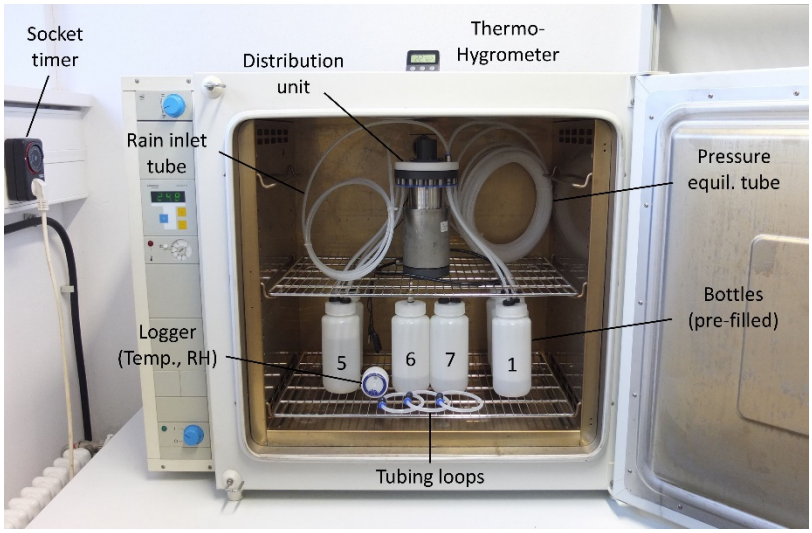

Fig. 5-2. Photograph of the evaporation experiment setup. Note that the bottles were pre-filled with water of known isotopic composition; i.e., no water flowed through the tubing, and the distribution unit did not rotate during the test.

For comparison, two additional bottles were placed into the oven – bottles 6 and 7 (both filled with 100 mL). Bottle 6 was closed, thus representing a best-case scenario. With this approach, potential diffusion through the bottle material was tested. Bottle 7, by contrast, was “open”; i.e., it featured two holes (diameter 6 mm) in its cap, to represent the worst case (no evaporation suppression).

Moreover, three identical LDPE tubing loops (häberle LABORTECHNIK, Lonsee-Ettlenschieß, Germany) were included in the oven experiment. They were partially filled with 0.5 mL of water and the tubing ends were connected to each other with a connector. All three loops had a circumference of 25 cm, which corresponds to the lengths of the tubing between the bottles and the distribution unit. This allowed for an estimate of diffusive water fluxes through the tubing material.

To determine evaporative mass losses during the experiment, the bottles and the tubing loops were weighed repeatedly (Voyager Pro VP2102C by Ohaus, Pine Brook, USA). Bottles 1 through 5 were disconnected from the distribution unit for this purpose. Samples for isotope analyses (1.6 mL in 2 mL vials) were gathered after 6, 16, and 26 weeks. In the case of bottles 1 to 5, water was withdrawn through the water tube with a syringe. Bottle

6 was sampled through a gastight sampling port in its cap (Mininert by VICI Precision Sampling, Baton Rouge, LA, USA) with a syringe. Samples from bottle 7 were taken with a Pasteur pipette through one of the holes in the cap. To account for these artificial mass losses, the bottles were weighed before and after sampling.

At the end of the test, the obtained water samples were analyzed for their isotopic composition using laser cavity ringdown spectroscopy (L2130-i by Picarro, Santa Clara, CA, USA). The results were expressed in per mil (‰) using the conventional delta notation relative to V-SMOW. The external precisions (±1σ), determined by repeated analyses of a control sample, were ±0.15 ‰ and ±0.6 ‰, for $\delta^{18}O$ and $\delta^{2}H$, respectively.

5.4.2. Results

5.4.2.1 Evaporative mass losses

The applied diurnal temperature regime (21–31°C; see Fig. A5-3) mostly resulted in small but measurable evaporative mass losses that increased over time (Table 5-1).

After 26 weeks, absolute mass losses ranged between 0.8 and 2.4 g for the bottles connected to the distribution unit (bottles 1 through 5). Bottle 6 (closed), representing the best case, showed a lower mass loss of 0.24 g, and in the case of bottle 7 (open; worst case), a loss of 24.42 g was encountered. The three tubing loops (each 25 cm long) lost about 0.14 g over the same time period (see Table A5-2).

These data suggest that the diffusive loss through the tubing material of the connected bottles (two tubes per bottle, hence 0.28 g; see tubing loop data) is similar to the flux through the bottle material of bottle 6 (0.24 g). As all connected bottles exhibited greater absolute mass losses, additional leakages, e.g., at the cable grommets in the bottle caps or at the distribution unit, seem likely. In this context, pressure fluctuations, induced by the diurnal temperature regime, probably play a role. It is also noteworthy that the blocked bottles, bottles 4 and 5, containing 300 and 400 mL of water showed the greatest losses (>2 g). This observation could point towards an influence of the bottle surface area in contact with liquid water on the diffusive water flux through the plastic. Nevertheless, the overall absolute losses are still rather small, particularly when compared to the worst-case scenario, an unprotected bottle (bottle 7).

This becomes clearer when the data are put in perspective with the original water amounts. Fractional losses of bottles 1 through 5 range from 0.40 % to 0.94 % orig; i.e., even after half a year the maximum loss was below 1 %. As expected, these values are somewhat higher than in case of the closed bottle (bottle 6; 0.24 % orig) but far below the loss recorded for the open bottle, bottle 7, which lost nearly a quarter of its water (24.42 % orig).

5.4.2.2 Isotopic shifts

The bulk of the obtained δ values scatter around the original isotopic signature ($\delta^{18}O$=-8.53 ‰, $\delta^{2}H$=-60.7 ‰; see Table 5-1). The calculated isotopic shifts, $\Delta\delta^{18}O$ and $\Delta\delta^{2}H$, mostly range between -0.07 ‰ and 0.30 ‰ and between -0.2 ‰ and 0.7 ‰, respectively (bottles 1 through 5).

These shifts are rather small. Keeping in mind that the reported external 1σ precisions, ±0.15 ‰ ($\delta^{18}O$) and ±0.6 ‰ ($\delta^{2}H$), apply to the original water and the water after oven exposure, the encountered shifts practically all lie within the analytical error. This also holds true for the shifts of the closed bottle, bottle 6.

The open bottle, bottle 7, by contrast, showed substantial shifts. After 26 weeks, the $\delta^{18}O$ and $\delta^{2}H$ values had increased by about 9.23 ‰ and 25.5 ‰, respectively.

5.5. Discussion

Following a "keep it simple" approach, we have designed an elementary and robust sampler, deliberately avoiding complexity such as pumps, solenoid valves, or remote controls (cf., Coplen et al., 2015; Hartmann et al., 2018; Nelke et al., 2018). Avoiding such complexities greatly reduces the failure risk in the field. We also avoided components that permanently consume power (e.g., normally closed solenoid valves during the "open" phase) and complex tubing systems that would possibly require parts of the sampling water to be used for tubing flushes. Hence, our collector is relatively easy to reproduce, although some technical skills are required.

Compared to other devices (Coplen et al., 2008; Hartmann et al., 2018), it has fewer but bigger bottles. The latter aspect implies that analyses do not have to be restricted to $\delta^{18}O$ and $\delta^{2}H$, but other parameters such as ^{3}H and major ions (incl. bicarbonate by titration), etc., could in principle be studied as well.

Most importantly, our device gathers integral samples over freely selectable collection periods (minutes to weeks) and effectively reduces post-sampling evaporation. In combination with the low power consumption, these features render it a potential candidate for autonomous rain sampling at remote, unmanned sites. Traditionally, precipitation samples for isotope analyses are mostly collected on a monthly integral basis (e.g., in the Global Network of Isotopes in Precipitation, GNIP; IAEA/WMO, 2019). Yet, due to the advent of laser-based isotope analyzers and the associated decreasing costs for analyses (Berman et al., 2009; Herbstritt et al., 2012; Wassenaar et al., 2018), shorter collection periods (e.g., weekly integral samples) have become more popular (e.g., Otte et al., 2017). An important advantage of sampling schemes with a higher temporal resolution is the gain in flexibility. They allow, for example, a correlation between isotope signature and meteorological variables (Akers et al., 2017; Hughes and Crawford, 2013; Rao et al., 2008), but data can still be aggregated to precipitation-weighted monthly values for seamless comparison with other monthly data sets (e.g., GNIP).

Due to the relatively low costs (parts <600 €), several automatic collectors can be deployed simultaneously to address spatial variability. A number of researchers reported pronounced spatial variability of the isotopic

composition of rain in small catchments (Fischer et al., 2017; Kato et al., 2013) or at the city scale (Chen et al., 2017). In these studies, $\delta^{18}O$ values partly varied by several ‰ within short distances (a few hundred meters to a few kilometers). In the case of throughfall, $\delta^{18}O$ values can even differ significantly on the plot scale, i.e., within meters, and differences of more than 1 ‰ (Allen et al., 2014, 2015; Kato et al., 2013) or even several ‰ (Hsueh et al., 2016) have been observed. Further, it has been shown that ignoring the spatial variability impairs isotope-based hydrograph separations (Cayuela et al., 2019; Fischer et al., 2017). These findings highlight the need for collector arrays or networks (see Lutz et al., 2018; Scholl et al., 1995, 1996). Using expensive, commercial equipment in such networks might be prohibitively expensive for many researchers. Rodgers et al. (2005), for instance, report resource constraints preventing the installation of a second sampler in their catchment to capture the local altitude effect. In such cases, an affordable custom-made alternative is extremely useful. This also applies to study areas in which vandalism or theft of monitoring equipment might be an issue (see Kongo et al., 2010; Otte et al., 2017; Pramana and Ertsen, 2016). In such settings, researchers on a limited budget would possibly hesitate to leave expensive equipment unattended at a remote site for longer time periods, and a low-cost alternative would be appreciated.

Although this work focused on the isotopes ^{18}O and ^{2}H, gathered samples could also be analyzed for other isotopes or their hydrochemistry. Since the funnel is permanently exposed, the sampler would act as a bulk sampler (collecting wet and dry deposition). Hydrochemical analyses could, for instance, include chloride for recharge estimations via the Chloride Mass Balance method (e.g., Eriksson and Khunakasem, 1969; Guan et al., 2010).

5.6. Potential modifications

While the presented sampler suits our purposes, we acknowledge that other researchers might have different expectations towards such a collector. Thus, we explicitly encourage others to modify our design and tailor it to their specific needs.

Potential modifications might address the number of bottles and their size. In addition, the tubing can be changed, but we suggest the use of opaque tubing for the exposed section from the funnel to the sampler itself to reduce the risk of algae growth, which has occasionally caused problems in rain collectors (Scholl et al., 1995). Although it might be tempting to replace the push-in ports by ordinary barbed hose fittings, we suggest not to do so for the following reasons. i) Given the potential risk of disconnection of tubing, the used ports are deemed a safe option. ii) Their handling is easier, particularly when dealing with tens of connections in a confined space. iii) They do not introduce an additional constriction.

Although we used a Texas Instruments microcontroller, we can imagine that the functionality of the sampler could also be achieved with parts from the popular Arduino ecosystem, though probably at the cost of greater power consumption.

Moreover, one could transform the timer-actuated into a volume-controlled rain sampler, for instance by means of a microcontroller-based tipping bucket system. The latter would calculate the filling status of a sampling bottle based on the recorded number of tips and automatically direct the water into the next bottle when the first one is full (see Muller et al., 2015).

Also, a transformation into a surface water sampler is feasible. To this end, one could combine the current device with a timer-triggered peristaltic or submersible pump. The microcontroller provides several unused input/output and communication pins and further unutilized resources to allow for such customizations.

5.7. Summary and conclusions

Our microcontroller-based automatic rain sampler enables timer-actuated integral rain sampling. The simple, low-cost device is robust and effectively minimizes post-sampling evaporation from the collection bottles and the associated isotope fractionation. The excellent performance of the device during an extensive evaporation experiment in a laboratory oven (26 weeks; 21–31°C) suggests that even multi-week field deployments in warm climates are feasible. In the spirit of open science, we share all relevant details on our sampler and encourage others to adapt it to their specific needs.

5.8. Data availability

All details needed to copy our sampler are freely available (Supplement and https://www.ufz.de/index.php?en=44048, last access: 15 June 2019, section Documentation). Data on the evaporation experiment, enabling a performance evaluation, are given in the main article and the Supplement.

5.9. Supplement

The supplement related to this article is available online at: https://doi.org/10.5194/hess-23-2637-2019-supplement. Parts of it are also presented in Appendix 5.

5.10. Author contributions

NM, GL, and TM conceptualized the sampler. GL was responsible for the detailed sampler design and programmed the microcontroller. GL, JF, ABABS, and TM conducted initial tests. NM carried out the evaporation experiment. SMW performed isotope and data analyses. NM wrote the manuscript with contributions from all co-authors.

5.11. Acknowledgments

This work has been supported by the project “Submarine Groundwater Discharge: Adaption of an Autonomous Aquatic Vehicle for Robotic Measurements, Sampling and Monitoring”, funded by The Research Council of Oman (TRC Research Contract No. TRC/RCP/15/001). We would also like to thank the UFZ workshop and Hendrik Zöphel (UFZ) for assistance in construction and Inga Schreiter, Sahand Farhang Darehshouri, and Claudia Cosma (TU Darmstadt) for help during the evaporation experiment. Moreover, we thank Martijn Westhoff for his efficient editorial handling and Rolf Hut and Manfred Gröning for their constructive reviews. We acknowledge support by the German Research Foundation and the Open Access Publishing Fund of Technische Universität Darmstadt.

5.12. References

Akers, P.D., Welker, J.M., Brook, G.A., 2017. Reassessing the role of temperature in precipitation oxygen isotopes across the eastern and central United States through weekly precipitation-day data. Water Resources Research 53, 7644–7661.

Allen, S.T., Brooks, J.R., Keim, R.F., Bond, B.J., McDonnell, J.J., 2014. The role of pre-event canopy storage in throughfall and stemflow by using isotopic tracers. Ecohydrology 7, 858–868.

Allen, S.T., Keim, R.F., McDonnell, J.J., 2015. Spatial patterns of throughfall isotopic composition at the event and seasonal timescales. Journal of Hydrology 522, 58–66.

Ankor, M.J., Tyler, J.J., Hughes, C.E., 2019. Development of an autonomous, monthly and daily, rainfall sampler for isotope research. Journal of Hydrology 575, 31–41.

Berman, E.S.F., Gupta, M., Gabrielli, C., Garland, T., McDonnell, J.J., 2009. High-frequency field-deployable isotope analyzer for hydrological applications. Water Resources Research 45, W10201.

Birkel, C., Tetzlaff, D., Dunn, S.M., Soulsby, C., 2011. Using lumped conceptual rainfall–runoff models to simulate daily isotope variability with fractionation in a nested mesoscale catchment. Advances in Water Resources 34, 383–394.

Bowen, G.J., Revenaugh, J., 2003. Interpolating the isotopic composition of modern meteoric precipitation. Water Resources Research 39, 1299.

Buda, A.R., DeWalle, D.R., 2009. Dynamics of stream nitrate sources and flow pathways during stormflows on urban, forest and agricultural watersheds in central Pennsylvania, USA. Hydrological Processes 23, 3292–3305.

Camacho Suarez, V.V., Saraiva Okello, A.M.L., Wenninger, J.W., Uhlenbrook, S., 2015. Understanding runoff processes in a semi-arid environment through isotope and hydrochemical hydrograph separations. Hydrology and Earth System Sciences 19, 4183–4199.

Cayuela, C., Latron, J., Geris, J., Llorens, P., 2019. Spatio-temporal variability of the isotopic input signal in a partly forested catchment: Implications for hydrograph separation. Hydrological Processes 33, 36–46.

Chen, F., Zhang, M., Wang, S., Qiu, X., Du, M., 2017. Environmental controls on stable isotopes of precipitation in Lanzhou, China: An enhanced network at city scale. Science of the Total Environment 609, 1013–1022.

Conroy, J.L., Noone, D., Cobb, K.M., Moerman, J.W., Konecky, B.L., 2016. Paired stable isotopologues in precipitation and vapor: A case study of the amount effect within western tropical Pacific storms. Journal of Geophysical Research – Atmospheres 121, 3290–3303.

Coplen, T.B., 2010. Sequential, time-integrated collector of precipitation, ground water, and surface water for analysis of isotopes. Patent US7687028 (B1).

Coplen, T.B., Neiman, P.J., White, A.B., Landwehr, J.M., Ralph, M., Dettinger, M.D., 2008. Extreme changes in stable hydrogen isotopes and precipitation characteristics in a landfalling Pacific storm. Geophysical Research Letters 35, L21808.

Coplen, T.B., Neiman, P.J., White, A.B., Ralph, F.M., 2015. Categorisation of northern California rainfall for periods with and without a radar brightband using stable isotopes and a novel automated precipitation collector. Tellus B, 67, 28574.

Eriksson, E., Khunakasem, V., 1969. Chloride concentration in groundwater, recharge rate and rate of deposition of chloride in the Isreal coastal plan. Journal of Hydrology 7, 178–197.

Fergusson, S.P., 1921. Improved Gages for Precipitation. Monthly Weather Review 49, 379–386.

Fischer, B.M.C., Stähli, M., Seibert, J., 2016. Pre-event water contributions to runoff events of different magnitude in pre-alpine headwaters. Hydrology Research 48, 28–47.

Fischer, B.M.C., van Meerveld, H.J., Seibert, J., 2017. Spatial variability in the isotopic composition of rainfall in a small headwater catchment and its effect on hydrograph separation. Journal of Hydrology 547, 755–769.

Gröning, M., 2019. Interactive comment on “Technical note: A microcontroller-based automatic rain sampler for stable isotope studies” by N. Michelsen et al., https://doi.org/10.5194/hess-2019-93-RC2.

Gröning, M., Lutz, H.O., Roller-Lutz, Z., Kralik, M., Gourcy, L., Pöltenstein, L., 2012. A simple rain collector preventing water re-evaporation dedicated for $\delta^{18}O$ and $\delta^{2}H$ analysis of cumulative precipitation samples. Journal of Hydrology 448–449, 195–200.

Guan, H., Love, A.J., Simmons, C.T., Makhnin, O., Kayaalp, A.S., 2010. Factors influencing chloride deposition in a coastal hilly area and application to chloride deposition mapping. Hydrology and Earth System Sciences 14, 801–813.

Hartmann, A., Luetscher, M., Wachter, R., Holz, P., Eiche, E., Neumann, T., 2018. Technical note: GUARD – an automated fluid sampler preventing sample alteration by contamination, evaporation and gas exchange, suitable for remote areas and harsh conditions. Hydrology and Earth System Sciences 22, 4281–4293.

Herbstritt, B., Gralher, B., Weiler, M., 2012. Continuous in situ measurements of stable isotopes in liquid water. Water Resources Research 48, W03601.

Herbstritt, B., Gralher, B., Weiler, M., 2018a. Real-time observations of stable isotope dynamics during rainfall and throughfall events. Hydrology and Earth System Sciences Discussions, https://doi.org/10.5194/hess-2018-301.

Herbstritt, B., Seeger, S., Rinderer, M., Weiler, M., 2018b. Low cost water vapour sampling for mobile in-situ measurements of stable water isotopes. EGU General Assembly 2018, Vienna, Austria, EGU2018-9188-1.

Hervé-Fernández, P., Oyarzún, C., Brumbt, C., Huygens, D., Bodé, S., Verhoest, N.E.C., Boeckx, P., 2016. Assessing the 'two water worlds' hypothesis and water sources for native and exotic evergreen species in south-central Chile. Hydrological Processes 30, 4227–4241.

Hsueh, Y.H., Allen, S.T., Keim, R.F., 2016. Fine-scale spatial variability of throughfall amount and isotopic composition under a hardwood forest canopy. Hydrological Processes 30, 1796–1803.

Hughes, C.E., Crawford, J., 2013. Spatial and temporal variation in precipitation isotopes in the Sydney Basin, Australia. Journal of Hydrology 489, 42–55.

IAEA, 2014. IAEA/GNIP precipitation sampling guide.

IAEA/WMO – International Atomic Energy Agency/World Meteorological Organization, 2019. Global Network of Isotopes in Precipitation. The GNIP Database. https://nucleus.iaea.org/ wiser (last access: 12 January 2019).

Kato, H., Onda, Y., Nanko, K., Gomi, T., Yamanaka, T., Kawaguchi, S., 2013. Effect of canopy interception on spatial variability and isotopic composition of throughfall in Japanese cypress plantations. Journal of Hydrology 504, 1–11.

Kennedy, V.C., Zellweger, G.W., Avanzino, R.J., 1979. Variation of Rain Chemistry During Storms at Two Sites in Northern California. Water Resources Research 15, 687–702.

Kongo, V.M., Kosgei, J.R., Jewitt, G.P.W., Lorentz, S.A., 2010. Establishment of a catchment monitoring network through a participatory approach in a rural community in South Africa. Hydrology and Earth System Sciences 14, 2507–2525.

Krupa, S.V., 2002. Sampling and physico-chemical analysis of precipitation: a review. Environmental Pollution 120, 565–594.

Laquer, F.C., 1990. Sequential Precipitation Samplers: A Literature Review. Atmospheric Environment 24A, 2289–2297.

Lutz, S.R., Krieg, R., Müller, C., Zink, M., Knöller, K., Samaniego, L., Merz, R., 2018. Spatial Patterns of Water Age: Using Young Water Fractions to Improve the Characterization of Transit Times in Contrasting Catchments. Water Resources Research 54, 4767–4784.

Michelsen, N., Reshid, M., Siebert, C., Schulz, S., Knöller, K., Weise, S.M., Rausch, R., Al-Saud, M., Schüth, C., 2015. Isotopic and chemical composition of precipitation in Riyadh, Saudi Arabia. Chemical Geology 413, 51–62.

Michelsen, N., van Geldern, R., Roßmann, Y., Bauer, I., Schulz, S., Barth, J.A.C., Schüth, C., 2018. Comparison of cumulative precipitation collectors used in isotope hydrology. Chemical Geology 488, 171–179.

Muller, C.L., Baker, A., Fairchild, I.J., Kidd, C., Boomer, I., 2015. Intra-Event Trends in Stable Isotopes: Exploring Midlatitude Precipitation Using a Vertically Pointing Micro Rain Radar. Journal of Hydrometeorology 16, 194–213.

Munksgaard, N.C., Wurster, C.M., Bird, M.I., 2011. Continuous analysis of $\delta^{18}O$ and δD values of water by diffusion sampling cavity ring-down spectrometry: a novel sampling device for unattended field monitoring of precipitation, ground and surface waters. Rapid Communications in Mass Spectrometry 25, 3706–3712.

Munksgaard, N.C., Wurster, C.M., Bass, A., Bird, M.I., 2012. Extreme short-term stable isotope variability revealed by continuous rainwater analysis. Hydrological Processes 26, 3630–3634.

Muñoz-Villers, L.E., McDonnell, J.J., 2013. Land use change effects on runoff generation in a humid tropical montane cloud forest region. Hydrology and Earth System Sciences 17, 3543–3560.

Nelke, M., Coltman, C., Lien, H., Walter, C., Udell, C., Selker, J., 2018. OPEnSLab-OSU/OPEnSampler: OPEnSampler v1.0. https://doi.org/10.5281/zenodo.2483259 (see also http://www.open-sensing.org/opensampler/ (last access: 10 February 2019).

Neuhaus, L., 2016. Verfahren mit einem elektronischen Probenfluidnehmer zum Erzeugen und Bereitstellen von in umgebungsluftdichten Behältern abgefüllten Fluidproben für die Analyse und/oder Grenzwert-Überwachung. Patent DE102015007049 (A1).

Neuhaus, L., 2019. Automatisches Wasserprobenentnahmesystem mit Verdunstungs- und Entgasungsschutz. https://www.liquidsampler.de/ (last access: 12 January 2019).

Otte, I., Detsch, F., Gütlein, A., Scholl, M., Kiese, R., Appelhans, T., Nauss, T., 2017. Seasonality of stable isotope composition of atmospheric water input at the southern slopes of Mt. Kilimanjaro, Tanzania. Hydrological Processes 31, 3932–3947.

Pangle, L.A., Klaus, J., Berman, E.S.F., Gupta, M., McDonnell, J.J., 2013. A new multisource and high-frequency approach to measuring $\delta^{2}H$ and $\delta^{18}O$ in hydrological field studies. Water Resources Research 49, 7797–7803.

Pramana, K.E.R., Ertsen, M.W., 2016. Towards systematic planning of small-scale hydrological intervention-based research. Hydrology and Earth System Sciences 20, 4093–4115.

Qu, S., Wang, Y., Zhou, M., Liu, H., Shi, P., Yu, Z., Xiang, L., 2017. Temporal ^{18}O and deuterium variations in hydrologic components of a small watershed during a typhoon event. Isotopes in Environmental and Health Studies 53, 172–183.

Rao, T.N., Radhakrishna, B., Srivastava, R., Satyanarayana, T.M., Rao, D.N., Ramesh, R., 2008. Inferring microphysical processes occurring in mesoscale convective systems from radar measurements and isotopic analysis. Geophysical Research Letters 35, L09813.

Robertson, J.K., Dolzine, T.W., Graham, R.C., 1980. Chemistry of Precipitation from Sequentially Sampled Storms. U.S. Environmental Protection Agency, EPA-600/4-80-004.

Rodgers, P., Soulsby, C., Waldron, S., Tetzlaff, D., 2005. Using stable isotope tracers to assess hydrological flow paths, residence times and landscape influences in a nested mesoscale catchment. Hydrology and Earth System Sciences 9, 139–155.

Saffarpour, S., Western, A.W., Adams, R., McDonnell, J.J., 2016. Multiple runoff processes and multiple thresholds control agricultural runoff generation. Hydrology and Earth System Sciences 20, 4525–4545.

Scholl, M.A., Ingebritsen, S.E., Janik, C.J., Kauahikaua, J.P., 1995. An Isotope Hydrology Study of the Kilauea Volcano Area, Hawaii. U.S. Geological Survey Water-Resources Investigations Report 95-4213.

Scholl, M.A., Ingebritsen, S.E., Janik, C.J., Kauahikaua, J.P., 1996. Use of precipitation and groundwater isotopes to interpret regional hydrology on a tropical volcanic island: Kilauea volcano area, Hawaii. Water Resources Research 32, 3525–3537.

Siebert, C., 2015. Automatischer Probennehmer mit atmosphärisch entkoppelter Speicherung wässriger Proben im Passiv- und Aktiv-Modus. Patent DE102014205633 (B4).

Spangenberg, J.E., 2012. Caution on the storage of waters and aqueous solutions in plastic containers for hydrogen and oxygen stable isotope analysis. Rapid Communications in Mass Spectrometry 26, 2627–2636.

Sprenger, M., Tetzlaff, D., Soulsby, C., 2017. Soil water stable isotopes reveal evaporation dynamics at the soil–plant–atmosphere interface of the critical zone. Hydrology and Earth System Sciences 21, 3839–3858

Tauro, F., Selker, J., van de Giesen, N., Abrate, T., Uijlenhoet, R., Porfiri, M., Manfreda, S., Caylor, K., Moramarco, T., Benveniste, J., Ciraolo, G., Estes, L., Domeneghetti, A., Perks, M.T., Corbari, C., Rabiei, E., Ravazzani, G., Bogena, H., Harfouche, A., Brocca, L., Maltese, A., Wickert, A., Tarpanelli, A., Good, S., Lopez Alcala, J.M., Petroselli, A., Cudennec, C., Blume, T., Hut, R., Grimaldi, S., 2018. Measurements and Observations in the XXI century (MOXXI): innovation and multi-disciplinarity to sense the hydrological cycle. Hydrological Sciences Journal 63, 169–196.

Terzer-Wassmuth, S., Araguas-Araguas, L.J., Wassenaar, L.I., Aggarwal, P.K., 2018. On the short-term (5-30 min.) precipitation isotope ($\delta^{18}O$, $\delta^{2}H$) variability in a temperate climate. EGU General Assembly 2018, Vienna, Austria, EGU2018-18997.

Tunaley, C., Tetzlaff, D., Birkel, C., Soulsby, C., 2017. Using high-resolution isotope data and alternative calibration strategies for a tracer-aided runoff model in a nested catchment. Hydrological Processes 31, 3962–3978.

van Huijgevoort, M.H.J., Tetzlaff, D., Sutanudjaja, E.H., Soulsby, C., 2016. Using high resolution tracer data to constrain water storage, flux and age estimates in a spatially distributed rainfall-runoff model. Hydrological Processes 30, 4761–4778.

Vermette, S.J., Drake, J.J., 1987. Simplified Wet-Only and Sequential Fraction Rain Collector. Atmospheric Environment 21, 715–716.

von Freyberg, J., Studer, B., Kirchner, J.W., 2017. A lab in the field: high-frequency analysis of water quality and stable isotopes in stream water and precipitation. Hydrology and Earth System Sciences 21, 1721–1739.

Wassenaar, L.I., Terzer-Wassmuth, S., Douence, C., Araguas-Araguas, L., Aggarwal, P.K., Coplen, T.B., 2018. Seeking excellence: an evaluation of 235 international laboratories conducting water isotope analyses by isotope-ratio and laser absorption spectrometer. Rapid Communications in Mass Spectrometry 32, 393–406.

Williams, M.R., Lartey, J.L., Sanders, L.L., 2018. Isotopic ($\delta^{18}O$ and $\delta^{2}H$) Integrity of Water Samples Collected and Stored by Automatic Samplers. Agricultural & Environmental Letters 3, 180009.

Windhorst, D., Kraft, P., Holly, H., Sahraei, A., Breuer, L., 2017. A mobile and self-sufficient lab for high frequency measurements of stable water isotopes and chemistry of multiple water sources. EGU General Assembly 2017, Vienna, Austria, EGU2017-4879.

Zannoni, D., Steen-Larsen, H.C., Rampazzo, G., Dreossi, G., Stenni, B., Bergamasco, A., 2019. The atmospheric water cycle of a coastal lagoon: An isotope study of the interactions between water vapor, precipitation and surface waters. Journal of Hydrology 572, 630–644.

Preface to Chapter 6

The previous chapters focused on elements of the natural, undisturbed water cycle – precipitation and water in the unsaturated zone under sand dunes. In the next chapter, we turn towards the following compartment of the hydrologic cycle and address shallow groundwater. While many studies have concentrated on deep groundwater in Saudi Arabia, the shallow zone is underrepresented in the literature. At the same time, this chapter touches upon the topic of human interactions with the water cycle, which also deserves more attention in the case of the kingdom.

In this work, we tracked human-induced water level changes in a Saudi Arabian cave by means of a new archive: YouTube videos. Although this might seem somewhat unconventional at the first glance, we have to acknowledge that creative geoscientists have always harnessed proxy data from at times unconventional archives. The main reason is that we are often interested in processes and events in the (distant) past and nature does usually not hand us the required data on a silver platter in our discipline. Although there are numerous examples reported in the literature, only two shall be mentioned here, perhaps not surprisingly from the world of isotopes.

When atmospheric ^{3}H concentrations increased substantially due to thermonuclear bomb tests conducted in the 1950s–1980s (see Chapter 2.2.), the isotope community realized that this tracer could be used to date young groundwaters. Hence, people also became interested in the natural background value, i.e., in the pre-bomb atmospheric ^{3}H concentration. Since only very few old rain or river water samples were available, Kaufman and Libby (1954) utilized vintage wines as an archive.

The isotope ^{36}Cl, an age tracer occasionally used to study old groundwaters was subject to some unconventional approaches as well. Plummer et al. (1997), for instance, capitalized on ^{14}C-dated fossil rat urine to reconstruct cosmogenic ^{36}Cl deposition over a period of 40,000 years.

While old wines and crystallized rat urine are physical archives, digital repositories also hold great potential and are increasingly used in environmental research. This current development is catalyzed by the advent of smartphones and the associated infrastructure.

Leijnse et al. (2007) studied radio links from cellular communication networks and derived precipitation amounts from signal attenuation within the network. Overeem et al. (2013) analyzed logged smartphone battery temperatures to model urban air temperatures. Seibert et al. (2019) designed a smartphone app to enable crowd-based stream level observations. These examples cover a wide spectrum of data types: i) data derived from signal noise (Leijnse et al., 2007), ii) repurposed information, i.e., the data was actually recorded for a different purpose (i.e., battery protection; Overeem et al., 2013), and iii) data deliberately collected for the very purpose (Seibert et al., 2019).

The YouTube approach that is utilized in the following chapter ranges somewhere between type 1 and type 2. In any case, it constitutes (Data) MacGyvering (*sensu* Hut, 2013).

References

Hut, R., 2013. New Observational Tools and Datasources for Hydrology – Hydrological data Unlocked by Tinkering. PhD thesis, TU Delft.

Kaufman, S., Libby, W.F., 1954. The Natural Distribution of Tritium. Physical Review 93(6), 1337–1344.

Leijnse, H., Uijlenhoet, R., Stricker, J.N.M., 2007. Rainfall measurement using radio links from cellular communication networks. Water Resources Research 43, W03201.

Overeem, A., Robinson, J.C.R., Leijnse, H., Steeneveld, G.J., Horn, B.K.P., Uijlenhoet, R., 2003. Crowdsourcing urban air temperatures from smartphone battery temperatures. Geophysical Research Letters 40, 4081–4085.

Plummer, M.A., Phillips, F.M., Fabryka-Martin, J., Turin, H.J., Wigand, P.E., Sharma, P., 1997. Chlorine-36 in Fossil Rat Urine: An Archive of Cosmogenic Nuclide Deposition During the Past 40,000 Years. Science 277, 538–541.

Seibert, J., Strobl, B., Etter, S., Hummer, P., van Meerveld, H.J., 2019. Virtual Staff Gauges for Crowd-Based Stream Level Observations. Frontiers in Earth Science 7, 70.

6. YouTube as a crowd-generated water level archive

Nils Michelsen [a,*], Heiko Dirks [b], Stephan Schulz [c], Stephan Kempe [a], Mohammed Al-Saud [d], Christoph Schüth [a]

[a] Technische Universität Darmstadt, Institute of Applied Geosciences, Darmstadt, Germany

[b] Dornier Consulting, Riyadh, Saudi Arabia

[c] UFZ – Helmholtz Centre for Environmental Research, Catchment Hydrology, Halle, Germany

[d] Ministry of Water & Electricity, Riyadh, Saudi Arabia

* Corresponding author (michelsen@geo.tu-darmstadt.de)

Published in Science of the Total Environment, 2016, Vol. 568, 189–195, DOI: 10.1016/j.scitotenv.2016.05.211

6.1. Abstract

In view of the substantial costs associated with classic monitoring networks, participatory data collection methods can be deemed a promising option to obtain complementary data. An emerging trend in this field is social media mining, i.e., harvesting of pre-existing, crowd-generated data from social media. Although this approach is participatory in a broader sense, the users are mostly not aware of their participation in research.

Inspired by this novel development, we demonstrate in this study that it is possible to derive a water level time series from the analysis of multiple YouTube videos. As an example, we studied the recent water level rise in Dahl Hith, a Saudi Arabian cave. To do so, we screened 16 YouTube videos of the cave for suitable reference points (e.g., cave graffiti). Then, we visually estimated the distances between these points and the water level and traced their changes over time. To bridge YouTube hiatuses, we considered own photos taken during two site visits. For the time period 2013–2014, we estimate a rise of 9.5 m. The fact that this rise occurred at a somewhat constant rate of roughly 0.4 m per month points towards a new and permanent water source, possibly two nearby lakes formed from treated sewage effluent. An anomaly in the rising rate is noted for autumn 2013 (1.3 m per month). As this increased pace coincides with a cluster of rain events, we deem rapid groundwater recharge along preferential flow paths a likely cause.

Despite the sacrifice in precision, we believe that YouTube harvesting may represent a viable option to gather historical water levels in data-scarce settings and that it could be adapted to other environments (e.g., flood extents). In certain areas, it might provide an additional tool for the monitoring toolbox, thereby possibly delivering hydrological data for water resources management.

6.2. Introduction

Integrated Water Resources Management (IWRM) requires a sound assessment of the available resources and their natural fluctuations over time. It is also crucial to understand how the system of interest responds to anthropogenic disturbances. Hence, monitoring represents an important tool within the framework of IWRM (GWP and INBO, 2009). Unfortunately, the installation and operation of monitoring networks come at substantial costs. Hence, participatory data collection methods, also known as citizen science or crowdsourcing approaches, may represent an attractive option to expand existing networks and to gather complementary data (Buytaert et al., 2016; Lowry and Fienen, 2013). Despite the rapidly gaining momentum in participatory methods within the water resources (Buytaert et al., 2014), there are still apparent tensions with traditional methods. Nevertheless, the concept is currently applied to key elements of the water cycle, i.e., precipitation (CoCoRaHS, 2016), soil moisture (SciStarter, 2016), groundwater (Little et al., 2016), streams (Lowry and Fienen, 2013), lakes (Järviwiki, 2016), and the ocean (WHOI, 2016). In such projects, the degree of participation varies considerably and contributions may include digitization of pre-existing data (Old Weather, 2016), sensor design, protection and basic maintenance of monitoring equipment (van de Giesen et al., 2014), data collection (Lowry and Fienen, 2013), sample collection (Good et al., 2014), or data analysis (Cyclone Center, 2016), also as part of the school curriculum (van de Giesen et al., 2014). Moreover, the ways in which the participants are approached and trained differ. They range from site visits with formal training in person (Little et al., 2016) to instructional online videos or slide shows (CoCoRaHS, 2016) and ad hoc instruction in the field by means of signage (Lowry and Fienen, 2013). Nevertheless, such projects have commonality in that the amateur scientists are approached in some way, thereby actively motivating them to contribute data through specific channels and often in a pre-defined data format (Daume et al., 2014).

Some years ago, however, researchers started to complement traditional crowdsourcing by extracting pre-existing, crowd-generated data from social media. Hence, such approaches are, in a way, also participatory, but the contributors are mostly not aware of their participation in a scientific study (Daume et al., 2014). To differentiate this emerging trend from classic, deliberate citizen science, the latter authors coined the term “opportunistic sensing model”. Initially, social media mining largely focused on cultural and social aspects within the Web 2.0 (e.g., Russell, 2014). Yet, recently, the concept became popular in other fields as well (Daume et al., 2014), including hydrology. Social media mining has, for instance, been applied to derive inundation depths during floods and to generate flood extent maps (e.g., Eilander et al., 2015; Fohringer et al., 2015; Smith et al., in press), mostly on the basis of Twitter and Flickr posts. The use of YouTube videos, by contrast, has been rather limited. While the video platform is often termed an archive, its role as a repository has been mostly limited to cultural aspects (e.g., Burgess and Green, 2009; Gehl, 2009). A notable exception in this regard is the recent study by Le Boursicaud et al. (2016). The authors reconstructed a flash-flood in a mountainous torrent on the basis of a high-quality YouTube video and a post-event field survey. They thereby demonstrated the potential

of the video platform to serve as a valuable source for data of hydrological relevance. We agree with this and further suggest that the analysis of YouTube footage in the hydrological context does not have to be limited to the study of short-term phenomena visible in a single video. Instead, we think that certain settings call for the integral analysis of multiple videos from the same location, enabling the tracing of medium- to long-term trends. In the present paper, we seek to demonstrate this method and its feasibility by reconstructing recent water level changes in a Saudi Arabian cave through the analysis of multiple YouTube videos.

6.3. Study site

Dahl Hith, also known as Ayn Hith (Arabic: *dahl* = cave, *ayn* = spring), is a more than 160 m deep cave, located approximately 30 km southeast of Riyadh at the base of the Sulaiy Limestone escarpment (Rausch et al., 2014b) (Lower Cretaceous; Fig. 6-1).

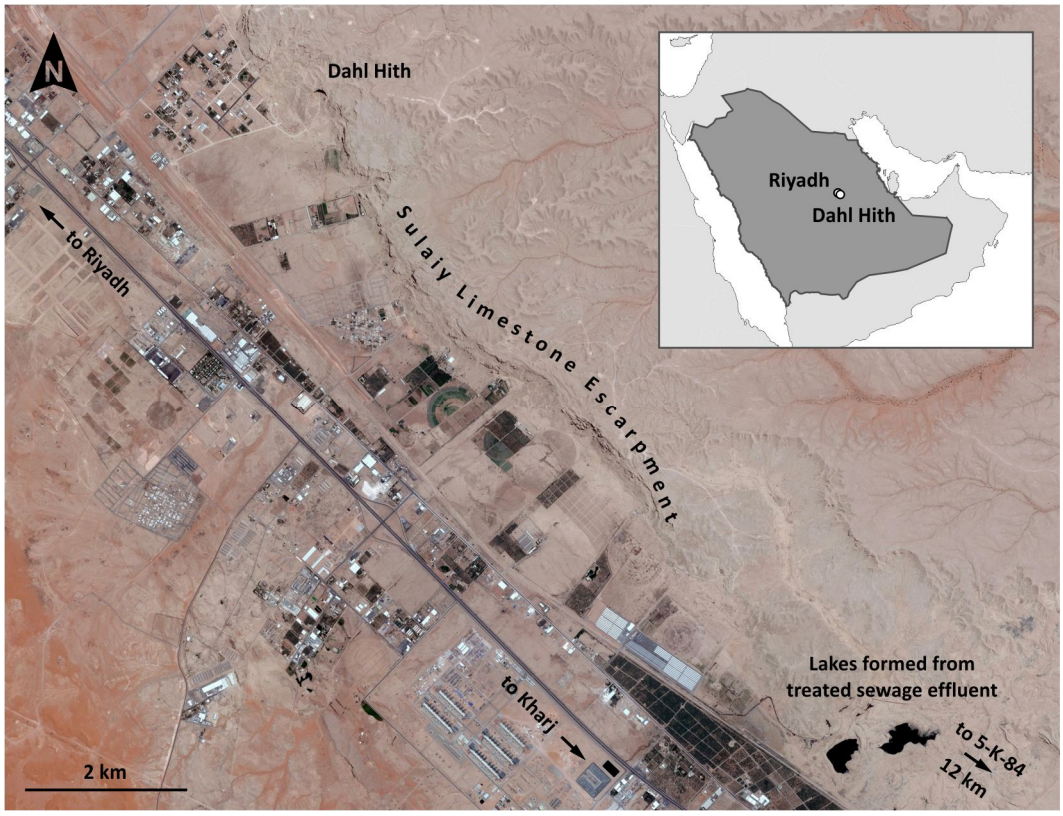

Fig. 6-1. Satellite image of the Dahl Hith area (5 June 2014; GoogleEarth Pro, modified; cave entrance at 24°29'10"N, 46°59'50"E; see also Appendix 6, Figs. A6-1 and A6-2). The closest observation well, 5-K-84, is located 22 km southeast of the cave (12 km southeast of the lakes at the bottom right corner).

It was formed by hypogene karstification of the underlying Upper Jurassic Hith Anhydrite (Kempe and Dirks, 2008). The latter is an important hydrocarbon cap rock on the Arabian Peninsula and Dahl Hith, the type locality,

represents one of the few locations were the anhydrite is exposed (Powers et al., 1966; Steineke et al., 1958; Wolpert et al., 2015).

During the past four decades, the water level inside the cave had dropped by more than 100 m due to agricultural water abstraction (Kempe and Dirks, 2008). The largely fossil groundwater was pumped from wells tapping the underlying Arab aquifer (limestone and anhydrite of Upper Jurassic age), but also from the cave itself. Parts of the corresponding pump station are still visible today (Appendix 6, Figs. A6-1 to A6-4). A few years ago, however, the water level started to rise. Given the fact that many aquifers on the Arabian Peninsula are overexploited and suffer from declining groundwater levels (Rausch et al., 2014a; Richey et al., 2015), this rise was somewhat surprising.

The cave has always attracted people – geologists, cavers and cave divers (Bjurström, 1997), as well as the general public. However, the number of visitors has strongly increased recently. The fact that the water has now reached a level at which it is reached by sunlight (Appendix 6, Figs. A6-5 and A6-6) even made it a popular swimming spot. Unfortunately, there is no observation well in the direct vicinity of the cave. The closest one is located 22 km to the southeast (well 5-K-84, Fig. 6-1). Hence, reliable data on the local piezometric changes are unavailable, resulting in the need to apply a non-traditional technique to reconstruct the water level development.

6.4. Materials and methods

Inspired by YouTube videos that we had stumbled upon in the course of a literature review, we conducted a systematic YouTube survey. We searched for “Dahl Hith” and “Ayn Hith”, using various ways of spelling (e.g., “Ain Heet”, incl. Arabic letters). Partly, we also included the search terms “cave”, “Riyadh”, and/or “Kharj” (another nearby city).

The appreciable number of obtained videos (74 videos by 42 users) reflects the site popularity, a remarkable smartphone penetration in Saudi Arabia, and the leading role of YouTube among social media websites in the country (CITC and KFUPM, 2016; for details see Appendix 6, Text A6-1). From the compiled videos, we selected 16 that were of reasonable quality and showed the water level. After bringing them into chronological order, we screened the footage for suitable reference points (e.g., cave graffiti, boulders, etc.) that appear in multiple videos. Then, we visually estimated the distances between the reference points and the water level and traced their changes over time. These estimations were greatly facilitated when swimmers were close to the section of interest, serving as scale (see Fig. 6-2). In most cases, the uploading date was regarded as the day of observation. Sometimes, however, also the exact date of the visit is provided as part of the footage description. To bridge occasional YouTube hiatuses, we complemented the videos by own photographs taken during two site visits.

Fig. 6-2. Examples of YouTube screenshots used in this study. a) Screenshot from a video by Mark Carreon (upload: 20 October 2013). The diver, Mark, serves as scale, thus facilitating the visual estimation of the distance between the water level and the graffito "J.B" (approx. 0.3 m). b) Screenshot from a video by Marcelo Cordova Jr. (upload: 1 August 2014). For the corresponding links, see Table 6-1 (IDs 5 and 15).

The considered YouTube videos and photographs provide water level data for the time period from January 2013 to December 2014. Yet, one cave graffito featuring a date allowed a glance into the year 1977 (Fig. 6-3). As it is located on the ceiling of the cave, we believe that it has been created by a swimmer. It thus serves as a proxy for a historical water level.

6.5. Results

The results of our YouTube data mining are presented in Table 6-1. During the two year study period, the water has apparently risen by about 9.5 m.

To illustrate this rise, we present selected levels on a photograph that had been taken during a previous site visit in 2012, i.e., before the actual study period (Fig. 6-4). The photo provides a visual impression of the situation.

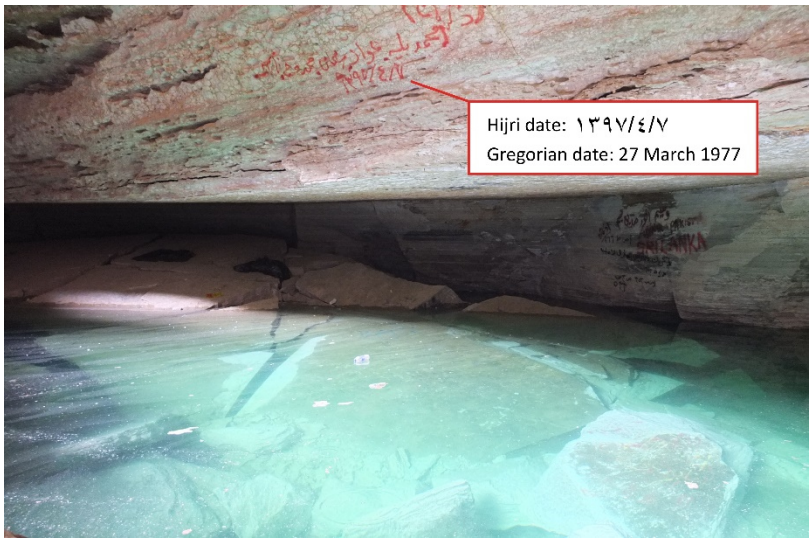

Fig. 6-3. Photograph (taken 29 November 2013) showing a graffito on the cave ceiling. The last line represents a date (in Arabic). Converting the Arabic date (Hijri calendar) into a Gregorian date yields 27 March 1977. The position of the graffito suggests that it was created by a swimmer and thus provides an estimate for the water level in 1977.

Table 6-1. Overview of used videos and photos with date (U: upload, V: visit) and examples of snapshot times useful for water level evaluations. The last two columns present our estimations of relative piezometric changes and the thus derived water levels above the reference (level in January 2013).

ID	Date	Link	Screenshot Time	Comment	Water Level [m]
1	18 Jan 2013 (U)	www.youtube.com/watch?v=JBlKxGCFOc0	0:12	reference	0.0
2	15 Jun 2013 (U)	www.youtube.com/watch?v=t1IKZBy9xQc	0:18, 0:35, 0:39	2.2 m higher than ID 1	2.2
3	23 Aug 2013 (U)	www.youtube.com/watch?v=fh_mtqMdHjM	3:51, 5:09	0.8 m higher than ID 2	3.0
4	1 Sep 2013 (U)	www.youtube.com/watch?v=6nze81IilXQ	0:01	0.2 m higher than ID 3	3.2
5	19 Oct 2013 (V)	www.youtube.com/watch?v=fGwDoLX9FdA	0:11, 0:52	0.1 m lower than ID 6	3.6
6	25 Oct 2013 (V)	www.youtube.com/watch?v=OqQuVPI1YwI	2:43, 3:41	1.5 m higher than ID 2	3.7
7	1 Nov 2013 (V)	www.youtube.com/watch?v=hIzpBjYdTD8	0:54, 1:05	0.3 m higher than ID 6	4.0
8	8 Nov 2013 (U)	www.youtube.com/watch?v=FXyNf_qNskA	0:07	0.3 m higher than ID 7	4.3
9	18 Nov 2013 (U)	www.youtube.com/watch?v=sQodFaGMILQ	9:36	0.5 m higher than ID 7	4.5
10	20 Nov 2013 (V)	own photo	n.a.	0.4 m higher than ID 9	4.9
11	29 Nov 2013 (U)	www.youtube.com/watch?v=IhqNlrOg0_4	0:03	0.4 m higher than ID 10	5.3
12	20 Dec 2013 (V)	www.youtube.com/watch?v=HdQ7-cNDyNI	0:37	0.7 m higher than ID 10	5.6
13	30 May 2014 (V)	www.youtube.com/watch?v=JSf1s9CrP1U	0:30, 1:47	1.5 m higher than ID 10	6.4
14	30 Jul 2014 (U)	www.youtube.com/watch?v=Y69kL-K8Y-k	0:32	0.6 m higher than ID 13	7.0
15	1 Aug 2014 (U)	www.youtube.com/watch?v=urPHGT340dw	0:14, 2:09	same as ID 14	7.0
16	4 Aug 2014 (U)	www.youtube.com/watch?v=mkITdMehbGk	0:05, 0:12	same as ID 14 and ID 15	7.0
17	6 Oct 2014 (U)	www.youtube.com/watch?v=rKcNLxLH6xQ	1:16, 1:40	0.7 m higher than ID 16	7.7
18	19 Dec 2014 (V)	own photo	n.a.	1.8 m higher than ID 17	9.5

Fig. 6-4. Dahl Hith photograph taken before the studied phase of the recent rise (30 May 2012). Lines represent selected water levels derived from YouTube videos and own photos and the associated numbers refer to the IDs in Table 6-1 (for ID 15, also compare Fig. 6-2b). The height of the boulder with the blue graffito on the left is about 2 m.

However, the temporal development is more obvious in Fig. 6-5. The plot reveals a more or less continuous rise at a pace of approx. 0.4 m per month. As a consequence of this remarkable rise, also the graffito marking the level in 1977 has drowned.

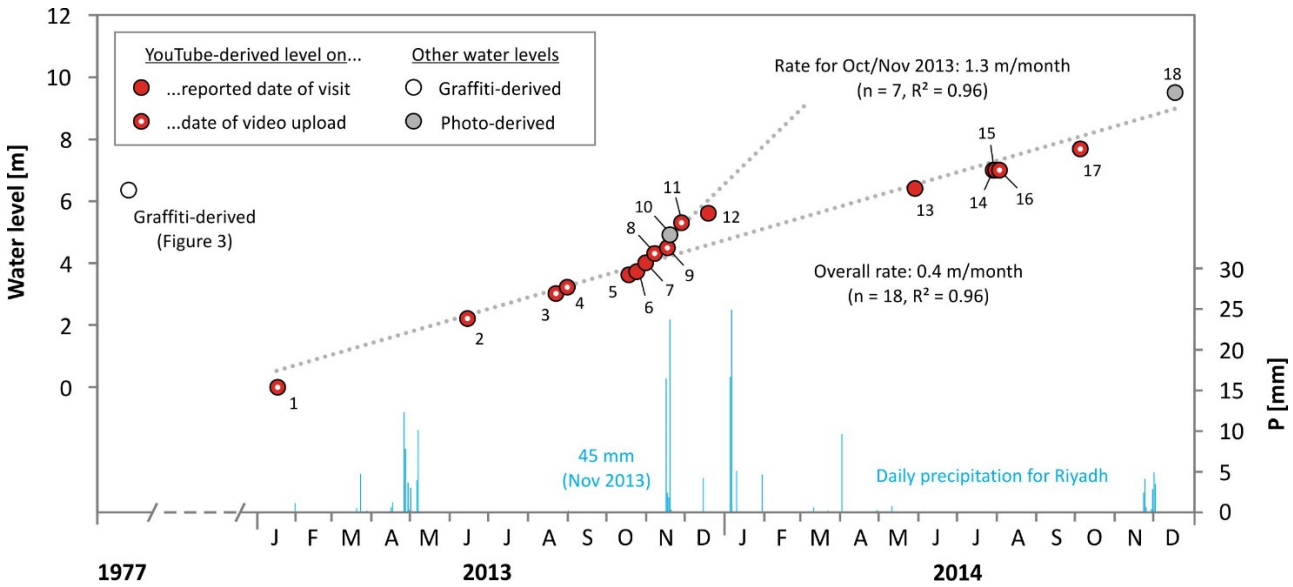

Fig. 6-5. Development of estimated Dahl Hith water levels (zero arbitrarily set to the level in January 2013). Numbers next to data points refer to IDs in Table 6-1. For comparison, daily precipitation data is included (station Riyadh Malaz; Ministry of Water & Electricity). Exact water levels between 1977 and 2013 are unknown, but based on an initial cave survey conducted by some of us (Appendix 6, Figs. A6-3 and A6-4), we estimate that the level in 2008 was several tens of meters deeper than in January 2013 (cf., piezometric data for well 5-K-84, Appendix 6, Fig. A6-7).

Although most aquifers on the Arabian Peninsula show declining groundwater levels (see Section 6.3.), rising groundwater is occasionally observed, particularly underneath big cities like Riyadh. Al-Othman and Ahmed (2012), for instance, report rates between 0.03 and 0.55 m per year for Eastern Riyadh, caused by leaky drinking water and sewage water systems as well as irrigation return flow. However, the rate observed at Dahl Hith clearly exceeds these values.

6.6. Discussion

6.6.1. Reason for the water level rise

The fact that the rise is so rapid and somewhat steady indicates a sudden change in the hydrogeological system, i.e., it points towards a new but permanent water source. A potential source matching these criteria are two artificial lakes formed due to the discharge of treated sewage effluent into a former quarry since spring 2008. These lakes are located 10 km southeast of the cave (Fig. 6-1). As the observation well 5-K-84 (mentioned in Section 6.3., but at first not deemed too relevant) is also situated in the southeast, this well becomes interesting again. Also here, a rapid rise of the groundwater is noted, interestingly since 2008 (approx. 8.2 m per year or 0.7 m per month; see Appendix 6, Fig. A6-7).

In view of the significant distances of 10 km (cave – lakes) and 12 km (lakes – observation well), the rapid responses as well as their magnitudes might seem unrealistic on the first glance. However, one has to keep in mind preferential flow paths caused by karstification and subsequent slumping in the area. Steineke et al. (1958), for example, describe the area, in which the Arab and Hith formations would be expected to crop out as a “nearly hopeless jumble of low hills representing complexly settled rocks”. Further, they state that “dropped masses of the younger Cretaceous rocks occupy the eastern part of the solution-collapse zone”. Also Powers et al. (1966) mention a “rather broad zone of badly slumped beds”. This slumping is also evident in the direct vicinity of Dahl Hith (see Appendix 6, Figs. A6-8 and A6-9).

Although the water level rise in the cave is overall rather stable, there is a deviation from the trend in autumn 2013 (Fig. 6-5). Here, the plot shows a faster rise of about 1.3 m per month. As this anomaly coincides with a cluster of precipitation events (45 mm in five days), we postulate rapid recharge along preferential flowpaths, e.g., the cave entrance (Appendix 6, Fig. A6-10). Such erratic, recharge-related overprints could modify the actually continuous trend and create a step-like pattern. Analyzing this phenomenon is, however, challenging with the available data because our observations are limited in number, restricted to a rather short time period, and distributed unevenly – unavoidable issues inherent to the utilized approach.

6.6.2. Discussion of the YouTube approach

Piezometric data derived from YouTube videos have to be regarded as estimates. A quantification of the associated error (and error propagation) would be in principle possible, after the water level has dropped again (cf., post-event field survey by Le Boursicaud et al., 2016). Then, one could physically measure previously estimated distances on-site. In the present case, however, this is not possible, due to the rise in water levels in the cave flooding the area of interest.

Moreover, there are drawbacks on the temporal scale. The observations are, for example, unevenly distributed, which is an occasional downside of crowdsourced data (cf., Lowry and Fienen, 2013). In the present case, the temporal distribution is probably linked to the water level situation, which has a direct impact on the site popularity. When the water in Dahl Hith was reached by sunlight, it attracted more visitors. As the latter shared their experiences on TV or through social media (see footage descriptions of IDs 12 and 3 on YouTube) the number of visitors increased further. At some point, however, the boom came to an end and Dahl Hith-related video uploads occurred more seldom again.

In terms of shortcomings on the temporal scale, also the often unknown actual observation times are noteworthy. Yet, as the studied system is rather sluggish, at least in comparison to surface water, we think that an uploading delay of a few days would not represent a major problem. In specific cases of doubt, one could try to contact the observer and ask for meta data or the original footage (Le Boursicaud et al., 2016). One way to do so is via the messaging option of YouTube (only available for registered users).

Water levels obtained with the YouTube approach are obviously less precise than those gathered by traditional measurements (e.g., by pressure transducers). However, the approaches should not be seen as competing but complementary methods. In case of Dahl Hith, for instance, the water level rise had not been anticipated and hence, no monitoring equipment had been installed before. Thus, we do not have the choice between traditional measurements and crowd-generated data shared on social media platforms. The latter simply represent the only source of information. We believe that in such data-scarce settings, it is justified to explore the potential of social media as a source of information.

At this point, we also emphasize that, even if one had foreseen the water level rise, the question of which monitoring strategy to use, would have not been a simple one. A pressure transducer installed in the cave would have been at risk of being stolen or damaged (cf., Lorenzen et al., 2011). Moreover, its recovery would have involved cave diving. In principle, also a time-lapse camera pointing at a staff gauge would have been an option. Such a camera has already been used in Saudi Arabia to observe a v-notch weir to monitor discharge into a cave (Schulz et al., 2016). However, also a camera is difficult to hide and cave visitors might feel offended being photographed without their knowledge. Finally, the method of Lowry and Fienen (2013) would have been worth considering. Their instructional signage encouraged citizen scientists in the US to read streamwater levels from

staff gauges and report the value via text message to a server. Although this would have allowed a near real-time monitoring, the response and performance by the citizen scientists would have been unpredictable. Hence, one would have probably not relied on this approach alone. Moreover, visual information, i.e., photographs and/or videos, has the potential to provide additional impressions, contextual information, and possibly useful proxy data, apart from the mere water level reading (Fohringer et al., 2015; Schulz et al., 2016).

6.7. Conclusions and outlook

In the present study, we demonstrated that it is possible to reconstruct medium- to long-term water level changes from YouTube videos. The systematic analysis of videos taken in Dahl Hith yielded a water level rise of about 9.5 m for the time period 2013–2014, with an average pace of about 0.4 m per month. Even short-term (weekly/monthly) trends such as the water level rise at 1.3 m per month after a cluster of rain events in autumn 2013, were captured.

Although our approach is beyond the standard suite of monitoring methods and can be called experimental, we could demonstrate that it is applicable to real-world problems. To the best of our knowledge, we thereby established a precedent of using YouTube for reconstructing historical water level changes over an extended time period (two years). We acknowledge that such an improvised method relying on visual estimations would be outperformed by more conventional monitoring methods (e.g., pressure transducers) in terms of precision and temporal resolution. Nevertheless, we are convinced that the approach represents a complementary form of data collection and is justified in data-scarce settings. Particularly in cases like the present one, we believe that the method is better than the alternative – having no data at all.

Although we demonstrated the approach by using a somewhat specific case, we think that it is transferable to other settings. It could, for instance, be applied to reconstruct stream stage, flood extents, lake levels, or spring discharge. The method does not allow for a continuous or real-time monitoring, but data mining the video platform might provide valuable snapshots. When installing a staff gauge or designing a weir for discharge monitoring, for example, information on previous minimum and maximum stream stages can be helpful. In such settings, the water level does not rise continuously like in case of Dahl Hith, but fluctuates. Hence, low level phases enable a physical on-site measurement of previously estimated shifts, allowing a hindsight validation and error estimation (see Section 6.6.2.).

The main factor influencing the success of the YouTube-based method is the number of potential contributors, which is in turn governed by the smartphone penetration and social media popularity in the studied area or country (Daume et al., 2014; Fohringer et al., 2015). Moreover, the number of site visitors plays a role (Lowry and Fienen, 2013). Although a large pool of potential contributors is helpful, it is interesting to note that occasionally, a single motivated person can make a difference in participatory approaches (Lowry and Fienen, 2013). In case YouTube does not yield enough data, other social media like Facebook, Twitter, Flickr, etc. might

provide useful information that can be analyzed in a similar fashion. Also the Panoramio picture database, accessible via GoogleEarth, represents a convenient way to retrieve site-specific photographs. Yet, we believe that video material may outperform static pictures in many cases. Videos allow for a better 3D perception of a situation and their multi-temporal character enables the tracking of moving objects, which can be helpful. In the hydrological context, the latter aspect is, for example, utilized in the estimation of stream surface velocity (e.g., Le Boursicaud et al., 2016).

We also envisage synergistic effects from the conjunctive use of several emerging trends, e.g., mining of social media for videos taken by unmanned aerial vehicles (UAVs). The latter have recently shown a rapid development and currently gain increasing attention in the scientific community (Jordan, 2015; Selker et al., 2015). Hence, we can imagine future studies to benefit from drone videos of hydrological relevance shared online. For example, for post-flood analyses, we see significant potential in this regard – searching "drone flood" on YouTube currently yields more than 100,000 results.

6.8. Acknowledgments

The first author was supported by the German Federal Ministry of Education and Research (BMBF) through its program International Postgraduate Studies in Water Technologies (IPSWaT; IPS10/P10). We thank all Dahl Hith visitors who shared their cave adventures on YouTube, thereby turning the video platform into a water level archive. We are particularly grateful to Mark Carreon and Marcelo Cordova Jr. who gave us permission to use screenshots from their videos for this paper (Fig. 6-2). We also thank an anonymous reviewer for insightful comments that greatly improved the manuscript.

6.9. Supplementary data

Supplementary data to this article can be found online at http://dx.doi.org/10.1016/j.scitotenv.2016.05.211 and in Appendix 6.

6.10. References

Al-Othman, A.A., Ahmed, I., 2012. Hydrogeological framework and its implication on water level rise in eastern ArRiyadh, Saudi Arabia. Environmental Earth Sciences 67(5), 1493–1502.

Bjurström, E., 1997. Diving in the desert. Aramco World 48(4), 40–47.

Burgess, J., Green, J., 2009. YouTube – Online Video and Participatory Culture. Polity Press, Cambridge, UK.

Buytaert, W., Zulkafli, Z., Grainger, S., Acosta, L., Alemie, T.C., Bastiaensen, J., DeBièvre, B., Bhusal, J., Clark, J., Dewulf, A., Foggin, M., Hannah, D.M., Hergarten, C., Isaeva, A., Karpouzoglou, T., Pandeya, B., Paudel,

D., Sharma, K., Steenhuis, T., Tilahun, S., VanHecken, G., Zhumanova, M., 2014. Citizen science in hydrology and water resources: opportunities for knowledge generation, ecosystems service management, and sustainable development. Frontiers in Earth Science – Hydrosphere 2, 1–21.

Buytaert, W., Dewulf, A., De Bièvre, B., Clark, J., Hannah, D.M., 2016. Citizen science for water resources management: toward polycentric monitoring and governance? Journal of Water Resources Planning and Management 142(2), 01816002.

CITC and KFUPM – Communications and Information Technology Commission and King Fahd University of Petroleum & Minerals, 2016. ICT survey results 2014, Individuals Report. CITC, Riyadh, Kingdom of Saudi Arabia. www.citc.gov.sa/English/Reportsandstudies/Studies/Pages/default.aspx (last access: 6 January 2016).

CoCoRaHS – Community Collaborative Rain, Hail & Snow Network, 2016. www.cocorahs.org (last access: 6 January 2016).

Cyclone Center, 2016. www.cyclonecenter.org (last access: 6 January 2016).

Daume, S., Albert, M., von Gadow, K., 2014. Forest monitoring and social media – complementary data sources for ecosystem surveillance? Forest Ecology and Management 316, 9–20.

Eilander, D., van Loenen, A., Roskam, R., Wagemaker, J., 2015. Real-time flood extent maps based on social media. EGU2015–9143, EGU General Assembly 2015. Geophysical Research Abstracts Vol. 17.

Fohringer, J., Dransch, D., Kreibich, H., Schröter, K., 2015. Social media as an information source for rapid flood inundation mapping. Natural Hazards and Earth System Sciences 15, 2725–2738.

Gehl, R., 2009. YouTube as archive – who will curate this digital Wunderkammer? International Journal of Cultural Studies 12(1), 43–60.

Good, S.P., Mallia, D.V., Lin, J.C., Bowen, G.J., 2014. Stable isotope analysis of precipitation samples obtained via crowdsourcing reveals the spatiotemporal evolution of superstorm Sandy. PLOS ONE 9(3), e91117.

GWP, INBO – Global Water Partnership and International Network of Basin Organizations, 2009. A Handbook for Integrated Water Resources Management in Basins.

Järviwiki, 2016. www.jarviwiki.fi (last access: 6 January 2016).

Jordan, B.R., 2015. A bird's-eye view of geology: the use of micro drones/UAVs in geologic fieldwork and education. GSA Today 24(7), 50–52.

Kempe, S., Dirks, H., 2008. Layla Lakes, Saudi Arabia: the world-wide largest lacustrine gypsum tufas. Acta Carsologica 37(1), 7–14.

Le Boursicaud, R., Pénard, L., Hauet, A., Thollet, F., Le Coz, J., 2016. Gauging extreme floods on YouTube: application of LSPIV to home movies for the post-event determination of stream discharges. Hydrological Processes 30, 90–105.

Little, K.E., Hayashi, M., Liang, S., 2016. Community-based groundwater monitoring network using a citizen-science approach. Groundwater 54(3), 317–324.

Lorenzen, G., Sprenger, G., Pekdeger, A., 2011. A simple method to hide data loggers safely in observation wells. Groundwater 49(3), 450–453.

Lowry, C.S., Fienen, M.N., 2013. CrowdHydrology: crowdsourcing hydrologic data and engaging citizen scientists. Groundwater 51(1), 151–156.

Old Weather, 2016. www.oldweather.org (last access: 6 January 2016).

Powers, R.W., Ramirez, L.F., Redmond, C.D., Elberg, E.L., 1966. Geology of the Arabian Peninsula – Sedimentary Geology of Saudi Arabia. USGS, Washington D.C.

Rausch, R., Dirks, H., Kallioras, A., Schüth, C., 2014a. The riddle of the springs of Dilmun – does the Gilgamesh Epic tell the truth? Groundwater 52(4), 640–644.

Rausch, R., Simon, T., Al Ajmi, H., Dirks, H., 2014b. The scarp lands of Saudi Arabia. Arabian Journal of Geosciences 7(6), 2437–2450.

Richey, A.S., Thomas, B.F., Lo, M.-H., Reager, J.T., Famiglietti, J.S., Voss, K., Swenson, S., Rodell, M., 2015. Quantifying renewable groundwater stress with GRACE. Water Resources Research 51, 5217–5238.

Russell, M.A., 2014. Mining the Social Web. Second ed., O'Reilly, Sabastopol, CA, USA.

Schulz, S., de Rooij, G.H., Michelsen, N., Rausch, R., Siebert, C., Schüth, C., Al-Saud, M., Merz, R., 2016. Estimating groundwater recharge for an arid karst system using a combined approach of time-lapse camera monitoring and water balance modelling. Hydrological Processes 30, 771–782

SciStarter, 2016. http://scistarter.com/project/1226-SMAP:%20Soil%20Moisture%20Active%20Passive?tab=project (last access: 6 January 2016).

Selker, J., Tyler, S., Higgins, C., Wing, M.G., 2015. Drone squadron to take earth monitoring to New Heights. Eos 96(19), 8–11.

Smith, L., Liang, Q., James, P., Lin, W., 2015. Assessing the utility of social media as a data source for flood risk management using a real-time modelling framework. Journal of Flood Risk Management, http://dx.doi.org/10.1111/ jfr3.12154 (in press).

Steineke, M., Bramkamp, R.A., Sander, N.J., 1958. Stratigraphic relations of Arabian Jurassic oil. In: Weeks, L.G. (ed.), Habitat of Oil. AAPG Special Publication. AAPG, Tulsa, 1294–1329.

van de Giesen, N., Hut, R., Selker, J., 2014. The Trans-African Hydro-Meteorological Observatory (TAHMO). Wiley Interdisciplinary Reviews – Water 1(4), 341–348.

WHOI – Woods Hole Oceanographic Institution, 2016. www.ourradioactiveocean.org (last access: 6 January 2016).

Wolpert, P., Bartenbach, M., Suess, P., Rausch, R., Aigner, T., Le Nindre, Y.-M., 2015. Facies analysis and sequence stratigraphy of the uppermost Jurassic- Lower Cretaceous Sulaiy formation in outcrops of Central Saudi Arabia. GeoArabia 20(4), 67–122.

7. Concluding remarks

While some of the aspects discussed in the previous chapters are specific to Saudi Arabia, others have a wider scope and are hopefully relevant for the broader international community.

7.1. Concluding remarks on Saudi Arabia

As most of Saudi Arabia's groundwater is fossil (i.e., non-renewable), its extraction constitutes groundwater mining. Given ubiquitous calls for sustainability in many disciplines – sometimes to an extent that the term reaches buzzword status (Hibbs, 2008; see also Wood, 2003) – one might be tempted to instinctively criticize this mining. Such criticism is easy to express from a western (i.e., temperate climate) perspective, but sustainable water use under the given climatic conditions (and the population number and growth) is simply unrealistic (Wood, 2003). Obviously, sensible measures should be introduced or rather intensified (e.g., water saving, desalination, irrigation efficiency improvement, selection of climate-adapted crops, rainwater harvesting, wastewater reuse), but groundwater will continue to be used and its mining is an accepted concept in arid areas (Lloyd, 1986). Yet, to mine this water in the most efficient way, a sound understanding of the hydrogeological system is required. The studies described in this thesis address parts of this system that were and still are underrepresented in the literature. Although they are meant as a contribution to the overall understanding and represent valuable pieces of the puzzle, the latter is still incomplete. In view of the size of the country and the spectrum of environments and associated processes, we also have to acknowledge that the puzzle is fairly large and that it will still take some time, and probably generations of researchers and consultants, to complete it – if this is possible at all.

Nevertheless, the insights gained in this research, but also other recent studies (see Preface), hopefully provide new perspectives on the system and highlight potential pathways for future research. In terms of the latter, additional precipitation studies are recommended. Although the currently available isotope analyses of Riyadh rainfall (Chapter 2) represent a first, robust data set that may serve as a reference for old and new groundwater isotope analyses (e.g., for the identification of modern and fossil waters), additional efforts seem appropriate. This is not the usual, generic call for more data – having more data is always better – but the pore water study (Chapter 3) has indicated that our current rain data set does not capture the full spectrum of isotopic compositions that may appear in Central Saudi Arabia. To this end, one would clearly have to make a long-term monitoring effort. Such an endeavor should not be limited to the capital, but given Saudi Arabia's size, a monitoring network would be desirable. The corresponding stations, selected based on hydro(geo)logical criteria (major catchments, outcrops of main aquifers, etc.), could be equipped with cumulative samplers (Tube-dip-in-water collectors with pressure equilibration tube; Chapter 4) or their robotic counterpart (Chapter 5). With respect to sampling intervals, one would have the choice between event samples, biweekly samples, or – like in GNIP – samples collected on a monthly basis.

Unlike in GNIP, however, the analyses should not be restricted to $\delta^{18}O$, $\delta^{2}H$, and ^{3}H, but also target the rain's chemical composition (see also Stone and Edmunds, 2016). Here, particularly additional Cl^- concentrations would be helpful to strengthen the basis for Chloride Mass Balance applications, allowing for groundwater recharge estimations (Eriksson and Khunakasem, 1969). Due to our currently available Cl^- analyses of Riyadh rainfall, the data situation for Central Saudi Arabia is better than elsewhere on the Arabian Peninsula. Imes and Wood (2007), for instance, used *four* rain samples for their Chloride Mass Balance in the United Arab Emirates. Nevertheless, we need more and especially spatially distributed data. These would allow us to apply the Chloride Mass Balance approach to the unsaturated zone of the vast dune areas in the region. Such studies would probably benefit from the conjunctive use of chloride and stable isotopes ($\delta^{18}O$, $\delta^{2}H$), providing different perspectives on the same phenomenon, current groundwater replenishment. The suggested investigation would have the potential to provide meaningful estimations on a large scale and to resolve the issue of rather contrasting recharge values reported in the literature for Saudi Arabian dune areas (see Chapter 3.6.2.).

Given the logistical efforts associated with the outlined ideas, this is not necessarily low-hanging fruit to be picked, but worth the effort.

7.2. Concluding remarks from an isotope perspective

While Chapters 2 and 3, dealing with Saudi Arabian rainfall and dune sand pore waters, are particularly useful for the country itself, their findings might also be relevant for other (arid) areas.

The isotopic analysis of sequentially collected rain samples during a storm event (23 April 2012; see Chapter 2.4.1.), for instance, revealed remarkable variations. The encountered $\delta^{18}O$ and $\delta^{2}H$ ranges cover about 7 and 38 ‰, respectively. Interestingly, these ranges correspond to approximately half of the total data scatter of all (integral) samples in this study, with respect to both isotopes. This case may serve as an effective warning against snapshot samples randomly taken during an event. Although even standard textbooks alert the reader to avoid this practice (e.g., Clark and Fritz, 1997), personal experience has shown that it is still somewhat common. The case hence underscores the need for integral samples that capture the entire event or sampling period. Accordingly, the calculation of average δ values and LMWLs requires weighting schemes.

Moreover, care must be taken when interpreting the data. The study of Riyadh rainfall revealed that several phenomena (continental effect, altitude effect, sub-cloud evaporation, and moisture recycling) can induce a masking effect and thus blur the original moisture source-related isotopic fingerprints of air masses. Initially, such a characteristic fingerprint does exist, due to the environmental conditions during primary evaporation (sea surface temperature, humidity, wind speed; Clark and Fritz, 1997; and references therein). Often, this isotopic signature is also reflected in rain resulting from this air mass (Yurtsever and Gat, 1981) and accordingly d has been used (and promoted) as a source indicator (see Andreo et al., 2004; Celle-Jeanton et al., 2001). However, the above-mentioned effects are rather efficient in altering the original fingerprint and particularly

sub-cloud evaporation in arid environments can strongly lower d, rendering it useless for source identification. In such cases, air mass back-trajectory models might be the better option.

In contrast to Chapters 2 and 3, the following two sections have a genuinely methodological character, although they were inspired by the work in Saudi Arabia as well, i.e., by the prevailing conditions and the resulting challenges. Interestingly, a reviewer of the sampler comparison manuscript (Chapter 4) wrote the following with respect to our chosen environmental conditions simulated with the lab oven (26 to 45°C; 5 % relative humidity): "[the test is] so extreme that it is hardly 'representative' of temperate zone samplers".

This is certainly true, but it is arid areas that represent our greatest challenge in terms of future monitoring. This is more or less readily apparent from GNIP, which forms the backbone of many isotope studies (despite the creation of new databases, e.g., Putman and Bowen, 2019). While the standard maps showing all stations in the repository suggest a mostly decent coverage (Appendix 7, Fig. A7-1), the picture changes when stations that only feature a few records are excluded. Setting an arbitrary threshold of at least 12 $\delta^{18}O$ values for a station (e.g., Crawford et al., 2014; Rozanski et al., 1993) yields the following.

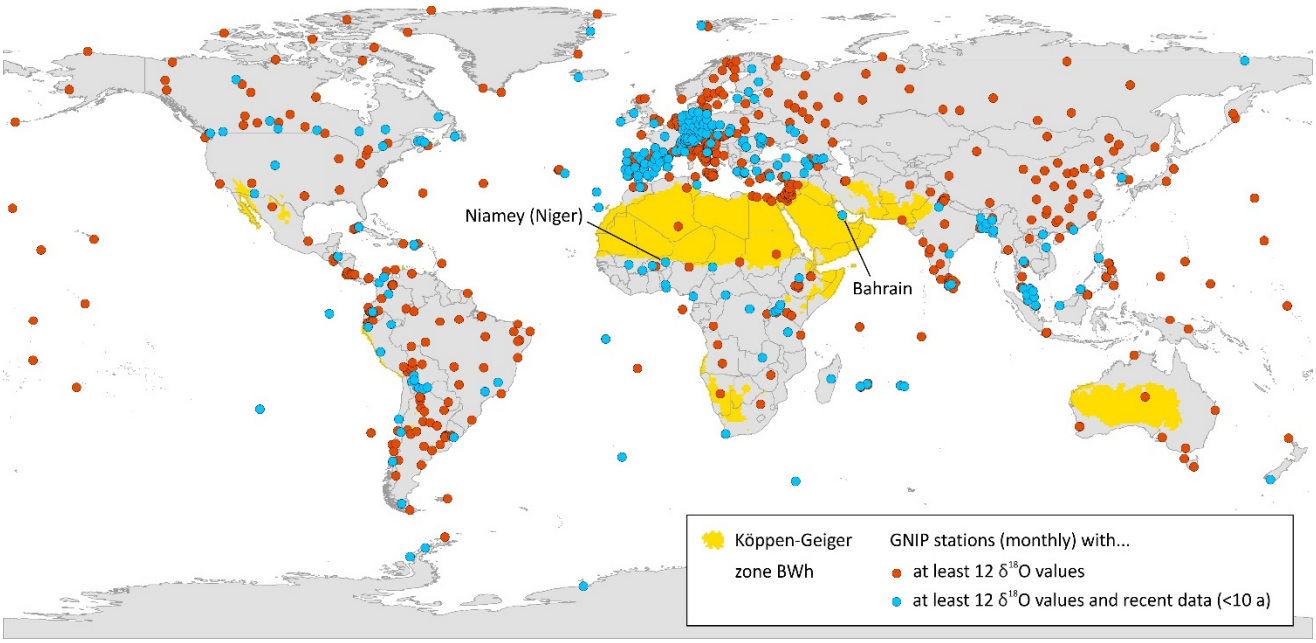

Fig. 7-1. Map showing the current state of the GNIP database (data source: IAEA/WMO, 2019). The yellow area represents the Köppen-Geiger zone BWh (hot deserts; Rubel and Kottek, 2010).

The map (Fig. 7-1) exhibits large gaps, despite repeated calls for contributions by the IAEA (see Chapter 4.2). Admittedly, a few of these gaps are misleading, because some countries run national networks and do not report (all) their data to the IAEA. Yet, the gaps in most arid areas are real. The Köppen-Geiger class BWh (hot deserts; shown in yellow) is the most common individual climate type by land area (14 %; Peel et al., 2007). Nevertheless, there are only a few stations located in this zone. To make matters worse, the map also features a temporal

dimension – stations with recently added data (within the last 10 years) are highlighted in blue. When applying this criterion, the number of BWh stations drops to two: Niamey (Niger) and Bahrain. The entire Sahel zone and the largest part of the Arabian Peninsula are thus devoid of a reliable station with recent data.

The situation becomes even more absurd, if we consider that it is these very areas, where our isotope techniques represent especially powerful tools for water resources assessments. Here, data on rain could serve as a valuable reference for analyses of rivers and lakes, pore waters in the unsaturated zone, or groundwaters.

Although global predictive models (see Chapter 4.2.) might seem to be a practical workaround, we ultimately need genuine data from these regions. Hopefully, the rigorous sampler comparison can make a small contribution towards this goal by helping researchers to select a suitable collector for their studies. Possibly, the developed automatic counterpart may be useful here as well – the target regions are not only arid, but large parts are also difficult to reach due to a limited road network (see Appendix 7, Fig. A7-2).

7.3. Concluding remarks from a crowdsourcing perspective

Crowdsourcing and citizen science methods are rapidly gaining momentum (Fig. 7-2). Nevertheless, there are still apparent tensions with traditional methods (Buytaert et al., 2014) and skepticism in terms of the quality of the data gathered with this "new" method (Nature editorial, 2015).

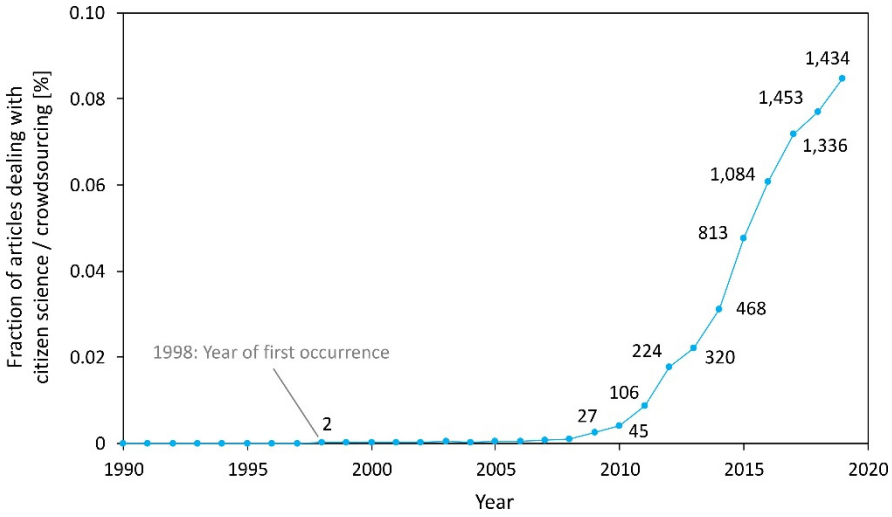

Fig. 7-2. Bibliometric analysis of the crowdsourcing/citizen science phenomenon. The terms were searched in the *Topic* field of the Web of Science Core Collection (Language: English, Document type: articles). The obtained number of articles per year was divided by the total number of English articles in that year for normalization. The resulting fractions (blue points) were complemented by the absolute number of crowdsourcing/citizen science articles in that year (black labels).

However, actually only the terms are new (see Fig. 7-2). The method itself has a rather long tradition, at least in other disciplines. In ornithology, for instance, the Christmas Bird Count is a well-established layperson-based

bird census that is carried out since 1900, mostly in the US and Canada (National Audubon Society, 2019). Further, oceanographers benefitted from a drift observation program initiated in 1864 by Georg Balthasar von Neumayer (then director of the Deutsche Seewarte). In this campaign, bottles were released from ships throughout the world's oceans and a message in the bottle requested its finder to send it back with information on the date and place of recovery (Bye, 2012).

What is new nowadays is that we have novel digital data sources, including smartphone-generated data (see Preface to Chapter 6). While such information also has its downsides (see Chapter 6.6.2.), it can be a useful addition to knowledge gathered in more traditional ways, particularly because many monitoring networks around the world are shrinking (e.g., Lorenz and Kunstmann, 2012; Walker et al., 2016). This phenomenon also occurs in the developed world as well, but the regions with the greatest data scarcity often coincide with regions suffering most from impacts from adverse hydrological circumstances (Walker et al., 2016), such as arid areas.

Although useful, the crowd-generated data are sometimes not deliberately collected for the given purpose, and hence not delivered in a readily usable format, like our YouTube videos. The latter required visual estimations that were somewhat laborious, but this effort is justified in certain cases (e.g., when the alternative is having no data). Further, this process could be facilitated by incorporating other emerging technologies enabling high-resolution 3D models of the area of interest, for example ground-based or air-borne 3D laser scanning. Moreover, conventional photos taken with commercial grade cameras can be combined in 3D with the structure from motion technique (Carrivick et al., 2016; and references therein). Such additional data would possibly enable a (partial) automatization of the analysis and increase the precision and accuracy of water level estimations.

Apart from constituting a new technique, our YouTube approach also has an outreach component. Admittedly, we had initially not realized this dimension of our work. This only changed during a European Geosciences Union (EGU) General Assembly in 2015, when a BBC science journalist approached us in the "MacGyver poster session" and eventually covered our study in a short article (https://www.bbc.com/news/science-environment-32324232), triggering additional, secondary articles. Although such "publications" do obviously not pay off in our traditional academic system (h-index, etc.), the case illustrated that our work is occasionally not only relevant in the ivory tower, but also interesting for the general public. The entire spectrum of geoscientific sub-disciplines has great societal relevance, but it is sometimes challenging to communicate this. In terms of hydrogeology, there are two main reasons – a limited hydroliteracy and our often sophisticated, difficult to understand methods.

A limited hydroliteracy it a quite common phenomenon, particularly when it comes to groundwater. The latter has been called an „invisible resource" (López-Vera, 2012; Megdal, 2018) that is „out of sight and out of mind" (Alley et al., 2016). While this seems to be an international phenomenon, it is interesting that it also prevails in

water-scare regions, including Saudi Arabia. Here, several surveys have revealed limited awareness of the water situation in Saudi Arabia (Alsaluli et al., 2015; Ouda et al., 2013).

While the communication of our research findings is hampered by the mentioned limited (ground)water awareness, also our methods contribute to the problem. Some of them (e.g., modeling, isotope techniques) are inherently difficult to explain to a layperson. However, in the YouTube case, we utilize one of the most popular social media websites as a water level archive and apply an easily comprehensible technique to reconstruct water level changes. Such simple, creative approaches hence hold a certain potential to spark greater interest for hydro(geo)logy among the general public.

Although outreach has only played a minor role in our discipline in the past decades, it has been acknowledged that there is a clear need for the hydro(geo)logical community to be more effective at promoting its work to the wider society and improve hydroliteracy among the general public (Tetzlaff et al., 2017). We hope and suggest that unconventional crowdsourcing approaches can contribute to this process.

7.4. References

Alley, W.M., Beutler, L., Campana, M.E., Megdal, S.B., Tracy, J.C., 2016. Groundwater Visibility: The Missing Link. Groundwater 54(6), 758–761.

Alsaluli, A., Ahmed, A., Davies, J., 2015. Public engagement in integrated urban water management in Saudi Arabia: teacher's perceptions in relation to water awareness. Water Science & Technology 15(4), 871–880.

Andreo, B., Liñán, C., Carrasco, F., Jiménez de Cisneros, C., Caballero, F., Mudry, J., 2004. Influence of rainfall quantity on the isotopic composition (^{18}O and ^{2}H) of water in mountainous areas. Application for groundwater research in the Yunquera-Nieves karst aquifers (S Spain). Applied Geochemistry 19, 561–574.

Buytaert, W., Zulkafli, Z., Grainger, S., Acosta, L., Alemie, T.C., Bastiaensen, J., DeBièvre, B., Bhusal, J., Clark, J., Dewulf, A., Foggin, M., Hannah, D.M., Hergarten, C., Isaeva, A., Karpouzoglou, T., Pandeya, B., Paudel, D., Sharma, K., Steenhuis, T., Tilahun, S., VanHecken, G., Zhumanova, M., 2014. Citizen science in hydrology and water resources: opportunities for knowledge generation, ecosystems service management, and sustainable development. Frontiers in Earth Science – Hydrosphere 2, 1–21.

Bye, J.A.T., 2012. Southern Ocean surface drift: old observations and new theories. Weather 67(7), 187–191.

Carrivick, J.L., Smith, M.W., Quincey, D.J., 2016. Structure from motion in the geosciences. Wiley Blackwell, Chichester.

Celle-Jeanton, H., Travi, Y., Blavoux, B., 2001. Isotopic typology of the precipitation in the Western Mediterranean region at three different time scales. Geophysical Research Letters 28(7), 1215–1218.

Clark, I.D, Fritz, P., 1997. Environmental Isotopes in Hydrogeology. Lewis Publishers, Boca Raton/New York.

Crawford, J., Hughes, C.E., Lykoudis, S., 2014. Alternative least squares methods for determining the meteoric water line, demonstrated using GNIP data. Journal of Hydrology 519, 2331–2340.

Eriksson, E., Khunakasem, V., 1969. Chloride concentration in groundwater, recharge rate and rate of deposition of chloride in the Israel coastal plain. Journal of Hydrology 7, 178–197.

Hibbs, B.J., 2008. Foreword: Ground Water in Arid Zones. Ground Water 46(3), 345–347.

IAEA/WMO – International Atomic Energy Agency/World Meteorological Organization, 2019. Global Network of Isotopes in Precipitation. The GNIP Database. https://nucleus.iaea.org/ wiser (last access: 17 November 2019).

Imes, J.L., Wood, W.W., 2007. Solute and isotope constraint of groundwater recharge simulation in an arid environment, Abu Dhabi Emirate, United Arab Emirates. Hydrogeology Journal 15, 1307–1315.

Lloyd, J.W., 1986. A review of aridity and groundwater. Hydrological Processes 1, 63–78.

Loizides, P., 1975. The sandy soils of the Kingdom of Saudi Arabia. In: Food and Agriculture Organization of the United Nations (eds.). Sandy Soils. FAO Soils Bulletin 25, 225–227.

López-Vera, F., 2012. Groundwater: The Invisible Resource. Water Resources Development 28(1), 141-150.

Lorenz, C., Kunstmann, H., 2012. The Hydrological Cycle in Three State-of-the-Art Reanalyses: Intercomparison and Performance Analysis. Journal of Hydrometeorology 13, 1397–1420.

Megdal, S.B., 2018. Invisible water: the importance of good groundwater governance and management. Npj Clean Water 1, 15.

National Audubon Society, 2019. https://www.audubon.org/conservation/science/christmas-bird-count (last access: 21 November 2019).

Nature editorial, 2015. Rise of the citizen scientist. Nature 524, 265.

Ouda, O.K.M., Shawesh, A., Al-Olabi, T., Younes, F., Al-Waked, R., 2013. Review of domestic water conservation practices in Saudi Arabia. Applied Water Science 3, 689–699.

Peel, M.C., Finlayson, B.L., McMahon, T.A., 2007. Updated world map of the K¨oppen-Geiger climate classification. Hydrology and Earth System Sciences 11, 1633–1644.

Putman, A.L., Bowen, G.J., 2019. Technical note: A global database of the stable isotopic ratios of meteoric and terrestrial waters. Hydrology and Earth System Sciences 23, 4389–4396.

Rozanski, K., Araguás-Araguás, L., Gonfiantini, R., 1993. Isotopic Patterns in Modern Global Precipitation. In: Swart, P.K., Lohmann, K.C., McKenzie, J., Savin, S. (eds.). Climate change in continental isotopic records. Geophysical Monograph 78, 1–36.

Rubel, F., Kottek, M., 2010. Observed and projected climate shifts 1901–2100 depicted by world maps of the Köppen-Geiger climate classification. Meteorologische Zeitschrift 19(2), 135–141.

Stone, A.E.C., Edmunds, W.M., 2016. Unsaturated zone hydrostratigraphies: A novel archive of past climates in dryland continental regions. Earth-Science Reviews 157, 121–144.

Tetzlaff, D., Carey, S.K., McNamara, J.P., Laudon, H., Soulsby, C., 2017. The essential value of long-term experimental data for hydrology and water management, Water Resources Research 53, 2598–2604.

Walker, D., Forsythe, N., Parkin, G., Gowing, J., 2016. Filling the observational void: Scientific value and quantitative validation of hydrometeorological data from a community-based monitoring programme. Journal of Hydrology 538, 713–725.

Wood, W.W., 2003. Water Sustainability: Science or Science Fiction? Perspective from One Scientist. In: Alsharan, A.S., Wood, W.W. (eds.) Water Resources Perspectives: Evaluation, Management and Policy. Developments in Water Science 50. Elsevier, 45–51.

Yurtsever, Y., Gat, J.R., 1981. Atmospheric Waters. In: Gat, J.R., Gonfiantini, R. (eds.). Stable Isotope Hydrology – Deuterium and Oxygen-18 in the Water Cycle. IAEA Technical Report Series No. 210, 103–142.

8. Acknowledgments

First and foremost, I would like to thank Prof. Dr. Christoph Schüth for his guidance, supervision, and steady support throughout my work. His laissez-faire leadership style led to a great atmosphere in our group and his curiosity and passion were truly inspiring. I am also grateful to Dr. Paul Königer for his encouragement and advice over the years, and for readily accepting my invitation to be co-supervisor.

Next, I want to express my gratitude to the GIZ and Dornier Consulting team in Saudi Arabia. During my employment as a hydrogeology consultant in Riyadh (2007–2010), but also during frequent research and consulting visits in the following years, I experienced a great working atmosphere as well as guidance and support by the whole team. Over the years, I got to know and appreciate many people there and I will not make an attempt to list all the colleagues with whom I worked together and from whom I learned so much. Exemplarily, I want to mention Prof. Dr. Randolf Rausch, Johannes Döhler, Stephan Dohm, Tilman Mieseler, Peter Forestier, and Prof. Dr. Martin Keller. Although we were far away from Schnittspahnstraße, the times in Riyadh still felt like home, also due to the "Darmstädter Invasion" through friends and colleagues from the institute such as Andreas Deckelmann, Heiko Dirks, Nico Trauth, and Gabino Tuñón Vettermann. While the conditions in Saudi Arabia were sometimes challenging, I enjoyed this exiting and formative phase a lot and will always keep fond memories of it. The projects enabling this time were mainly funded by the Saudi Arabian Ministry of Water & Electricity (now Ministry of Environment, Water & Agriculture), which is also thanked here.

After the greatly acknowledged initial support of my research by the BMBF through an IPSWaT scholarship, I continued to work on the thesis for several years without formal funding. Interestingly, this was exactly the time when I learned how this publishing thing works. In fact, most of the papers where submitted during this time. The research during this phase was enabled by my freelance work as a consultant and a more or less constant flux of assignments by clients such as GIZ and Dornier Consulting, as well as UFZ. In this context, I am particularly grateful to Tilman Mieseler, Thomas Müller, and Jan Friesen. Importantly, I am not only thankful for the money you paid me. The collaborations were fruitful and the interesting assignments in Saudi Arabia, in the United Arab Emirates, and in Oman also served as a constant reminder that our research is important beyond the ivory tower and helps to solve real-world problems. I really enjoyed working with you guys.

Besides my coauthors (e.g., Dr. Stephan Weise, Dr. Robert van Geldern), I would also like to thank colleagues from outside my own "bubble" – editors, reviewers, conference attendees, etc., who showed interest in my work and were sometimes surprisingly supportive. I particularly recall a situation at an isotope conference in autumn 2014, in which Prof. Dr. Michael Böttcher looked at my poster and asked the magic five words: "Have you published this already?" – a key moment, because before, I had no idea of what was publishable in a decent ISI journal. In hindsight, and without exaggerating, I would say that this was one of the most motivating situations and decisive moments during the journey. Thank you.

Moreover, I express my gratitude to all members of the Hydrogeology group at the Institute of Applied Geosciences. The atmosphere in the Hydrogeology team has always been particularly friendly and truly supportive. Among these colleagues, I want to explicitly mention the lab team (Rainer Brannolte, Claudia Cosma, Zahra Neumann, Steffi Schmidt) as well as Dr. Stephan Schulz. When Stephan joined the Saudi Arabia project, things changed dramatically. Suddenly, there was an enthusiastic colleague and friend on the same level with whom I could discuss ideas. These were fruitful in-depth discussions, which went far beyond previous conversations that too often felt uni-directional. Occasionally, his motivating comments were as brief as they were effective and untranslatable: “Is’ doch cool, Alter!”.

I am also extremely grateful to my family for their steady and unconditional support. My parents did probably not fully understand this geoscience thing and much less the world of isotopes, but trusted me blindly and believed in my decisions. Thank you so much.

Finally, I want to thank Inga. I thank you for tremendous and continuous support that you provided in so many situations and in so many ways. You were more than patient with me (I am still kind of surprised), but also created gentle pressure when necessary: “…yes, Nils, this [scientific but possibly weird] idea sounds somewhat interesting, but please…after you completed the PhD degree.”.

Appendix 1

Supplementary data for Chapter 1

Details on the Web of Science analysis (Chapter 1.1.)

The database was screened in the Advanced Search mode with the following query (on 24 November 2019):

TS=(Country Name) AND SO=("Advances in Water Resources" OR "Groundwater" OR "Ground Water" OR "Hydrogeology Journal" OR "Hydrological Processes" OR "Hydrological Sciences Journal" OR "Hydrology and Earth System Sciences" OR "Hydrology Research" OR "Journal of Hydrology" OR "Water Research" OR "Water Resources Research")

where TS is the Topic (comprising title, abstract, keywords, keywords plus) and SO is the Source (journal title).

Further criteria were the Time period (*1969–2019*), the Language (*English*), and the Document type (*article*). In some cases, it was necessary to use multiple search terms for the same country, for example when the official country name is not necessarily the commonly used name:

TS=(Czechia OR "czech republic")… or *TS=(Eswatini OR Swaziland)*…

In other cases, certain terms had to be excluded:

TS=(" oman " NOT romania)…

Regarding the list of journals, one has to keep in mind that not all existed during the entire search period. Moreover, the selected journals are meant as proxies with a clear water focus. Water-related articles that appeared in other journals (e.g., multi-disciplinary journals) are not found with this search strategy.

Fig. A1-1. Photograph of selected rock art at a location locally known as “Graffiti Rock 1” (24°18’58”N, 45°38’23”E). Numerous depictions of animals such as bovine suggest a savanna type climate. Note the contrast to the present day environment around the site (upper left photo).

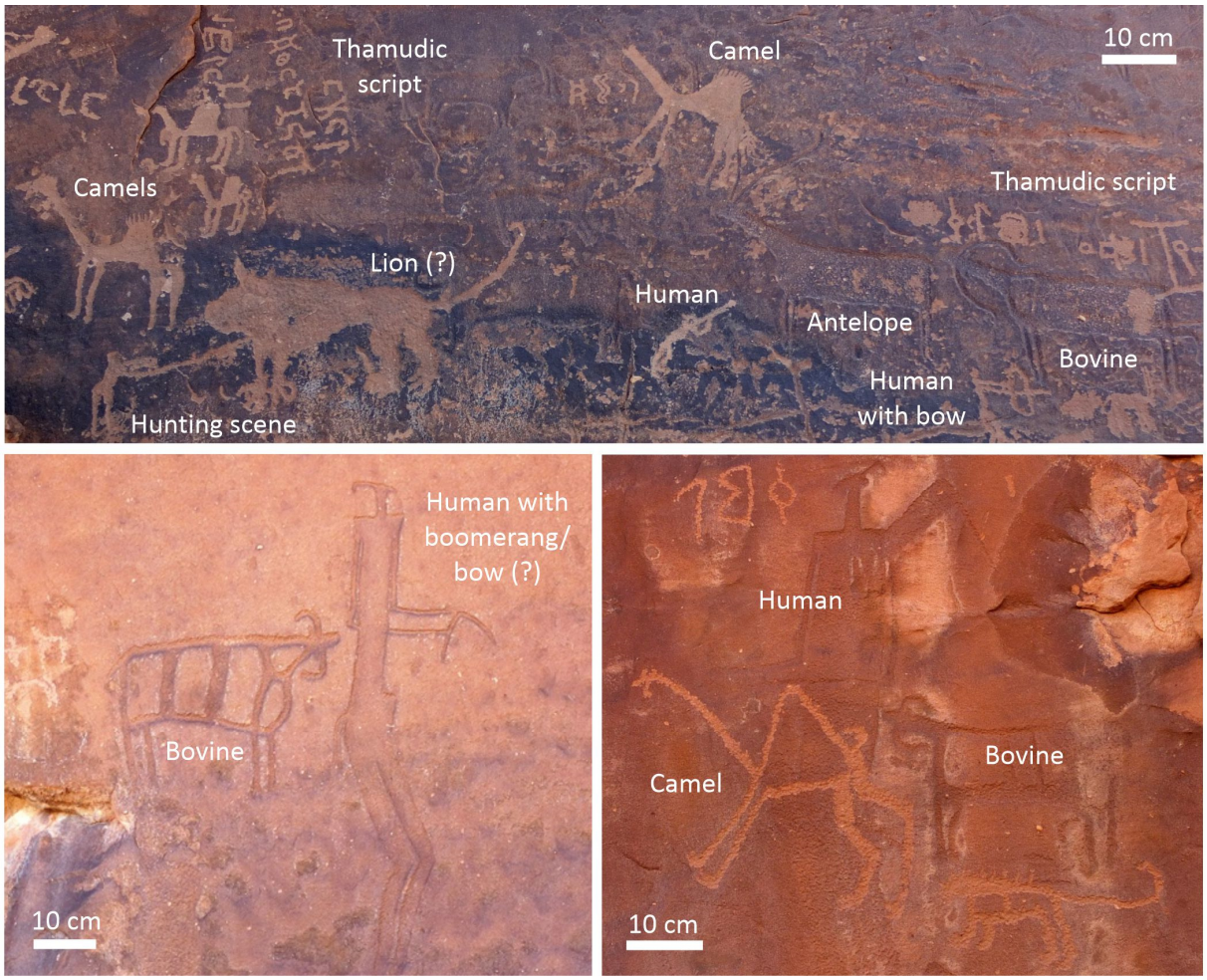

Fig. A1-2. Photograph of selected rock art at the Jubbah petroglyph site (28°1'55"N, 40°55'6"). Note the different generations of petroglyphs with faded (i.e., older) savanna type animals (e.g., bovine) and fresher (i.e., younger) desert type animals (camel) and Thamudic script.

Appendix 2

Supplementary data for Chapter 2

HYSPLIT modeling results

The air mass back-trajectories were modeled with HYSPLIT (Draxler and Rolph 2015, Rolph 2015). As mentioned in the main article (Section 2.3.4.), the required cloud elevation was obtained from METAR reports (Meteorological Aviation Routine Weather Report). Occasionally, these indicated multiple cloud layers. In such cases, the layer with the most intense cloud cover was utilized for the modeling.

In a first step, the air masses were traced back for four days and the last "maritime contact" of the air parcel was treated as the moisture source. Mostly, this last contact had occurred within three days prior the rain event. In six cases, no such contact was observed within four days, making further modeling with extended time periods necessary (up to eight days).

The following maps present the air mass back-trajectories calculated for the 28 rain events sampled in Riyadh as part of this study (red lines). The maps are labeled with the sample ID and the corresponding modeling time period. Abbreviations on the maps indicate the last maritime contact (MS=Mediterranean Sea, RS=Red Sea, AS=Arabian Sea, AG=Arabian Gulf).

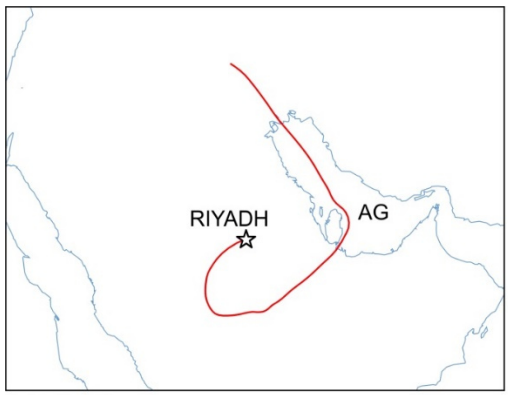

1 (4 days)

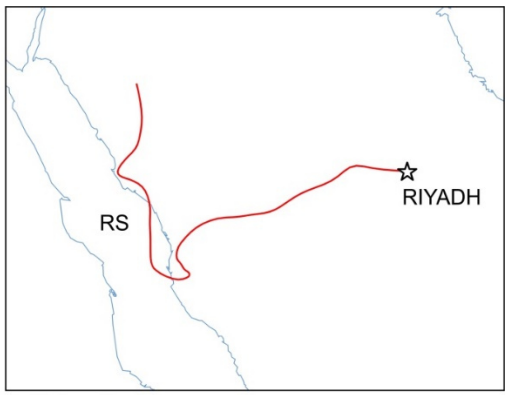

2 (4 days)

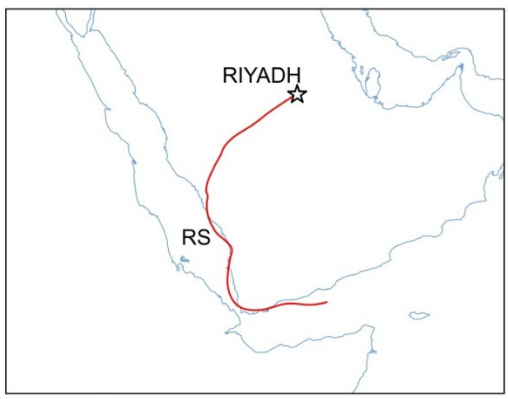

3 (4 days)

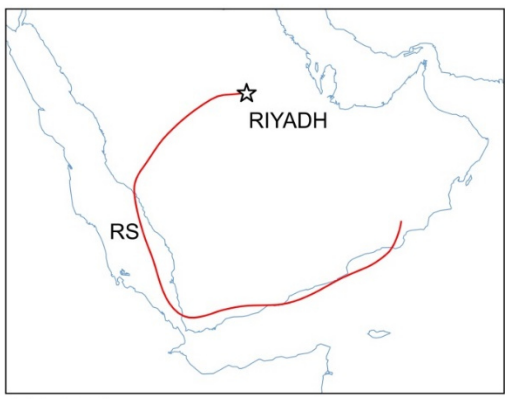

4 (4 days)

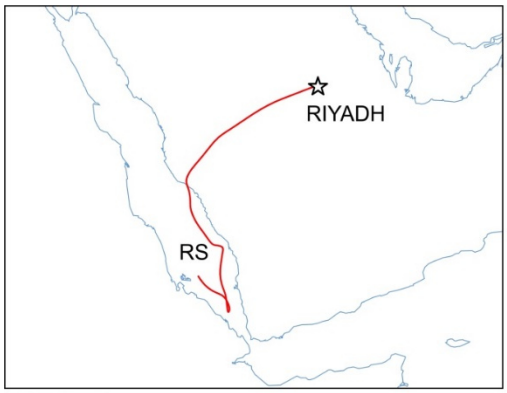

5 (4 days)

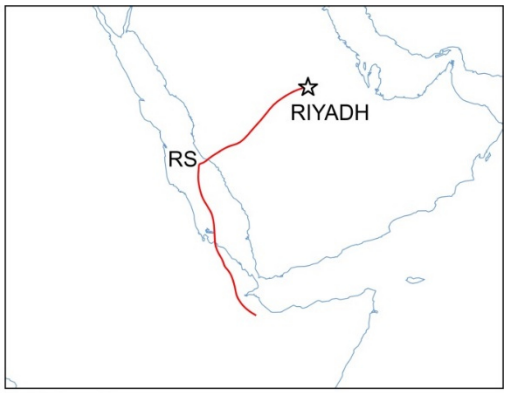

6 (4 days)

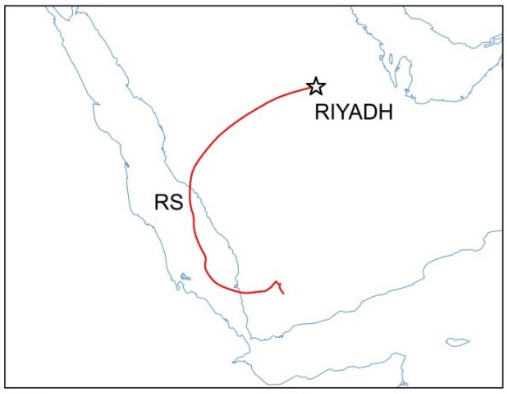

7 (4 days)

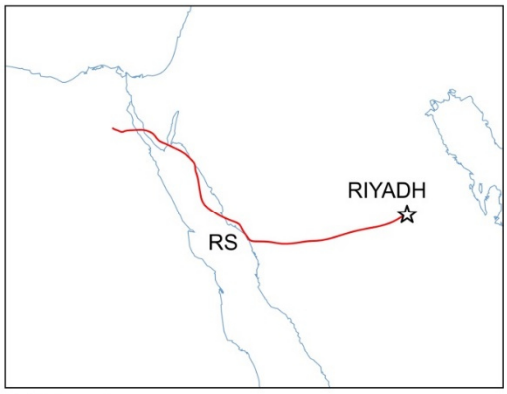

8 (4 days)

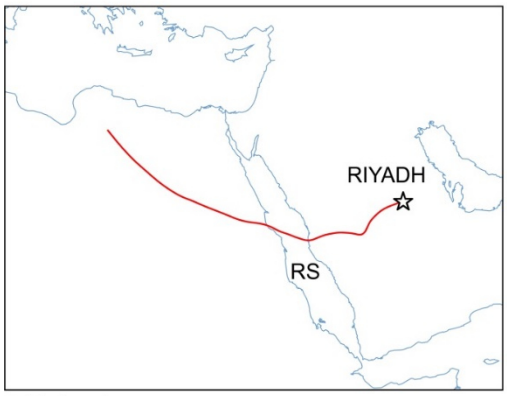

9 (4 days)

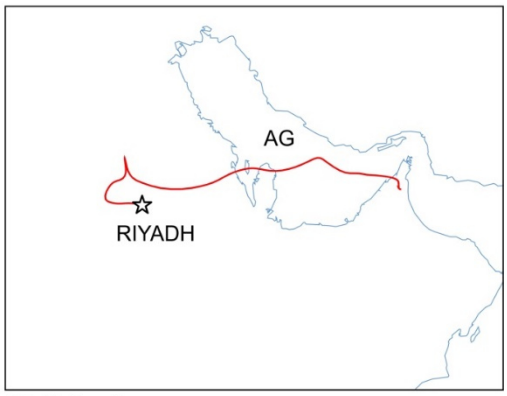

10 (4 days)

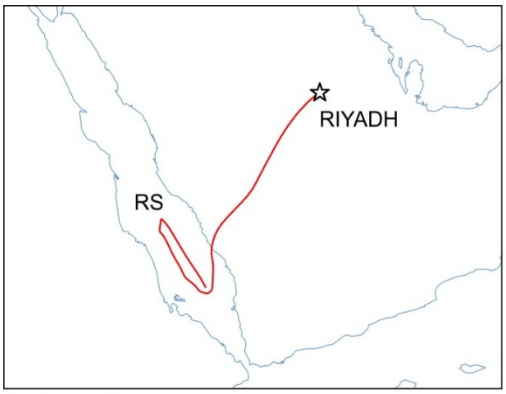

11 (4 days)

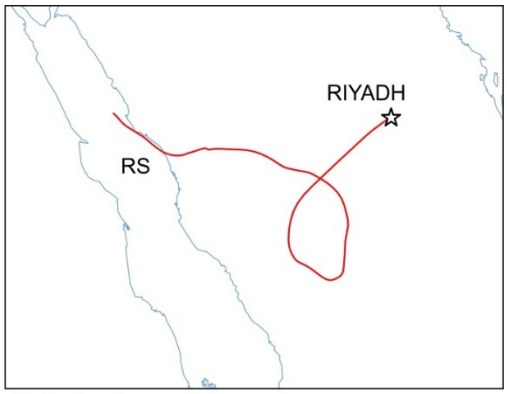

12 (5 days)

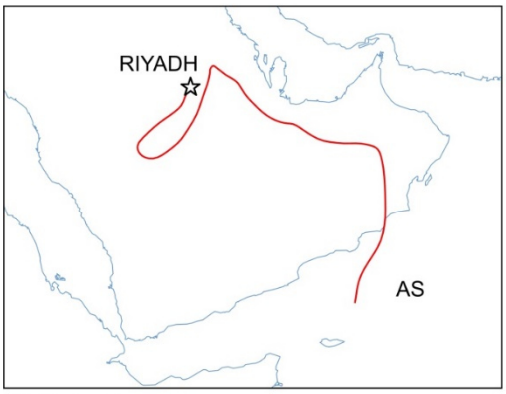

13 (5 days)

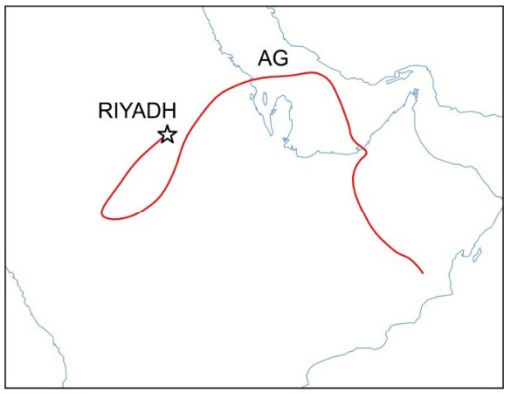

14 (4 days)

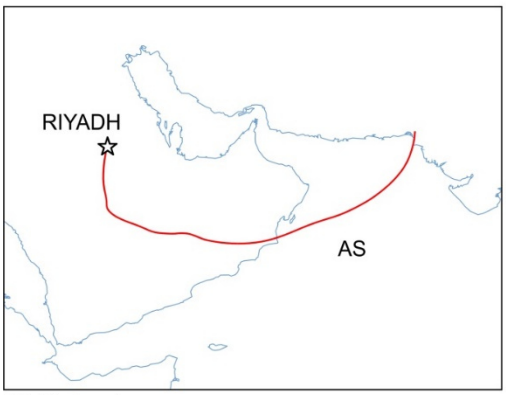

15 (4 days)

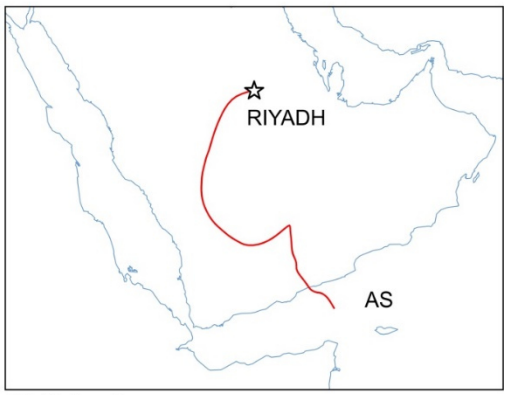

16 (4 days)

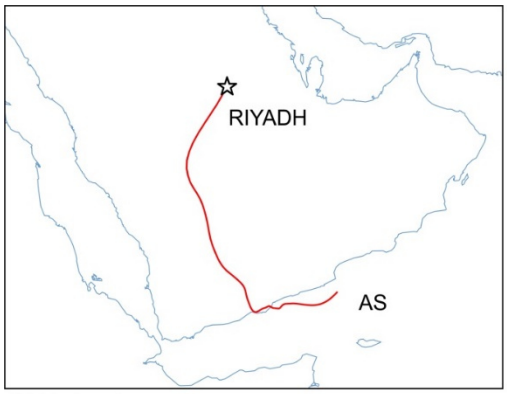

17 (4 days)

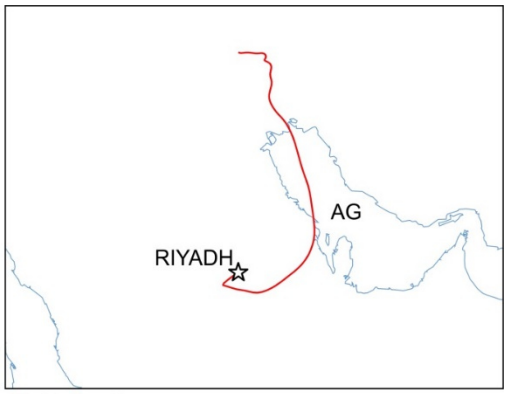

18 (4 days)

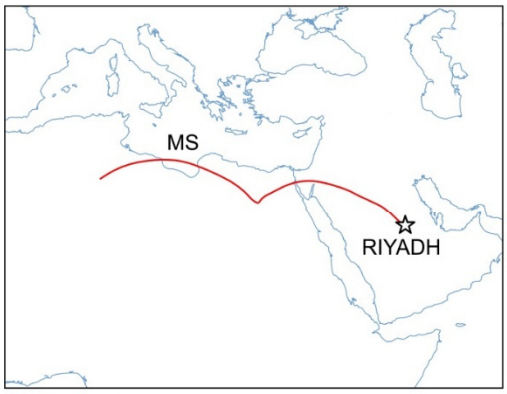

19 (4 days)

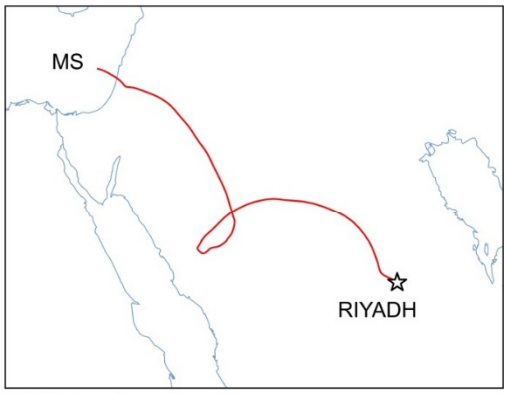

20 (6 days)

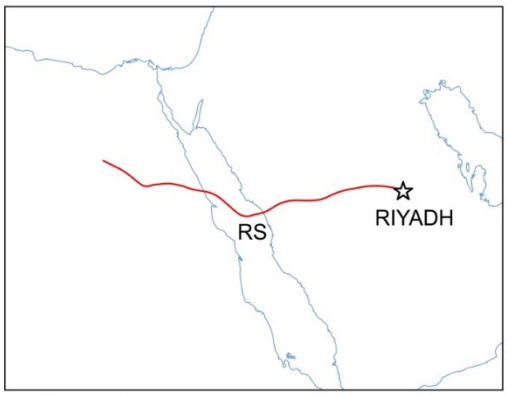

21 (4 days)

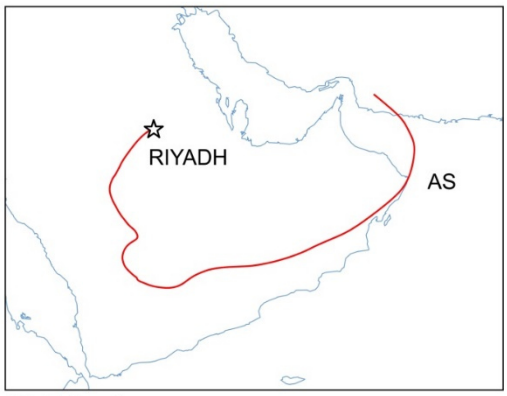

22 (8 days)

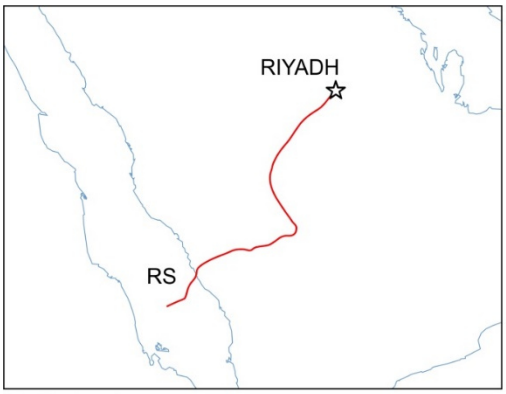

23 (6 days)

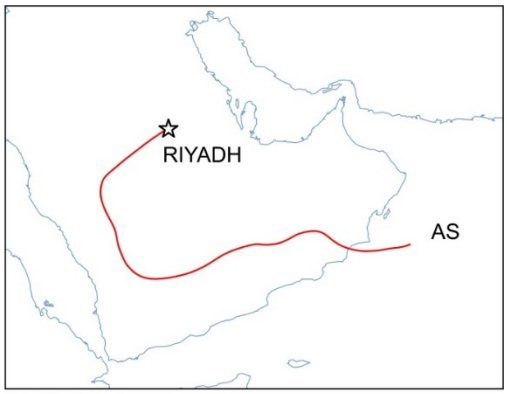

24 (5 days)

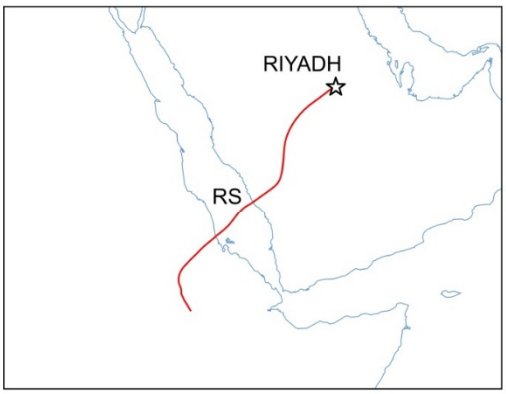

25 (4 days)

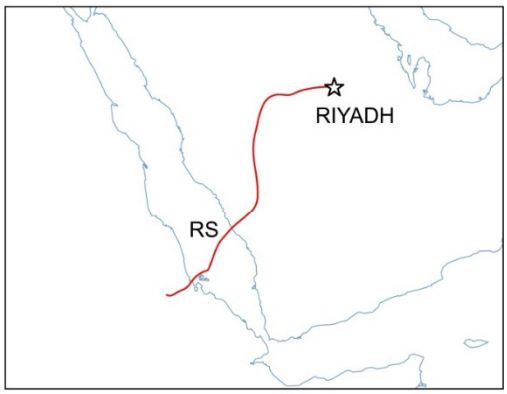

26 (4 days)

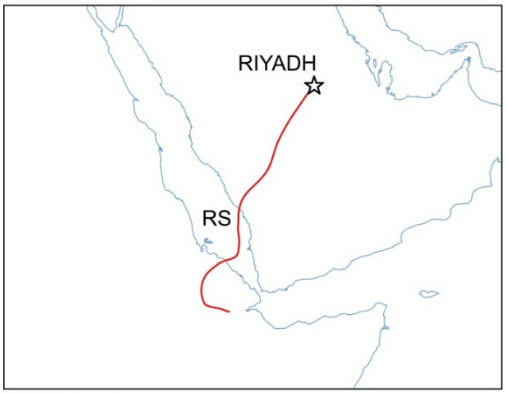

27 (4 days)

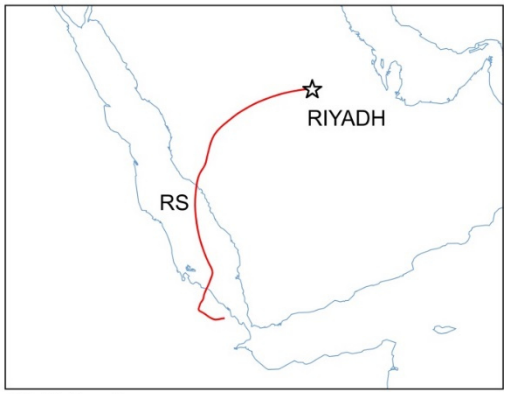

28 (4 days)

LMWL parameters for Riyadh and other GNIP stations

Table A2-1: LMWL parameters obtained for Riyadh and selected GNIP stations by applying the six regression methods presented in Crawford et al. (2014). $rmSSE_{av}$ values given in bold represent the lowest value for a given site.

Method	$\delta^{18}\overline{O}_w$	$\delta^{2}\overline{H}_w$	a	SE_a	b [‰]	SE_b [‰]	$rmSSE_{av}$
Riyadh (event data; n=48; this study, refs in Table 2-1)							
OLSR	0.37	16.7	4.4907	0.3591	13.5537	1.2221	1.0536
RMA			5.1087	0.3515	12.8007	1.2295	1.0197
MA			5.7625	0.4051	12.0039	1.3787	1.0526
PWLSR			5.2197	0.3844	14.8219	0.8982	**1.0028**
PWRMA			5.8345	0.3949	14.5975	0.9228	1.0499
PWMA			6.4843	0.4272	14.3603	0.9983	1.1373
Bahrain (monthly data; n=9; IAEA/WMO, 2015)							
OLSR	-0.69	7.5	5.6274	0.2669	9.0465	0.7871	1.0376
RMA			6.1591	0.2639	8.7245	0.7949	**1.0142**
MA			6.7124	0.2909	8.3895	0.8578	1.0370
PWLSR			5.4814	0.2796	11.2229	0.7332	1.0212
PWRMA			6.0765	0.2867	11.6324	0.7518	1.0152
PWMA			6.7029	0.3084	12.0636	0.8088	1.0672
Salalah, Oman (event data; n=59; IAEA/WMO, 2015, originally Wushiki, 1991)							
OLSR	-0.80	5.1	4.9822	0.3953	8.9674	0.2888	1.0653
RMA			5.8076	0.3885	8.9075	0.2944	1.0237
MA			6.7178	0.4572	8.8415	0.3341	1.0645
PWLSR			5.1834	0.1809	9.242	0.2942	**1.0075**
PWRMA			5.3603	0.1824	9.3832	0.2966	1.0082
PWMA			5.5312	0.1867	9.5196	0.3036	1.0164
Qairoon Hairiti, Oman (event data; n=43; IAEA/WMO, 2015, originally Wushiki, 1991)							
OLSR	-0.59	7.3	1.94	0.7892	8.7257	0.4813	1.6191
RMA			5.41	0.7706	10.5888	0.4943	1.1362
MA			14.63	2.1324	15.5369	1.3005	1.6857
PWLSR			2.19	0.8446	8.6297	0.5484	1.5253
PWRMA			5.84	1.0183	10.7806	0.6612	**1.1317**
PWMA			15.14	2.1907	16.2726	1.4224	1.7200
Global*							
OLSR	n.d.	n.d.	8.21	0.002	12.2	0.02	1.002
RMA			8.26	0.002	12.5	0.02	**1.001**
MA			8.30	0.002	12.9	0.02	1.002
PWLSR			8.21	0.003	12.6	0.02	1.004
PWRMA			8.28	0.003	13.1	0.02	1.002
PWMA			8.36	0.003	13.6	0.02	1.004

* For details on calculation procedure, see Crawford et al. (2014)

We applied the six regression methods outlined in Crawford et al. (2014) to the data sets available for Riyadh (this study, refs in Table 2-1) and selected GNIP stations in the region, namely Bahrain, Salalah, and Qairoon

Hairiti (IAEA/WMO, 2015). For comparison, the results from Crawford et al. (2014) for the global data set are included.

The obtained slopes show the order $a_{OLSR} < a_{RMA} < a_{MA}$. The same pattern is observed when considering the precipitation-weighted counterparts, i.e., $a_{PWLSR} < a_{PWRMA} < a_{PWMA}$. This is in line with the findings of Crawford et al. (2014). Yet, there is no general rule which regression method is the most suitable. The mentioned authors suggest the $rmSSE_{av}$ value as indicator. In case of Riyadh, the PWLSR method yields the lowest $rmSSE_{av}$. Although this does not apply to most other sites, the PWLSR sub set has been selected for ease of comparison in Table 2-3 (main text).

Appendix 3

Supplementary data for Chapter 3

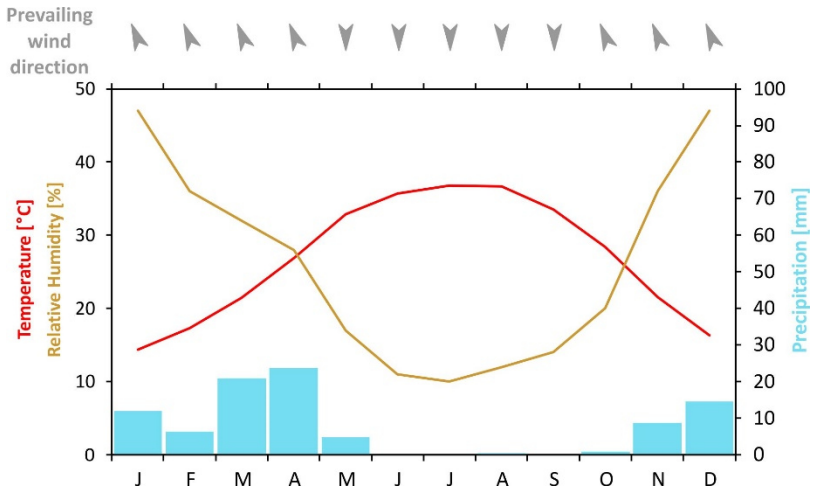

Fig. A3-1. Climate chart for the closest official weather station "Riyadh Old" (based on data by JRCC/PME, 2016; 1985–2010). The mean annual temperature, relative humidity, and precipitation account for 26.8°C, 26 %, and 93 mm, respectively.

Fig. A3-2. Photo of the interdune setting and the augering works for the first borehole (AH 1).

Fig. A3-3. Photo of the augering works for the second borehole (AH 2). Note the white PVC pipe that was used to stabilize the upper layer of dry, loose sand.

Grain size distribution and loss on ignition

Six samples were selected for grain size analysis. The samples were dried at 105°C, split with a custom-made riffle splitter, and about 200 g of sand were analyzed by wet sieving (DIN, 2017; Udden, 1914). Representative sub-samples of 40 to 50 g were used for a loss on ignition test (550°C, 20 h) to estimate the organic matter content (DIN, 2002).

The analyzed samples are mostly dominated by medium and fine sand (Table A3-1). The silt and clay fractions are consistently low and scatter between about 1 and 6 %. These values are typical for dune sands and compare well with data on Saudi Arabian dunes reported in the literature (Dincer et al., 1974; Lopez et al., 2014, 2015).

The loss on ignition values, reflecting the organic matter contents, are all low and range between 0.36 and 0.56 %.

Table A3-1. Grain size fractions and loss on ignition values of the six analyzed sand samples.

AH	Depth [cm]	Very coarse sand [%]	Coarse sand [%]	Medium sand [%]	Fine sand [%]	Very fine sand [%]	Silt and clay [%]	Loss on ignition [%]
1	200	0.8	12.3	35.7	32.0	13.1	6.1	0.56
1	400	0.4	20.4	38.6	27.0	9.6	4.0	0.39
2	53	0.0	1.6	50.0	41.9	5.8	0.7	0.36
2	125	0.0	2.7	53.0	35.0	6.1	3.3	0.39
2	333	0.9	18.7	35.8	21.1	19.3	4.2	0.40
2	500	1.6	26.1	26.0	21.2	22.7	2.3	0.41

Modeling of evaporative fractionation in soils

The following section describes the applied Craig and Gordon (1965) model as summarized by Benettin et al. (2018).

The model incorporates equilibrium and kinetic fractionation during the phase transition from the liquid to the vapor phase. Neglecting resistance to transport in the liquid phase, the water vapor composition is expressed as follows:

$$\delta_E = \frac{(\delta_L - \varepsilon^+)/\alpha^+ - h\delta_A - \varepsilon_k}{1 - h + 10^{-3}\varepsilon_k} \quad \text{(A3-1)}$$

where δ_L and δ_A represent the isotopic compositions of the evaporating surface and the atmosphere, and h is the relative humidity of the atmosphere. The remaining parameters are fractionation factors: α^+ and ε^+ are equilibrium fractionation factors and ε_k is a kinetic fractionation factor. Note that δ values and fractionation factors may here refer to hydrogen or oxygen isotopes (also applies to the following paragraphs, unless otherwise noted).

The equilibrium fractionation factor α^+ quantifies the difference between the isotopic signatures of the liquid and the vapor phase at isotopic equilibrium and is expressed as the ratio of the liquid water and vapor isotope ratios. To calculate α^+, as a function of temperature T [K], the equations by Horita and Wesolowski (1994) are used:

$$10^3 ln\left[\alpha^+\left({}^2H\right)\right] = 1158.8(T^3/10^9) - 1620.1(T^2/10^6) + 794.84(T/10^3) - 161.04 + 2.9992(10^9/T^3) \quad \text{(A3-2)}$$

$$10^3 ln\left[\alpha^+\left({}^{18}O\right)\right] = -7.685 + 6.7123(10^3/T) - 1.6664(10^6/T^2) + 0.3504(10^9/T^3) \quad \text{(A3-3)}$$

The equilibrium isotopic separation between liquid and vapor phase is then calculated as $\varepsilon^+=(\alpha^+-1)10^3$ [‰].

The kinetic fractionation factor ε_k describes isotopic effects that are related to the higher diffusivities of isotopically lighter water molecules. Here, a simplified expression is used (Horita et al., 2008):

$$\varepsilon_k = \Theta n(1-h)(1-D_i/D)10^3 \ \ [‰] \quad \text{(A3-4)}$$

where θ [–] is a weighting term that expresses the potential impact of the evaporation flux on the ambient moisture. For small water bodies, a value of 1 is commonly assumed (Gat, 1996). D_i/D is the ratio between the diffusivities of the heavy and light isotopes. The corresponding values reported by Merlivat (1978) are well-established: $D_i/D({}^2H)=0.9755$ and $D_i/D({}^{18}O)=0.9723$. The parameter n [–] describes the aerodynamic conditions above the evaporating surface and ranges from 0.5 to 1. The former value is considered for turbulent regimes such as open water surfaces (e.g., lakes) that are subject to wind-induced air mass mixing. The latter value is chosen for diffusion-dominated settings (e.g., dry soils).

Now, the case of an isolated water volume (with initial isotopic composition δ_0) evaporating into the atmosphere is considered. Assuming that evaporation is the only flux, the residual liquid volume decreases progressively. To express the evaporated fraction, x [–] is used. Hence, the remaining liquid fraction is 1–x. Assuming constant fractionation factors during the evaporation process, the isotopic composition of the remaining liquid δ_L can be expressed as (Gonfiantini, 1986)

$$\delta_L = (\delta_0 - \delta^*)(1-x)^m + \delta^* \quad \text{(A3-5)}$$

The term δ^* [‰] is the limiting isotopic composition, i.e., the composition approached by a desiccating water volume. The parameter m [–] is the "temporal enrichment slope" (Gibson et al., 2016).

$$\delta^* = (h\delta_A + \varepsilon_k + \varepsilon^+/\alpha^+)/\left(h - 10^{-3}(\varepsilon_k + \varepsilon^+/\alpha^+)\right) \quad \text{(A3-6)}$$

$$m = \left(h - 10^{-3}(\varepsilon_k + \varepsilon^+/\alpha^+)\right)/(1 - h + 10^{-3}\varepsilon_k) \quad \text{(A3-7)}$$

Equation A3-5 may represent an isolated volume of precipitation with initial isotopic composition δ_P, which is subject to evaporation into an atmosphere with an isotopic composition δ_A. If the latter is not known, it is

commonly assumed to be in isotopic equilibrium with precipitation, warranting the use of the following equation (Gibson et al., 2008).

$$\delta_A = (\delta_P - \varepsilon^+)/\alpha^+ \quad \text{(A3-8)}$$

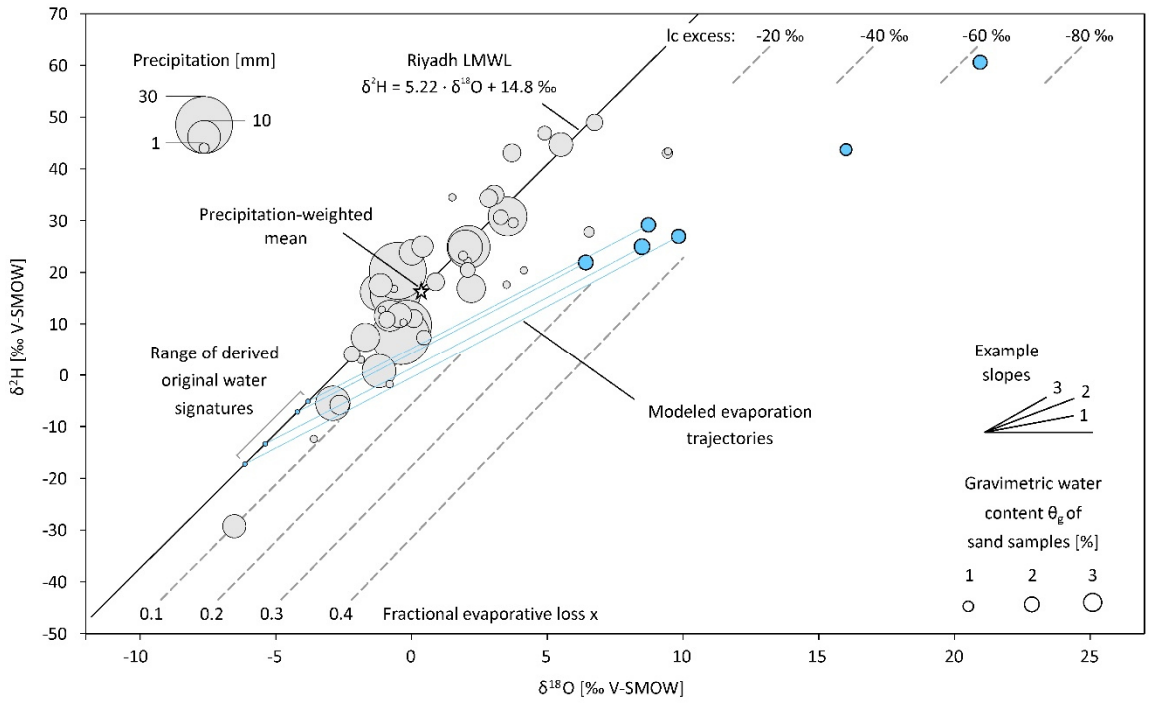

Fig. A3-4. Relation between δ^2H and $\delta^{18}O$ for the AH 1 pore waters (water content θ_g represented by bubble size). For comparison, isotopic data on Riyadh rain events (grey) and the corresponding LMWL are included (rain amount as bubble size; Michelsen et al., 2015). Colored lines are modeled, nearly linear evaporation trajectories.

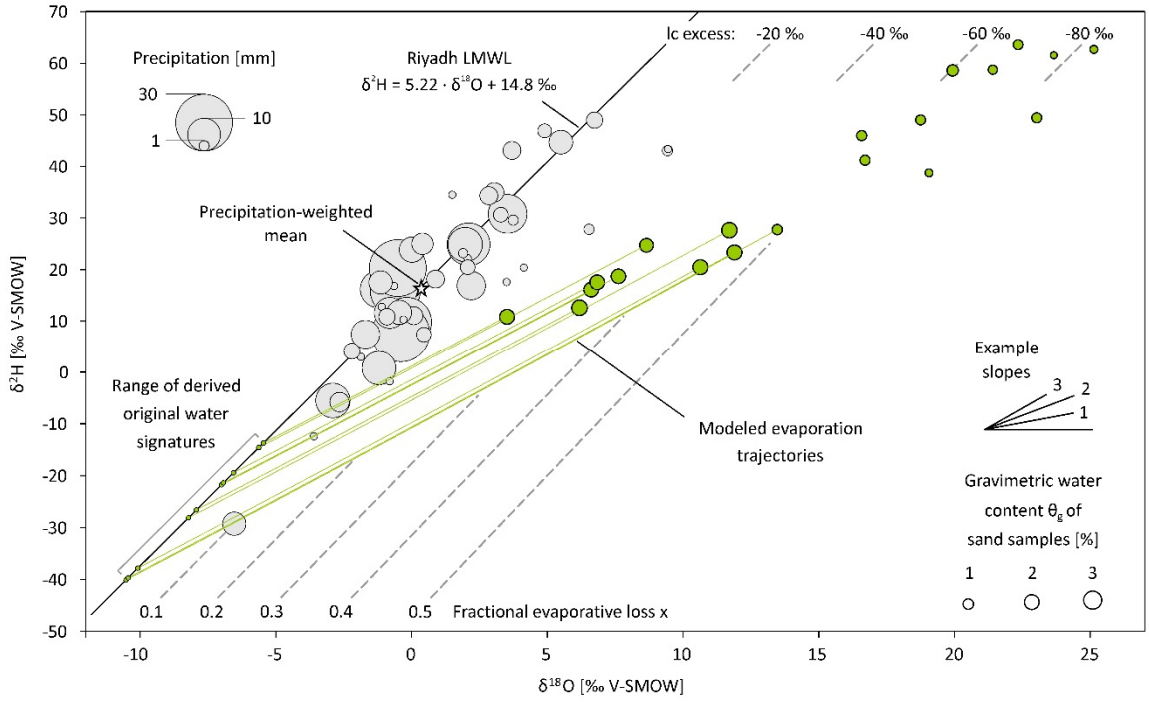

Fig. A3-5. Relation between δ^2H and $\delta^{18}O$ for the AH 2 pore waters (water content θ_g represented by bubble size). For comparison, isotopic data on Riyadh rain events (grey) and the corresponding LMWL are included (rain amount as bubble size; Michelsen et al., 2015). Colored lines are modeled, nearly linear evaporation trajectories.

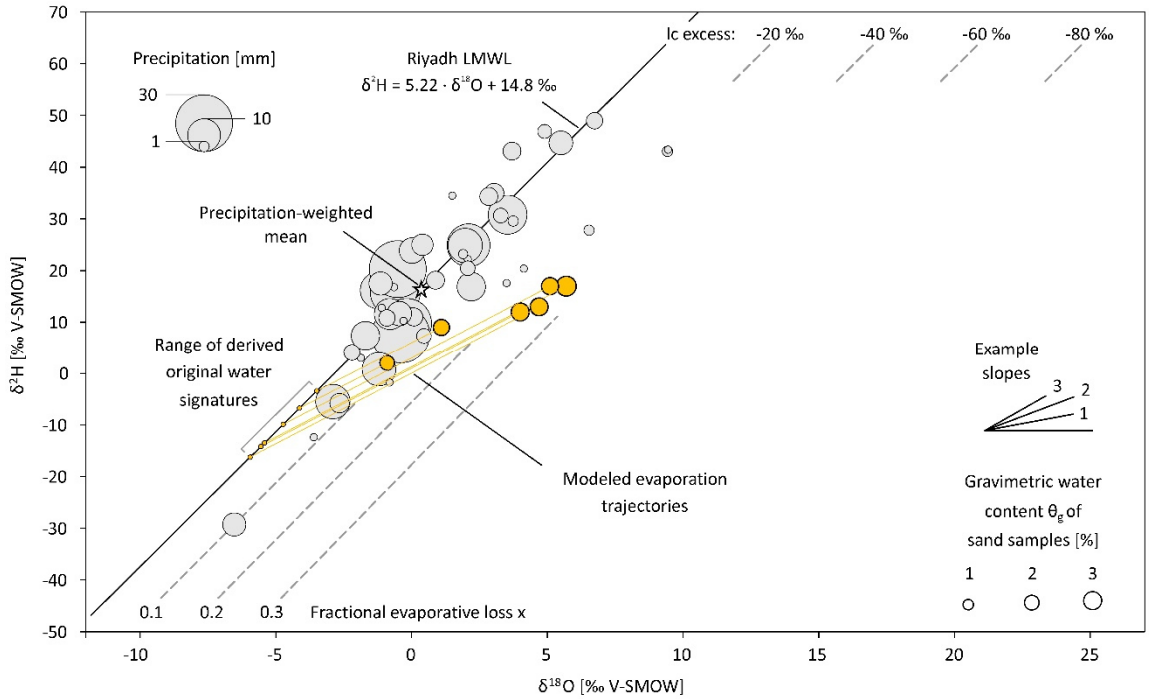

Fig. A3-6. Relation between δ^2H and $\delta^{18}O$ for the AH 3 pore waters (water content θ_g represented by bubble size). For comparison, isotopic data on Riyadh rain events (grey) and the corresponding LMWL are included (rain amount as bubble size; Michelsen et al., 2015). Colored lines are modeled, nearly linear evaporation trajectories.

References

Benettin, P., Volkmann, T.H.M., von Freyberg, J., Frentress, J., Penna, D., Dawson, T.E., Kirchner, J.W., 2018. Effects of climatic seasonality on the isotopic composition of evaporating soil waters. Hydrology and Earth System Sciences 22, 2881–2890.

Craig, H., Gordon, L.I., 1965. Deuterium and oxygen 18 variations in the ocean and the marine atmosphere. In: Tongiorgi, E. (ed.). Stable Isotopes in Oceanographic Studies and Paleotemperatures. Consiglio Nazionale delle Ricerche, Laboratorio di Geologia Nucleare, Pisa, 9–130.

DIN – Deutsches Institut für Normung, 2017. DIN EN ISO 17892-4, Geotechnical investigation and testing – Laboratory testing of soil – Part 4: Determination of particle size distribution. Deutsches Institut für Normung e.V.

DIN – Deutsches Institut für Normung, 2002. DIN 18128, Soil – Investigation and testing – Determination of ignition loss. Deutsches Institut für Normung e.V.

Dincer, T., Al-Mugrin, A., Zimmermann, U., 1974. Study of the infiltration and recharge through the sand dunes in arid zones with special reference to the stable isotopes and thermonuclear tritium. Journal of Hydrology 23, 79–109.

Gat, J.R., 1996. Oxygen and hydrogen isotopes in the hydrologic cycle. Annual Review of Earth and Planetary Sciences 24, 225–262.

Gibson, J.J., Birks, S.J., Edwards, T.W.D., 2008. Global prediction of δ_A and δ^2H-$\delta^{18}O$ evaporation slopes for lakes and soil water accounting for seasonality. Global Biogeochemical Cycles 22, GB2031.

Gibson, J.J., Birks, S., Yi, Y., 2016. Stable isotope mass balance of lakes: a contemporary perspective. Quaternary Science Reviews 131, 316–328.

Gonfiantini, R., 1986. Environmental isotopes in lake studies. In: Fritz, P., Fontes, J. (eds.). Handbook of Environmental Isotope Geochemistry – The Terrestrial Environment. Elsevier, 113–168.

Horita, J., Rozanski, K, Cohen, S., 2008. Isotope effects in the evaporation of water: a status report of the Craig–Gordon model. Isotopes in Environmental and Health Studies 44(1), 23–49.

Horita, J., Wesolowski, D., 1994. Liquid-Vapor Fractionation of Oxygen and Hydrogen Isotopes of Water from the Freezing to the Critical-Temperature. Geochimica et Cosmochimica Acta 58, 3425–3437.

JRCC/PME – Jeddah Regional Climate Center South West Asia/Presidency of Meteorology and Environment, 2016. Climate Data for Saudi Arabia. Surface Annual Climatological Report for station Riyadh Old (1985–2010).

Lopez, O., Stenchikov, G., Missimer, T.M., 2014. Water management during climate change using aquifer storage and recovery of stormwater in a dunefield in western Saudi Arabia. Environmental research Letters 9, 075008.

Lopez, O.M., Jadoon, K.Z., Missimer, T.M., 2015. Method of Relating Grain Size Distribution to Hydraulic Conductivity in Dune Sands to Assist in Assessing Managed Aquifer Recharge Projects: Wadi Khulays Dune Field, Western Saudi Arabia. Water 7, 6411–6426.

Merlivat, L., 1978. Molecular diffusivities of $H_2{}^{16}O$, $HD^{16}O$, and $H_2{}^{18}O$ in gases. The Journal of Chemical Physics 69, 2864–2871.

Michelsen, N., Reshid, M., Siebert, C., Schulz, S., Knöller, K., Weise, S.M., Rausch, R., Al-Saud, M., Schüth, C., 2015. Isotopic and chemical composition of precipitation in Riyadh, Saudi Arabia. Chemical Geology 413, 51–62.

Udden, J.A., 1914. Mechanical composition of clastic sediments. Bulletin of the Geological Society of America 25, 655–744.

Appendix 4

Supplementary data for Chapter 4

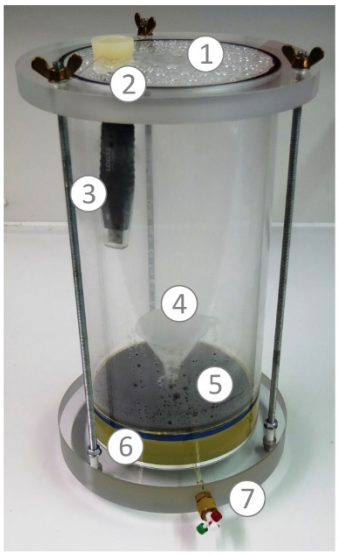

1. Hole for funnel (Ø 5 mm)
2. Access port (Ø 26 mm) with rubber plug
3. Temp. & RH data logger
4. Funnel with ball
5. Float
6. Distilled water (600 mL)
7. Sampling port (Mininert)

Fig. A4-1. Photograph of the Float 2 collector. The collector body is made of acrylic glass (inner diameter 140 mm, wall thickness 5 mm). Note the re-condensed water on the collector walls and ceiling.

Evaporation mapping

Initially, the dry air from the pressurized air system of the laboratory was released into the oven through a simple, bent copper pipe (diameter 16 mm), mounted into an inlet port in the back wall. The pipe extended about 25 cm into the oven, i.e., the air entered the chamber in a central position. A preliminary test with open beakers in the original laboratory oven indicated that the beaker position on a given rack had an influence on the evaporation rate. The evaporation was systematically mapped by placing 208 small beakers (25 mL), each filled with 10 mL of water, into the 30°C warm oven for 48 h (Fig. A4-2). Evaporative mass losses were determined by weighing the 208 beakers before and after exposure in the oven.

Fig. A4-2. Array of 208 beakers, each filled with 10 mL of water, applied to map the evaporation in the oven. For better stability, the beakers were sandwiched between two oven racks.

The result was a rather heterogeneous evaporation distribution, with elevated values near the walls and especially in the center of the oven (Fig. A4-3a). The latter effect was attributed to the rather concentrated release of the dry air beneath the central beakers.

Aiming at a homogeneous evaporation, we installed a custom-made dry air diffuser onto the copper pipe and placed a porous filter mat between the diffuser and the beaker rack (see ③ and ② in Fig. A4-4). These measures caused a much more homogeneous evaporation pattern (Fig. A4-3b), which eventually allowed us to place the collectors to be tested almost anywhere on the rack. Only very peripheral positions had to be avoided.

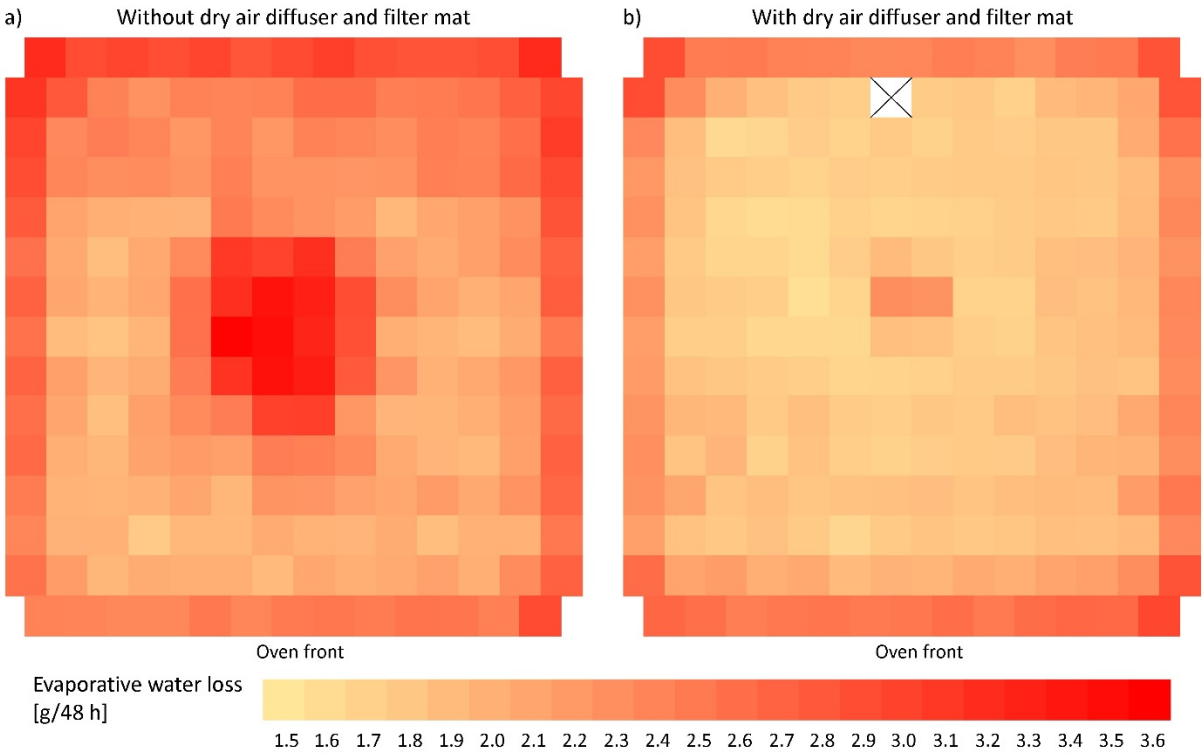

Fig. A4-3. Water mass losses from beakers after 48 h at 30°C illustrate the spatial evaporation pattern in the laboratory oven a) without and b) with the dry air diffuser and the filter mat. Each square represents one beaker.

Fig. A4-4. Photograph of the modified laboratory drying oven. The modifications ensure dry conditions and a homogeneous evaporation distribution in the oven.

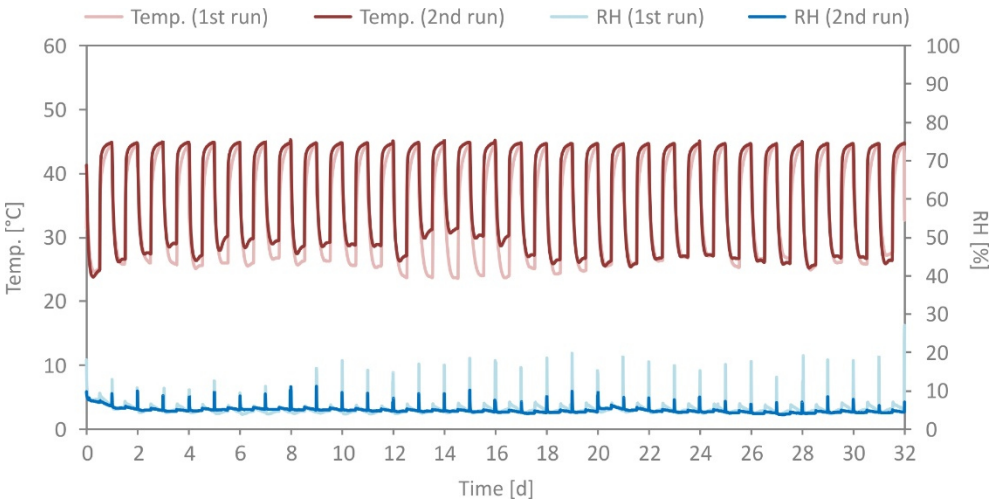

Fig. A4-5. Temporal development of temperature and relative humidity in the laboratory oven during the two runs. Note the diurnal temperature regime with daytime temperatures reaching 45°C. The low relative humidities in the oven (RH_{mean}, 1st run = 5.3 %, RH_{mean}, 2nd run = 5.0 %) are a result of the silica gel and the flushing with dry air (see Fig. A4-4). The daily peaks of the relative humidity are caused by the nighttime cooling and ambient laboratory air entering the oven when the door is opened once a day to weigh the collectors.

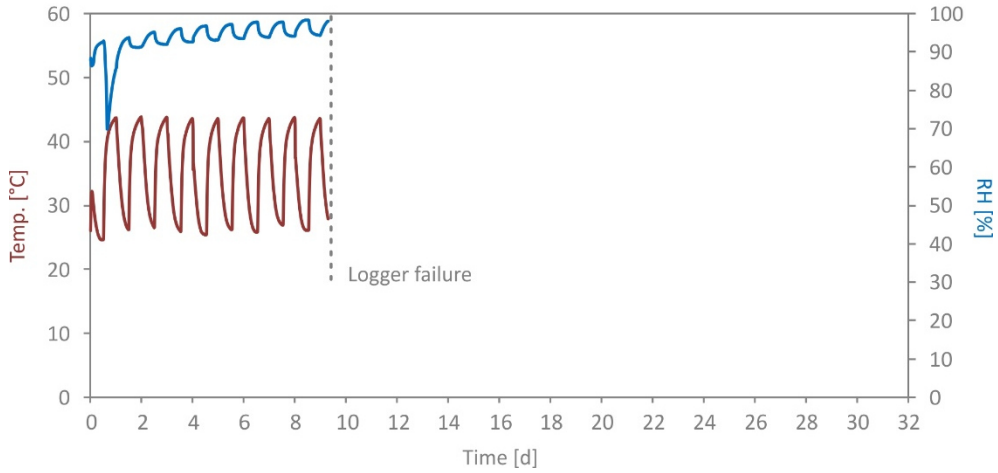

Fig. A4-6. Temporal development of temperature and relative humidity in the Tube-dip-in-water collector (1st run). The evaporation in the collector leads to an elevated relative humidity (RH_{mean} 93.5 %). The logger failure (after about 9 days) was probably caused by condensed water in the logger.

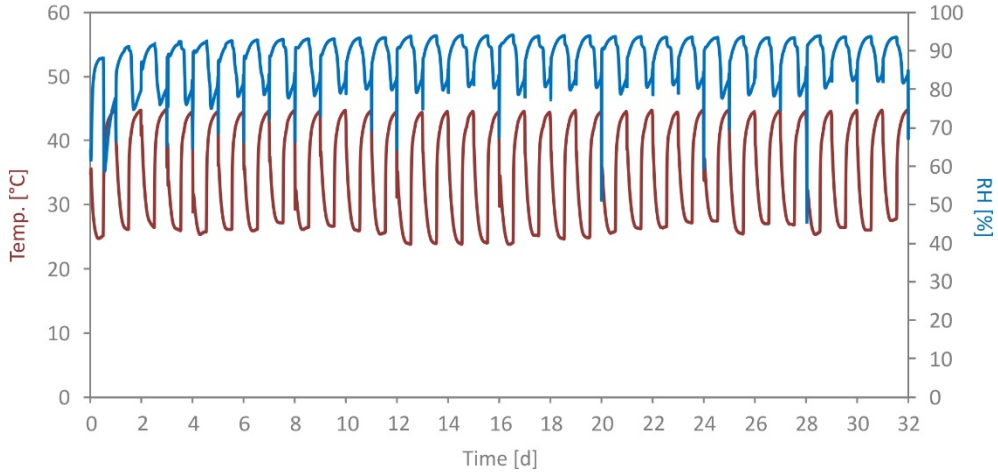

Fig. A4-7. Temporal development of temperature and relative humidity in the Floating balls collector (1st run). The high relative humidity values (RH_{mean} 87.7 %) indicate that evaporation is not effectively reduced.

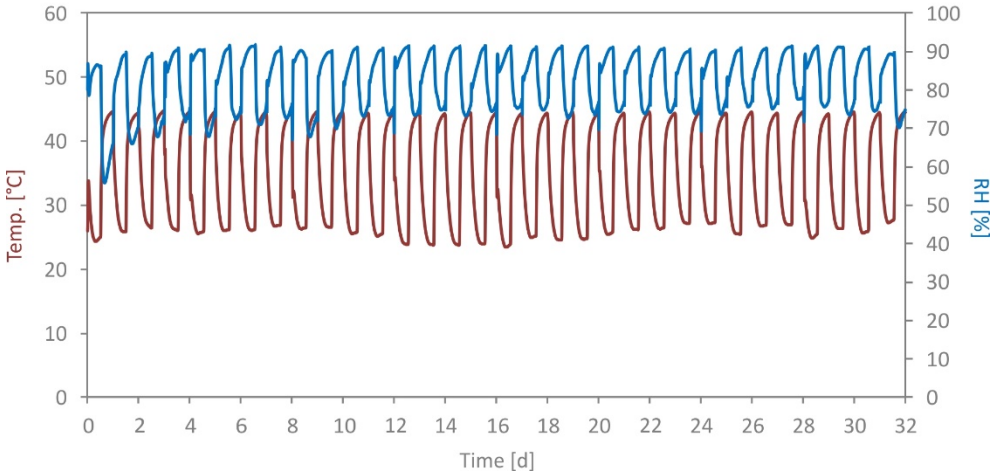

Fig. A4-8. Temporal development of temperature and relative humidity in the Float 1 collector (1st run). The high relative humidity values (RH_{mean} 82.3 %) indicate that evaporation is not effectively reduced.

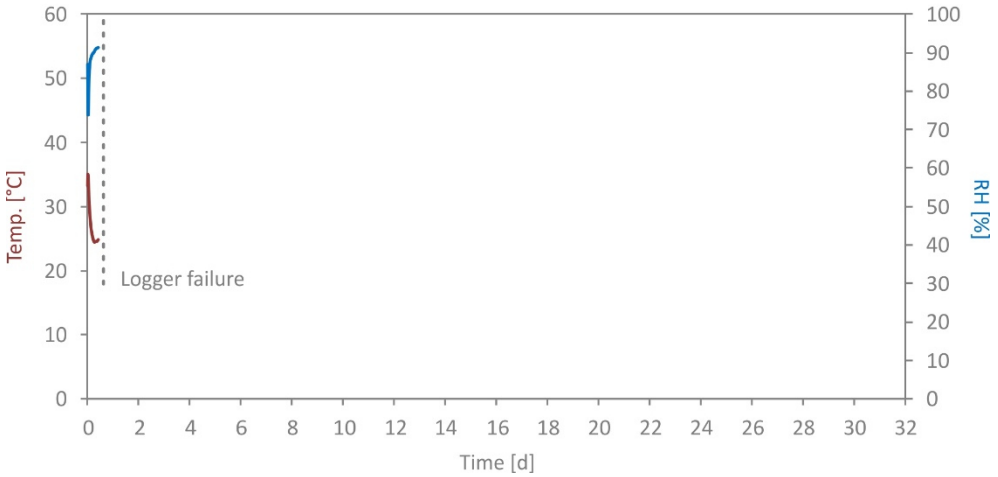

Fig. A4-9. Temporal development of temperature and relative humidity in the Reference 1 collector (1st run). The logger failure (on the first day) was probably caused by condensed water in the logger.

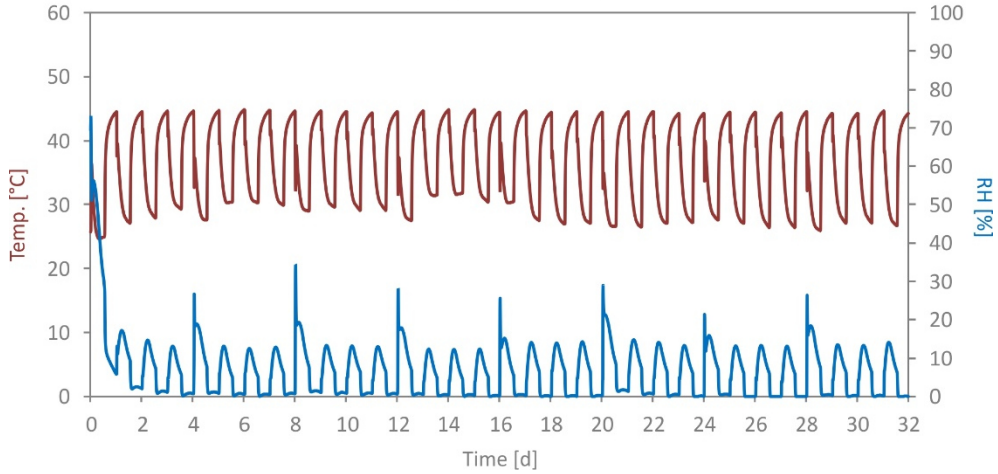

Fig. A4-10. Temporal development of temperature and relative humidity in the Oil collector (2nd run). The low relative humidities (RH_{mean} 6.9 %) indicate an effective evaporation suppression by the oil layer. The peaks occurring every four days reflect the sampling during which the collector was opened, allowing moist ambient laboratory air to enter the bottle.

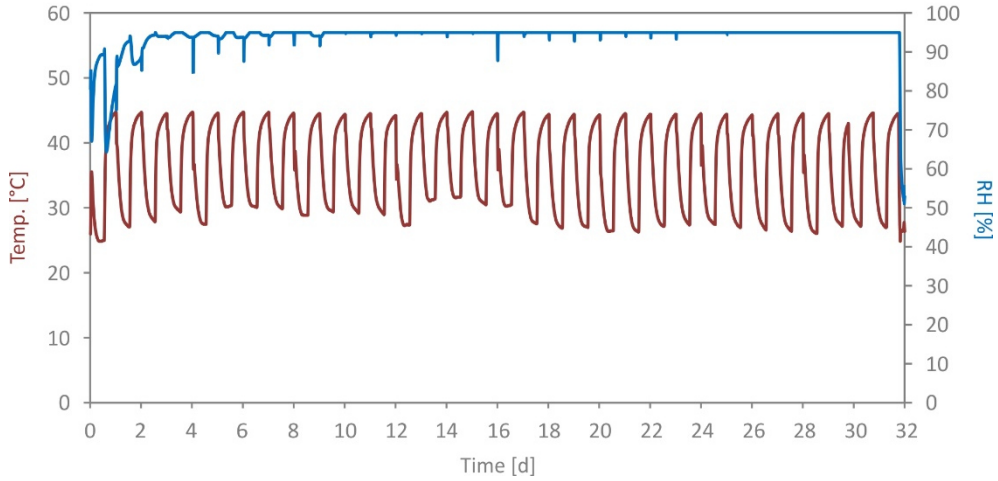

Fig. A4-11. Temporal development of temperature and relative humidity in the Float 2 collector (2nd run). The high relative humidity values (RH_{mean} 93.9 %) indicate that evaporation is not effectively reduced. This is also evident from condensed water on the lid and the wall of the collector (see Fig. A4-1).

Table A4-1. Cumulative evaporative mass losses Δm over time [g]. The total mass losses after 32 d (Δm_{fin}) are expressed as absolute mass losses [g], as percentages of the original water mass of 600 g [%-orig.], and as percentages normalized to the corresponding reference collector [%-ref.] (Δm_{ref} = 100 %).

Time [d]	Tube-dip-in-water	Floating balls	Float 1	Ref 1	Oil	Ball-in-funnel	Float 2	Ref 2	
0	0.0	0.0	0.0	0.0	0.0	0.0	0.0	0.0	
1	2.0	1.1	1.0	0.9	0.3	0.8	2.1	0.7	
2	2.3	2.0	1.7	1.4	0.3	1.4	2.8	1.3	
3	2.8	2.9	2.5	1.9	0.4	2.0	3.5	1.7	
4	2.8	3.8	2.9	2.4	0.5	2.6	4.2	2.4	
5	4.0	4.7	3.9	3.6	0.6	3.2	4.9	3.6	
6	4.0	5.5	3.9	4.1	0.6	3.8	5.6	4.2	
7	4.1	6.1	4.3	4.6	0.6	4.4	6.4	4.7	
8	4.2	6.9	4.8	5.1	0.7	5.0	6.9	5.2	
9	4.5	7.7	5.7	6.1	0.9	5.9	8.1	6.2	
10	4.7	8.3	6.3	6.6	0.9	6.5	8.9	6.8	
11	4.9	9.1	6.9	7.2	1.0	7.2	9.6	7.3	
12	5.0	9.7	7.4	7.7	1.1	7.8	10.2	7.9	
13	5.3	10.5	8.1	8.6	1.3	8.5	11.2	8.9	
14	5.3	11.1	8.5	9.1	1.3	9.1	12.0	9.6	
15	5.4	11.7	9.0	9.6	1.4	9.8	13.0	10.2	
16	5.5	12.4	9.4	10.1	1.4	10.4	13.6	10.7	
17	6.0	13.3	10.3	11.1	1.6	11.2	14.8	11.9	
18	6.1	13.9	10.8	11.8	1.6	11.8	15.1	12.4	
19	6.3	14.6	11.3	12.3	1.7	12.3	15.9	12.9	
20	6.3	15.4	11.8	12.8	1.8	13.0	16.5	13.5	
21	6.7	16.3	12.6	13.9	2.0	13.9	18.0	14.6	
22	6.9	17.0	13.1	14.6	2.1	14.5	18.5	15.1	
23	6.9	17.6	13.6	15.1	2.2	15.1	19.1	15.7	
24	7.0	18.4	14.1	15.5	2.2	15.6	19.7	16.3	
25	7.4	19.4	14.9	16.7	2.4	16.4	21.1	17.8	
26	7.6	20.3	15.4	17.3	2.4	17.0	21.7	18.4	
27	7.7	21.2	16.0	17.9	2.4	17.7	22.5	18.9	
28	7.7	21.8	16.3	18.3	2.5	18.2	22.9	19.5	
29	8.1	22.6	17.2	19.5	2.6	18.9	23.8	20.6	
30	8.1	23.3	17.7	20.0	2.8	19.6	24.5	21.2	
31	8.1	24.0	18.2	20.5	2.8	20.2	25.1	21.7	
32	8.4	24.7	18.9	21.1	2.8	20.8	25.5	22.1	Δm_{fin} [g]
	1.4	4.1	3.2	3.5	0.5	3.5	4.2	3.7	Δm_{fin} [%-orig.]
	40	117	90	100	13	94	115	100	Δm_{fin} [%-ref.]

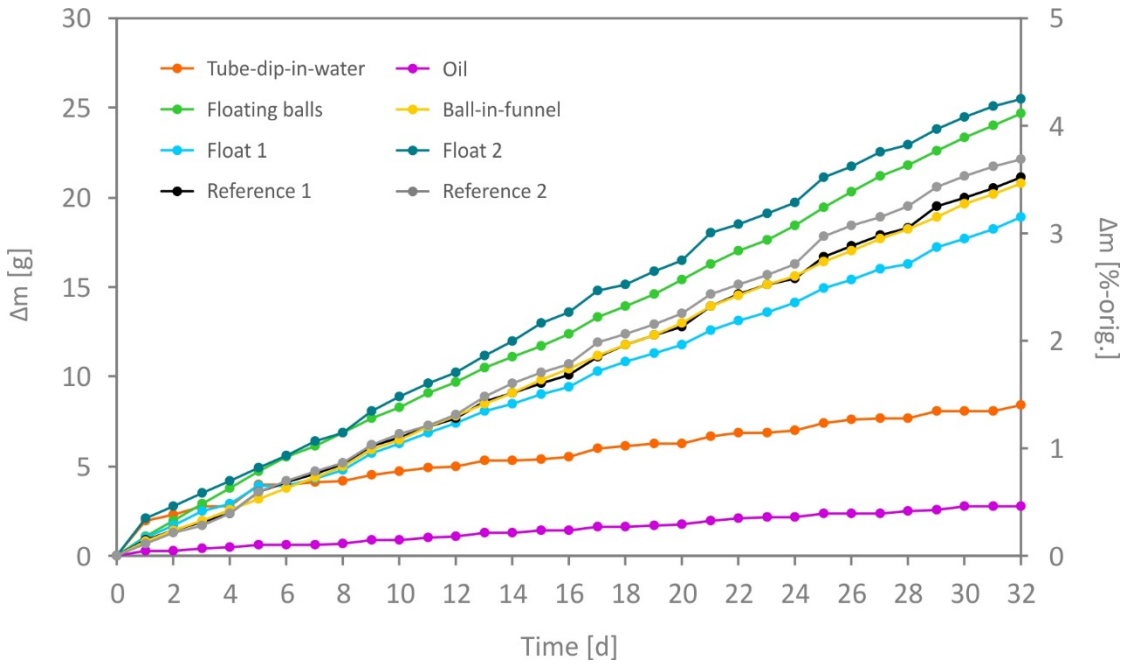

Fig. A4-12. Temporal development of the cumulative evaporative water loss Δm, expressed as absolute mass [g] (left axis) and as percentage of the original water mass of 600 g [%-orig.] (right axis).

Table A4-2. Measured δ-values and deuterium excess (d) values for the tested collectors [all values in ‰ VSMOW].

Day	Tube-dip-in-water			Floating balls			Float 1			Reference 1			Oil			Ball-in-funnel			Float 2			Reference 2		
	$\delta^{18}O$	$\delta^{2}H$	d	$\delta^{18}O$	$\delta^{2}H$	d	$\delta^{18}O$	$\delta^{2}H$	d	$\delta^{18}O$	$\delta^{2}H$	d	$\delta^{18}O$	$\delta^{2}H$	d	$\delta^{18}O$	$\delta^{2}H$	d	$\delta^{18}O$	$\delta^{2}H$	d	$\delta^{18}O$	$\delta^{2}H$	d
0	-8.62	-61.1	7.9	-8.62	-61.1	7.9	-8.62	-61.1	7.9	-8.62	-61.1	7.9	-8.62	-61.1	7.9	-8.62	-61.1	7.9	-8.62	-61.1	7.9	-8.62	-61.1	7.9
4	-8.50	-60.5	7.5	-8.32	-60.4	6.2	-8.44	-60.6	6.9	-8.42	-61.1	6.3	-8.60	-61.2	7.6	-8.48	-60.9	7.0	-8.50	-60.8	7.2	-8.44	-60.7	6.8
8	-8.69	-61.2	8.3	-8.34	-60.5	6.3	-8.28	-59.9	6.3	-8.47	-61.1	6.7	-8.61	-61.4	7.5	-8.29	-60.4	6.0	-8.41	-60.5	6.8	-8.41	-60.7	6.5
12	-8.65	-61.0	8.2	-8.15	-60.0	5.3	-8.20	-59.8	5.8	-8.33	-60.4	6.2	-8.59	-60.8	7.9	-8.24	-60.4	5.5	-8.28	-60.1	6.1	-8.33	-60.5	6.1
16	-8.39	-60.7	6.4	-7.73	-59.0	2.9	-8.14	-60.3	4.8	-8.23	-60.2	5.6	-8.55	-60.9	7.5	-8.07	-60.0	4.5	-8.14	-59.6	5.5	-8.13	-59.9	5.2
20	-8.37	-59.9	7.1	-7.90	-59.5	3.7	-8.12	-60.3	4.7	-8.00	-59.5	4.5	-8.59	-61.0	7.7	-7.96	-59.7	3.9	-8.07	-60.0	4.6	-8.09	-59.5	5.2
24	-8.28	-60.0	6.2	-7.73	-59.1	2.7	-8.04	-59.7	4.6	-7.84	-58.9	3.8	-8.58	-60.7	8.0	-7.87	-59.7	3.2	-8.02	-59.4	4.8	-7.96	-59.7	3.9
28	-8.38	-60.3	6.7	-7.53	-58.4	1.9	-7.94	-59.1	4.5	-7.92	-59.3	4.1	-8.55	-61.1	7.3	-7.63	-58.9	2.1	-7.87	-58.7	4.3	-7.83	-58.9	3.7
32	-8.34	-60.1	6.6	-7.37	-57.7	1.3	-7.87	-58.9	4.1	-7.55	-57.8	2.6	-8.58	-60.7	8.0	-7.57	-58.9	1.7	-7.82	-58.8	3.8	-7.69	-59.1	2.5

Table A4-3. Calculated deviations from the original δ values and deuterium excess (d) values for the tested collectors [all values in ‰ VSMOW].

Day	Tube-dip-in-water			Floating balls			Float 1			Reference 1			Oil			Ball-in-funnel			Float 2			Reference 2		
	$\Delta\delta^{18}O$	$\Delta\delta^{2}H$	Δd	$\Delta\delta^{18}O$	$\Delta\delta^{2}H$	Δd	$\Delta\delta^{18}O$	$\Delta\delta^{2}H$	Δd	$\Delta\delta^{18}O$	$\Delta\delta^{2}H$	Δd	$\Delta\delta^{18}O$	$\Delta\delta^{2}H$	Δd	$\Delta\delta^{18}O$	$\Delta\delta^{2}H$	Δd	$\Delta\delta^{18}O$	$\Delta\delta^{2}H$	Δd	$\Delta\delta^{18}O$	$\Delta\delta^{2}H$	Δd
0	0.00	0.0	0.0	0.00	0.0	0.0	0.00	0.0	0.0	0.00	0.0	0.0	0.00	0.0	0.0	0.00	0.0	0.0	0.00	0.0	0.0	0.00	0.0	0.0
4	0.12	0.5	-0.4	0.30	0.7	-1.7	0.18	0.4	-1.0	0.20	0.0	-1.6	0.02	-0.1	-0.3	0.13	0.2	-0.9	0.12	0.3	-0.7	0.18	0.4	-1.0
8	-0.07	-0.1	0.4	0.28	0.6	-1.6	0.34	1.2	-1.5	0.15	0.0	-1.2	0.00	-0.3	-0.4	0.33	0.7	-1.9	0.21	0.6	-1.1	0.21	0.3	-1.3
12	-0.03	0.1	0.3	0.47	1.1	-2.6	0.42	1.3	-2.0	0.29	0.6	-1.7	0.03	0.3	0.0	0.38	0.7	-2.3	0.34	1.0	-1.7	0.29	0.5	-1.8
16	0.23	0.3	-1.5	0.89	2.1	-5.0	0.48	0.7	-3.1	0.39	0.9	-2.2	0.06	0.2	-0.4	0.55	1.1	-3.4	0.48	1.5	-2.3	0.49	1.2	-2.7
20	0.25	1.2	-0.8	0.72	1.6	-4.1	0.50	0.8	-3.2	0.62	1.6	-3.3	0.03	0.0	-0.2	0.66	1.3	-4.0	0.55	1.1	-3.3	0.53	1.5	-2.7
24	0.34	1.0	-1.7	0.89	2.0	-5.1	0.58	1.4	-3.2	0.78	2.1	-4.1	0.04	0.4	0.1	0.75	1.4	-4.6	0.60	1.7	-3.1	0.66	1.3	-3.9
28	0.24	0.8	-1.1	1.09	2.7	-6.0	0.68	2.0	-3.4	0.70	1.8	-3.8	0.06	0.0	-0.5	0.99	2.2	-5.7	0.75	2.4	-3.6	0.79	2.2	-4.1
32	0.28	0.9	-1.3	1.25	3.4	-6.6	0.75	2.2	-3.8	1.07	3.3	-5.3	0.04	0.4	0.1	1.05	2.2	-6.2	0.80	2.3	-4.1	0.93	2.0	-5.4

Craig and Gordon model

In an attempt to gain further insights into the processes governing the observed isotope shifts in our experiments, we utilized the Craig and Gordon (1965) model as implemented in the *Hydrocalculator* (Skrzypek et al., 2015; Excel version in their Supplementary material).

For the non-steady state model, we selected the mean ambient conditions recorded in the oven (T_{mean}=35.5°C, RH_{mean}=5 %). We assumed that vapor in the headspace was in equilibrium with the original water ($\delta^{18}O$=-8.62 ‰, $\delta^{2}H$=-61.1 ‰), i.e., these values are also used to determine the isotope composition of the air ambient moisture (δ_A in *Hydrocalculator*; Option 2).

With the default values for the kinetic fractionation constant C_k (14.2 and 12.5 ‰ for $\delta^{18}O$ and $\delta^{2}H$, respectively; cf., Gonfiantini, 1986), the fits between the generated lines and the measured data in the corresponding plots ($\delta^{18}O$ and $\delta^{2}H$ vs residual fraction f, $\delta^{18}O$ vs $\delta^{2}H$) were unsatisfactory. This finding can be explained by the fact that the *Hydrocalculator* was designed for evaporation from open water, e.g., from lakes. Because evaporation in our experiments took place inside containers, the interface between the water and the free atmosphere was less turbulent. This means that we had to adjust the C_k values to mimic the conditions in the collectors. The above-mentioned default values correspond to a turbulence parameter n of 0.5 (Gonfiantini, 1986), but n can reach unity in case of very stagnant interfaces (Horita et al., 2008). Hence, we modified the C_k values in the model by using n as fitting parameter:

$$C_k = n \cdot (1 - D_i/D) \cdot 10^3 \qquad \text{(Horita et al., 2008)}$$

where D_i/D is the ratio of the molecular diffusion coefficients and the subscript i stands for the heavy isotope water molecule. As values for D_i/D, those presented by Merlivat (1978) were used, i.e., 0.9723 and 0.9755 for ^{18}O and ^{2}H, respectively.

The resulting fits are shown in Fig. A4-13 and A4-14. As reference, also the lines representing the case n=0.5 are included (grey, dashed lines). For nearly all collectors, the obtained n was greater than 0.5. This finding suggests that isotope-fractionating molecular diffusion out of the collectors plays a dominant role in our experiments. Evaporation, by contrast, is less important in terms of fractionation. In this context, it is also noteworthy that the highest n values (0.828 and 0.883), indicating the most stagnant conditions, were determined for the Floating balls collector and the Ball-in-Funnel collector, which seems plausible. In case of the former device, floating balls form a macro-porous layer above the water surface, promoting stagnant conditions. In case of the Ball-in-funnel collector, the table tennis ball reduces vapor exchange.

With these n values, it was also possible to capture the relatively low slopes (2.5 to 3.4) in the dual isotope plots (right column in Fig. A4-13 and A4-14).

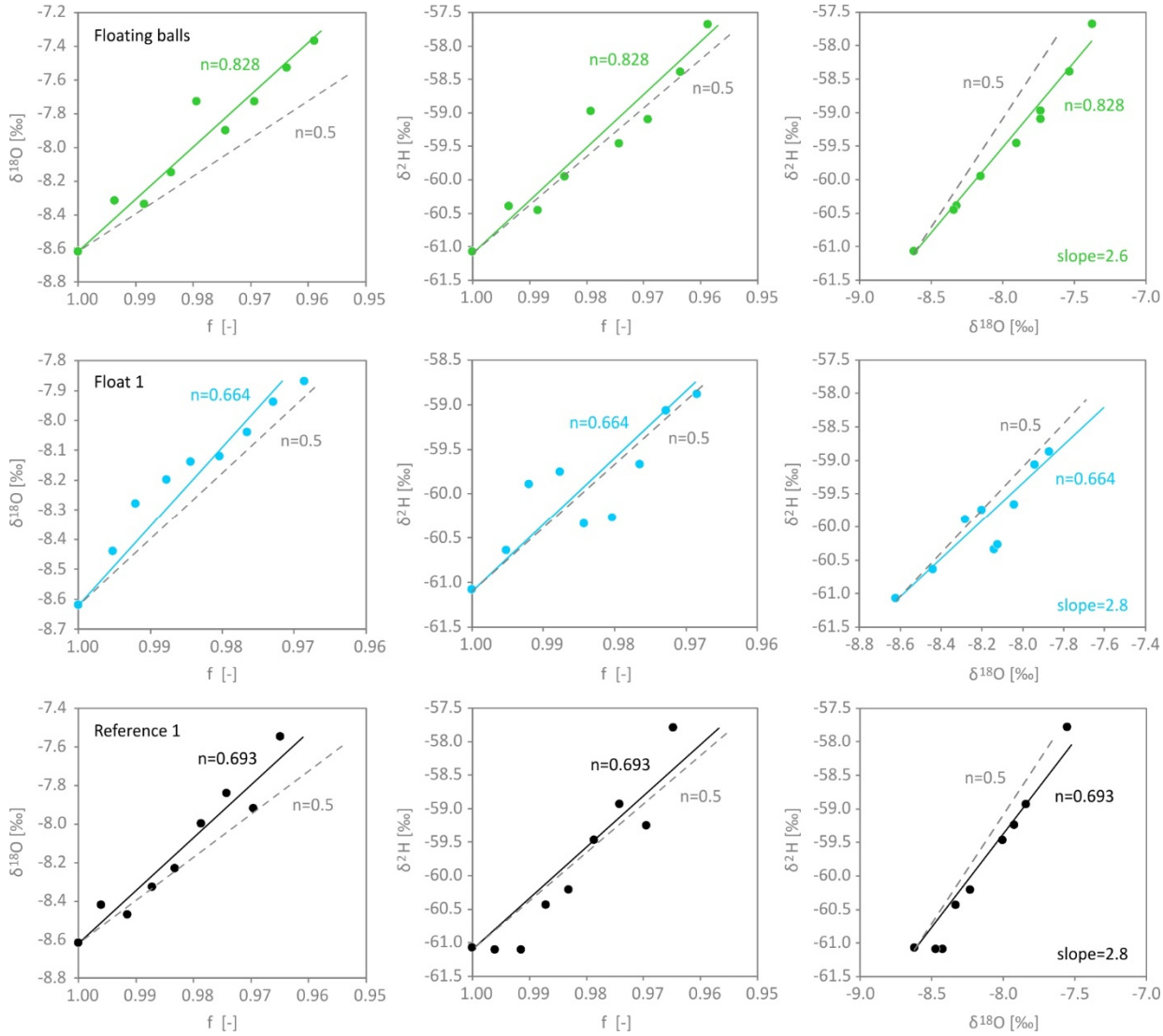

Fig. A4-13. Scatter plots showing the results of the modeling exercise for the Floating balls, the Float 1, and the Reference 1 collector.

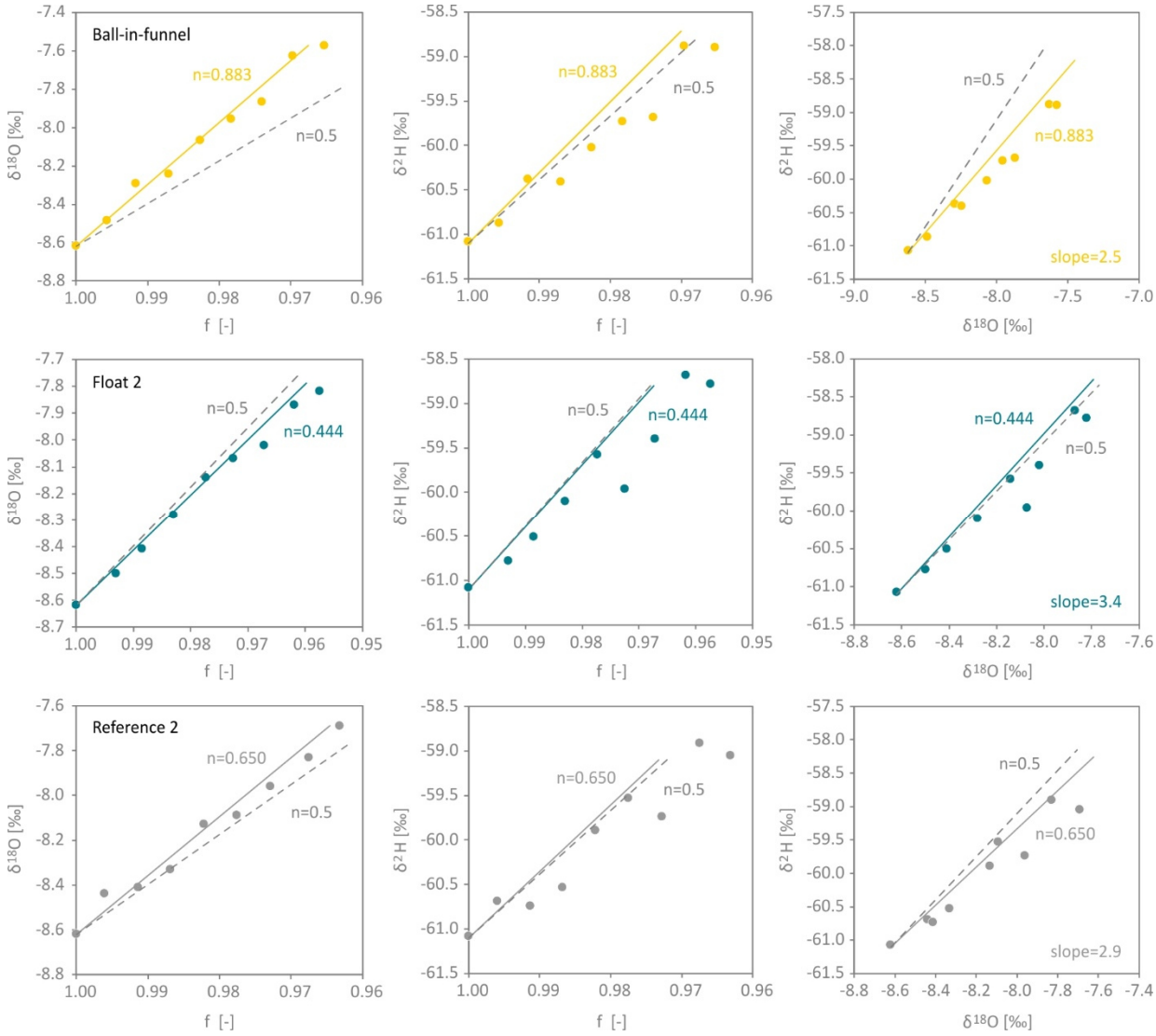

Fig. A4-14. Scatter plots showing the results of the modeling exercise for the Ball-in-funnel, the Float 2, and the Reference 2 collector. Note: In case of the Tube-dip-in-water and the Oil collector, isotope shifts and mass losses were rather small and hence we made no attempt to model the conditions in these devices.

References

Craig, H., Gordon, L.I., 1965. Deuterium and oxygen 18 variations in the ocean and the marine atmosphere. In: Tongiorgi, E. (ed.). Stable Isotopes in Oceanographic Studies and Paleotemperatures. Consiglio Nazionale delle Ricerche, Laboratorio di Geologia Nucleare, Pisa, 9–130.

Gonfiantini, R., 1986. Environmental isotopes in lake studies. In: Fritz, P., Fontes, J.C. (eds.). Handbook of Environmental Isotope Geochemistry, Vol. 2: The Terrestrial Environment. Elsevier, Amsterdam, 113–168.

Horita, J., Rozanski, K, Cohen, S., 2008. Isotope effects in the evaporation of water: a status report of the Craig–Gordon model. Isotopes in Environmental and Health Studies 44(1), 23–49.

Merlivat, L., 1978. Molecular diffusivities of $H_2{}^{16}O$, $HD^{16}O$, and $H_2{}^{18}O$ in gases. The Journal of Chemical Physics 69, 2864–2871.

Skrzypek, G., Mydłowski, A., Dogramaci, S., Hedley, P., Gibson, J.J., Grierson, P.F., 2015. Estimation of evaporative loss based on the stable isotope composition of water using Hydrocalculator. Journal of Hydrology 523, 781–789. Online and offline versions also available at http://hydrocalculator.gskrzypek.com/ (last access: 8 April 2018).

Appendix 5

Supplementary data for Chapter 5

Pre-test of tubing materials

To identify the most suitable tubing material, a pre-test was conducted. To this end, different materials were selected, namely PU (black and transparent), silicone, Tygon (E3603), rubber, FKM (recommended by Hartmann et al., 2018), PE (LDPE), PTFE, and PVC (Fig. A5-1, Table A5-1). Tubing sections of 25 cm length were used to create tubing loops (mostly by push-in connectors). These loops were partially filled with 0.5 mL of water and placed in an oven (duplicates or triplicates). Here, a diurnal temperature regime (21–31°C; monitored with log32TH loggers by Dostmann electronic, Wertheim, Germany) was simulated for one week. Water losses were determined gravimetrically.

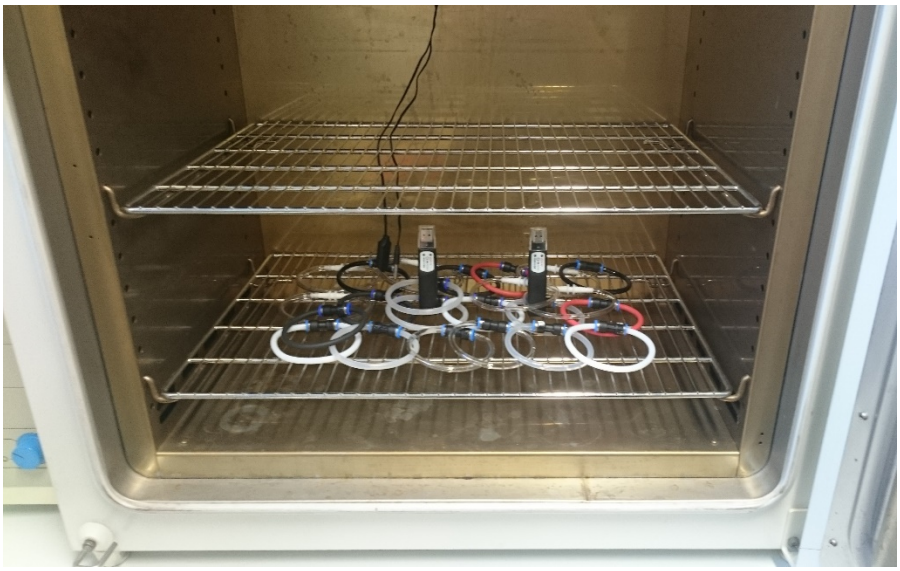

Fig. A5-1. Setup of the pre-test of tubing materials.

Although the tubing loops had nearly identical dimensions (lengths, inner diameters, wall thicknesses), the recorded mass losses differed substantially. While the loops made of LDPE and PTFE (IDs 7 and 8) showed no measurable mass losses after one week, the silicone loops (ID 3) lost 0.35 and 0.36 g of water. These results highlight the importance of the tubing material in terms of diffusive water vapor fluxes and demonstrate the superiority of LDPE and PTFE among the tested materials. Given that LDPE is cheaper than PTFE (by a factor of 10), we selected this tubing material for our automatic rain sampler.

Table A5-1. Results of the pre-test of tubing materials.

Loop ID	Description	Supplier	Approx. price [€/m]	Dimensions (Inner diameter x wall thickness) [mm]	Total mass at first day [g]	Total mass after 7 days [g]	Mass loss Δm after 7 days [g]
1a	PU (black)	Landefeld	0.79	4 x 1	10.69	10.54	0.15
1b	PU (black)	Landefeld	0.79	4 x 1	10.79	10.63	0.16
2a	PU (transparent)	Landefeld	0.79	4 x 1	10.90	10.75	0.15
2b	PU (transparent)	Landefeld	0.79	4 x 1	10.81	10.68	0.13
3a	Silicone	häberle	3.40	4 x 1	10.66	10.30	0.36
3b	Silicone	häberle	3.40	4 x 1	10.66	10.31	0.35
4a	Tygon E3603	häberle	3.05	4 x 0.8	5.27	5.02	0.25
4b	Tygon E3603	häberle	3.05	4 x 0.8	5.27	5.06	0.21
4c	Tygon E3603	häberle	3.05	4 x 0.8	5.28	5.03	0.25
5a	Rubber	häberle	4.30	4 x 1	11.10	11.06	0.04
5b	Rubber	häberle	4.30	4 x 1	9.41	9.36	0.05
6a	FKM	häberle	13.30	4 x 1	12.33	12.31	0.02
6b	FKM	häberle	13.30	4 x 1	10.77	10.75	0.02
6c	FKM	häberle	13.30	4 x 1	10.68	10.66	0.02
7a	PE (LDPE)	häberle	1.30	4 x 1	9.20	9.20	0.00
7b	PE (LDPE)	häberle	1.30	4 x 1	7.59	7.59	0.00
7c	PE (LDPE)	häberle	1.30	4 x 1	7.57	7.56	0.01
8a	PTFE	häberle	14.10	4 x 1	14.06	14.06	0.00
8b	PTFE	häberle	14.10	4 x 1	12.41	12.41	0.00
8c	PTFE	häberle	14.10	4 x 1	14.21	14.21	0.00
9a	PVC	häberle	1.35	4 x 1	9.65	9.61	0.04
9b	PVC	häberle	1.35	4 x 1	9.74	9.70	0.04
9c	PVC	häberle	1.35	4 x 1	9.66	9.62	0.04

PU: Polyurethane

LDPE: Low-density polyethylene

PTFE: Polytetrafluoroethylene

PVC: Polyvinyl chloride

Tubing-bottle connections

The water and air tubes are guided through the bottle caps by means of cable grommets. The used KAB SNAP 9 cable grommets (see bill of materials) are suitable for tubing diameters between 5.0 and 7.0 mm. They were installed by drilling two 16 mm bores into the bottle caps and pushing the conical part of the grommets through the bores.

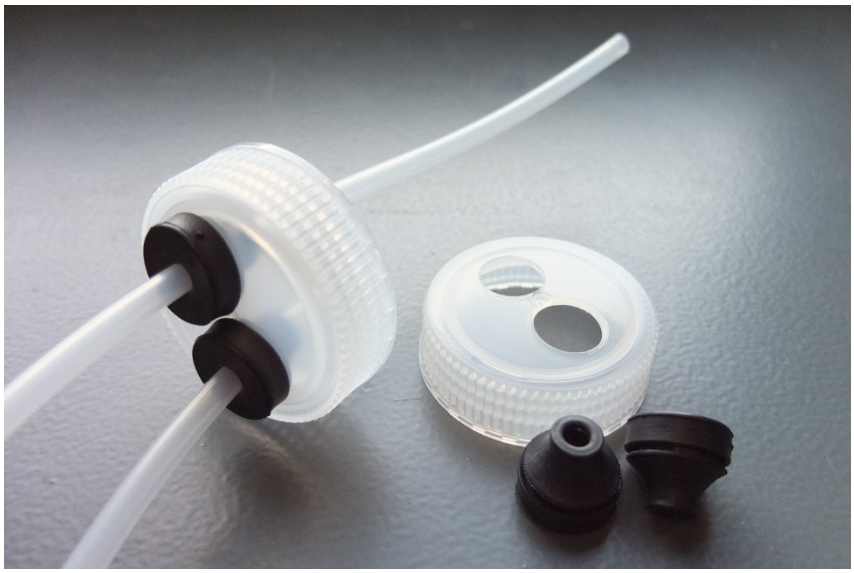

Fig. A5-2. Bottles caps with cable grommets. Note that the water tube (rain inlet) extends to the bottom of the bottle, whereas the air tube extends just below the cable grommet.

Further details on the evaporation experiment in the laboratory oven

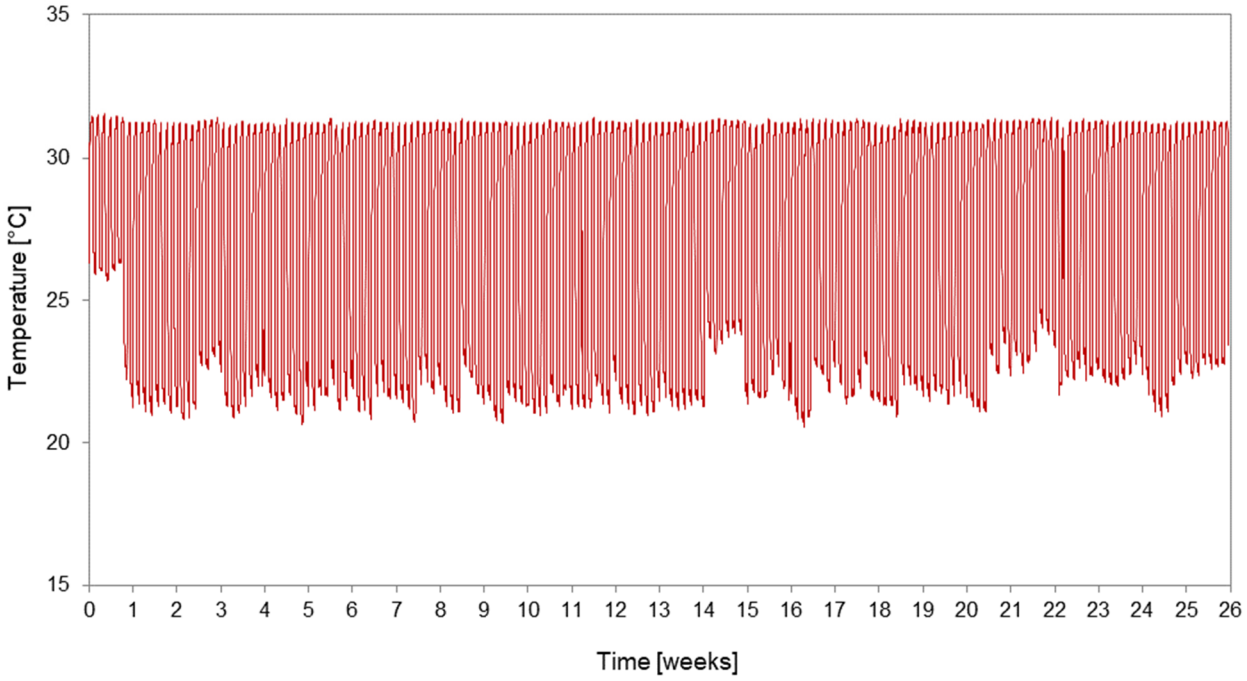

Fig. A5-3. Temperatures during the evaporation experiment in the laboratory oven (T_{mean}=26.7°C). Note the diurnal regime with simulated nighttime and daytime temperatures of approx. 21°C and 31°C. Anomalies in the nighttime temperatures are caused by occasional technical problems with the air-conditioning system of the laboratory.

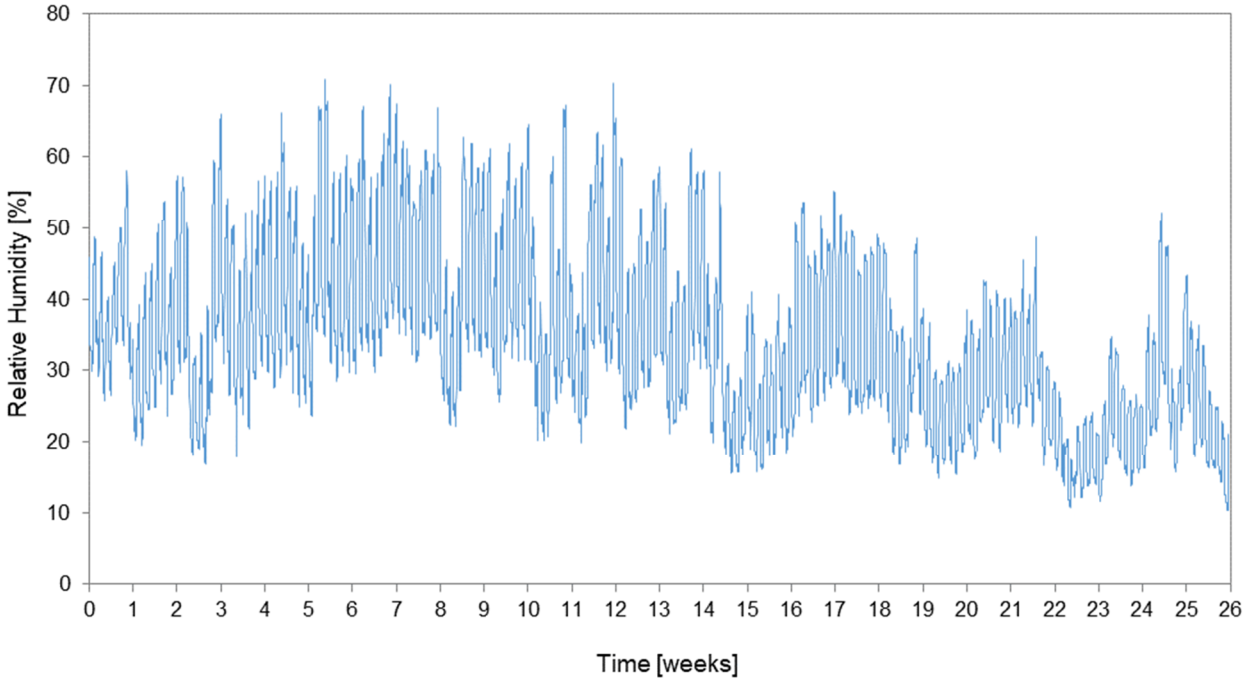

Fig. A5-4. Relative humidities during the evaporation experiment in the laboratory oven (RH_{mean}=34.4 %).

Table A5-2. Absolute masses and mass losses of the three identical tubing loops (LDPE; 25 cm) during the evaporation experiment. Initially, all loops contained 0.5 mL of water.

Loop ID	Total mass at first day [g]	Total mass after 6 weeks [g]	Mass loss Δm after 6 weeks [g]	Total mass after 16 weeks [g]	Mass loss Δm after 16 weeks [g]	Total mass after 26 weeks [g]	Mass loss Δm after 26 weeks [g]
1	7.56	7.53	0.03	7.47	0.09	7.41	0.15
2	7.47	7.44	0.03	7.38	0.09	7.33	0.14
3	7.53	7.50	0.03	7.44	0.09	7.39	0.14

Appendix 6

Supplementary data for Chapter 6

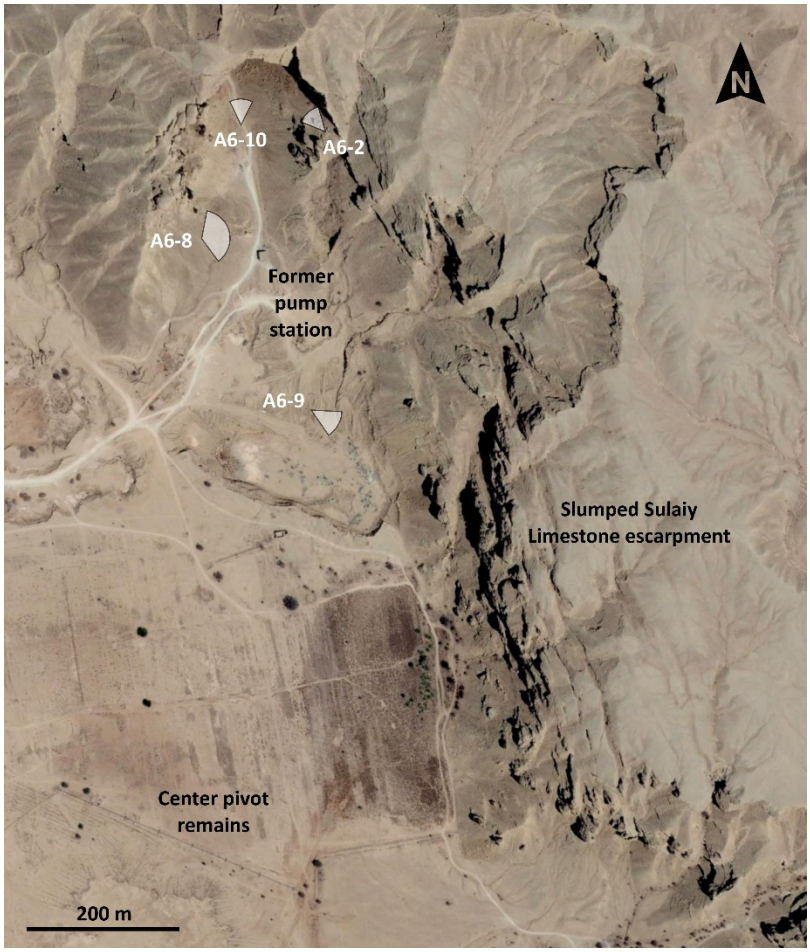

Fig. A6-1. Satellite image of Dahl Hith and its vicinity (12 August 2015; GoogleEarth Pro, modified; cave entrance at 24°29’10’’N, 46°59’50’’E). Symbols indicate photographer’s perspective for Fig. A6-2, A6-8, A6-9, and A6-10. Note the pump station and center pivot remains, testifying to intensive irrigation activities in the past.

Fig. A6-2. Entrance of Dahl Hith at the foot of the Sulaiy Limestone escarpment (approx. 100 m high). Note the cave visitors in the foreground, serving as scale.

Fig. A6-3. Cave graffiti in Dahl Hith (19 February 2008). These graffiti were probably created by swimmers in the 1970s–1990s, when the water level dropped due to agricultural water abstraction.

Fig. A6-4. Water level in Dahl Hith (19 February 2008). Due to the low water level at that time, additional photography equipment (slave flash) was necessary.

Fig. A6-5. Water level in Dahl Hith (20 November 2013; now reached by sunlight). Due to the recent water level rise, the “graffiti wall” (completely exposed in 2008, Fig. A6-3), was half-drowned in 2013.

Fig. A6-6. Water level in Dahl Hith (19 December 2014; now reached by sunlight). Due to further water level rise, the “graffiti wall” (compare Fig. A6-3 and A6-5) has drowned completely.

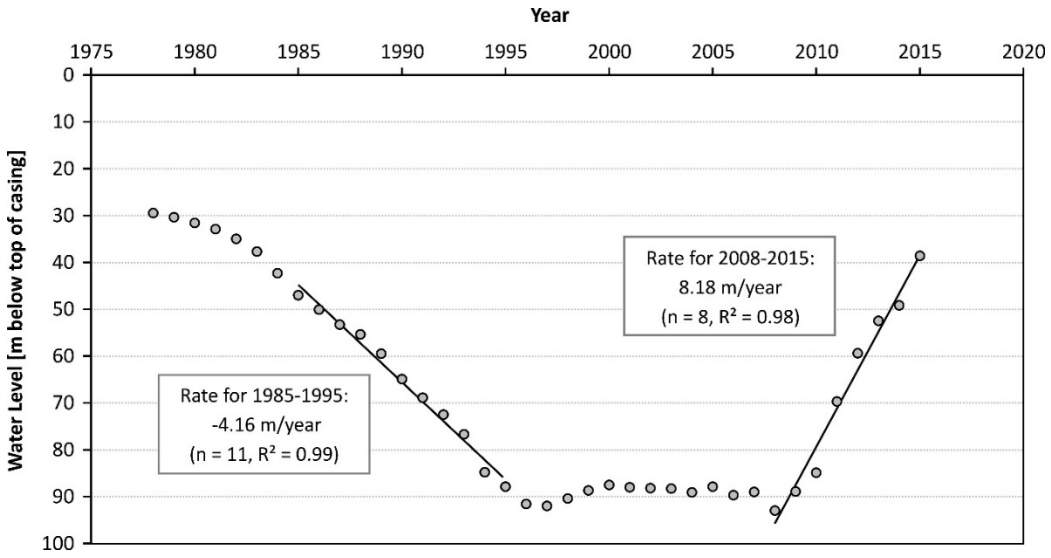

Fig. A5-7. Development of the groundwater level in observation well 5-K-84 (Sulaiy Formation; total depth: 300 m; 24°21’06’’N, 47°09’49’’E). The well is located 22 km southeast of Dahl Hith and 12 km southeast of the artificial lakes. Due to agricultural water abstraction in the area, the groundwater level had dropped during the 1980s and 1990s. Since 2008, the water level has been rising again.

Fig. A6-8. Panorama photograph of the Dahl Hith vicinity (19 December 2014). Note the slumped Sulaiy Limestone in the south (see Fig. A6-9 for close-up view; compare the roughly horizontal bedding in the center of the picture).

Fig. A6-9. Close-up view of the slumped Sulaiy escarpment (19 December 2014).

Fig. A6-10. Photograph of the Dahl Hith entrance with fresh traces of surface runoff in the foreground (20 November 2013; one day after a rain event).

Text A6-1. Extract of CITC and KFUPM (2014) survey results.

The survey relies upon 3,000 interviews with inhabitants from across Saudi Arabia (age range: 12-65 years). Although the survey covers various aspects of the information and communications technology sector, the figures on smartphone penetration and social media use are particularly relevant for the present study.

It can be summarized that Saudi Arabia shows a remarkable smartphone penetration: approx. 67 % of the respondents owned a smartphone and approx. 72 % used a smartphone (CITC and KFUPM, 2014; page 68). Moreover, the study indicates that about 91 % of the respondents used social media (CITC and KFUPM, 2014; page 81). The users were also asked, which social media platforms they had used in the preceding six months (multiple choice). YouTube was the most popular platform (approx. 70 %), followed by Facebook (approx. 59 %), Twitter (approx. 53 %), Instagram (approx. 41 %), Google+ (approx. 21 %), etc. (CITC and KFUPM, 2014; page 82).

For further information, the reader is referred to the full report available at:
www.citc.gov.sa/English/Reportsandstudies/Studies/Pages/default.aspx (last access: 6 January 2016).

Appendix 7

Supplementary data for Chapter 7

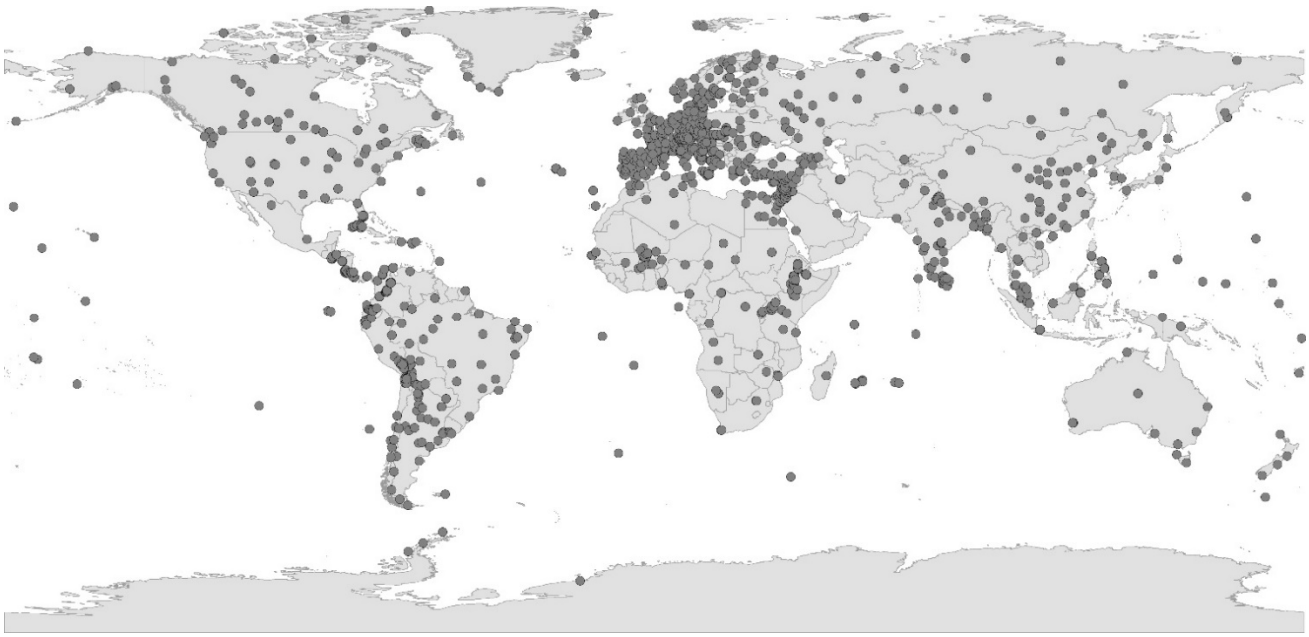

Fig. A7-1. Map showing all monthly GNIP stations (data source: IAEA/WMO, 2019).

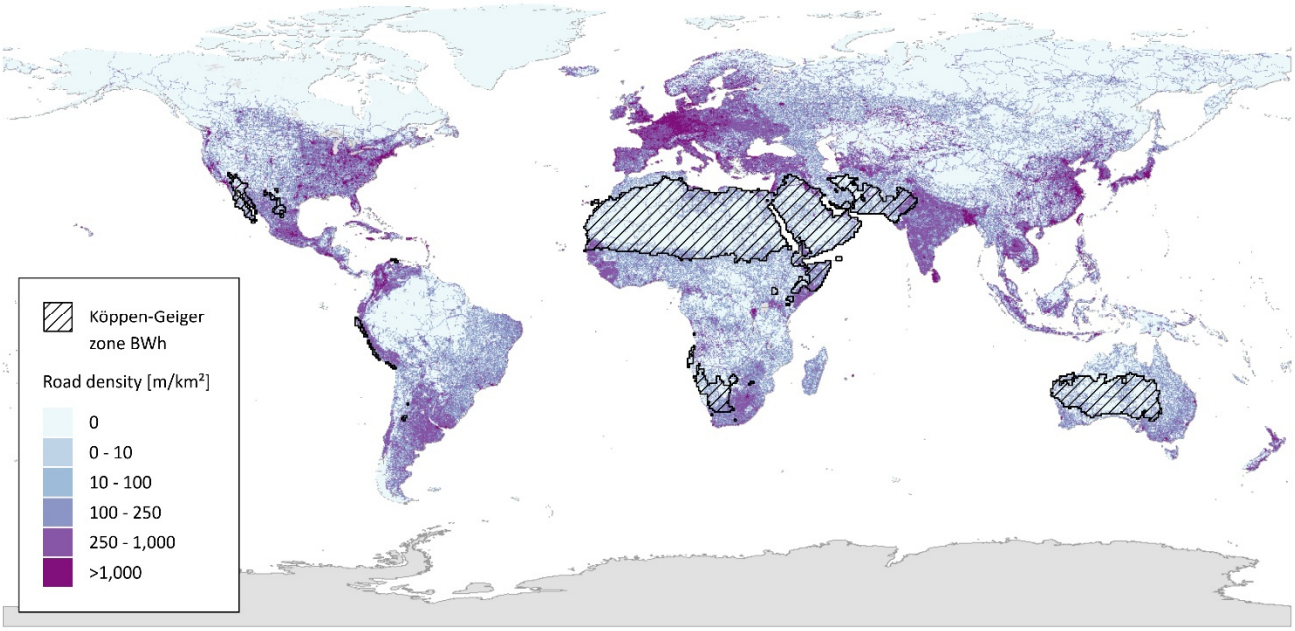

Fig. A7-2. Map showing the global road density (GloBio, 2019; Meijer et al., 2018). The hatched area represents the Köppen-Geiger zone BWh (hot deserts; Rubel and Kottek, 2010). Note the particularly low road density in this zone.

References

GloBio, 2019. https://www.globio.info/download-grip-dataset (last access: 28 November 2019).

IAEA/WMO – International Atomic Energy Agency/World Meteorological Organization, 2019. Global Network of Isotopes in Precipitation. The GNIP Database. https://nucleus.iaea.org/ wiser (last access: 17 November 2019).

Meijer, J.R., Huijbregts, M.A.J., Schotten, K.C.G.J., Schipper, A.M., 2018. Environmental Research Letters 13, 064006.

Rubel, F., Kottek, M., 2010. Observed and projected climate shifts 1901–2100 depicted by world maps of the Köppen-Geiger climate classification. Meteorologische Zeitschrift 19(2), 135–141.